

Effects of Dissolved Gas Supersaturation and Bubble Formation on Water Treatment Plant Performance

Paolo Scardina

Dissertation submitted to the Faculty of the
Virginia Polytechnic Institute and State University
In partial fulfillment of the requirements for the degree of

Doctor of Philosophy

In

Civil Engineering

Marc Edwards, Chair

Bill Knocke

John Little

John Novak

Alan Esker

January 19, 2004

Blacksburg, Virginia

Keywords: Bubble Formation, Air Binding, Filtration, Water Treatment, Coagulation

Copyright 2004, Paolo Scardina

Effects of Dissolved Gas Supersaturation and Bubble Formation on Water Treatment Plant Performance

Paolo Scardina

Advisor: Dr. Marc Edwards

ABSTRACT

Gas bubbles that form within water treatment plants can disrupt drinking water treatment processes. Bubbles may form whenever the total dissolved gas pressure exceeds the local solution pressure, a condition termed dissolved gas “supersaturation.” This project investigated how bubble formation affects conventional drinking water treatment and examined factors that can reduce these problems.

Gas bubbles attached to coagulated floc particles can reduce settling efficiency and create “floating floc.” In laboratory experiments, bubbles formed on the surface of the mixing paddle, since this was the location of minimum pressure within the system. The formation and stability of floating floc was dependent on many different factors including the amount and type of dissolved gas supersaturation and surface chemistry of the mixing paddle. The intensity and duration of rapid mixing also controlled the amount of floating floc.

Bubbles forming in filter media can block pore spaces and create headloss, a process popularly termed “air binding.” During benchscale filtration experiments, bubbles were released upwards from the media in a burping phenomenon, and bubbles could also be pushed downwards by fluid flow. Burping is beneficial since it partly alleviates the bubble induced headloss, but the media disruptions might also decrease filter efficiency (particle capture). Bubble formation within filters can be reduced by increasing the pressure inside the filter via greater submergence (water head above the media), lower hydraulic flow rate, or use of a more porous media. The mode of filter operation (declining or constant flow rate) will also affect the local filter pressure profile.

Dissolved gas supersaturation and bubble formation are detected in on-line turbidity devices and particle counters causing spurious measurements. The use of bubble traps usually reduced these problems, but one device worsened turbidity spikes. Flow disturbances may also release bubbles upstream of the on-line turbidimeter, which can cause spikes in turbidity readings.

ACKNOWLEDGEMENTS

Many thanks extended to my adviser Marc Edwards, and also to my committee members. The author appreciates the help of Kenneth Craft, Jr, Julia Novak, and all the water utilities that provided valuable information and on-site sampling. This work was supported by a grant from the American Water Works Association Research Foundation (AWWARF). The generous funding provided by the Virginia Tech Via Fellowship is also appreciated.

TABLE OF CONTENTS

ABSTRACT.....	ii
ACKNOWLEDGMENTS	iii
LIST OF TABLES.....	vii
LIST OF FIGURES	viii
AUTHOR’S PREFACE.....	xi
CHAPTER 1: AIR BINDING OF GRANULAR MEDIA FILTERS.....	1
Abstract.....	1
Introduction.....	1
Materials and Methods.....	2
Filter Apparatus	2
Testing Solutions and Dissolved Gas Supersaturation	4
Experimental Matrix	6
Results and Discussion	6
Filter Hydraulics in Relation to Total Dissolved Gas (TDG).....	6
Experimental Confirmation of Predicted Trends in Air Binding.....	12
Bubble Behavior within the Filter during Runs.....	15
Implications for Filter Operation	21
Other Influential Factors: Atmospheric Pressure and Interstitial Velocity.....	25
Summary and Conclusions	27
Acknowledgements.....	28
References.....	28
CHAPTER 2: INTERFERENCE TO PARTICLE COUNT AND ON-LINE TURBIDITY MEASUREMENTS FROM BUBBLE FORMATION	30
Abstract.....	30
Introduction.....	30
Interferences from Bubbles.....	32
Materials and Methods.....	36

Analysis of Particle Counters.....	36
Laboratory Analysis of Turbidimeters.....	37
Results and Discussion	39
Preliminary Examination of Bubble Interferences in Particle Counters.....	39
Preliminary Examination of Bubble Interferences in Turbidimeters.....	46
Discussion.....	51
Summary and Conclusions	55
Acknowledgements.....	56
References.....	56

CHAPTER 3: FUNDAMENTALS OF BUBBLE FORMATION DURING

COAGULATION AND SEDIMENTATION PROCESSES	60
Abstract.....	60
Introduction.....	60
Materials and Methods.....	62
Results and Discussion	64
Fundamental Background on Bubble Formation during Coagulation and Mixing.....	64
Generalized Observations Related to Bubble Phenomenon in Jar Tests	73
Quantitative Results in Relation to Background, Theory, and General Observations	77
Additional Considerations	86
Summary and Conclusions	88
Acknowledgements.....	89
Appendix.....	89
References.....	91

CHAPTER 4: ADDRESSING PROBLEMS WITH GAS SUPERSATURATION

AT POTABLE WATER TREATMENT PLANTS.....	95
Abstract.....	95
Introduction.....	95

Materials and Methods.....	96
Results and Discussion	97
Design of Coagulation Mixers and Bubble Formation.....	97
Analysis of Bubble Formation at Treatment Plants.....	100
Mitigating the Effects of Bubble Formation.....	115
Summary and Conclusions	119
Acknowledgements.....	119
References.....	120
APPENDIX I	121
Prediction and Measurement of Bubble Formation in Water Treatment.....	121
APPENDIX II.....	142
Practical Implications of Bubble Formation in Conventional Treatment.....	142
AUTHOR’S VITA.....	164

LIST OF TABLES

1.1	Benchscale Filter Experimental Conditions.....	7
1.2	Calculated Local Pressure Profile in the Clean Bed Filter of Experiment 7	9
2.1	On-line Turbidimeters Used in this Study	38
3.1	Illustrative Calculation of Effect of Gas Type and Temperature Relative to Bubble Formation.....	67
3.A1	Comparison of the Amirtharajah and Mills (1982) and This Study	89
4.1	Single Comparison of Waters Supersaturated and Undersaturated with Dissolved Gas	102
4.2	On-site Analysis of Dissolved Gas Supersaturation and Bubble Formation at Various Water Treatment Plants.....	103
4.3	Analysis at Utilities B and C.....	108

LIST OF FIGURES

1.1	Benchscale Filter Schematic	3
1.2	Predicted Pressure Profiles as a Function of Flow Rate for the Clean Bed Benchscale Filter.....	9
1.3	Scenarios for Bubble Formation Using Predicted Pressure Profiles through the Clean Bed Filter of Two Experiments	10
1.4	Predicted Filter Pressure Profile of Clean Bed Filters for Various Experiments	12
1.5	High Porosity ($\epsilon = 0.40$) Filtration Experiments	14
1.6	Low Porosity ($\epsilon = 0.28$) Filtration Experiments	14
1.7	Effluent Total Dissolved Gas (TDG) Profiles (Top), and Change in Supersaturation with Depth during Experiment 2 (Bottom).....	16
1.8	Volume of Bubbles Trapped in the Filter Based on Weight Loss Measurements (Top), and the Comparison of Degassing from Solution to that Trapped in the Filter (Bottom)	18
1.9	Retention Ratio during Two Filter Runs (Top), and the Average Retention Ratio as a Function of Flow Rate (Bottom)	20
1.10	Total Water Production for Various Experimental Conditions	22
1.11	Comparison of Bubble Formation on Dual and Mono Media Filters.....	23
1.12	Amount of Degassing (Difference between the Influent and Effluent TDG) and Average Detention Time (Dt) through the Top 15.2 cm of Media for Mono and Dual Media Experiments	24
2.1	Minimum Outlet Pressure Required to Prevent Gaseous Cavitation in Particle Counters (Data from Dillenbeck, 1987).....	34
2.2	Representative Particle Count Data on Two Filters at Utility X	42
2.3	Particle Counter Modifications for This Study.....	43
2.4	Particle Counts at Different Manifold Tubing Heights at Utility X	44
2.5	Actual Particle Counts at Utility X on 7-31-2002	44
2.6	Turbidity Measurements from Three Different On-line Turbidimeters with an Influent Supersaturated with Dissolved Gas at 0.23 atm Gauge Pressure	48

2.7	Turbidity during High Levels of Dissolved Gas Supersaturation (0.23 atm gauge pressure).....	50
2.8	Effects of Dissolved Carbon Dioxide Supersaturation on Turbidity Measurements of Instrument B.....	51
2.9	Effects of Dissolved Carbon Dioxide Supersaturation on Turbidity Measurements of Instrument C.....	52
2.10	Measurements of Benchtop Turbidity for Solutions Supersaturated with Either Dissolved Nitrogen or Carbon Dioxide.....	55
3.1	Floating Floc Collected above a Filter at a Water Treatment Plant.....	61
3.2	Gas Bubble Formation by Heterogeneous Nucleation: Schematic (Top) and on the Mixing Paddle (Bottom).....	65
3.3	Gas Bubbles Form until Equilibrium Is Reached Between Water and Local Atmosphere (Left), and Conceptualization of Gas Transfer Kinetics as System Approaches Equilibrium via Bubble Formation (Right).....	66
3.4	Calculated Local Solution Pressure at the Outer Most Tip of the Paddle Estimated for the Jar Tester at a Depth of 6.0 cm.....	70
3.5	Crude Manometer Tube Affixed to Mixing Paddle.....	71
3.6	Change in Local Solution Pressure while Mixing for the Front and Back of the Paddle Face (Top) and for the Front Face as a Function of Different Mixing Speeds (Bottom).....	72
3.7	Preliminary Alum Experiment.....	73
3.8	Quantification of Alum Floating Floc by Estimating the Surface Diameter (a.) and the Depth/Thickness (b.) of the Floating Floc.....	74
3.9	Variations in Floating Floc as a Function of the Rapid Mix Length.....	76
3.10	Visual Observations of Bubble Nucleation on Paddle during Nucleation Experiments.....	78
3.11	Factors Affecting Gas Bubble Nucleation and Floating Floc.....	79
3.12	Floating Floc as a Function of Initial TDG and Length of Rapid Mixing.....	82
3.13	Comparison of Alum and Iron (III) Chloride Coagulants.....	84
3.14	Picture of Ferric (III) Chloride Jar Tests (30 mg/L as Fe).....	85
3.15	High Rate Mixing Experiments at 1300 rpm.....	87

3.A1	Bubble Formation after Rapid Mixing in Solutions Supersaturated with Dissolved Carbon Dioxide (Top) and Nitrogen (Bottom)	90
4.1	Mixing Velocity Where the Local Solution Pressure Equals the Total Dissolved Gas (TDG) Pressure at a Given Depth, as Calculated by the Energy Equation.....	98
4.2	Operational Curves for Different Mixing Scenarios.....	101
4.3	Effects of the Rate of Flocculation on the Amount of Floating Floc.....	102
4.4	Floating Floc at Utility A.....	106
4.5	Water Flow Schematic from the Sedimentation Basin to the Filters at Utility D.....	110
4.6	Schematic of Upflow Clarifier at Utility F	111
4.7	Bubble Release (Burping) from the Upflow Clarifier at Utility F.....	112
4.8	Diurnal Variation of TDG in the Filter Influent for All Four Filters at Utility G (Top), and Change in the Total Dissolved Gas (TDG) through Each Filter at Utility G (Bottom).....	114
4.9	Change in the Dissolved Oxygen and Carbon Dioxide for All Filters at Utility G	116
4.10	Decision Tree for Reducing Bubble Formation, Floating Floc, and Hindered Settling	117
4.11	Decision Tree for Reducing Filter Air Binding and Burping	118

AUTHOR'S PREFACE

Gas bubbles forming in a drinking water treatment plant are known to disrupt conventional treatment (coagulation, sedimentation, filtration) and to interfere with turbidity and particle count measurements. Bubbles interfere with particle agglomeration during coagulation, attach to coagulated floc particles thereby reducing settling in the sedimentation basin, form within granular media filters and produce headloss, carry media out of filters during backwashing, and cause spurious turbidity or particle count measurements. Although many treatment plants are adversely affected by these problems on a daily or seasonal basis, very little experiment work has been done to understand the fundamental science behind this phenomenon or to develop practical mitigation strategies. This research will address these deficiencies.

This dissertation is organized in chapters that describe results for a specific area of conventional water treatment, and is a seamless continuation of the author's M.S. thesis examining the fundamental science of bubble formation (Appendix I and II). Consequently, a reader interested in a complete and logical development of this graduate research should read Appendix I and Appendix II first (M.S. Thesis) and then Chapters 1 – 4 which present results for the Ph.D. The work from the M.S. thesis has already been published in *Journal of Environmental Engineering* 2001, 127, 11, 968-973 (Appendix I) and *Journal American Water Works Associate* 2002, 94, 8, 85-94 (Appendix II).

A gas bubble can form in solution when the total dissolved gas (TDG) pressure exceeds the local solution pressure, where the TDG is the sum of the partial pressure of each gas species dissolved in solution. When this condition occurs, the water is “supersaturated” with respect to dissolved gas (Appendix I). A water can become supersaturated with dissolved gas by microbiological, chemical, and physical processes, either in the source water or directly in the treatment plant (Appendix II). To assess the potential for bubble formation, a total dissolved gas probe (TDGP) can be used to measure the TDG of a water, which can then be compared to the local solution pressure in the plant as determined by either direct measurements or calculations. A TDGP is also a powerful tool for diagnosing the source of dissolved gas supersaturation.

Chapter 1 “Air Binding in Granular Media Filters” has been accepted for publication in *Journal of Environmental Engineering* during 2004 and is an investigation of bubble formation in granular media filters through a phenomenon termed “air binding.” A benchscale filter was

used for all laboratory filtration experiments that either contained only a sand media or a dual media (sand and anthracite). Most experiments were constant head, such that any headloss caused by bubbles reduced the effluent flow rate. During filtration experiments, bubbles were discovered to move within the filter media. Trapped bubbles can be released upwards from the media in a burping phenomenon, and bubbles can be pushed through the media by fluid drag. Although burping could allow particles and pathogens to pass through the filter, burping also alleviates the bubble induced headloss. Filter operation affects the local solution pressure within the filter, and the location of potential bubble formation in filters can be predicted based on measurements of the clean bed headloss with depth and the influent total dissolved gas. Bubble formation in filters can be reduced by increasing the local pressure via greater submergence (water head above the media), lowering hydraulic flow rate, or using a more porous media. The mode of filter operation (declining or constant flow rate) will also affect the local filter pressure profile. A dual media filter with an anthracite top layer induced more bubble formation, due to the anthracite's hydrophobicity. The lower density and higher porosity anthracite layer also allowed more burping, leading to much greater water production in situations where the water was supersaturated with dissolved gas.

Chapter 2, "Interference to Particle Count and On-line Turbidity Measurements from Bubble Formation," has been submitted to *Journal of Environmental Engineering*. Experiments in the laboratory and at full-scale treatment plants confirmed that gas bubbles can often measure as false particle counts or turbidity. Bubbles can form within the measurement cell of particle counters via gaseous cavitation, since this is the location of high fluid velocity and minimum pressure in the system. When the pressure within a particle counter at a water utility was increased, the corresponding particle counts consistently decreased, indicative of bubbles forming within the apparatus. In a laboratory study, an applied pressure of 20 psi was required to suppress gas bubbles forming within the particle counter for levels of supersaturation encountered at water treatment plants. Several on-line turbidimeters were tested in the laboratory using water supersaturated with dissolved gas. The problems caused by dissolved gas supersaturation and bubble formation varied for each instrument. One instrument was prone to spurious turbidity spikes even at low levels of dissolved gas supersaturation, and a significant quantity of gas developed in the measurement cell of another instrument which steadily increased the detected turbidity. The third instrument was relatively immune to bubble

formation during normal operation, but the turbidity spiked during flow disruptions that caused bubbles in the influent line to be swept into the instrument. The bubble reject functions and bubble traps of the instruments helped mitigate variability in the turbidity data, except in a few cases where use of one bubble trap actually caused more problems.

Chapter 3, “Fundamentals of Bubble Formation during Coagulation and Sedimentation Processes” is an analysis of disruptions caused by bubbles during conventional coagulation and sedimentation. This chapter describes the creation of “floating floc” and has been submitted to the *Journal of Environmental Engineering*. A benchtop conventional jar tester was used to simulate coagulation and sedimentation processes in treatment plants. Gas bubbles formed on the mixing paddle during rapid mixing via heterogeneous nucleation, as the paddle surface is the location of lowest pressure due to high fluid velocities. High rate mixers often are appealing for large velocity gradients (G values) and rapid chemical dispersal, but the high rate mixing can induce lower solution pressures that can exacerbate bubble formation. The larger gas bubbles rose to the water surface quickly; whereas, many of the smaller gas bubbles remained in the water and attached to coagulant floc creating floating floc at the water surface. Floating floc could dramatically reduce particle removal efficiency during sedimentation. Both iron and aluminum coagulants were susceptible to this problem. In some instances, previously settled floc was buoyed by bubble growth, and the agglomerate was floated to the water surface. Many factors affected the amount of bubble formation and corresponding floating floc, including the surface chemistry of the mixing paddle, presence of surfactants, solution temperature, and whether the dissolved gas supersaturation was due to nitrogen, oxygen, or carbon dioxide. Future research should examine the role of different gases in greater detail.

Chapter 4, “Addressing Problems with Gas Supersaturation at Potable Water Treatment Plants,” has been submitted to *Journal American Water Works Association* and explains some design and operational considerations that reduce the effects of bubble formation within a treatment plant. Several site visits at treatment plants afflicted with bubble formation provide practical confirmation of hypotheses developed in the laboratory phase of research. That work indicated that the amount of floating floc can be reduced by altering the mixing protocol within the plant. Decreasing the mixing speed or increasing the depth of the paddle will help reduce the potential for bubble formation during rapid mixing. If the paddle speed is fixed, the amount of floating floc passes through a maximum at a specific time duration of rapid mixing;

consequently, treatment plants can reduce floating floc problems by altering mixing rate or the mixing time. For instance, decreasing the duration and intensity of mixing can prevent many bubbles from forming at all; whereas, increased mixing speed and duration of rapid mixing can eventually detach bubbles from particles and allow natural floc settling to occur. The case studies present a sampling and data analysis protocol that help utilities diagnosis the source of bubble formation. Two decision trees were also developed to guide utilities in finding solutions. Whenever possible, the source causing the dissolved gas supersaturation and/or bubble formation should be eliminated. If the source of dissolved gas supersaturation cannot be eliminated, then additional treatment step(s) should be installed to remove the dissolved gas.

CHAPTER 1

AIR BINDING IN GRANULAR MEDIA FILTERS

Paolo Scardina and Marc Edwards
418 Durham Hall, Blacksburg, VA 24061

ABSTRACT:

Gas bubbles that form in water treatment filters create headloss similar to solid particles. Gas bubbles can form in solution whenever the total dissolved gas (TDG) pressure exceeds the local solution pressure. The local solution pressure within a filter, and therefore the location where bubbles could potentially form, can be predicted using measurements of the clean bed headloss at a given depth and influent TDG measurements. Bubble formation within filters can be reduced by increasing the pressure within the filter via greater submergence (water head above the media), lower hydraulic flow rate, or use of a more porous media. Bubbles were observed to move both up- and downwards through the filter media due to drag and buoyant forces. Bubbles trapped in the bed can also be released from the media in a “burping” phenomenon, which can reduce the extent of headloss buildup. Burping is more significant at lower flow rates and within a lower density, higher porosity, hydrophobic media such as anthracite.

INTRODUCTION:

If gas bubbles form in filters, they disrupt filter operation through a process popularly termed “air binding.” Air binding increases backwashing frequency when compared to situations where bubbles do not form (Water Quality and Treatment, 1999; Scardina and Edwards, 2002). During backwashing, released gas bubbles can carry and float media out of the filter or cause undesirable intermixing of dual media. Large holes through the media can develop from gas release during normal filter operation, which increases the likelihood of pathogen escape to the finished water, and gas bubbles forming in turbidimeters might contribute to spuriously final filter turbidity measurements (HACH, 1997).

A gas bubble can form within a filter via heterogeneous nucleation whenever the total dissolved gas (TDG) pressure—as determined by the summation of the aqueous gas partial pressures—exceeds the local solution pressure (Scardina and Edwards, 2001):

$$[(TDG = pN_2 + pO_2 + pCO_2 + pAr + pH_2O) > \text{Local Pressure}] \quad (\text{Equation 1.1})$$

⇒ Possible Bubble Formation.

In such circumstances we term the water “supersaturated” with respect to total dissolved gas. Dissolved gas supersaturation can occur from mechanical, chemical, or microbial processes (Scardina and Edwards, 2002). Dissolved gas concentrations and partial pressures will vary significantly throughout a plant, and it is not uncommon for a utility to treat waters that range from -0.2 atmospheres (atm) gauge pressure (undersaturated with dissolved gas) to greater than +0.2 atm gauge pressure (supersaturated with dissolved gas).

Although disruptions from gas bubbles plague many utilities on a daily or seasonal basis, little experimental work has focused on the fundamental factors that control bubble formation or the behavior of trapped bubbles within filters. Existing filtration models do not account for, nor do they attempt to predict, bubble formation within filter media (i.e., O’Melia and Ali, 1978; Appleton et al., 2001; Head and Shepherd, 2001); consequently, a systematic study of bubble formation in filters was undertaken.

MATERIALS AND METHODS:

Filter Apparatus

A mono media benchscale sand filter with an internal diameter of 4.13 cm (1 5/8 inches) was used for this study (Figure 1.1). The filter sand media was captured between a 0.417 and 0.589 mm sieve, and this sand media was supported by an intermediate (a mix of 0.32 - 0.64 cm) and ballast (~2.5 cm) material. Two filter bed porosities (ϵ) were tested using the same sand. A high porosity ($\epsilon = 0.40$) was obtained by allowing the media to settle naturally after backwashing; whereas, a lower porosity ($\epsilon = 0.28$) was created by rapping the column until the media appeared completely compressed. For all experiments, the overall depth of filter media was 30.5 cm by adding media as necessary. In one study, half of the sand was replaced with an anthracite top layer ($\epsilon = 0.47$), which was passed and retained on a 2.0 cm and 0.85 cm sieves, respectively. In this dual media study, both media settled naturally after backwashing.

Static tubes were positioned at 1.5, 13.0, 24.4, and 38.6 cm below the filter media surface to measure headloss with depth. The fourth static tube (at 38.6 cm) was located in the filter

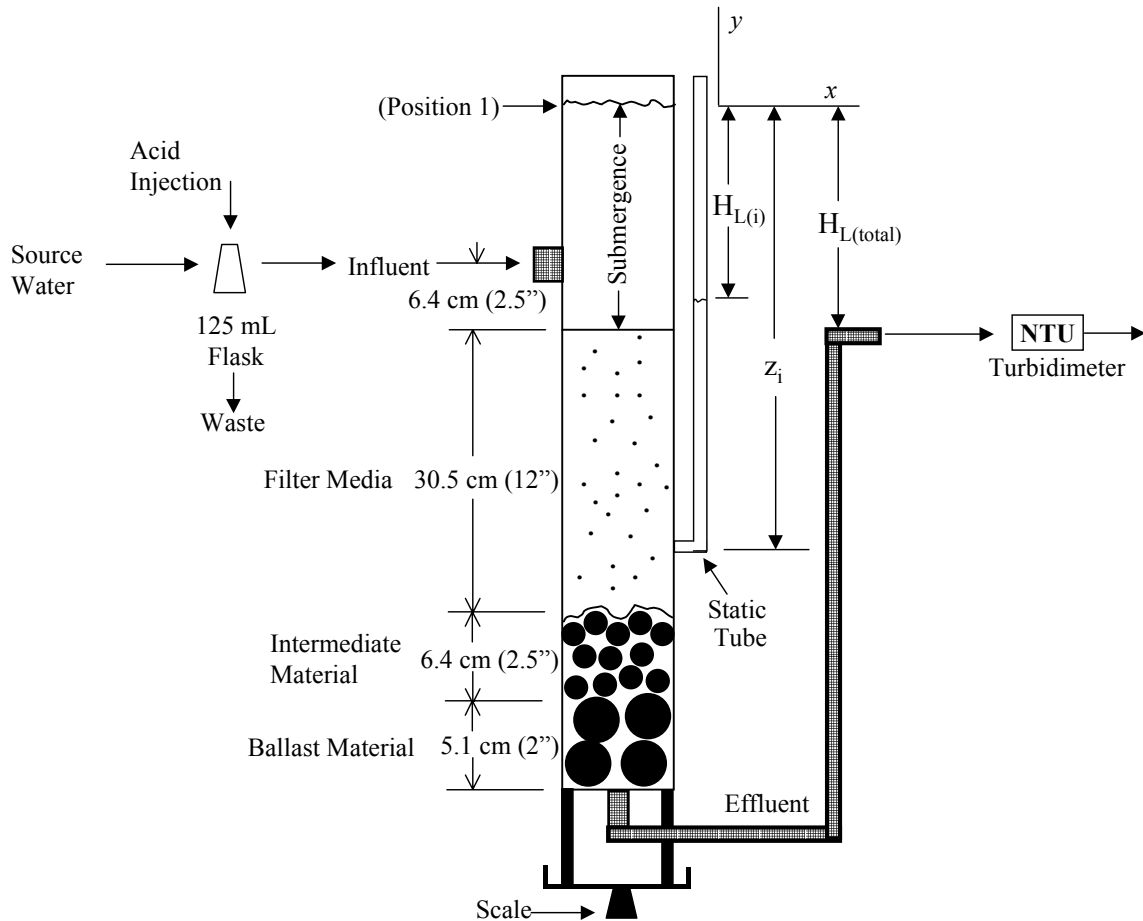


Figure 1.1 – Schematic of the Benchscale Filter Used in this Study.

underdrain and determined the total headloss of the filter (approximate height of the effluent outlet).

The submergence (water head above the media) and the height of the effluent outlet were altered for specific experiments. Typical filter operation was a declining flow and constant head mode with an initial effluent flow of 9.8 L/hr (approximately 3 gpm/ft² for this benchscale filter) ± 5% unless otherwise indicated. A filter effluent valve was partially closed as noted in one experiment to control the hydraulic flow rate.

The filter effluent emptied into a 60 mL reservoir that was open to the atmosphere, and approximately 30% of that flow was diverted to a HACH 2100N turbidimeter flow-through cell equipped with a bubble trap. The turbidimeter was calibrated every three months as per manufacturer recommendations.

The entire filter was set upon an Ohaus scale capable of measuring the filter apparatus mass to ± 0.5 g. Any gas bubbles that formed within the media displaced a volume of water from the filter leading to an overall decrease in the mass of the apparatus. The submergence (height of water above the sand media) was monitored to ± 0.5 mm, and the water in the headloss tubes was measured to $\pm 1/16^{\text{th}}$ inch. QA/QC testing suggested that the weight of the apparatus was reproducible upon replicate measurements to within ± 1 gram. To estimate the cumulative volume of gas trapped in the media, each mL of gas bubble formed was assumed to displace 1 gram of water.

After each experiment the filter was backwashed to dislodge any trapped gas bubbles. A typical backwash would not remove some gas bubbles that were attached to filter media even with high washing flow rates ($\sim 200\%$ bed expansion), so a degassed water (boiled and then cooled to room temperature) was placed into the column for at least 12 hours to remove/dissolve any remaining gas bubbles. A final backwash at 50% bed expansion was performed at the start of each new filter run.

Testing Solutions and Dissolved Gas Supersaturation

Most experiments used an influent water that was supersaturated with dissolved gas. The corresponding total dissolved gas (TDG) pressure was referenced to the local barometric pressure and reported as a gauge pressure. For example, a solution at equilibrium with the local atmosphere (100% saturation) would have a gauge pressure of 0 atm. Any supersaturation or undersaturation with respect to dissolved gas would be reported as a positive or negative gauge pressure, respectively. The distilled source water used in these experiments was initially undersaturated with dissolved gas at approximately -0.08 atm gauge pressure.

The following procedure was used to create a dissolved gas supersaturation of 0.10 ± 0.03 atm gauge pressure in the water influent to the filter. The source water was first equilibrated with the atmosphere (0.0 atm gauge pressure of TDG) via diffused aeration at a temperature of about 20 °C (± 1.5 °C). Next, sodium bicarbonate was added to the aerated waters at a final concentration of 3 mM. This alkaline water was then pumped into a 125 mL flask where 0.06 M nitric acid was also added to pH 5 (Figure 1.1), thereby converting the bicarbonate (HCO_3^-) alkalinity to dissolved carbon dioxide:



This supersaturated water (0.1 atm gauge pressure) was immediately introduced to the filter. This method was chosen for its simplicity and reliability, and at the time of this work, there was no reason to suspect that dissolved carbon dioxide would behave significantly different than other gases in water. In experiments without dissolved gas supersaturation, sodium nitrate (0.01 M) electrolyte was added to the distilled water, and experiments confirmed that this salt concentration had little effect on bubble formation. No turbidity particles were added to the filter influent waters.

The total dissolved gas (TDG) pressure of the water was measured with a total dissolved gas probe (TDGP or saturometer) manufactured by Sweeney Aquametrics (± 0.0026 atm gauge pressure). The local barometric pressure measured by the TDGP was the pressure datum (gauge pressure) for the reported TDG data. The TDGP also measured and compensated for the solution temperature (± 0.1 °C).

As gases left solution (degassing) to form bubbles, the TDG would decrease through the filter, so that the volume of bubbles formed per liter of water passing through the filter could be estimated from the measured decrease in TDG pressure through the filter and dissolved gas calculations. Since the water was aerated initially, the starting concentrations of nitrogen, oxygen, and carbon dioxide could be calculated with Henry's gas law (Henry's constants were adjusted to the solution temperature) and the measured barometric pressure. Henry's gas law is considered a better approximation for dissolved gases in dilute solutions such as from atmospheric gases, rather than Raoult's law (Betterton, 1992). The amount of dissolved carbon dioxide supersaturation was also known, such that the total initial TDG was 0.1 atm gauge pressure. The Scardina and Edwards modified closed system equilibrium model (2001) was used in conjunction with the measured TDG loss through the filter to determine the percent reduction of each dissolved gas from solution (i.e., the transfer of each dissolved gas species to the bubble(s)). This model is a modified closed system equilibrium where a volume of gas is allowed to form (Scardina and Edwards, 2001). The difference between the concentration of each dissolved gas in the influent and effluent was the number of moles transferred to the bubbles per liter of solution passing in the filter. The ideal gas law was then used to estimate the

volume of bubbles formed by assuming the pressure in the bubbles was approximately the barometric pressure.

Experimental Matrix

This study investigated how design and operational parameters of a filtration system influence gas bubble formation and air binding (Table 1.1). Design parameters—such as the media porosity and type of filter media (mono- versus dual media)—and different operational parameters (flow rate and submergence) were varied for benchscale laboratory experiments. For clarity, each experimental condition was assigned an experiment number (Table 1.1).

RESULTS AND DISCUSSION:

Results are presented in five sections including 1) predicting bubble formation in clean bed filters based on hydraulic profiles and dissolved gas measurements, 2) experimental confirmation of predictions, 3) bubble phenomena observed in filters during a run, 4) implications for filter operation, and 5) other factors influencing air binding.

Filter Hydraulics in Relation to Total Dissolved Gas (TDG)

The concept of negative gauge pressures developing in filters is widely understood (AWWA, 1999). For instance, if the filter effluent outlet is too low, a corresponding negative gauge pressure within the filter can draw/suck air into the filter through valves. During design of new filters, models can be used to predict the development of negative gauge pressures within the filter (Stevenson, 2001).

Hydraulic models also provide a useful starting point for considering the early stages of bubble growth in a clean filter media. The initial pressure profile (P_i) through a clean filter at depths (z_i) corresponding to each static tube can be calculated using the energy equation:

$$\frac{P_1}{\lambda} + \frac{V_1^2}{2g} + z_1 = \frac{P_i}{\lambda} + \frac{\alpha V_i^2}{2g} + z_i + H_{L(i)}. \quad (\text{Equation 1.2})$$

In the calculations for these experiments, the water surface was chosen to be position 1, since P_1 , V_1 , and z_1 would then be zero (Figure 1.1). The velocity component (V_i) in equation 1.2 would be the average superficial velocity, i.e. the flow rate divided by the filter surface area. The

Table 1.1 – Benchscale Laboratory Filter Experimental Matrix.

Experiment	Media Porosity	Initial Flow Rate L/hr (gpm/ft ²)	Submergence ¹ cm (inches)	Total Headloss ² cm (inches)	Measured Influent TDG atm, gauge
1	0.40	9.8 (3)	15.2 (6)	15.2 (6)	0.10
2	0.40	9.8 (3)	76.2 (30)	15.2 (6)	0.10
3	0.40	9.8 (3)	76.2 (30)	15.2 (6)	0.00
4	0.40	9.8 (3)	15.2 (6)	15.2 (6)	-0.08
5	0.40	41.0 (12.5)	76.2 (30)	76.2 (30)	0.10
6	0.28	9.8 (3)	40.6 (16)	40.6 (16)	0.10
7	0.28	9.8 (3)	15.2 (6)	40.6 (16)	0.10
8	0.28	9.8 (3)	76.2 (30)	40.6 (16)	0.10
9	0.28	9.8 (3)	76.2 (30)	40.6 (16) ³	0.10
10	0.28	4.3 (1.3)	15.2 (6)	15.2 (6)	0.10
11	0.28	19.7 (6)	76.2 (30)	76.2 (30)	0.10
12	0.40	9.8 (3)	15.2 (6) ⁴	15.2 (6) ⁴	0.10
13	0.47 & 0.40 ⁵	14.4 (4.4)	76.2 (30)	15.2 (6)	0.10

¹Submergence was the height of water above the filter media (Figure 1.1).

²The total headloss ($H_{L(Total)}$) was the height (depth) of the effluent outlet, as measured from the water surface (Figure 1.1).

³Experiment 9: Effluent outlet was 76.2 cm below the water surface, and a partially closed effluent valve controlled the flow rate and total headloss.

⁴Experiment 12 was at constant flow and varying ΔH_L . The starting submergence was 15.2 cm.

⁵Experiment 13 was a dual anthracite and sand media.

calculated Reynolds number indicated that the hydraulic flow through the media was laminar for all experiments, so alpha (α) in Equation 1.2 would be 2. Although some error would be inherent with this approach, the minimum local solution pressure (P_i) (gauge pressure) at a given depth (z_i) in the clean bed filter can then be estimated by using the measured z_i (negative number in Equation 1.2), the measured headloss (H_{Li} , a positive number in Equation 1.2), and the calculated V_i .

Likewise, if the local solution pressure is known (P_i), the potential for classical vaporous hydrodynamic cavitation within the filter can be predicted from the cavitation number (σ):

$$\sigma = \frac{P_i - P_v}{\frac{1}{2}\rho V^2}. \quad (\text{Equation 1.3})$$

For this calculation, the absolute pressure (gauge pressure + barometric pressure) is used for P_i , and the variables P_v and ρ are the solution vapor pressure and solution density, respectively. For flow through a filter, the velocity variable (V) in Equation 1.3 would be the interstitial velocity within the media: the superficial velocity divided by the porosity. While it can be complex, vaporous cavitation often occurs if σ is less than about 3 (Young, 1989).

The pressure profile through the filter was calculated (Equation 1.2) at the start of each experiment (Table 1.2). The velocity head does not markedly affect the local pressure, nor was it high enough to cause vaporous cavitation in the clean bed filter (Equation 1.3): the minimum cavitation number calculated in experiment 7 was 8.8×10^5 . However, flow through the porous media does lead to a significant headloss with depth that can counter the tendency for increased hydrostatic pressure with depth. Measurements through the clean bed at the start of experiment 7 indicate that the local gauge pressure (P_i) was positive throughout the filter (0.011 – 0.017 atm gauge pressure) and was a minimum at static tube 3 (Table 1.2). Thus, this is the location within the filter where the likelihood of bubble formation is greatest for a given influent water. From a more important practical perspective, air binding is not expected to occur in the clean bed of this particular filter as long as the influent dissolved gas supersaturation did not exceed 0.011 atm gauge pressure (Equation 1.1), since this is the lowest pressure within the filter under the given conditions.

If the submergence is maintained at a constant level and the initial flow is controlled by the height of the effluent outlet (or at treatment plants by adjusting an effluent outlet valve), the pressure will increase with depth in a clean bed if the flow rate is decreased, or the pressure will decrease with depth if the flow rate is increased (Figure 1.2). There is also a flow rate (for a mono media filter) at which pressure remains roughly constant with depth (Figure 1.2). The latter condition occurs when the increased hydrostatic pressure from depth cancels the decrease in pressure due to headloss through the filter with depth.

These concepts can be used to predict when and where bubbles might form within a filter, i.e. situations where the dissolved gas pressure exceeds the local solution pressure (Equation 1.1). Bubble growth within clean filters can be described by four possible scenarios, using the

Table 1.2 – Calculated Hydraulic Pressure Profile in the Clean Bed Filter for Experiment 7. [flowrate = 9.8 L/hr (3 gpm/ft²), $\epsilon = 0.28$, submergence = 15.2 cm (6 inches), and total headloss = 40.6 cm (16 inches)]

Static Tube	z_i (m)	Superficial Velocity V_i (m/s)	$\frac{(2)V_i^2}{(2g)}$ (m)	$H_{L(i)}$ (m)	P_i (atm, gauge)
1	(-) 0.167	0.002	4.08E-07	0.014	0.015
2	(-) 0.282	0.002	4.08E-07	0.157	0.012
3	(-) 0.396	0.002	4.08E-07	0.287	0.011
4*	(-) 0.538	0.002	4.08E-07	0.357	0.017

*Position 4 was located at the filter underdrain (2.5 cm ballast), where less flow restrictions ($\epsilon = 0.33$) led to higher local pressures.

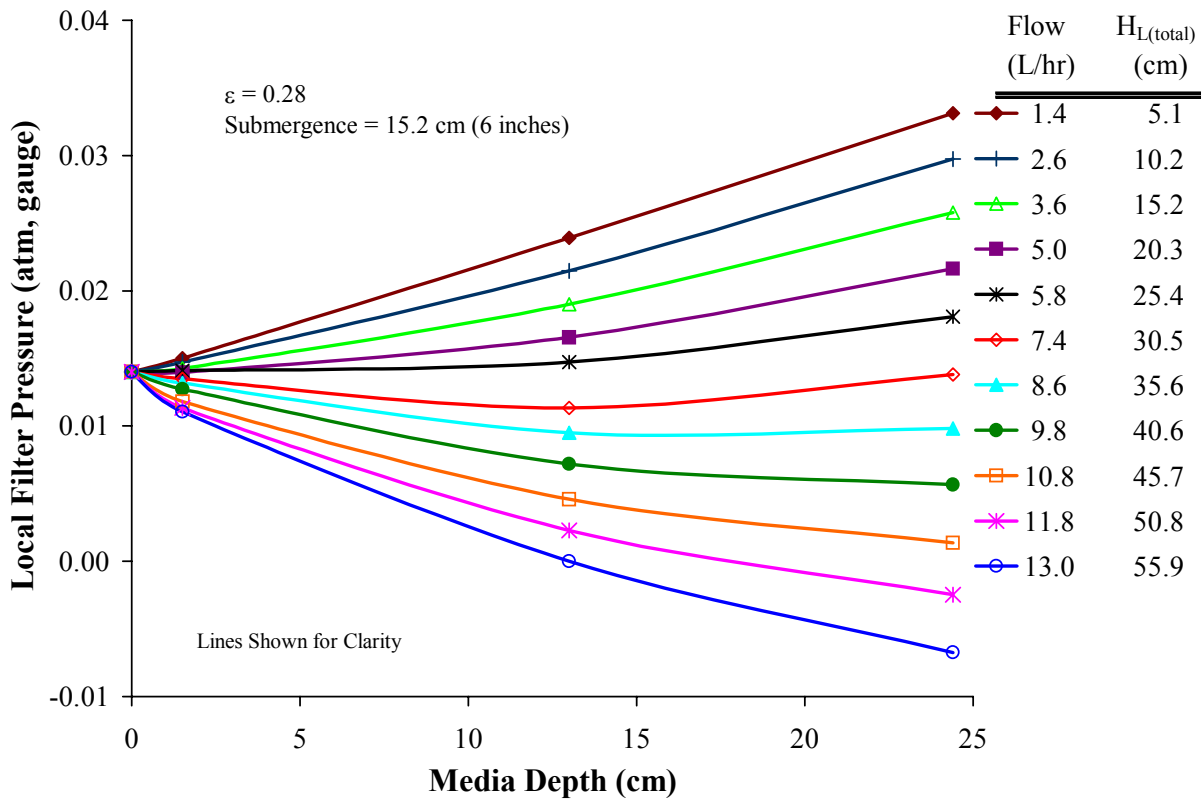


Figure 1.2 – Predicted Pressure Profiles at Depth for the Clean Bed Benchscale Filter using the Energy Equation (Equation 1.2) and the Measured Headloss for a Given Flow Rate.

actual/predicted pressure profile through the filter bed and hypothetical levels of influent dissolved gas concentration (Figure 1.3):

- Scenario 1: The lowest pressure within the filter is greater than the influent dissolved gas pressure, so bubbles cannot grow at any point.
- Scenario 2: The highest pressure in the filter is less than the influent dissolved gas pressure in the influent, so bubbles can form throughout the entire filter bed depth.
- Scenario 3: The water is supersaturated with gas at the top of the bed relative to hydraulic pressure profile (0.022 atmospheres dissolved gas versus hydraulic profile of experiment 10 in Figure 1.3) but not at the bottom, so bubbles grow only in the top of the filter bed.
- Scenario 4: The water is supersaturated with gas at the bottom of the bed but not at the top (0.013 atm of dissolved gas versus hydraulic profile in experiment 7 in Figure 1.3), so bubbles can grow only at the bottom of the filter.

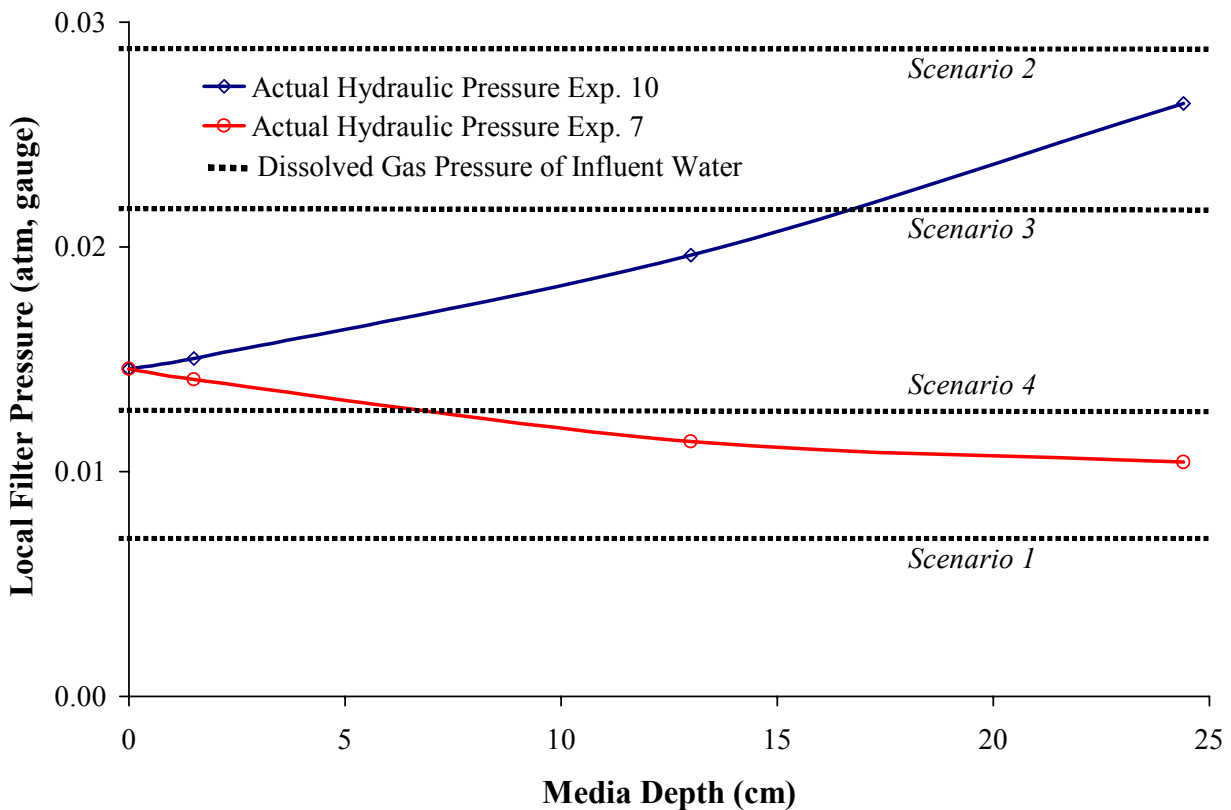


Figure 1.3 – Scenarios for Bubble Formation Using Predicted Pressure Profiles Calculated by the Energy Equation (Equation 1.2) through the Clean Bed Filter of Two Experiments.

In some circumstances, decreasing the initial flow rate would shift a clean filter from a situation favoring bubble growth at depth (Scenario 4) to no bubble growth (Scenario 1), potentially eliminating air binding problems at the expense of lower water production rates. Thus, there can also be a critical flow rate below which air binding will not occur in a filter, although if the influent is highly supersaturated with dissolved gas it might not be possible to reduce flow rates far enough to avoid supersaturation at the top of the bed.

Since the clean bed hydraulic pressure profiles are relatively easy to obtain and interpret relative to the measured influent dissolved gas pressure, it was instructive to retroactively consider each profile for the range of filtration experiments conducted (Figure 1.4). For a given flow rate, a lower media porosity had higher headloss with depth, which altered the pressure profile in the clean bed (e.g., Experiment 1 versus 7 in Figure 1.4). From this perspective, a higher porosity media is expected to be less susceptible to air binding problems if all other factors are equal. This is another reason why it might be possible to produce more water with a higher porosity media, in addition to a greater interstitial volume available for trapping particles.

Increasing the filter submergence (depth of water above filter) adds a constant amount of pressure throughout the depth of the filter (Experiments 1 versus 2 and 6 versus 7 in Figure 1.4). In fact, for a given flow rate and influent dissolved gas level, if submergence is increased above a critical level, the TDG pressure of the water in the filter can become undersaturated relative to the local pressure in the filter (Scenario 1). For instance, the point of minimum pressure in the filter for experiment 1 and 2 occurred at the top of the bed. The 15.2 cm of submergence in experiment 1 would maintain undersaturation throughout the bed if the influent contained less than 0.015 atm gauge pressure of dissolved gas. However, increasing the submergence to 76.2 cm in experiment 2 would maintain undersaturation throughout the bed for water containing up to 0.073 atm gauge pressure of dissolved gas. In this case, a filter highly susceptible to air binding could be made immune to such problems if operation was possible with a higher submergence (shifting to Scenario 1). Likewise, in constant flow filtration where submergence increases during a filter run, some problems with bubble formation in the media might be lessened or even reversed as the run progresses.

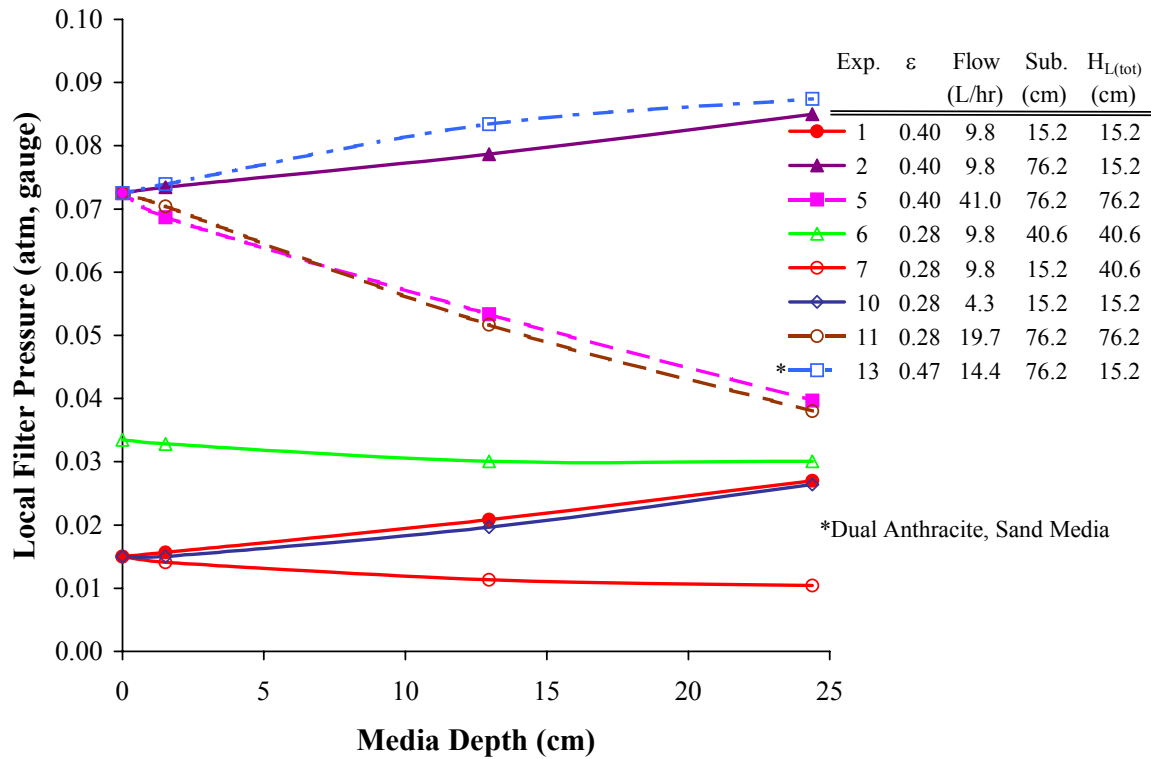


Figure 1.4 – Predicted Filter Pressure Profile Calculated by the Energy Equation (Equation 1.2) of Clean Bed Filters for Various Experiments.

Experimental Confirmation of Predicted Trends in Air Binding

Experiments (Table 1.1) were conducted with variable filter pressure profiles as per Figure 1.4 and influent dissolved gas pressures to examine the phenomenon of air binding. Since most experiments were at a constant submergence, any headloss development would decrease the effluent flow rate (declining flow rate operation). Over the first 80 hours of the filter run in cases satisfying Scenario 1 (experiment 3 and 4) for which bubbles are not predicted to form at any depth of the filter, only very small reductions (< 10%) in flow rate were noted when treating a water to which no particulate matter was added (Figure 1.5). However, under the same flow conditions with a supersaturated influent at 0.1 atm gauge pressure, Scenario 2 was imposed on the system (experiment 1 and 2), in which bubble formation was possible at all depths of the filter, and the flow rate was reduced by about 50% over the same time period.

When the submergence was increased from 15.2 cm (experiment 1) to 76.2 cm (experiment 2) and flow was unchanged, the flow declined at a slightly lower rate (Figure 1.5). With the higher submergence, the minimum 0.073 atm gauge pressure (located at the top of the

media) was initially anticipated to produce a much greater benefit compared to the 0.015 atm gauge pressure at the lower submergence (Figure 1.4), but this did not significantly occur with an influent of 0.1 atm gauge pressure.

When the media porosity was decreased ($\epsilon = 0.28$) and all other factors remained the same (Figure 1.6), flow through the filter decreased at a more rapid rate, as was predicted previously (i.e., Figure 1.4). A 50% reduction of the initial 9.8 L/hr flow occurred in only 19 hours with the lower porosity media (experiment 7 in Figure 1.6), compared to 59 hours for the higher porosity media ($\epsilon = 0.40$) (experiment 1 in Figure 1.5). At the lower porosity, increasing the submergence seemed to have a more significant role in reducing air binding impacts. While a 15 versus 40 cm submergence (experiments 7 vs. 6, respectively) produced similar trends, a 76 cm submergence (experiment 8) approximately doubled the run time. Maintaining this same submergence but lowering the effluent outlet to 76 cm below the water surface (experiment 9) required partially closing an effluent valve to mimic the flow rate (9.8 L/hr) and total headloss (40.6 cm) of experiment 8. As might be expected, filter performance and susceptibility to bubble growth (experiment 8 versus 9) was not significantly different if headloss was controlled by the height of the effluent outlet or an effluent valve, because the pressure profiles in the filters were identical—although extensive bubble formation was observed at the partially closed valve toward the end of the run, which may have produced additional flow restrictions (Figure 1.6).

After 84 hours in experiment 6, the flow rate had dropped to approximately 17% of the initial flow. It was deemed of interest to determine if bubble induced headlosses could be at least partly reversed if the dissolved gas pressure in the influent water was reduced. To accomplish this, a degassed water was created by boiling and then cooling to 20 °C, leading to a solution with very little dissolved gas (approximately 0 atm absolute pressure). When this water was applied to the filter, gas bubbles gradually disappeared, and the flow rate was restored to 83% of its initial value after 21 hours (Figure 1.6). Although this exercise would not be practical for a water utility, diurnal water quality changes, where the source water becomes undersaturated with dissolved gas, could partially re-dissolved some of the formed gas bubbles. Furthermore, backwash sequencing could be modified to maximize filter run length. For example, if a filter was operated when the influent was both supersaturated and undersaturated with dissolved gas, then some of the bubble induced headloss could be potentially reduced when the influent was undersaturated with dissolved gas, thereby extending the filter run.

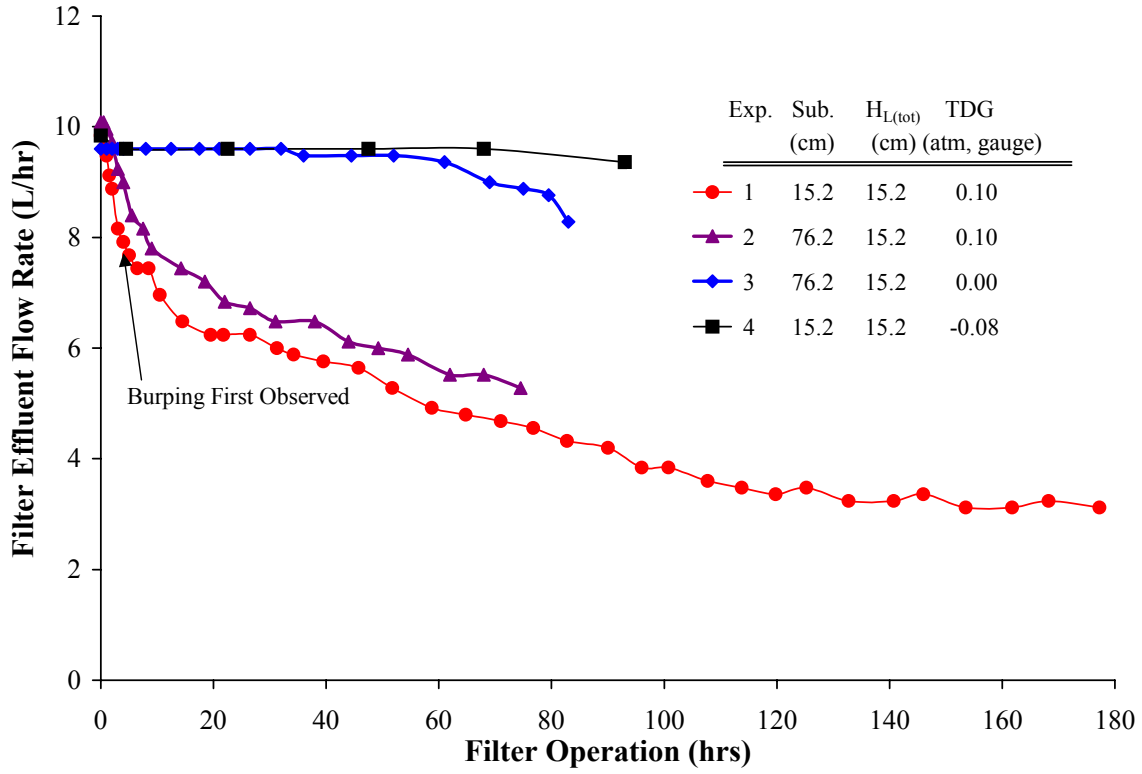


Figure 1.5 – High Porosity ($\epsilon = 0.40$) Filtration Experiments.

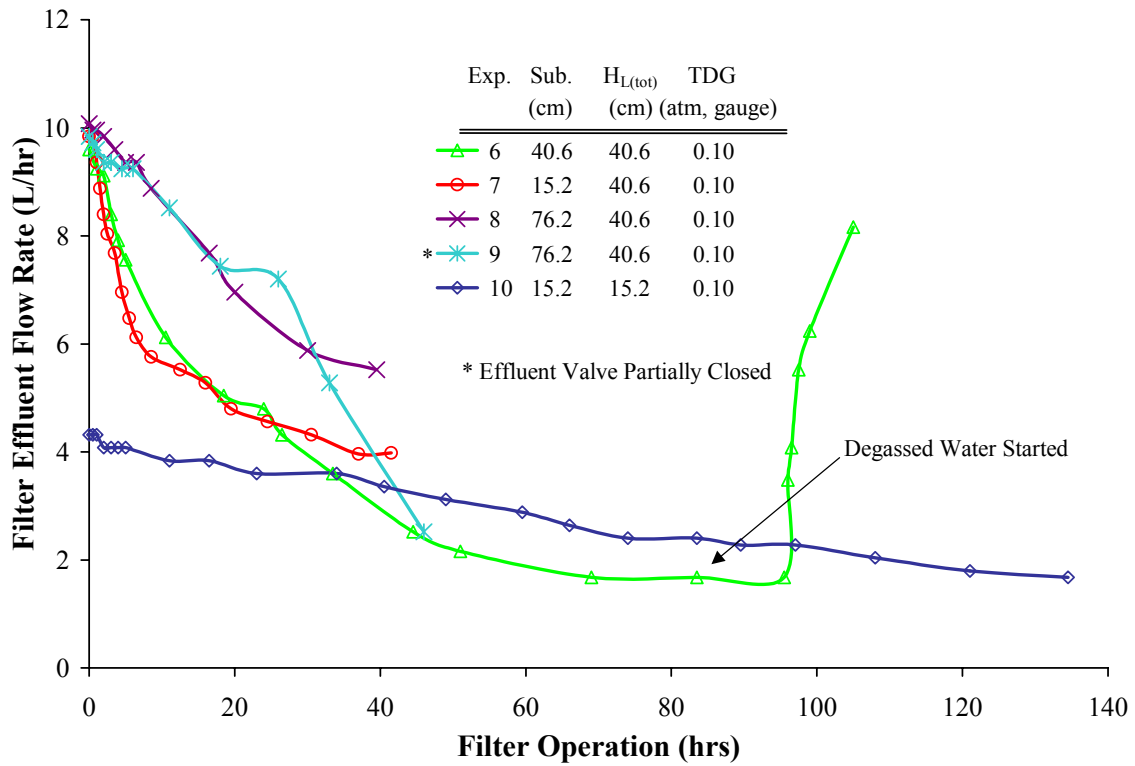


Figure 1.6 – Low Porosity ($\epsilon = 0.28$) Filtration Experiments.

Bubble Behavior within the Filter during Runs

The filter clean bed pressure profiles allowed predictions as to the location of bubble formation in the filter based on equilibrium. However, dissolved gas mass transfer to gas bubbles (degassing) is also very important, and the rate of degassing depends on many factors including the flow rate, the difference between influent dissolved gas pressure and the local solution pressure, the total surface area of bubbles within the bed, and the presence of nucleation sites (Scardina and Edwards, 2001; Harvey, 1975). There was little degassing in the early phases of filter runs, since the effluent TDG pressures were essentially the same as the influent TDG (Figure 1.7, top). This also confirms that the loss of gases at the top of the filter to the atmosphere (gas transfer across the air-water interface) was relatively low. Yet, the effluent TDG typically decreased steadily throughout the run as more degassing (bubble formation) occurred within the filter, which would be expected since flow rate typically decreased (greater time for mass transfer) and more gas bubbles would be present (additional surface area for mass transfer) (Figure 1.7, top). The oscillatory nature of the effluent TDG usually mimicked the influent TDG, such that a lower influent TDG corresponded to a lower measured effluent TDG.

In one filter run (experiment 2) this had important implications from the perspective of dissolved gas supersaturation as a function of column depth. In the beginning of experiment 2, the water was supersaturated at all depths of the filter, and as the run progressed, effluent concentrations of dissolved gas had decreased to the point where the water was supersaturated only in the top portions of the bed (Figure 1.7, bottom). If a system could be designed where all of the bubbles formed in the very top layer of a filter, then bubble formation may not occur throughout the filter. The bubbles in the top layer could then potentially be released naturally or by physical agitation. In all other experiments, while degassing occurred, the water still remained supersaturated throughout the entire filter bed depth.

Bubble dynamics within the filter also exerted important controls on the rate of headloss buildup. Early in the run of experiments 1 and 2, bubbles were visually present on top of the sand media after 30–60 minutes of run time, consistent with the prediction that this was the point of minimum pressure in the filter under this set of flow conditions (Figure 1.4). As the run progressed, bubbles were observed to form within the media, just below the top of the media. Further bubble growth was observed to physically displace the media, and after the bubbles reached a size of approximately 1 cm, the buoyant forces were such that the bubbles were

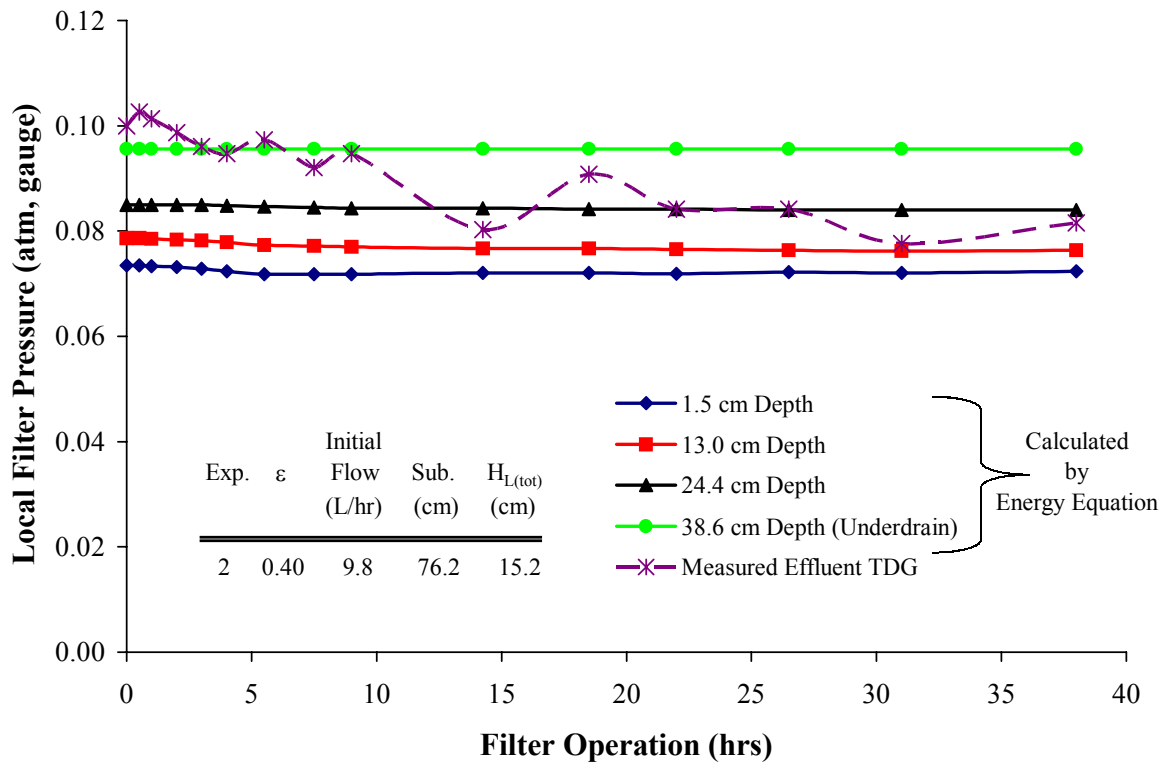
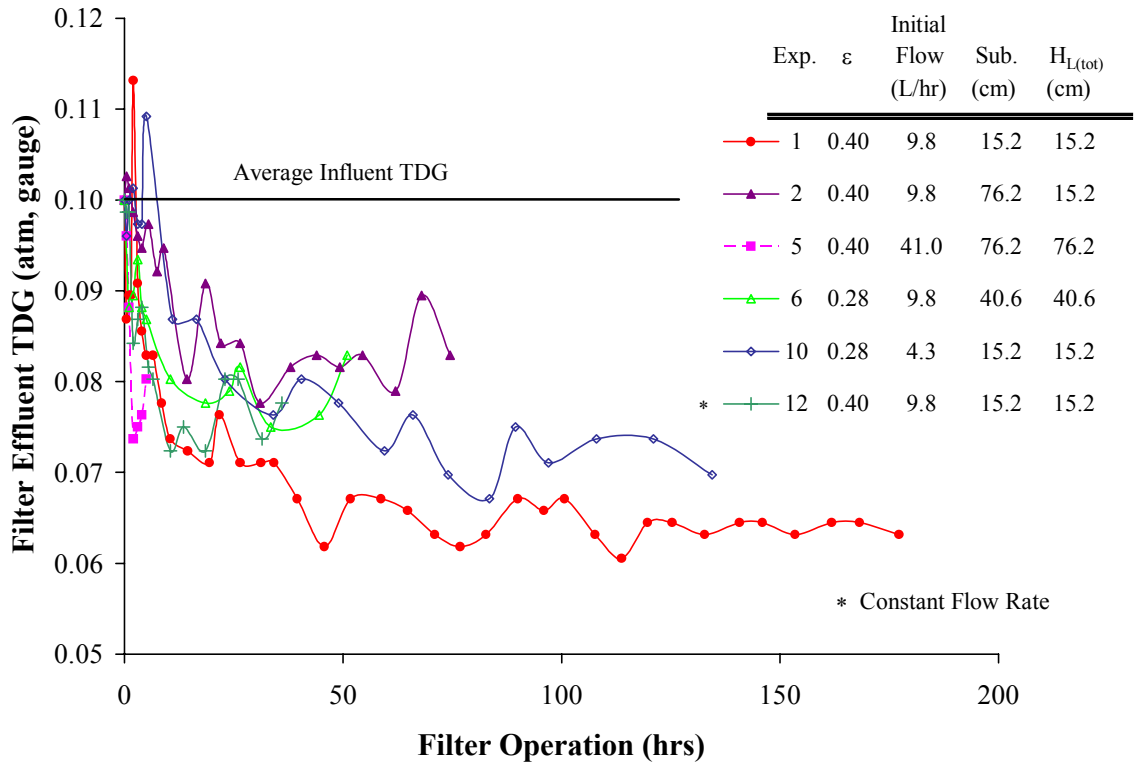


Figure 1.7 – Effluent Total Dissolved Gas (TDG) Profiles (Top), and Change in Supersaturation with Depth during Experiment 2 (Bottom).

released from within the media to the water surface. This disruption occasionally triggered release of several other bubbles located nearby in the filter as a “burp.” Burping was observed in all benchscale experiments. The onset of burping correlated to when the flow rate began to noticeably asymptote towards a constant value, since burping could be beneficial by alleviating at least part of the bubble induced flow restrictions (headloss in the media) (Figure 1.5). Some sand grains remained attached to the bubbles as they floated to the water surface above the filter. Yet, burping could also cause larger pathways in the media where pathogens could escape to the finish water, and burping from a upflow clarifier configuration would transport previously trapped turbidity and pathogens back into the system.

Gas bubbles were also observed to form in the underdrain in all experiments except experiment 2, which is the one run where the water became undersaturated with gas at depth in the filter (Figure 1.7, bottom). However, even in experiment 2, one bubble formed after 22 hours of operation in the bottom of the sand media (1 cm above the top of the underdrain where the calculated local filter pressure was approximately 0.088 atm gauge pressure) and traveled downwards in the bed until it reached the top of the underdrain where it remained until the end of the test. Thus, bubbles can be hydraulically pushed downwards in the bed by drag forces or rise upwards due to burping or buoyant forces.

These general observations are strongly supported by filter weight loss measurements, which provide insight to the cumulative volume of bubbles captured in the filter during the run (Figure 1.8, top). For all experiments, the rate of bubble formation (increasing or changing bubble volume per changing time) was higher at the beginning of the experiments (steeper slope within the first 10 hrs of operation in Figure 1.8, top), and this observed rate decreased after the onset of burping. Since the rate of bubble formation eventually stabilized at a constant value, the system reached a steady-state with respect to newly formed bubbles and burping (Figure 1.8).

In addition, as described previously, the volume of bubbles forming in the filter bed could also be estimated with a modified closed system equilibrium model by measuring the influent and effluent TDG and assuming that any degassing from the water went to bubble growth (Scardina and Edwards, 2001). In the early phases of the filter run, the calculated volume of bubbles based upon TDG measurements correlated well to measurements of weight loss in the filter (Figure 1.8, bottom). When burping started to occur, a portion of the gas that had formed in the filter was released to the water surface (atmosphere) and no longer contributed to

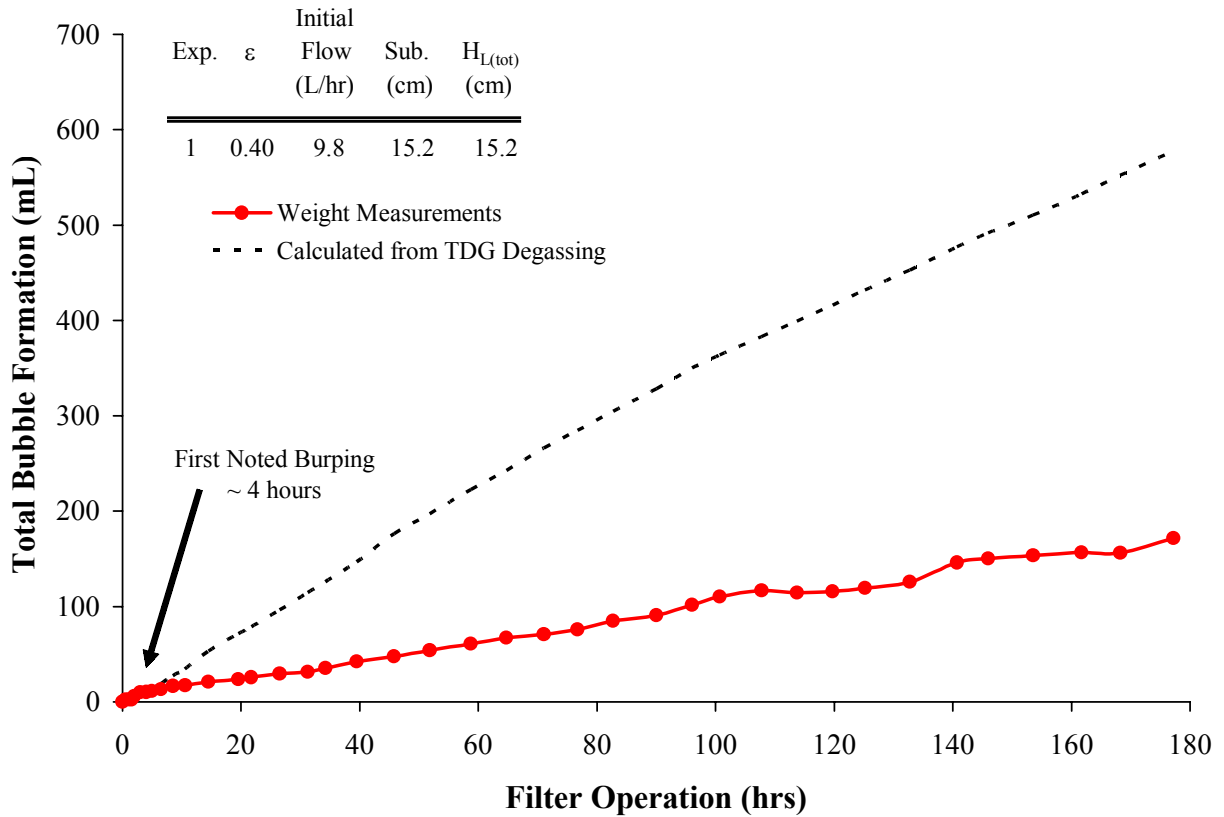
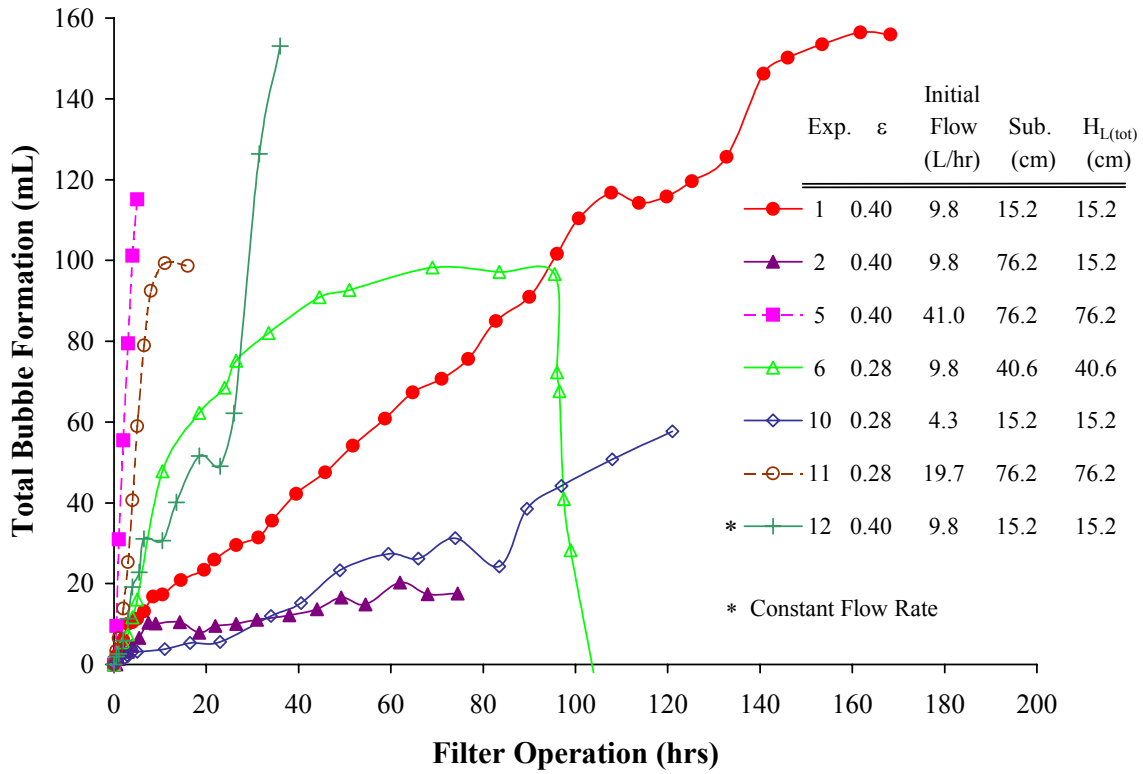


Figure 1.8 – Volume of Bubbles Trapped in the Filter Based on Weight Loss Measurements (Top), and the Comparison of Degassing from Solution to that Trapped in the Filter (Bottom).

decreasing filter weight (Figure 1.8, bottom). By the end of experiment 1, it is estimated that the total volume of gas bubbles degassed within the filter over the entire length of this experiment was 580 mL, but most of this headloss was actually burped to the atmosphere, since the measured volume of trapped bubbles was only 170 mL.

To better describe this phenomenon, a term “retention ratio” was defined as the ratio between the actual bubble volume trapped in the filter versus the total amount of degassing calculated from TDG measurements, for a given filter operation time:

$$\text{Retention Ratio} = \frac{(\text{Bubble Volume in Filter})_{\text{Weight Measurements}}_{(\text{Time} = t)}}{(\text{Total Bubble Volume})_{\text{TDG Measurements}}_{(\text{Time} = t)}}. \quad (\text{Equation 1.4})$$

If the gas retention ratio was 1, the volume rate of degassing (calculated from TDG measurements) would be equal to the rate at which bubbles volume increased in the filter (weight measurements), and losses due to burping would be insignificant. If the gas retention ratio was 0, then none of the degassed bubbles would be retained in the filter, since all would be lost from burping. Although there was considerable variation in the retention ratio due to irregular burping, the retention ratio started near 1 in experiment 1 and approached a lower value of 0.3 (Figure 1.9, top). At this point, the filter has reached a steady-state with respect to newly formed bubbles and burping, as described previously.

An average gas retention ratio was calculated for four runs at different flow rates for data collected after the onset of burping but well before steady state (Figure 1.9, bottom). As flow rate and interstitial velocity increased, the retention ratio increased as well. Since bubble release must be governed by some balancing of drag versus buoyant forces, greater downward forces on the bubbles at higher velocities might be acting to prevent burping, and it is also possible that the higher flow can physically drive (push) bubbles further into the media as observed previously. This was evident also in experiments 1 and 6. Although both experiments had the same flow rate, more bubbles were retained in the lower porosity media (higher interstitial velocity) (experiment 6 in Figure 1.9, top). In addition, bubble formation would be expected at greater media depths with higher flow or lower porosities, as indicated by the filter pressure profiles (Figure 1.4). The net result was that filter air binding was much worse at higher flow rates or higher interstitial velocities (lower porosities). In general, this was related to a greater degassing

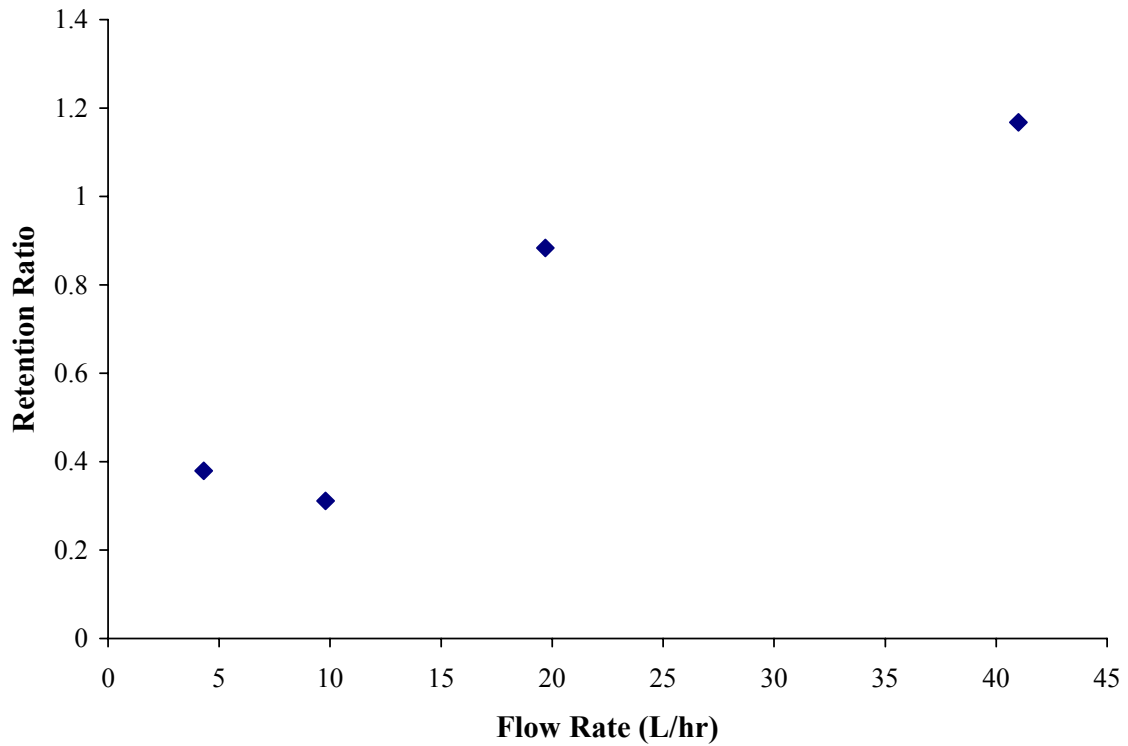
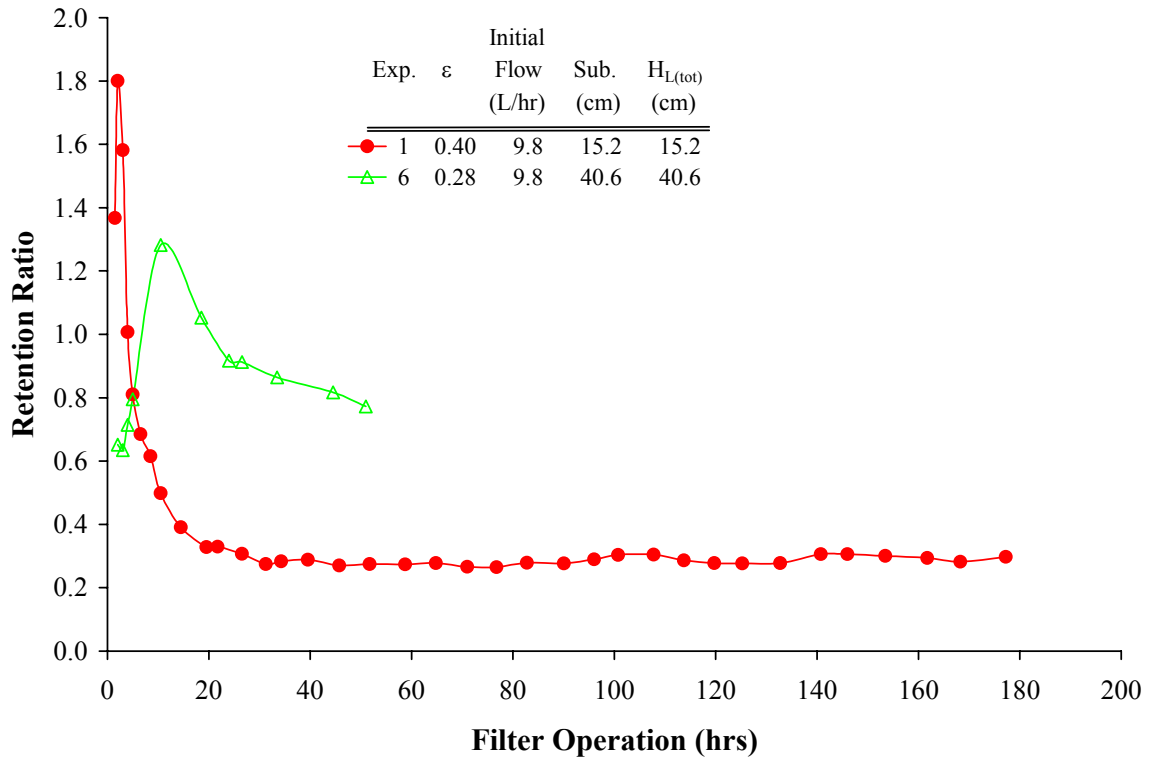


Figure 1.9 – Retention Ratio (Equation 1.4) during Two Filter Runs (Top), and the Average Retention Ratio (Equation 1.4) as a Function of Flow Rate (Bottom).

per volume of water treated and much more effective retention of bubbles within the media at higher flow rates.

Furthermore, considered from the perspective of total water production before backwashing, air binding phenomena also have important impacts (Figure 1.10). While runs were not extended to the point where clear conclusions can be drawn, it appeared that the greater water production early in a run at higher flow rates could lead to more air binding problems and less total production. Future work should examine this possibility for the higher levels of supersaturation that we have encountered in practice (up to 0.2 atm gauge pressure).

Implications for Filter Operation

The previous results have implications for selection of slow sand, dual media, and the mode of filter operation. At extremes of low flow, filter pressure will always increase with depth. If the water could also completely equilibrate with dissolved gas at the very top of the bed by bubble formation, the retention ratio could be near 0, since bubbles are released very easily in the top of the bed and the water would be undersaturated throughout the filter depth.

As mentioned earlier, constant flow versus constant head modes of filter operation are also controlling factors in air binding. For the constant flow run (experiment 12), the average retention ratio was approximately 0.90, which was close to that obtained during declining flow experiments with higher initial flow rates. As bubbles formed during the constant flow experiment, the average interstitial velocity in the bed at the end of the run had increased to 1.7 cm/s based on interstitial space not occupied by bubbles, which was similar to the higher flow experiments (2.1 and 1.5 cm/s for experiments 5 and 11, respectively). It is, therefore, not surprising that significantly more bubbles were retained in the filter media during the constant flow mode than in equivalent experiments with declining flow (Experiments 1 versus 12 in Figure 1.8, top). The increasing submergence during the constant flow experiment increased the local filter pressure, but the influent dissolved gas pressure always exceeded the local pressure at all depths of the filter (Scenario 2 in Figure 1.3). Thus, in this experiment the higher submergence during the run was not expected to reverse bubble formation, although it could in practice if the local filter pressure exceeded the TDG pressure.

The analysis of an anthracite and sand dual media is of interest since many utilities operate these filters, and it was anticipated that the higher porosity, lower density, and more

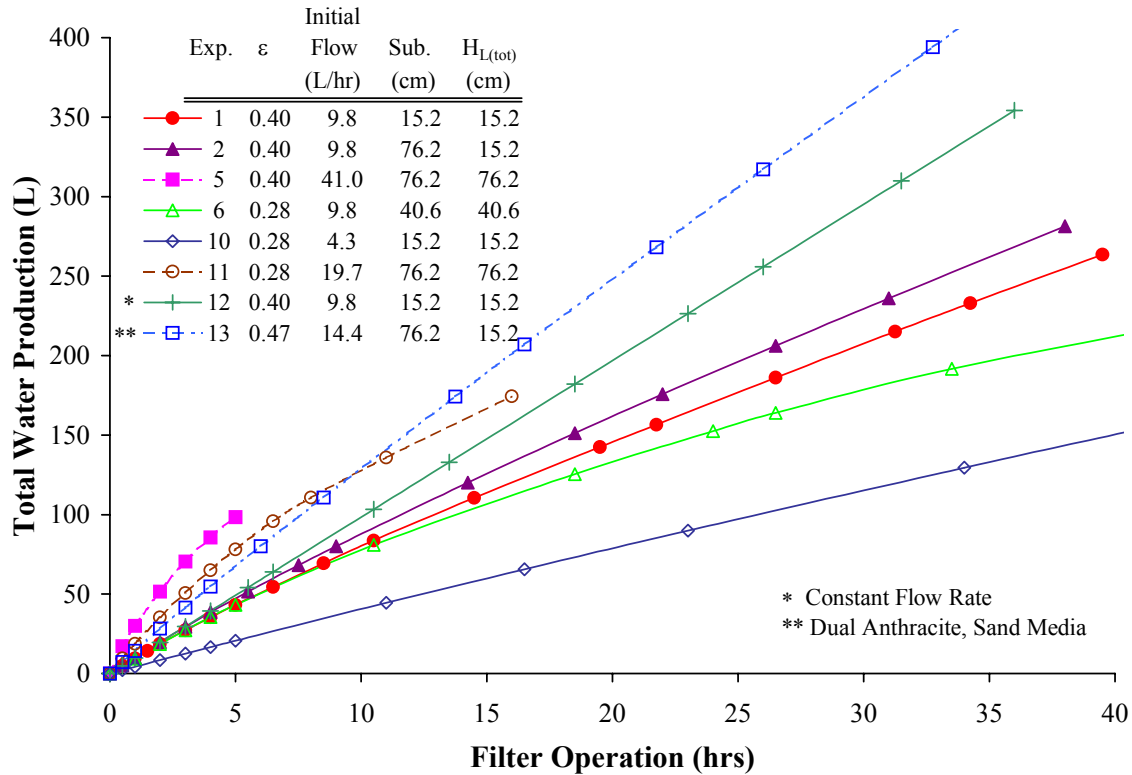


Figure 1.10 – Total Water Production for Various Experimental Conditions.

hydrophobic anthracite top layer could fundamentally alter bubble formation (Ryan and Hemmingsen, 1998). To test this idea, 50% of the original sand media was replaced with a 15.2 cm depth anthracite top layer, and all other experimental conditions were similar to experiment 2 (Table 1.1). Less headloss occurred within the anthracite media ($\epsilon = 0.47$ for the anthracite compared to $\epsilon = 0.40$ for the sand media), corresponding to a higher initial flow rate and higher local filter pressures (Figure 1.4) compared to the mono media system (experiment 2).

With the anthracite present, bubbles became visible more quickly and were more numerous when compared to the equivalent mono media run (experiment 2), which might indicate enhanced bubble nucleation due to anthracite's hydrophobicity. If any factors caused an existing filter media to become more hydrophobic, such as the sorption of organic compounds, then more bubbles may nucleate/form on the media. Estimates of total bubble formation within the filter from TDG measurements confirmed that more bubbles were forming in the dual media filter; however, overall weight loss indicated that burping was very effective at releasing the

bubbles from this top layer (Figure 1.11). It is speculated that the lower density and larger pore size of the anthracite contributed to easier release of the trapped gas.

The effluent TDG measurements from the dual media filter also indicated an interesting trend. The amount of degassing in the filter increased at the beginning of the run but then rapidly decreased after 9 hours of operation, since the effluent TDG eventually approximately equaled the influent TDG (Figure 1.12, top). This was contrary to all other experiments, where the amount of degassing (influent TDG – effluent TDG) either continually increased or stabilized at a constant value (i.e. experiment 2 in Figure 1.12, top).

Differences in mass transfer could potentially explain the degassing in these experiments. The average detention time of water in the anthracite layer (15.2 cm depth) was estimated using the flow rate, a calculated media porosity based upon the volume of bubbles trapped in the filter from weight loss data, and the assumption that bubbles occupied voids only in the anthracite layer. For comparison, the average detention time was also estimated in the mono media filter (experiment 2), assuming that bubbles predominantly only formed in the top 15.2 cm of the

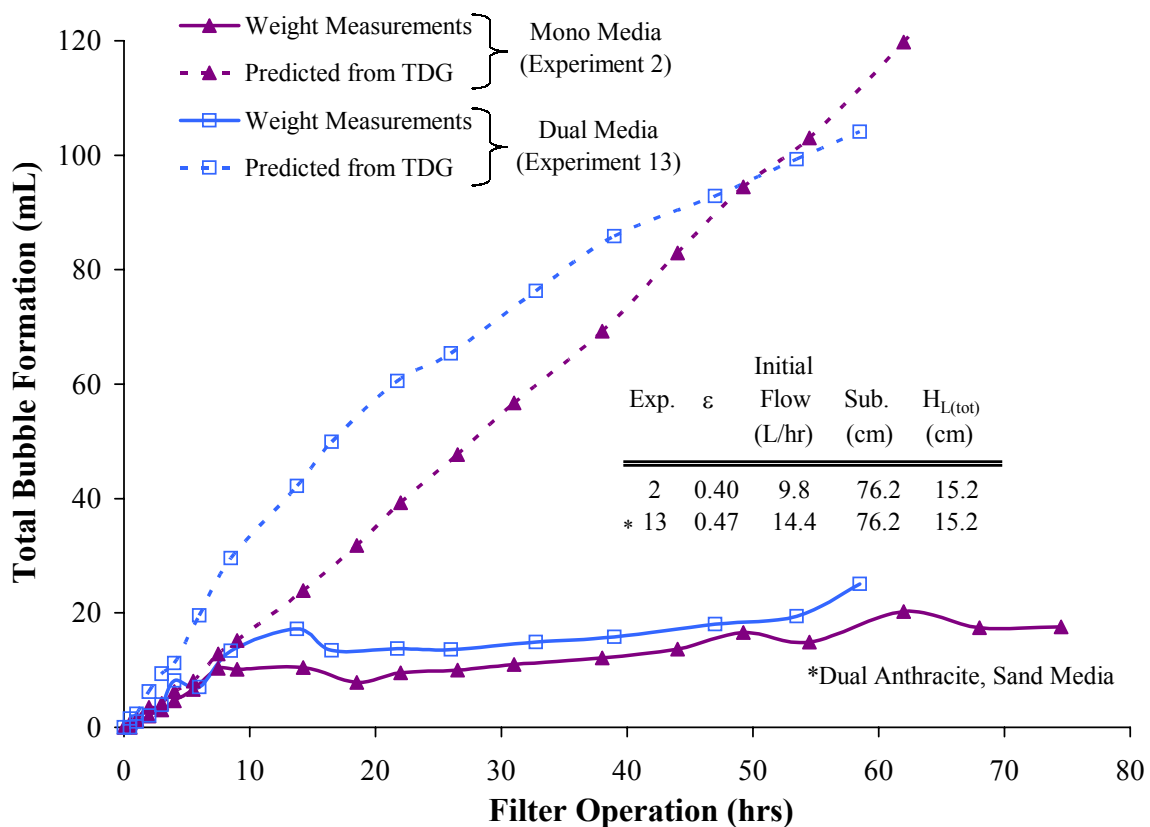


Figure 1.11 – Comparison of Bubble Formation on Dual and Mono Media Filters.

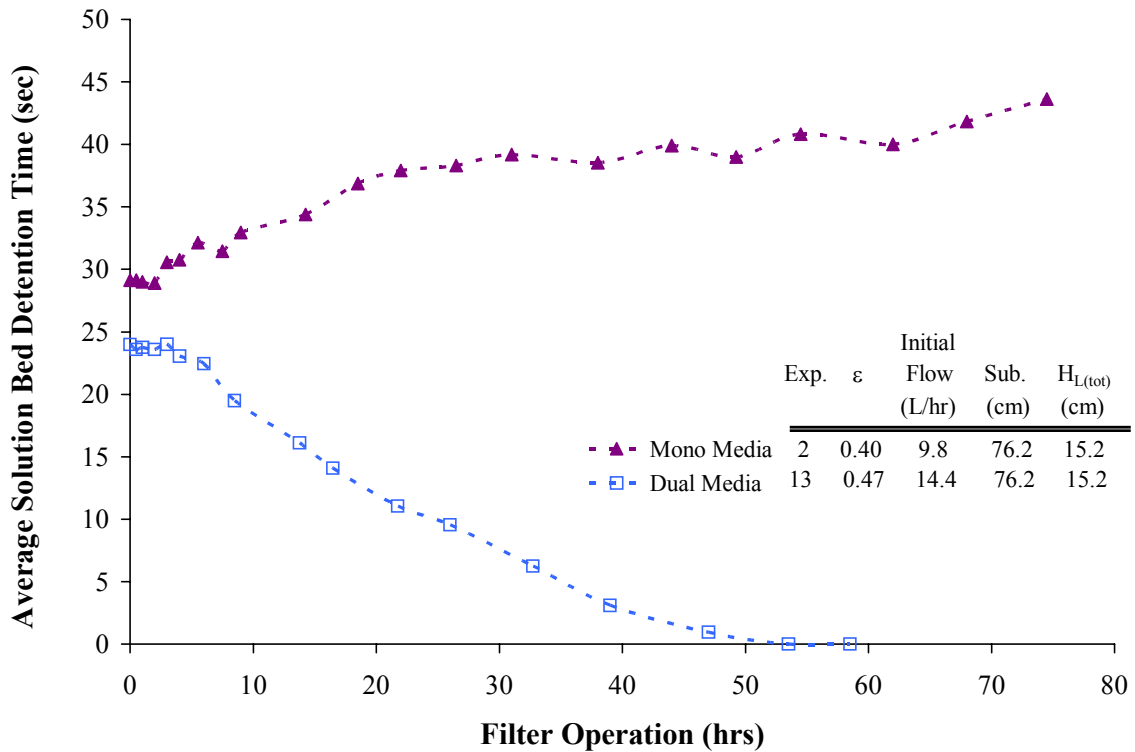
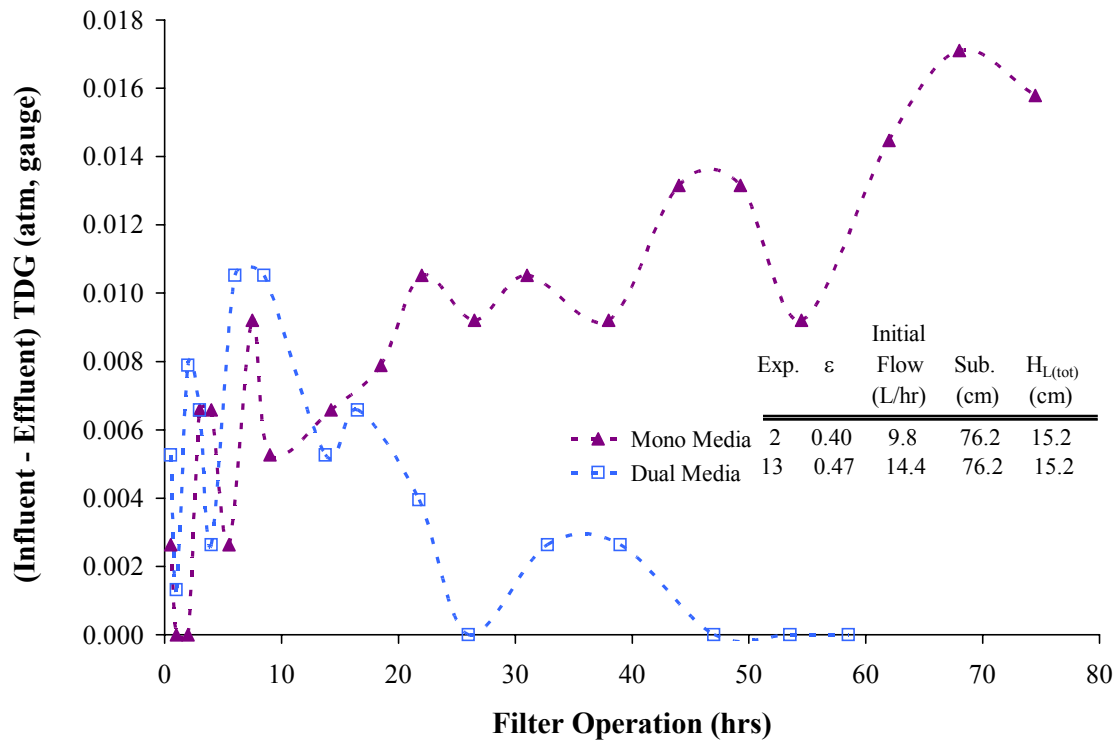


Figure 1.12 – Amount of Degassing in the Filter (Difference between the Influent and Effluent TDG) (Top) and Average Detention Time (Dt) through the Top 15.2 cm of Media (Bottom) for Mono and Dual Media Experiments.

media (i.e. Figure 1.7, bottom). While the detention time through the mono media filter increased during the experiment, the detention time of water in the anthracite layer decreased dramatically to where there was insufficient time for the water to degas, despite the presence of extensive bubble surface area for gas transfer (Figure 1.12, bottom). In fact, the calculated porosity in the anthracite layer at the end of the experiment was less than 0.1, suggesting that most of the pore space was filled with bubbles. Having the anthracite layer, therefore, caused most of the bubble formation in the top of the filter rather than throughout the whole media depth, with the additional benefit of reduced degassing at extended run times. We note that while the anthracite layer greatly increased water production (Figure 1.10) and decreased headlosses (more burping), the lowered detention time might reduce particle removal efficiency in practice. This should be addressed in future research.

Other Influential Factors: Atmospheric Pressure and Interstitial Velocity

Several other important phenomena might contribute significantly to bubble formation during filter runs, including changing barometric pressure and interstitial velocities. With respect to barometric pressure, a slight but significant decrease in flow rate was observed at the end of the control experiment 3 for which the water was initially undersaturated throughout the filter depth (Figure 1.5). Retrospective examination of local weather records indicated that the barometric pressure rapidly dropped toward the end of this filter run from about 0.943 to 0.932 atm absolute pressure due to a passing weather storm. This change probably caused the water, which was initially at equilibrium with the atmosphere at the start of the run (after aeration), to become supersaturated by about 0.011 atm gauge pressure. Although the pressure profile for experiment 3 (experiment 2) in Figure 1.4 suggests that gas dissolution should not have occurred at this level of supersaturation, TDG measurements at the final sampling time seemed to confirm a very slight removal of gas from the water, although the difference of 0.0026 atm gauge pressure was the detection limit. This sensitivity to external atmospheric pressure was unanticipated, and it illustrates the larger complexity of air binding in relation to external environmental factors.

It could also be speculated, that significant temperature changes could affect filter air binding. For example, a colder water that warms within a treatment plant during the winter could potentially become supersaturated with dissolved gas as a result of warming, consequently

inducing bubble formation. As described by Henry’s gas law constants, a water at equilibrium can hold less dissolved gas at higher solution temperatures. A given quantity of dissolved gas, therefore, would impose a higher dissolved gas pressure at higher solution temperatures, which could eventually lead to dissolved gas supersaturation with respect to the local solution pressure within a filter.

Lastly, although the preliminary calculations suggested that the velocity component did not significantly impact the local solution pressure (Table 1.2), the maximum interstitial velocity must have been increasing markedly during some runs. For example, at the end of experiment 1, 78% of the total pore space including the underdrain was occupied by bubbles. Therefore, the average interstitial velocity had to increase by at least a factor of 1.4 during the run based on the final flow rate of 3.1 L/hr. Considering that bubbles were not distributed uniformly with depth, maximum velocity in the column could have been much higher than twice the average velocity, which could be compounded by particle deposition in real filters.

Classical cavitation theory considered bubbles forming from water vapor (vaporous cavitation), and increasing interstitial velocities could not induce vaporous cavitation in these experiments. However, a review of the literature has revealed that dissolved gases have also been considered as composition in “gaseous” cavitation. In other words, whenever gases are dissolved in water, the phenomenon of gaseous cavitation can occur at certain critical velocities and local pressures as described by (Naylor and Millward, 1984):

$$O_{ci} = \frac{p_o - (p_v + p_c)}{0.5\rho V^2}, \quad (\text{Equation 1.5})$$

where O_{ci} is the cavitation inception number, p_o is the pressure at the point of concern, p_v is the vapor pressure of water, p_c is the “correction pressure” from dissolved gases, ρ is density, and V is velocity. With 1 atm absolute pressure TDG (0 atm gauge pressure) in water, p_c in the above equation was determined to be 0.61 atm by Naylor and Millward (1984). The net result is that gaseous cavitation can occur in water at equilibrium with the atmosphere (0 atm gauge pressure) at much lower flow rates than is possible for completely degassed water. For instance, at a water flow rate of 3 m/sec, room temperature, and 0 atm gauge pressure, Naylor and Millward (1984) readily observed bubbles from gaseous cavitation in flow experiments even at 0.3 atm local gauge pressure. Although many systems, including hydraulic pumps or filters, are designed to

prevent negative gauge pressures (vaporous cavitation), the Naylor and Millward (1984) study indicate that cavitation can still be problematic, since gaseous cavitation could occur at even low flow rates with water supersaturated with dissolved gas. This issue is also deserving of more study.

SUMMARY AND CONCLUSIONS:

- Bubble formation (air binding) can occur within a filter at points where the total dissolved gas (TDG) pressure exceeds the local pressure within the filter.
- Factors that affect the local pressure profile through a clean bed filter include flow rate, submergence, porosity, and the mode of operation. When the filter pressure profile increases with depth, bubble formation will be more likely in the upper part of the filter, and when the pressure within the filter decreases with depth, bubble formation will be more likely in the lower part of the filter.
- The locations within the filter where degassing is possible can change by modifying a filter pressure profile, the extent of degassing (bubble formation) from water as it passes through the filter, and the presence of particles in the water.
- Trapped bubbles can be released upwards from the media in a burping phenomenon, and bubbles can also be pushed down within the media by fluid drag. Burping can partly alleviate the bubble induced headloss. If the run is continued long enough, a steady state situation is attained between the rate of newly formed bubbles and the rate of bubble (gas) release by burping.
- Burping was increased at lower flow rates and in filters with a higher porosity media. The net result is that filters with lower interstitial velocities could experience overall less air binding problems.
- A dual media filter with an anthracite top layer allows more degassing (bubble formation) and burping (bubble release) in the anthracite layer. The net result was greater water production with dual media in situations where the water was supersaturated with TDG. However, there is reason to speculate that these benefits might be achieved at the expense of reduced particle removal efficiencies.

ACKNOWLEDGMENTS:

This work was supported by the American Water Works Association Research Foundation (AWWARF) under grant 2821. The opinions, findings, conclusions, or recommendations are those of the writers and do not necessarily reflect the views of AWWARF.

REFERENCES:

Appleton, Davison, T. S., and Pearce, J. (2001). "Rapid Gravity Filter Modeling." *Advances in Rapid Granular Filtration in Water Treatment*. Conference Proceedings, The Chartered Institution of Water and Environmental Management, London, UK, pg 23-32.

Betterton, E.A. (1992). "Henry's Law Constants of Soluble and Moderately Soluble Organic Gases: Effects on Aqueous Phase Chemistry." *Gaseous Pollutants: Characterization and Cycling*, Edt. J.O. Nriagu, John Wiley and Sons, Inc, New York.

HACH Model 2100N Laboratory Turbidimeter Instruction Manual. (1997). HACH Company.

Harvey, H. H. (1975). "Gas Disease in Fishes—A Review." *Proc., Chemistry and Physics of Aqueous Gas Solutions., Electrothermics and Metallurgy and Industrial Electrolytic Divisions, Electrochemical Society*, Princeton, N.J., 450-485.

Head, R. and Shepherd, D. (2001). "Practical Experience of Using Rapid Gravity Filter Models to Improve Operational Performance at Water Treatment Works." *Advances in Rapid Granular Filtration in Water Treatment*. Conference Proceedings, The Chartered Institution of Water and Environmental Management, London, UK, pg 381-390.

O'Melia, C. R. and Ali, W. (1978). "The Role of Retained Particles in Deep Bed Filtration." *Progress in Water Technology*, Vol. 10, pg 167-187.

Naylor, F., and Millward, A. "A Method of Predicting the Effect of the Dissolved Gas Content of Water on Cavitation Inception." *Proc Instn Mech Engineers*, V. 198C, No 12 (1984).

Ryan, W. L. and Hemmingsen, E. A. (1998). "Bubble Formation at Porous Hydrophobic Surfaces." *J. of Colloid and Interface Science*, 197, 101-107.

Scardina, P. and Edwards, M. (2001). "Prediction and Measurement of Bubble Formation in Water Treatment." *Journal of Environmental Engineering*, Vol. 127, 11, pg 968.

Scardina, P. and Edwards, M. (2002). "Practical Implications of Bubble Formation in Conventional Treatment." *Journal American Water Works Association*, Vol. 94, 8, pg 85.

Stevenson, D. G. (2001). "Exploration of Variables in Granular Media Filtration Using the Filterflex Model." *Advances in Rapid Granular Filtration in Water Treatment*. Conference Proceedings, The Chartered Institution of Water and Environmental Management, London, UK, pg 1-10.

Water Quality and Treatment: A Handbook of Community Water Supplies. (1999). Ed., Letterman, R. D. McGraw Hill, Inc. (5th ed.).

Young, F. R. (1989). *Cavitation*. McGraw-Hill, London.

CHAPTER 2

INTERFERENCE TO PARTICLE COUNT AND ON-LINE TURBIDITY MEASUREMENTS FROM BUBBLE FORMATION

Paolo Scardina,¹ Raymond D. Letterman,² and Marc Edwards¹

¹Virginia Tech; 418 NEB; Blacksburg, VA 24061

²Syracuse University; 220 Hinds Hall; Syracuse, NY 13244-1190

ABSTRACT:

Particle count and on-line turbidity measurements are affected by bubble formation, and the water industry does not routinely employ methodology that will determine when bubbles cause spurious measurements. Bubbles were measured as particle counts in laboratory experiments and at a full-scale utility, and particle counts decreased when the pressure in the measurement cell was increased during sampling. For example, if a water was supersaturated with dissolved gas, particle counts were nearly 3 orders of magnitude higher when the sample was not pressurized, compared to the same measurement made at an applied pressure of 15 psi. Failure to account for these spurious signals can cause water treatment operators and researchers to draw faulty conclusions about efficiency of water treatment in removing particles. In laboratory experiments, spurious turbidity spikes, increasing turbidity, and gas accumulation in the measurement cell occurred in on-line turbidimeters. Instrument features such as electronic “bubble reject” and in-line bubble traps may reduce the effect of bubbles on the measured turbidity, but in some cases they make the situation worse.

INTRODUCTION:

The water industry relies on particle count and turbidity measurements to monitor the quality of treated water. In recent years effluent turbidity regulations have decreased to 0.3 NTU or lower, and utilities are striving for even better performance under the worthy goals established by the Partnership for Safe Water. Consequently, in many treatment plants operators now strive to meet filtered water turbidity goals of 0.1 NTU or even less. Since filtered water quality changes of 0.01 NTU would have been deemed insignificant a decade ago, the industry needs to better understand when such signals are valid and when they are not. That is, many plants are implementing expensive treatment changes to improve water quality based on the premise that

data from particle counters and turbidimeters is trustworthy at these low levels. If the data from these devices was questionable, it might cause water plant operators to implement the wrong operational change, engineers to select and install inferior treatment processes, and researchers to draw erroneous conclusions. Poor understanding of problems with turbidity and particle count measurements can directly compromise the integrity and economics of potable water treatment.

Most regulators and water industry professionals are familiar with the same limitations of turbidity and particle counting devices. The response of these instruments is known to vary with the size, type, and composition of the particle, particle concentration, and differences in instrument design. Even when researchers have measured aliquots of “standard” samples in the laboratory using different calibrated instruments, particle counts can vary by factor of 2-3 and turbidity can vary by 20-30% (Hart et al., 1992; Van Gelder et al., 1999). When filter effluent samples were collected from 3 different treatment plants and transported to a laboratory, total particle counts differed by a factor of 4 to 18 among 3 different types of instruments (Van Gelder et al., 1999). Although it is relatively unusual to cross check these devices in the field, a recent laboratory test compared on-line turbidimeters that were connected in series and found a variation between the instruments of 3 to 10 times (Slatts et al., 2003).

Despite these known issues of inconsistency, experienced scientists still generally believe that these devices are reasonable surrogates for counts of real particles, and it is commonly assumed that data from a given reputable instrument will give results that are at least qualitatively accurate. In other words, particle counts on a given sample might differ by a factor of 10 from one device to another, but if treatment A reduced particle counts by 25% relative to treatment B as measured by a single counter, then treatment A is usually assumed to be superior to treatment B.

In further considering quality assurance and quality control (QA/QC), we note that particle counters and turbidimeters are among the few standard analytical devices for which possible matrix effects are not explicitly tested. This is because all dilution water gives at least some turbidity or particle count signal, sometimes salts must be added to samples to allow for the analysis (i.e., electrical zone sensing), the devices only work within fairly narrow concentration ranges, and industry accepted standards are not even available for particle counters (e.g., Van Gelder et al., 1999; Lewis et al., 1992). Indeed, other than calibrating these instruments with calibration standards made from “particle-free“ dilution water, the only routine check on proper

instrument operation is to run sample blanks with particle-free water. *Standard Methods* recommends that particle count and size distribution data be discarded from all channels in which the sample blank measurement is more than 5% of the count for a sample of interest (APHA et al., 1998).

Furthermore, it is also extremely rare that quantitative or qualitative trends in real-world data from these devices are confirmed using independent methods. For instance, it is possible to capture particles on a filter, and then quantify and size the particles using a microscope (e.g., Hunt et al., 1997). The fact that such confirmation is not routinely done is not surprising, since even the concentration of particles in calibration standards are determined only by other particle counters and are not confirmed by independent methods (Van Gelder et al., 1999). It is fairly commonplace to compare trends between data from particle counters and turbidimeters, and it is believed by some that these methods are somewhat independent. A few studies have even directly compared the usefulness of particle counters and turbidimeters as a surrogate for cryptosporidium cyst removal (Logsdon et al., 1985; LeChevallier and Norton, 1992).

In summary, the water industry depends on valid particle counting and turbidity measurements, and the turbidity measurement is explicitly used in regulations. If the signal from these instruments was dependent on the water chemistry of the sample, it would be problematic since the industry does not routinely implement QA/QC checks for matrix effects.

INTERFERENCES FROM GAS BUBBLES:

Standard Methods recognizes that bubbles can be a potential interference in all types of particle count and turbidity measurements (APHA et al., 1998). In fact, particle counters have been used to determine bubble size distributions in aerated water (i.e., Han *et al.*, 2002). However, QA/QC procedures that explicitly test for bubble interference in real samples are not available. Instead, for particle counters, *Standard Methods* (1998) states “Samples measured at different temperature or pressure than when collected and those with biological activity may develop entrained air bubbles that interfere with measurement accuracy. If any gas bubbles are visible, let sample stand for a short time to degas naturally or use a mild vacuum to speed degassing.” Even if bubbles were visible in samples and an operator were to apply a vacuum to speed degassing, there is still no information on how one could confidently make measurements that were not confounded by bubbles. It is also noteworthy that only visible bubbles that pre-

exist in samples are mentioned, and for this reason, bubble traps are installed on turbidimeters and particle counters to at least partly remove the bubbles from the water before it is introduced to the measuring device (Broadwell, 2001).

Problems from pre-existing bubbles are also mentioned in the Interim Enhanced Surface Water Treatment Rule, which states “Fluctuations in continuous measurements should be investigated since they may be due to air bubbles....” However, no guidance is given as to what utilities should do about this problem if it is identified, nor is there a methodology to distinguish between these bubble induced fluctuations and filter effluent turbidity spikes that are routinely deemed indicative of potential pathogen breakthrough during filtration. It is critically important to know when each phenomenon is occurring, since bubbles do not pose a public health threat, while breakthrough of real particles is an obvious and important concern.

Other industries have also noted interferences from bubbles in particle counting. When monitoring for oil contamination, Rossi et al. (2003) stated that it is widely known that the greatest interference is from bubbles, and that counters actually detect both “hard particles” (i.e., real particles) and “soft particles” (i.e., bubbles). In the case of oil quality, gas bubbles are often considered a significant source of contamination, so this detection is not always deemed a disadvantage.

Some very important work has been done in the semiconductor industry to detect and eliminate bubble interferences in particle counts. Specifically, when particle counters were used to monitor the purity of chemicals, extensive data was gathered that suggested bubbles were forming within the flow cells of the instruments (Dillenbeck, 1987). That study conducted QA/QC to determine acceptable operating conditions using a pressurized air sample delivery system. First, a needle valve was installed downstream of the flow measurement cell, and for a target pressure applied to the sample upstream of the instrument, the valve was adjusted to maintain the manufacturer’s recommended flow rate. After recording particle counts on a sample, the process was then repeated for the same sample but at a higher pressure upstream of the particle counter. The net effect was to incrementally increase the pressure within the flow cell during measurement and measure the instrument response.

When the Dillenbeck results are plotted versus influent gas pressure, a curve is obtained that clearly indicates the problem of spurious signals in the sample of interest (Figure 2.1). Sometimes a pressure of 20 psi was required to repress false positive counts from bubbles in

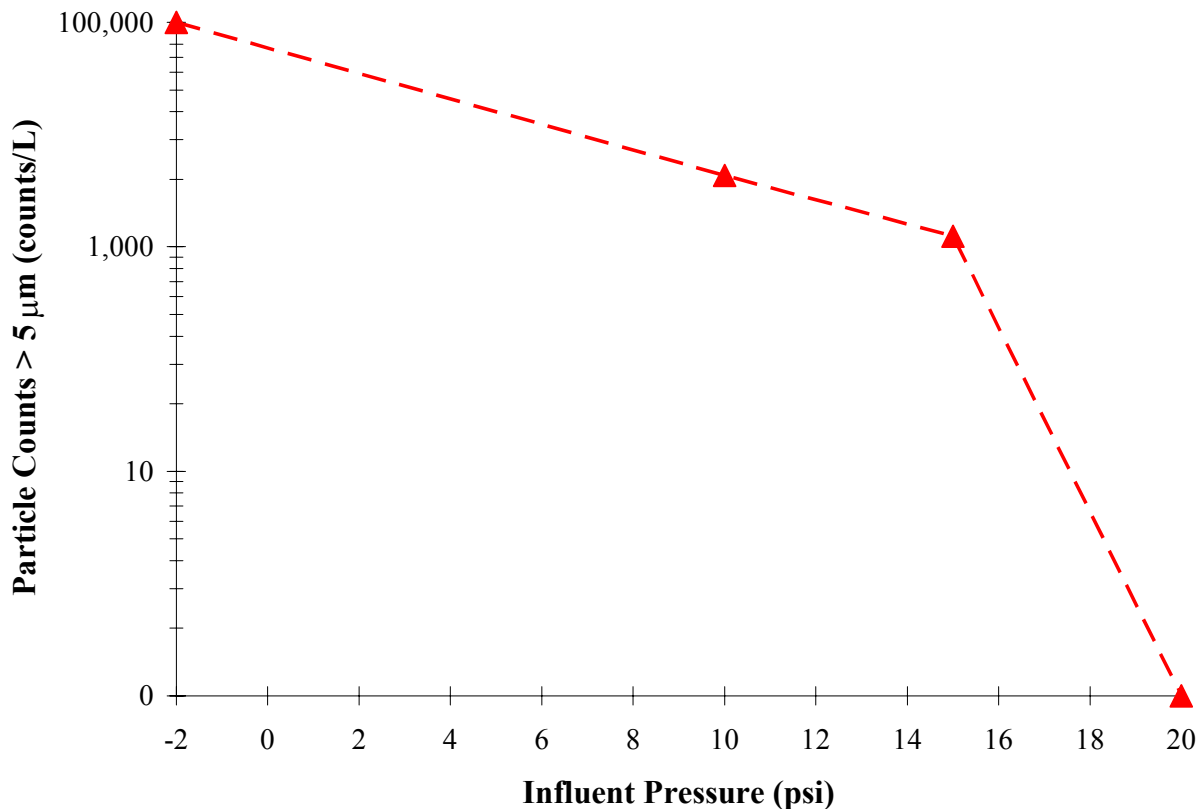


Figure 2.1 – Minimum Outlet Pressure Required to Prevent Gaseous Cavitation in Particle Counters (Data from Dillenbeck, 1987). Testing Was Conducted at the Recommended Flow Rate of 100 ml/min for 30% H₂O₂ Solution. We Estimated the Negative Outlet Pressure at -2 psi as Imposed by Use of a Downstream Syringe that “Pulled” the Sample through the Flow Cell.

solution. It is worth noting that 20 psi translates to a constant head of 46 ft water above the flow measurement cell. The data in Figure 2.1 also confirms the potential for even more serious problems with devices that pull samples through the instrument with a vacuum (Lewis et al., 1992). According to Broadwell (2001), vacuum grab samplers have almost completely replaced more expensive pressure driven samplers in the water industry.

It is noteworthy that, Dillenbeck believed the gas bubbles were forming directly within the particle counter as opposed to the possibility of entrained bubbles that pre-existed in the sample. Such a phenomenon is not anticipated in *Standard Methods*, and bubble traps could not prevent this interference. Although this phenomenon is alluded to in a particle counting book (Broadwell, 2001), it creates an additional concern about the quantitative accuracy of particle count data. The Dillenbeck approach provides a simple and sound method to detect problems with bubbles for any sample. Specifically, any decrease in particle count with higher pressure (at

constant flow) can only be attributed to reduced bubble formation in the measurement cell—we are aware of no other reason why relatively small increases in hydrostatic pressure should decrease counts in a given channel.

Although there is no routine QA/QC employed by the water industry to detect this potential interference from gas bubbles, there have been hints of a potential problems detected in a few instances when additional QA/QC was employed. For instance, in a recent study by the National Sanitation Foundation (NSF, 2000), the average turbidity of on-line turbidimeters compared to benchtop units was 0.082 versus 0.05 NTU, respectively. More importantly, some values from the continuous on-line devices were considered erroneously high, since certain measurements were 4 to 5 times higher in this same device after the water had been micro-filtered than before it had been micro-filtered. When the body of the device was drained and then refilled, the on-line turbidimeter would measure 0.02-0.03 NTU for a short time before returning to higher values. The authors felt that an accumulation of micro-bubbles in the on-line device was responsible for the difference (NSF, 2000). Because of this contrasting and perplexing behavior, data from the on-line turbidimeter was excluded from consideration, and the authors decided to rely on the benchtop devices.

Sakaji and Lai (1995) have reported even stronger evidence of a serious problem. Acting on a request to verify particle removal data for Giardia size particles, they noted that particle counters installed on individual filters gave data that was about 10 times lower than for the combined filter effluents. After ruling out the possibility of particle contamination between the filter and the combined effluent monitor and then explicitly ruling out variations between the instruments themselves, conversations with an instrument representative focused attention on a positive interference from bubbles forming before the devices. When the authors applied backpressure to the sensors using a rotometer downstream of the device or if they otherwise increased backpressure by raising the effluent outlet, particle counts could be decreased by about 10 times, directly implicating a positive interference from bubbles. Although their data was not inconsistent with the belief of Dillenbeck that gas bubbles were forming within the measurement cell, Sakaji and Lee believed the bubbles were forming in the influent plumbing to the apparatus and swept into the counter. Applying the backpressure somehow reduced the source of bubble formation. These authors noted that maintaining positive backpressure is essential to obtaining reasonable particle counts, and they further anticipated “There might be a great deal of

variability in the conditions under which micro-bubbles form due to the variations in water quality between utilities.”

If micro-bubbles were forming within certain particle counters and turbidimeters, this problem could help resolve some very perplexing results in the literature that have defied other rational mechanistic explanations to date (e.g., see Becker et al., 2002; Becker et al., 2003). Specifically, it has often been observed in studies examining pre-oxidation and filter performance that little or no improvement occurs in filter effluent turbidity. However, dramatic improvements in filter effluent particle counts are often noted following ozonation. For instance, Wilczak et al. (1992) and Becker et al. (2002) reported one or two order of magnitude improvements in filtered water particle counts when using ozonation versus the same treatment without ozone. In comparison, ozone had little or no noticeable effect on turbidity before and after the filters. Oddly, this effect is often independent of ozone dose.

The logical conclusion drawn was that ozonation dramatically improved particle removal by the filters, and that particle counters were much more sensitive in detecting improvements to treated water quality than was possible using turbidity measurements on the same sample. However, if it were shown that certain particle counters were sometimes impacted by a positive interference from counting bubbles when certain turbidimeters were not, and if application of ozonation somehow reduced the extent of bubble formation within the device, the scientific interpretations would be dramatically different.

The three goals of this paper are to 1) examine the potential problem of bubble formation in particle counters and to report on preliminary experiments verifying the phenomenon, 2) present the results of experiments that examine the effect of gas supersaturation and bubble formation on on-line turbidimeter measurements, and 3) describe preliminary tests on the effectiveness of bubble traps in mitigating these problems. Thereafter, a discussion section highlights important implications of the results to the water industry.

MATERIALS AND METHODS:

Analysis of Particle Counters

Experiments using a particle counter were conducted at a water utility using water drawn directly from the full-scale filter effluent. The distribution manifold of the particle counter was modified so that the pressure within the system could be varied by adjusting the height of the

overflow. During these experiments, a peristaltic pump continually operated to provide the necessary pressure head at all overflow heights, since filter hydraulics did not always allow head to be increased without a pump. A HIAC-ROYCO PC-320 particle counter was also used in preliminary laboratory experiments using distilled-deionized water pre-filtered through a 0.2 μm pore size membrane. The distilled and deionized water, by its nature, is highly undersaturated at 0.8 atm absolute pressure total dissolved gas (TDG) as measured by a total dissolved gas probe (TDGP). Supersaturated samples of this water were created containing 1.2 atm absolute pressure dissolved gas using pressurized nitrogen.

Laboratory Analysis of Turbidimeters

The three on-line and one benchtop turbidimeter used in this part of the study represent the two basic types of flow cells (open and closed to the atmosphere) and the two types of light sources (tungsten filament bulb and light emitting diode) (Table 2.1). Instruments A and B have internal or attached bubble traps, and instrument C has an external (detached) trap that was mounted on the test stand next to the flow cell. Unless indicated, all experiments incorporated the bubble traps. All instruments were calibrated to manufacturer specifications. Each of the turbidimeters was capable of electronically processing the measured points and computing a running average to suppress abrupt fluctuations in the turbidity record, and all analog data was converted to digital and compiled by a computer. It should be noted that instrument A with its open to the atmosphere design cannot be subjected to backpressure.

All test suspensions were prepared in a 250 L polypropylene tank that had an adjustable low speed mixer (8 cm diameter paddle) positioned in the middle of the tank. Test suspensions were transferred with a peristaltic pump [4.2 L/min (1.1 gpm)] from a tap at the bottom of this larger tank to a 40 L (10 gal) head tank above the instruments, which supplied via gravity the influent to all on-line instruments. The target flow rates for the instruments A, B, and C were 0.4, 2.3, and 0.5 L/min, respectively.

The driving force for gas bubble formation in these experiments was dissolved gas supersaturation (Scardina and Edwards, 2001). All test waters were initially supersaturated with dissolved gas by acidifying to $\text{pH } 3.9 \pm 0.5$ a water of known alkalinity, converting the bicarbonate alkalinity to supersaturated carbon dioxide (CO_2). This method was chosen for its

Table 2.1 – On-line Turbidimeters Used in this Study.

Instrument	Type of Flow Cell	Flow Cell Volume (mL)	Light Source	Calibration Material
A	Open to Atmosphere	910	Tungsten Filament Bulb	Diluted Commercial Formazin
B	Closed to Atmosphere	600	Two 860 nm Light Emitting Diodes	Diluted Commercial Formazin
C	Closed to Atmosphere	30	Tungsten Filament Bulb	Commercial PSL Suspensions

simplicity in creating dissolved gas supersaturation in large volumes of water, and at the time of these experiments, there appeared to be no evidence that dissolved carbon dioxide would give a response different than other dissolved gas(es) supersaturation. The dissolved gas supersaturation influent to the instruments was measured with a total dissolved gas probe (TDGP) manufactured by Common Sensing, Inc. Most dissolved gas supersaturation levels are reported as gauge pressures referenced to the local barometric pressure.

Each experiment began by filling the large tank with 240 L deionized water from a reverse osmosis unit at a temperature between 22 and 27 °C. Following addition of sodium bicarbonate, 14 mL of 4000 NTU commercial formazin suspension was added to the large tank, which gave a test suspension turbidity of about 0.26 NTU as measured with the benchtop turbidimeter. At the end of each experiment, the system was rinsed and filled with the deionized water, and the instruments were kept filled with deionized water between experiments.

During each experiment grab samples were collected from a number of locations in the experimental apparatus and measured using the benchtop turbidimeter, which did not appear to be impacted by the level of gas supersaturation (up to 0.2 atm gauge pressure) or sampling location. Two methods for handling the grab sample before placement into the meter also did not have a significantly different effect on the benchtop turbidity results.

RESULTS AND DISCUSSION:

Preliminary Examination of Bubble Interferences in Particle Counters

Although Dillenbeck (1987) believed interferences arose from bubble formation in the flow measurement cell, he did not propose a potential mechanism for this phenomenon other than to cite the high flow rates of water through the particle count measurement cell as a potential cause. Based on flow cell dimensions and flow rates given in Broadwell (2001) and consideration of likely flow profiles/regimes in the flow cell, maximum velocities within the measurement cell of particle counters (where the particles are detected) is likely to range between 0.88-6.66 m/s. These values are below the 10 m/s velocity range at which classical vaporous bubble cavitation can occur, where bubbles spontaneously form when the local solution pressure becomes less than the liquid vapor pressure in a process analogous to boiling; consequently, this potential mechanism of bubble formation can be ruled out as the cause.

However, a literature review revealed that dissolved gases (nitrogen, oxygen, etc.) could also constitute part of the bubble composition, which has been described as “gaseous” cavitation. Gaseous cavitation can occur whenever the local solution pressure becomes less than the total dissolved gas (TDG) pressure. An everyday example of gaseous cavitation is the immediate release of bubbles that occurs when carbonated beverages are opened.

The phenomenon of gaseous cavitation has received very little direct study, but Naylor and Millward (1984) have gathered considerable practical data. The authors used a flume to determine the role of velocity and local solution pressure in controlling inception of cavitation as measured by bubbles visible to the human eye. The following equation is cited:

$$O_{ci} = \frac{p_o - (p_v + p_c)}{0.5\rho V^2}, \quad (\text{Equation 2.1})$$

where O_{ci} is the cavitation inception number, p_o is the local solution pressure at the point of concern, p_v is the vapor pressure of water, p_c is the “correction pressure” from dissolved gases, ρ is the solution density, and V is the water velocity. With 1 atm absolute pressure TDG in the water, p_c in the above equation was determined to be 0.61 atm by Naylor and Millward (1984), such that at a velocity of 1 m/sec, gaseous cavitation is predicted whenever the local solution pressure drops below 1.05 atm absolute pressure in the flow cell. With 1.2 atm absolute pressure

of TDG in the water at the same velocity, gaseous cavitation is predicted to occur if the local solution pressure becomes less than 1.36 atm absolute pressure within the flow cell.

Recent field work has demonstrated that actual dissolved gas concentrations in water collected at treatment plants can vary from 0.8-1.4 atm absolute pressure (Scardina and Edwards, 2004b). At the lower end of dissolved gas content (0.8 atm absolute pressure), gaseous cavitation is not predicted to occur at any velocity of up to 6 m/sec in the flow cell if the sample is pressure driven. At 1.4 atm absolute pressure however, a positive backpressure of at least 20 psi (47 ft of hydrostatic pressure) is required to prevent gaseous cavitation in the flow cell at these velocities. Clearly, when it is considered that the flow cell is not only the point of highest velocity but also minimum pressure in the system, gaseous cavitation is a very real possibility in circumstances practically relevant to water treatment application.

To test this idea unambiguously, a preliminary experiment was conducted using three waters of various total dissolved gas content synthesized in the laboratory. Within the time frame of sampling, no bubbles were visible in the water or on the sides of the sample container. Thus, the samples always passed the *Standard Methods* criteria of being bubble free during introduction of the sample.

When a backpressure of 15 or 20 psi was applied to a particle counter and the samples were supplied under pressure, particle counts in the 5-10 μm channel always averaged less than 16 counts per liter regardless of which sample was tested. This confirmed that the samples were essentially particle free and that the process of supersaturating the water with nitrogen did not add particles to the water.

When the same samples were pulled through the measurement cell at the specified flow rate with a syringe, as would be the case with the common grab sampler, particle counts in the water supersaturated at 1.2 atm absolute pressure increased to $22,000 \pm 1200$ particles per liter. Bubbles were clearly visible in the water that emerged from the particle counter, but not in the sample influent before it entered the counter. This is strong and direct proof that gaseous cavitation was occurring within the measurement device itself. When the same test was conducted on water at 0.8 atm absolute pressure, the count decreased to 50 ± 15 counts per liter.

If this had been a routine measurement, the “blank” sample would have been the sample at 0.8 atm absolute pressure, since this was unaltered distilled, deionized, and filtered water. Based on the *Standard Method* QA/QC criteria (i.e., discard data from channels if the counts are

not at least 20 times higher than the blank), the “particles” counted in the water supersaturated at 1.2 atm absolute pressure would be deemed highly significant. In other words, there would be no way of knowing that this positive interference was not due to hard particles, since such particles were not present in significant concentrations and the signal is almost exclusively due to bubbles.

This clearly points to a very large problem with gaseous cavitation within the flow measurement cell if the sample is pulled through the instrument, creating a negative pressure. However, even if the sample was driven through the device without installation of a valve to apply backpressure, dissolved gas supersaturation still presented problems. Specifically, particle counts in water supersaturated with 1.2 atm absolute pressure TDG were $15,500 \pm 400$ during triplicate analysis. This is nearly 3 orders of magnitude higher than the counts obtained for the same sample but with 15-20 psi backpressure.

Another test simulated how aeration could affect the problem of bubble formation. When water supersaturated with dissolved gas was vigorously aerated for 3 seconds, allowed to sit 5 minutes, and then passed through the particle counter using the pressurized sampling device but without a valve for back pressure, particle counts decreased by a factor of 950 relative to the same sample before aeration. Dosing of 2 mg/L ozone, via pipette from a solution of ozone saturated gas but without aerating the sample, had an insignificant effect on particle measurements in the original sample or on the sample blank. In summary, dosing of ozone itself had no impact, but brief aeration greatly alleviated dissolved gas supersaturation and decreased the extent of positive interference from bubbles by about 3 orders of magnitude. The same samples were measured on a benchtop turbidimeter, and none were significantly impacted by either ozonation, aeration, or dissolved gas supersaturation.

The next step was to prove that this phenomenon was occurring at full-scale treatment plants. Utility X was selected because the staff reported large diurnal and seasonal variations in treated water particle counts, but only small variations were occurring in treated water turbidity measurements. Consistent with the conventional interpretation, the utility trusted their particle counter to be at least qualitatively accurate, and they had conducted many optimization studies to improve the quality of treatment and prevent potentially harmful filter effluent spikes. The original filters with older media had spurious spikes that were not observed with the “newer

filters” (Figure 2.2), which initially suggested that the filter performance was truly being compromised due to “worn out” media.

During a site visit to examine this problem, unfortunately, the filter effluent spikes were not at their worst. Nonetheless, the evaluation started with modification of the particle counter to test for measurement artifacts from bubbles. As is typical, the particle counter at the plant had an overflow manifold (Figure 2.3). A portion of the flow goes out the overflow, which creates a constant hydraulic pressure within the sensor as well as a constant flow rate through the device. If the overflow opens to the atmosphere, and the filter head is sufficient, then adding extra tubing and increasing the height of the overflow can increase the backpressure pressure within the device (Figure 2.3). To maintain flow at the desired rate, a valve was adjusted downstream of the sensor. This is an ideal way to test for bubble effects, since any significant difference in particle counts in normal versus higher backpressure operation is almost unquestionably due to bubbles.

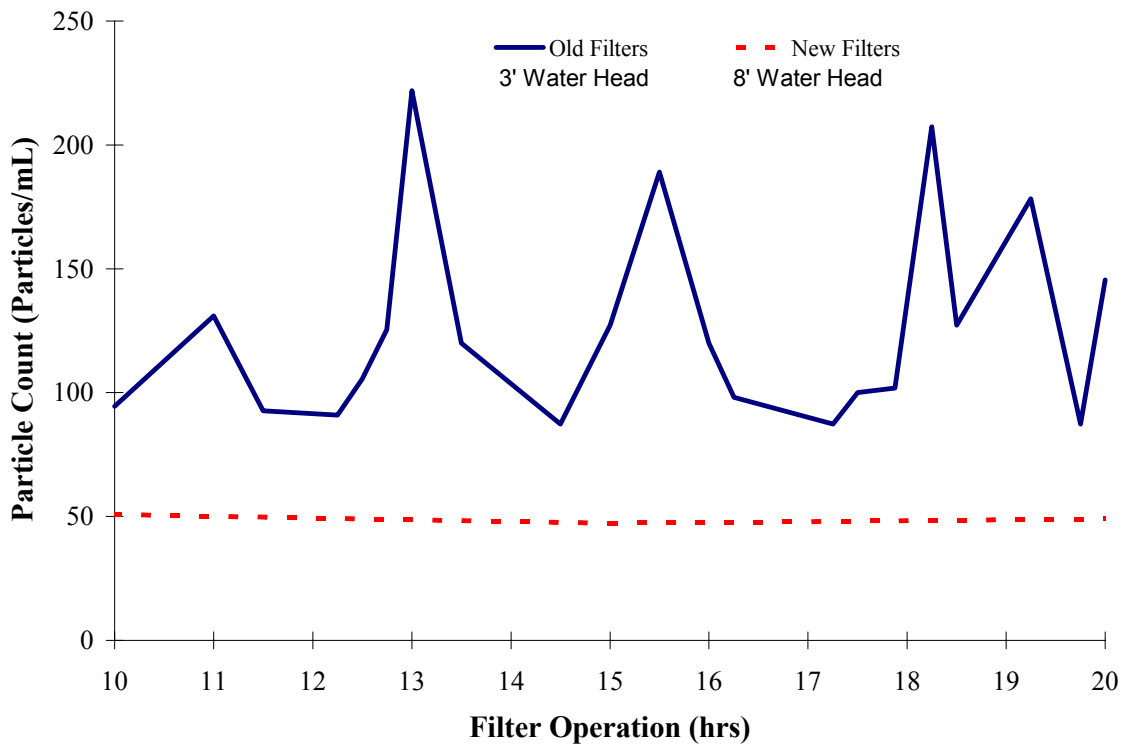


Figure 2.2 –Representative Particle Count Data on Two Filters at Utility X.

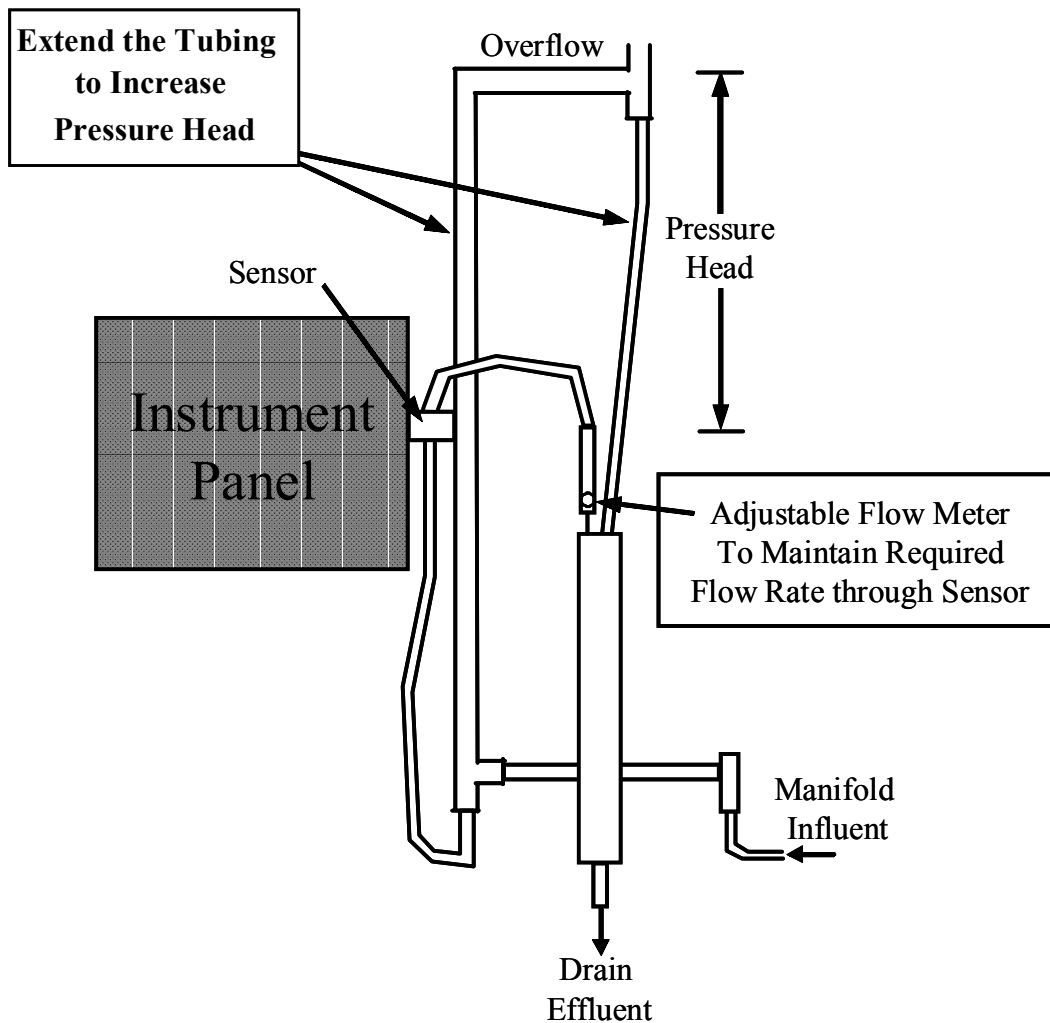


Figure 2.3 – Particle Counter Modifications for This Study.

After modifying the particle counter flow manifold at Utility X, the pressure head on the system could be varied between 1.8 ft (0.55 m) and 12.5 ft (3.81 m). The flow rate through the sensor was always maintained at the required 65 mL/min. The backpressure of the particle counter system was first varied toward the end of a filter run (85 hours of a 90 hour run) when the “particle counts” and “filter spikes” were starting to occur. The data confirmed, with greater than 95% confidence, that when backpressure on the particle counter was increased by increasing height of the overflow, particle counts decreased (Figure 2.4). When the overflow height was returned to 1.8 ft, the counts promptly measured as their original value.

This filter was then backwashed and allowed to ripen, and similar results were obtained (Figure 2.5). Operating with the overflow raised at 12.5 ft (3.81 m) (increased pressure), the

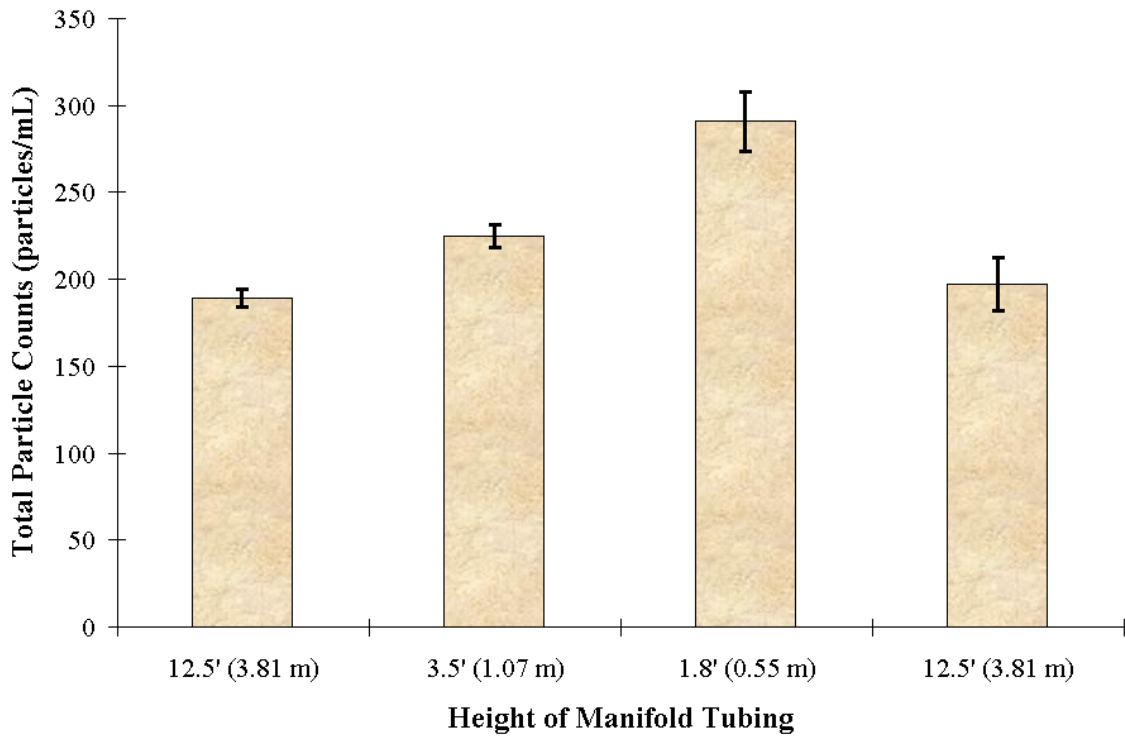


Figure 2.4 – Particle Counts at Different Manifold Tubing Heights at Utility X. Error Bars Indicate 95% Confidence.

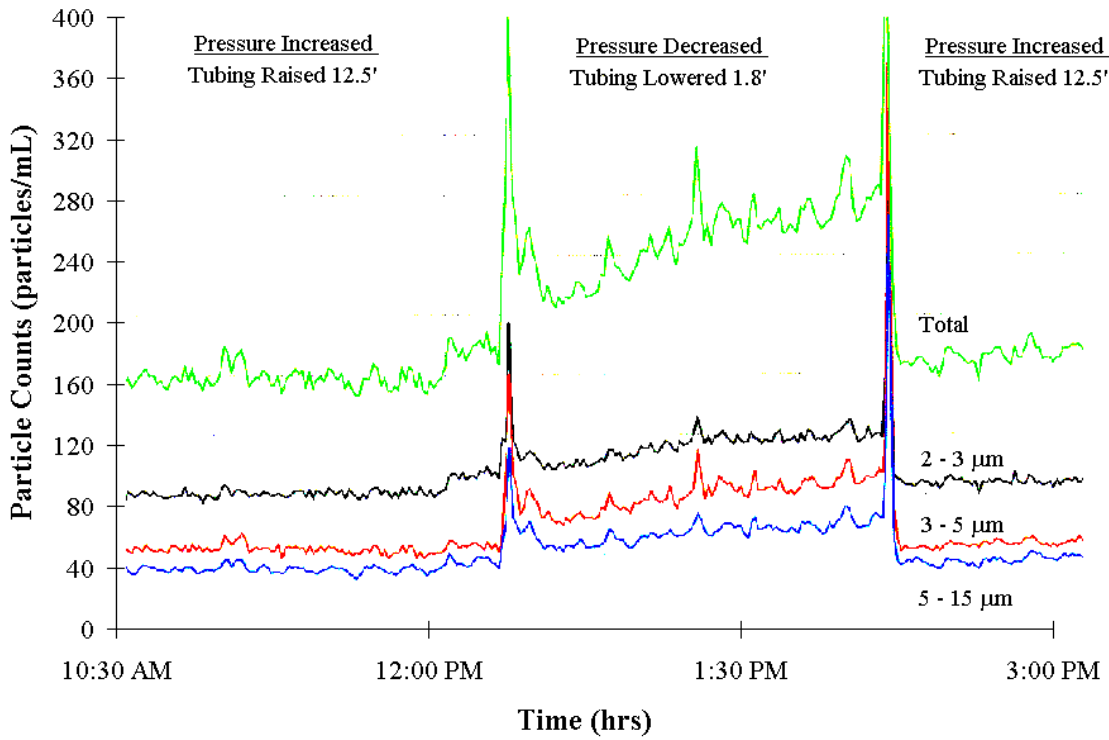


Figure 2.5 – Actual Particle Counts at Utility X on 7-31-2002.

total particle counts were steady at an average of 160 – 170 particles/mL, and lowering the overflow manifold to 1.8 ft (0.55 m) (decreased pressure) increased the total particle counts to approximately 240 – 270 particles/mL (Figure 2.5). The total particle counts returned to 160 – 170 particles/mL after raising the manifold overflow again to 12.5 ft (3.81 m). The manifold was then lowered to 1.8 ft (0.55 m) causing another increase in the particle counts (data not shown). These findings were highly reproducible from day to day. We further note that there is no way to know that increasing the overflow to 12.5 feet completely eliminated the problem of bubble formation and spurious signal in the sensor, only that we are confident that it reduced the extent of the positive interference.

In conclusion, the measured particle counts at this utility were highly dependent on the pressure within the measurement cell, and the most likely explanation is bubble formation via gaseous cavitation. It should be noted that the water during these measurements was actually undersaturated with dissolved gas (approximately -0.04 atm gauge pressure), and that during other visits to the plant, dissolved gas supersaturation as high as +0.2 atm gauge pressure had been measured during algal blooms. Problems with effluent spikes at the plant were retroactively noted to be consistent with periods of dissolved gas supersaturation as noted by floating floc and “air binding” of filters. Finally, an investigation revealed that the older filters had only 3 ft (0.91 m) of water head above the filter media (submergence), while the newer filters had 8 ft (2.44 m) of submergence (Figure 2.2). This extra submergence would greatly hinder formation of bubbles, since the hydrostatic pressure within the particle counter and in the filter would be higher (e.g., Scardina and Edwards, 2004a).

In summary, the weight of the evidence strongly suggests that many particle counters are subject to very significant positive interferences from bubble formation originating via gaseous cavitation. The extent of the problem worsens with lower backpressure on the instrument, higher velocities within a given flow cell, and higher dissolved gas content of the source water among other contributing factors. Moreover, as noted by the test with ozonation, interpreting the data of such devices as even qualitatively accurate could lead to grossly erroneous scientific conclusions. Finally, there is no QA/QC routinely employed by the water industry that can detect if and when a problem is occurring on a transient or continuous basis.

Preliminary Examination of Bubble Interferences in Turbidimeters

During some full-scale plant visits, operators and plant supervisors were not generally willing to speak with us “on the record” about problems they were having with turbidity measurements. Operators have a strong sense of pride in achieving low and stable turbidity values, and therefore, it is perhaps not surprising that there is some concern associated with unexplained spikes and variations in turbidity. In at least 2 utilities treating waters supersaturated with dissolved gas, operators were having problems with bubbles forming during measurements with benchtop turbidimeters. Specifically, bubbles were often visible within the grab samples, the turbidity measurements fluctuated unpredictably with time, and measurements made between different operators varied dramatically given differences in sample collection. Some operators found that pulling a partial vacuum on the water as recommended by manufacturers (HACH, 1997) or putting the sample into an ultrasound bath had rarely produced any benefits or reduced bubble interference—it may have even exacerbated the problem. It was generally believed that the best procedure was to let the sample sit for 15-30 minutes and allow the bubbles to degas. In so doing, variations in benchtop measurements made between operators had been reduced to about $\pm 30\%$ compared to $\pm 400\%$ (or worse).

All full-scale plants experiencing problems with benchtop turbidimeters also observed some “spikes” and erratic measurements within their on-line turbidity and particle counters. At times, bubbles were visibly apparent in the on-line devices, and some spikes increased the turbidity to above 10 NTU. Corresponding measurements using the benchtop devices after allowing samples to sit for 30 minutes consistently led to turbidities less than 0.1 NTU. The low turbidities for benchtop measurements were not changed when the contents of the cuvette were rapidly mixed. In some plants, the body, tubing, and sensor of the on-line meter was gradually filled with gas requiring periodic cleaning to remove the gas, and in some cases the meters had to be serviced every 30 minutes to give reasonable data. Again, these effects were all worsened under conditions of dissolved gas supersaturation including algae blooms, air entrainment in pipelines, and time periods of increasing water temperature.

The laboratory study sought to confirm these observations. The influent feed solution to the on-line instruments had a constant 0.26 NTU via a formazin standard and a variable dissolved gas content created by acidifying a bicarbonate solution. As a starting point, it was noted that if the on-line devices were not affected by bubbles, their measurements should be in

agreement with those for the benchtop sample from the feed tank. A baseline was established for each on-line instrument using “blank” water that had a very low potential to form gas bubbles. Although this water contained 0.006 M bicarbonate (and formazin at 0.26 NTU), the feed solution was not acidified so that the carbon dioxide supersaturation was close to 0.0 atm gauge pressure. The average turbidity for instruments A and B were similar to the benchtop turbidimeter (0.26 NTU), which would be expected for a blank run with no dissolved gas supersaturation. Yet, the average turbidity of instrument C (0.180 NTU) was less than the average benchtop reading. This interesting discrepancy was observed in a previous study (Letterman et al., 2002) and was probably caused by different methods used to calibrate and “zero” the two devices.

During subsequent experiments when the feed solution was supersaturated with dissolved gas, the measured TDG at the effluent of the on-line turbidimeters was on average 30% lower than the measured TDG of the feed tank, and the difference appeared to be somewhat independent of the initial amount of dissolved gas supersaturation in the feed tank. This observed degassing could have occurred in the head tank, distribution manifold, or within the instruments (measurement cell or bubble traps), but it is likely indicative of bubble formation somewhere within the experimental apparatus.

When bubbles interfere with the on-line measurements, the turbidity would be expected to deviate from the benchtop measurements, with more relative scatter within the data set. With the influent feed solution supersaturated to 0.10 atm gauge pressure, some turbidity spikes began to occur in instrument C towards the end of the experiment. Instruments A and B did not seem to be affected by this low level of dissolved gas supersaturation, since the turbidity of both devices remained essentially unchanged throughout the run.

At a higher influent supersaturation of 0.23 atm gauge pressure, the on-line turbidity measurements became more erratic (Figure 2.6). Instrument C was very erratic and prone to many more turbidity spikes. For this experiment, the bubble reject option was “on” for instruments A and B. The turbidity readings for instrument B continuously increased during the run, from about 0.25 to 0.7 NTU, but there was no evidence of the erratic turbidity spikes that were very apparent for instrument C. The measurement cell of instrument B was opened at the end of the experiment, and it was the only instrument with confirmed gas accumulation within the measurement cell. Some very small turbidity spikes occurred with instrument A, but the

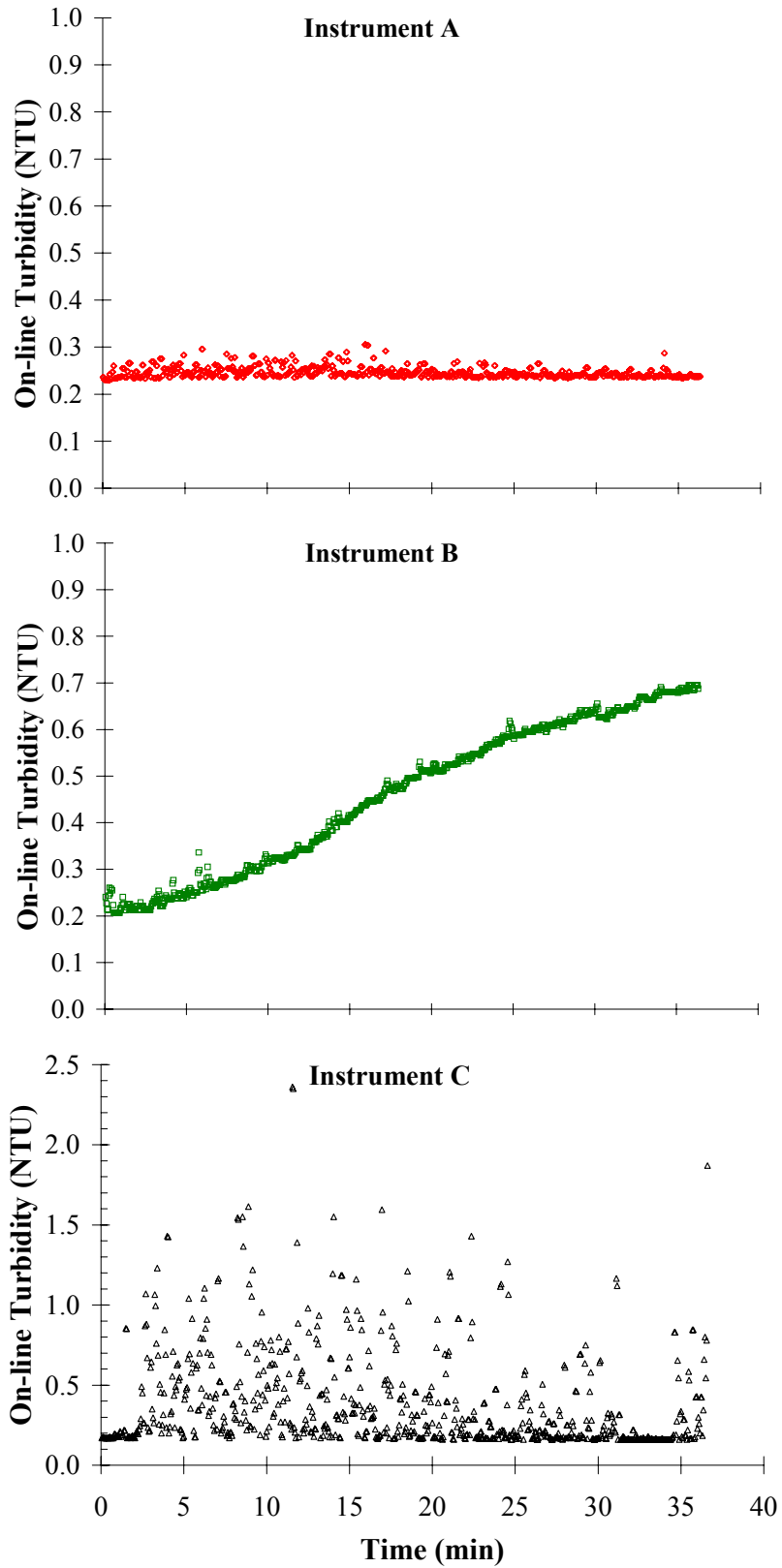


Figure 2.6 – Turbidity Measurements from Three Different On-line Turbidimeters when the Influent Water Was Supersaturated with Dissolved Gas at 0.23 atm Gauge Pressure.

measured turbidity never exceeded 0.3 NTU. Therefore, instrument A was not affected by the high level of dissolved gas supersaturation, since the turbidity remained relatively constant during this experiment.

Since bubble formation disrupted some of the turbidity measurements during the preliminary assessment, additional experiments tested the effectiveness of bubble reject functions and bubble traps for reducing turbidity data disruptions. In order to more easily compare all of the results, the data collected from each experiment was rank ordered to determine the fraction of data less than a given turbidity. The corresponding 95th, 50th, and 10th turbidity percentiles could then be established for a given data set. A simple turbidity ratio between the 95th and 50th percentile values was then used to compare all data sets:

$$\text{Turbidity Ratio} = \frac{95^{\text{th}}\%}{50^{\text{th}}\%}. \quad (\text{Equation 2.2})$$

If gas supersaturation and bubble formation had a negligible effect on the on-line measurements, the 95th, 50th, and 10th values should be essentially equal and close in magnitude to the turbidity measured by the benchtop instrument, corresponding to a turbidity ratio of 1. When bubbles interfere with the on-line measurements, the relative difference between the 95th and 50th, and eventually, between the 50th and 10th percentiles increases, such that the derived turbidity ratio would become greater than 1.

Except for one experiment at the highest carbon dioxide supersaturation (0.24 atm gauge pressure), instrument A was not affected by dissolved gas supersaturation, as indicated by a consistent turbidity ratio of approximately 1 (Figure 2.7). Furthermore, instrument A appeared to be stable even without its bubble trap or bubble reject function.

While utilizing its bubble reject feature and bubble trap, instrument B was also insensitive to dissolved gas supersaturation until the level of supersaturation reached about 0.24 atm gauge pressure (Figure 2.8). At this point, as described above, gas accumulated in the measurement cell, which had significant adverse effects on the turbidity measurements. The performance of instrument B was worsened when either the bubble reject feature or bubble trap was not used, and deviation in the turbidity data (turbidity ratio) was usually the highest when both devices were not used (Figure 2.8).

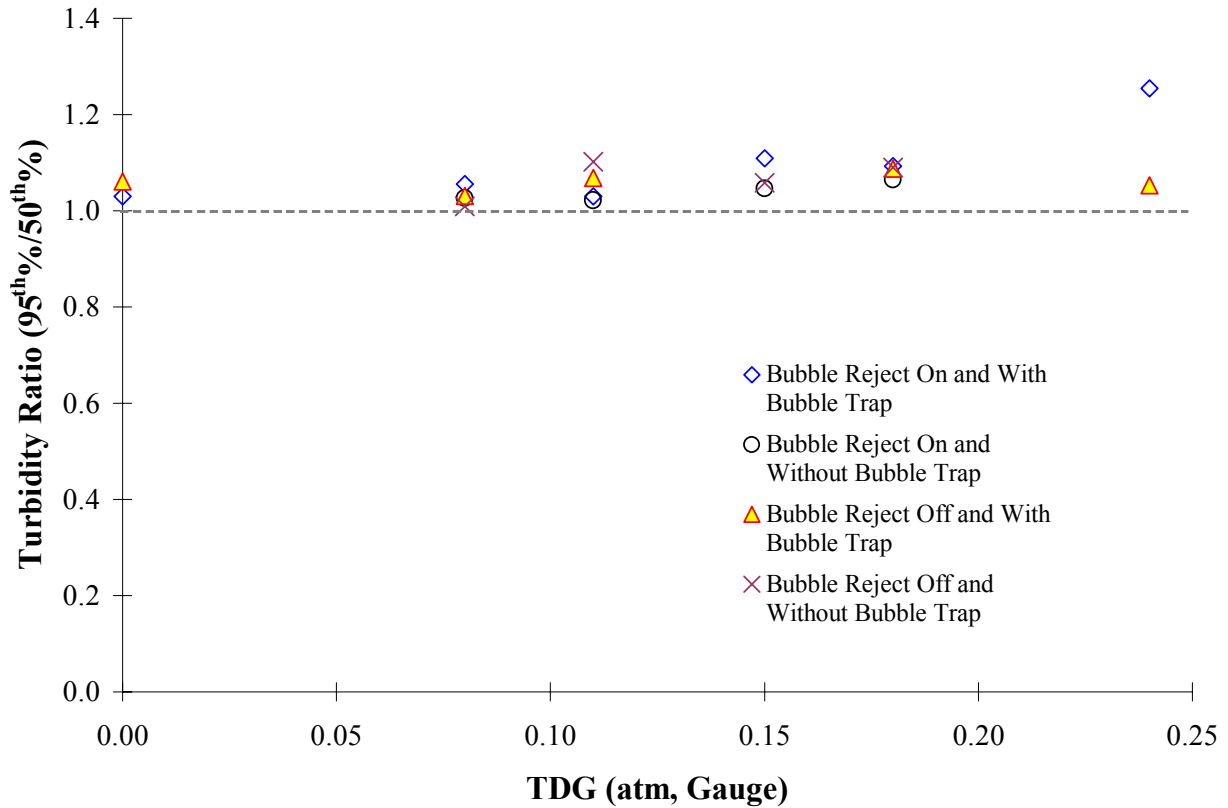


Figure 2.7 – Effects of Dissolved Carbon Dioxide Supersaturation on Turbidity Measurements of Instrument A. Turbidity Ratio is the Ratio of the 95th and 50th Percentile of All Data Collected for a Given Experiment. A Ratio of 1 Indicates Little Variation in the Turbidity Data and Little Effects from Gas Bubbles.

Since instrument C did not have an electronic bubble reject function, it was only tested with and without the bubble trap. The turbidity data for instrument C was erratic and inconsistent, and performance actually improved slightly with its bubble trap removed (Figure 2.9). The specific cause of this anomaly was not identified but may have been associated with small changes in pressure and bubble evolution at the inlet and outlet flow connections of the bubble trap.

During these experiments, opportunities arose to observe other deviations in turbidity measurements. Two disturbances affected turbidity measurements with instrument A, when the entire apparatus was being tested with tap water from an unfiltered water source. The first disturbance was an impact (repeated finger tap) on the tubing between the flow distribution manifold and this instrument. This impact was observed to dislodge a bubble that moved into the flow cell of the instrument, causing the turbidity to rise from 0.4-0.55 NTU range to

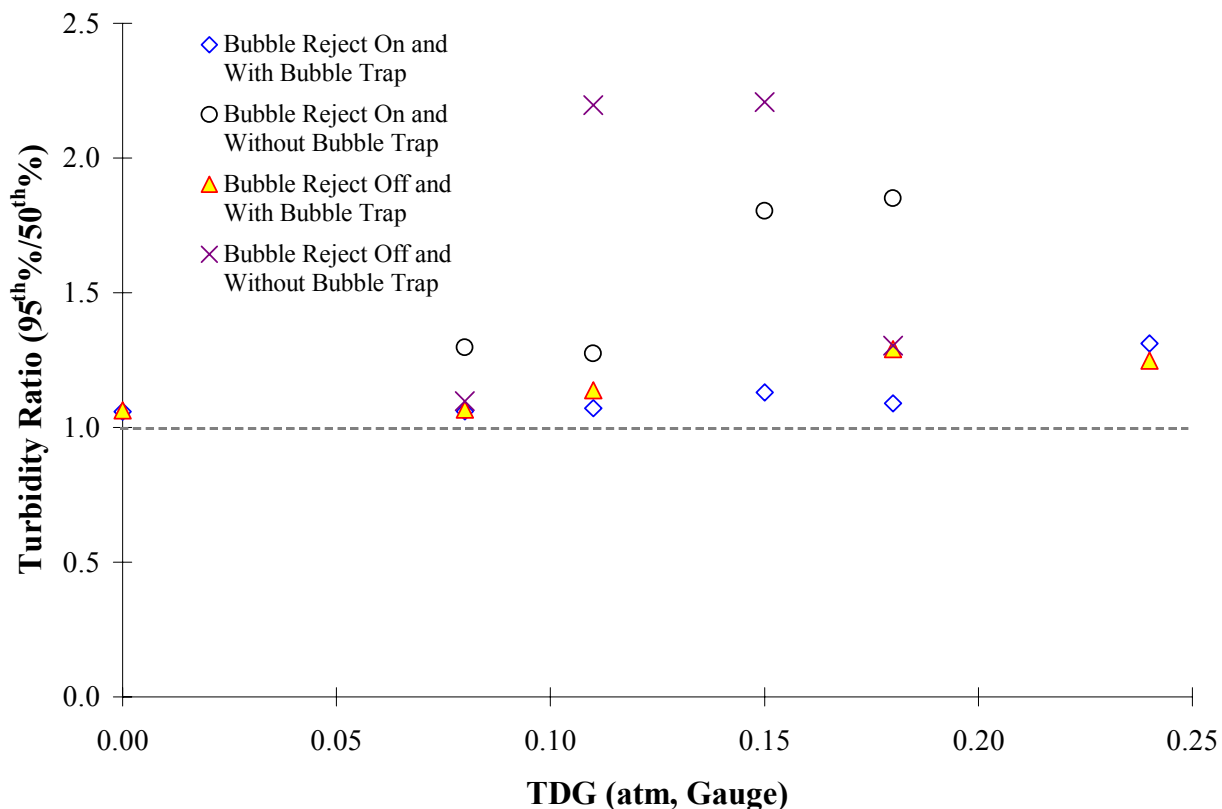


Figure 2.8 – Effects of Dissolved Carbon Dioxide Supersaturation on Turbidity Measurements of Instrument B. Turbidity Ratio is the Ratio of the 95th and 50th Percentile of All Data Collected for a Given Experiment. A Ratio of 1 Indicates Little Variation in the Turbidity Data and Little Effects from Gas Bubbles.

approximately 0.9 NTU. The turbidity then gradually decreased over a period of about 8-12 minutes to the range of values that were being recorded by the other instruments. The second disturbance occurred when the operational flow rate of instrument A increased from 114 to 462 mL/min, which led to a turbidity change of 0.35 to 0.90 NTU, respectively. These were crude and unplanned observations, but it does indicate that such disturbances should be avoided in the operation of on-line turbidimeters in treatment plants.

Discussion

It is clear that improved QA/QC is necessary for the proper use of particle counters and turbidimeters in water treatment applications where dissolved gas supersaturation occurs. In

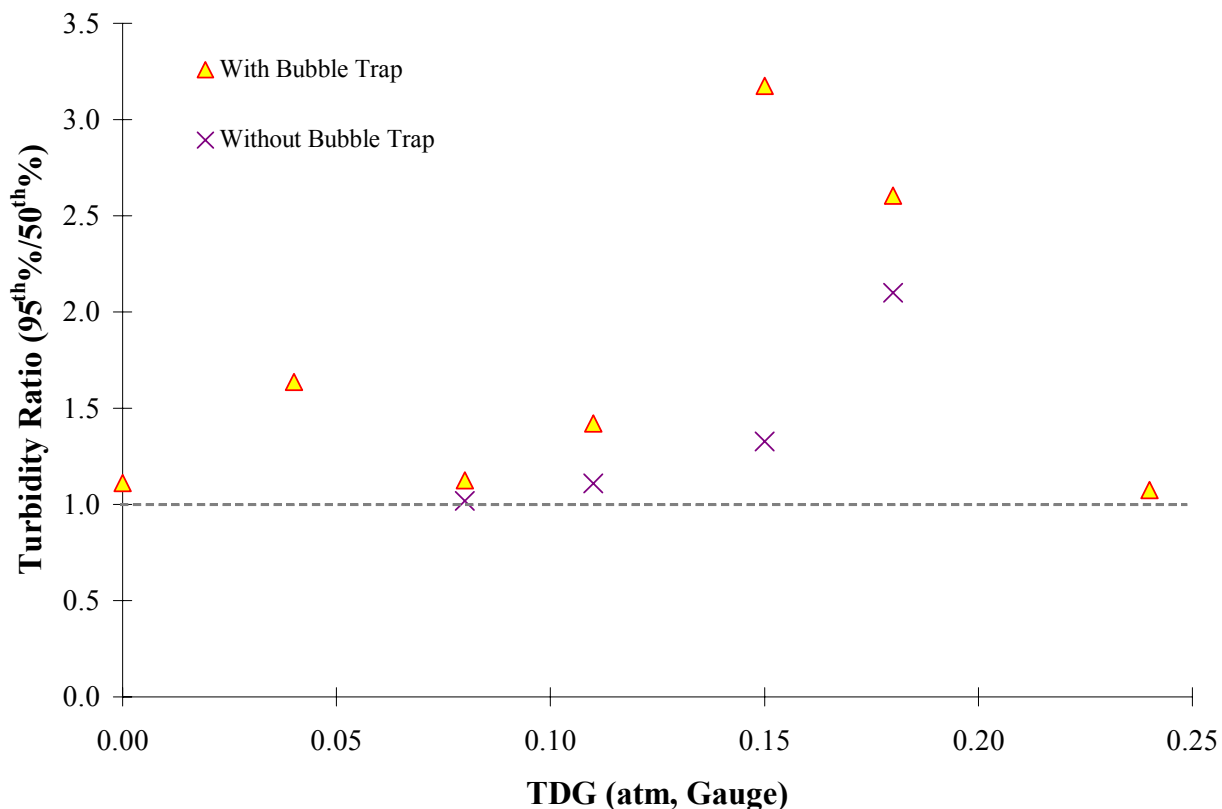


Figure 2.9 – Effects of Dissolved Carbon Dioxide Supersaturation on Turbidity Measurements of Instrument C. Turbidity Ratio is the Ratio of the 95th and 50th Percentile of All Data Collected for a Given Experiment. A Ratio of 1 Indicates Little Variation in the Turbidity Data and Little Effects from Gas Bubbles. Instrument C Does Have a Bubble Reject Function.

particular, scientific conclusions drawn from particle counter studies, where such QA/QC did not explicitly occur, needs careful re-evaluation. For example, we note that data documenting benefits of ozonation in reducing effluent particle counts, when no corresponding change was detected in effluent turbidity, has given rise to an industry consensus (as opined in Van Gelder et al., 1999 and others) that particle counters are more sensitive to actual particulate content in water than turbidimeters. We believe that this conclusion deserves scrutiny.

During preliminary experiments conducted herein, a test was conducted of ozonation that allowed the effect of ozone to be differentiated from the effect of aeration, which can be scientifically useful (i.e., Edwards and Benjamin, 1991). That test on a sample initially supersaturated with dissolved gas indicated that ozone itself had no effect on particle counts, whereas the aeration led to a nearly three order of magnitude reduction in particle counts.

However, the reduced particle counts were due to a reduced level of positive interference from bubbles, and this data was completely misleading in terms of true improvements to water quality. In the same test, turbidity measurements using a benchtop device were not impacted, but merely because bubbles did not seem to interfere with the turbidity measurement in the first place. In this case, which is the type of evidence that has led to the conclusion that particle counters are more useful than turbidimeters, it is clearly the turbidimeter that is providing better actual performance data.

In retrospect, the fact that the particle counts vary diurnally and seasonally (e.g., Becker et al., 2003) is not inconsistent with expected diurnal and seasonal variations in dissolved gas content during algal blooms and changes in water temperature (Scardina and Edwards, 2002). Dramatic increases in filter run length after aeration (i.e., ozonation) can also be expected based on reduced air binding within filters (i.e., Scardina and Edwards, 2001-2002) if dissolved gas supersaturation was alleviated. It is possible that this could explain certain improvements to filtration reported in the literature after ozonation (Edwards et al., 1991 and 1994). Similarly, the observation that ozone dose is relatively unimportant to obtain improved particle counts is also consistent with findings of this work, since it was the brief aeration that alleviated the supersaturation causing the positive interference. In summary, the industry needs to be cognizant of the fact that dissolved gas can give rise to particle count artifacts when using existing and accepted protocols.

Turbidity measuring devices vary dramatically in their response to dissolved gas supersaturation. Sometimes, the interference leads to fluctuations in effluent turbidity or increased “noise.” In other cases, a slow and steady change in turbidity occurred due to bubble accumulation in the measurement chamber (i.e., instrument B Figure 2.8) that would be hard to differentiate from a problem in treatment. Thus, we do not see how a treatment plant operator could be certain of knowing when a problem was caused by bubbles or when it was caused by a true treatment problem. This is especially true given that operators do not know what to look for and measurements of dissolved gas content are not yet routinely made at treatment plants (Scardina and Edwards, 2001-2002).

Furthermore, differences in water quality, which were not even initially considered by these authors, can also have dramatic effects on turbidity measurements. For example, as stated previously, dissolved carbon dioxide supersaturation was initially chosen due to its simplicity of

supersaturating large volumes of water in the on-line turbidimeter study. Yet, a separate analysis found different degrees of bubble formation when the dissolved gas was either carbon dioxide or nitrogen for the same initial level of supersaturation (Scardina and Edwards, 2004c). A simple laboratory experiment using a benchtop turbidimeter tested whether the type of dissolved gas affected the observed turbidity. To test this idea, a benchtop turbidimeter was equipped with a bubble trap and data was collected in the “average” mode, such that bubble induced disruptions should have been minimized. Water initially at a known supersaturation was poured into an overhead reservoir (3L), and the flow rate through the meter was set to manufacturer specifications.

Small turbidity spikes were observed with dissolved carbon dioxide supersaturation (Figure 2.10). Whenever fresh solution was poured into the reservoir, bubble formation was visible inside the reservoir, and large turbidity spikes resulted, suggesting that the bubble trap did not effectively remove all influent bubbles. Surprisingly, the average measured turbidity increased at each incremental increase in dissolved nitrogen supersaturation but not in dissolved carbon dioxide supersaturation (Figure 2.10). The type of dissolved gas supersaturation, therefore, could be another factor affecting turbidity and particle count measurements. These results were not anticipated but are consistent to the observations in another study (Scardina and Edwards, 2004c). Since most of the previous experiments were conducted with dissolved carbon dioxide, the observed disruptions could have been potentially worse if dissolved nitrogen had been used in the earlier experiments (i.e. different water quality).

Lastly, it is also likely that if these artifacts were routinely overcome by application of backpressure, then particle counting and turbidity measurements could become a much better guide to treatment performance than it currently is observed. For instance, in a study of cryptosporidium removal in granular media filters, excellent agreement was observed between cyst removal and that of 5 mm microspheres ($R^2 = 0.93$, log-log plot) in three filter studies during all phases of filter operation (Emelko, 2001). As has been commonly reported in numerous other studies, particle counts ($> 2 \mu\text{m}$) or turbidity was a poor reflection (R^2 in the range of 0.27) of cyst removal (Emelko, 2001). All explanations for this lack of agreement have focused exclusively on the potential differences in behavior between cysts and natural particles during filtration. However, if turbidity and particle counters were actually subject to bubble interferences noted in this study and if the bubble counts varied along with supersaturation of the

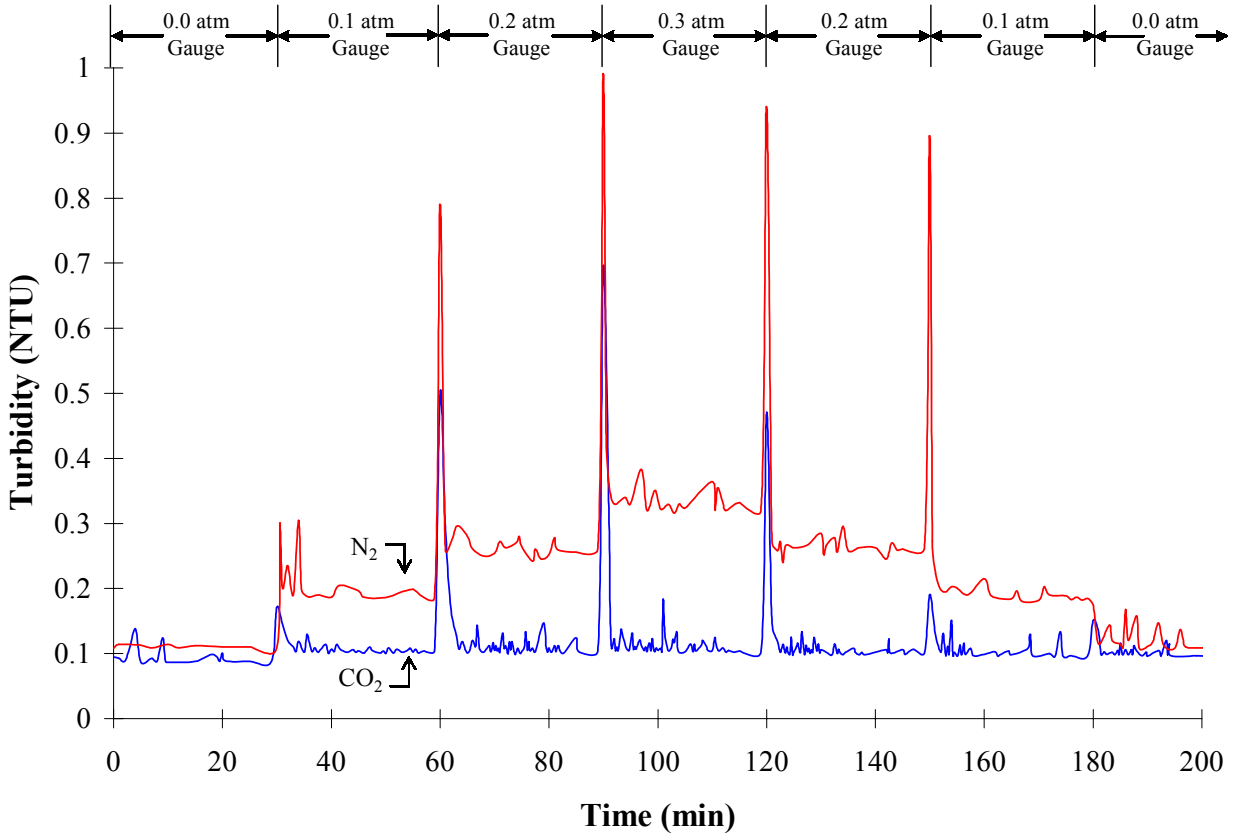


Figure 2.10 – Measurements of Benchtop Turbidity for Solutions Supersaturated with Either Dissolved Nitrogen or Carbon Dioxide. The Benchtop Turbidimeter Was Equipped with a Bubble Trap.

water and other factors during a filter run (Scardina and Edwards, 2004a), this artifact might be a significant cause for the poor correlations between cyst removal, turbidity, and particle counts. In all particle count data presented in this paper, particle counts had essentially zero correlation to actual particles in the water, since the entire signal was almost exclusively attributable to bubbles.

SUMMARY AND CONCLUSIONS:

- Dissolved gas supersaturation and bubble formation can affect particle count and turbidity measurements. Very limited QA/QC is performed on these instruments, which needs to be improved to account for conditions of dissolved gas supersaturation that can lead to bubble formation. The lack of reliable QA/QC has led to incorrect conclusions with particle count data.

- Bubbles were measured as particle counts in laboratory experiments and at a full-scale utility. Particle counts decreased when the pressure within the system (measurement cell) was increased. In some cases, a hydrostatic pressure of 46 ft of water might be required to suppress bubble formation in particle counters, and vacuum samplers increased particle counts.
- The effects of dissolved gas supersaturation to on-line turbidity measurements varied. One instrument was prone to spurious turbidity spikes at 0.10 and 0.24 atm gauge pressure dissolved gas supersaturation. The turbidity as measured by a second device gradually increased throughout the experiment when the water was supersaturated at 0.24 atm gauge pressure, and gas accumulation occurred in the measurement cell of this instrument. A third turbidimeter was immune to dissolved gas supersaturation but was sensitive to abrupt changes in flow rate. Bubble mitigation devices, such as the bubble reject feature and bubble traps, usually helped reduce disruptions caused by gas bubbles. Using the bubble trap for one of the instruments, though, did appear to be detrimental in some experiments.

ACKNOWLEDGMENTS:

This work was supported by the American Water Works Association Research Foundation (AWWARF) under grant 2821. The opinions, findings, conclusions, or recommendations are those of the writers and do not necessarily reflect the views of AWWARF.

REFERENCES:

- Becker, W.C., K.K. Au, C.R. O'melia, and J.S. Young. (2002). The Use of Oxidants to Enhanced Filter Performance. Proceedings of the 2002 Water Quality Technology Conference.
- Becker, W.C., L. Graffney, R. Metzger, and P. Maier. (2003). Diurnal Filtered Water Particle Count Variations: Causes and Control. Proceedings of the 2003 AWWA Annual Conference.

- Broadwell, M. (2001). *A Practical Guide to Particle Counting for Drinking Water Treatment*, Lewis Publishers, Boca Raton.
- Dillenbeck, K. (1987). Advances in Particle-Counting for Semiconductor Process Chemicals. *Microcontamination*.
- Edwards, M., and M.M. Benjamin. (1991). A Mechanistic Study of Ozone-Induced Particle Destabilization. *Journal American Water Works Association*, V. 83, No. 6, 96-105.
- Edwards, M., M.M. Benjamin, and J.E. Tobiason. (1994). Effects of ozonation on coagulation of NOM using polymer alone and polymer/metal salt mixtures. *Journal American Water Works Association*, V. 86, No. 1, 105-116.
- Elmelko, M. B. (2001). Removal of Cryptosporidium Parvum by Granular Media Filtration. University of Waterloo. PhD Dissertation.
- HACH Model 2100N Laboratory Turbidimeter Instruction Manual*. (1997). HACH Company.
- Han, M.Y., Y.H Park, and T.J. Yu. (2002). Development of a New Method of Measuring Bubble Size. *Water Science and Technology: Water Supply*, V. 2, No. 2, 77-83.
- Hart, V.S., C.E. Johnson, and R.D. Letterman. (1992). An Analysis of Low-Level Turbidity Measurements. *Journal American Water Works Association*, V. 84, N. 12, 40-46.
- Hunt, D.J., B. Bars, and Met One Inc. (1997). Particle Counter Size and Count Calibration System. Proceedings of the 1997 WQTC.
- LeChevallier, M.W. and W.D. Norton. (1992). Examining Relationships Between Particle Counts and Giardia, Cryptosporidium, and Turbidity. *Journal American Water Works Association* V84, 12, 54.

- Letterman, R.D., C.E. Johnson, S. Viswanathan, and J. Dawarakanathan. (2002). A Study of Low-Level Turbidity Measurements,” AWWARF Final Report.
- Lewis, C.M., E.E. Haresheimer, and C.M. Yentsch. (1992). Selecting Particle Counters for Process Monitoring. *Journal American Water Works Association*, V. 84, N. 12, 46-53.
- Logsdon, G.S., V.C. Thurman, E.S. Frindt, and J.G. Stoecker. (1985). Evaluating Sedimentation and Various Filter Media for Removal of Giardia Cysts. *Journal American Water Works Association* Vol. 77, 2, 61.
- Naylor, F., and A. Millward. (1984). A Method of Predicting the Effect of the Dissolved Gas Content of Water on Cavitation Inception. *Proc Instn Mech Engineers*, V. 198C, No 12.
- National Sanitation Foundation. (July 2000). Environmental Technology Report. Physical Removal of Cryptosporidium oocysts and Giardia cysts in Drinking Water. NSF 00/10/EPAADW395.
- Rossi, P., and K.A. Young. An Online Particle Counter as a CBM-Enabling Technology. Hiac Technical Notes. http://www.particle.com/whitepapers_hiac/PM4000_CBm.htm. Accessed on 12/12/2003.
- Sakaji, R.H., and H.H. Lai. (1995). Tiny Bubbles- No Cause to Feel Fine. Proceedings of the 1995 WQTC in New Orleans. 89-97.
- Scardina, P. and M. Edwards. (2001). Prediction and Measurement of Bubble Formation in Water Treatment. *Journal of Environmental Engineering*, Vol. 127, 11, pg 968.
- Scardina, P. and M. Edwards. (2002). Practical Implications of Bubble Formation in Conventional Treatment. *Journal American Water Works Association*, Vol. 94, 8, pg 85.

- Scardina, P. and M. Edwards. (2004a). Air Binding in Granular Media Filters. Scheduled for Publication in *Journal of Environmental Engineering*.
- Scardina, P. and M. Edwards. (2004b). Addressing Problems with Gas Supersaturation at Potable Water Treatment Plants. Submitted to *Journal American Water Works Association*.
- Scardina, P. and M. Edwards. (2004c). Fundamentals of Bubble Formation during Coagulation and Sedimentation Processes. Submitted to *Journal of Environmental Engineering*.
- Slaats, L.P.M., W.G. Rosenthal, M. Siegers, R.H.S. Beuken, and J.H.G. Vreeburg. (2003). Processes Involved in the Generation of Colored Water. AWWARF Final Report.
- Standard Methods for the Examination of Water and Wastewater*, 20th ed. (1998). APHA, AWWA, and WEF, Washington, DC.
- Van Gelder, A.M., Z.K. Chowdhury, and D. F. Lawler. (1999). Conscientious Particle Counting. *Journal American Water Works Association*, V. 91, N. 12, 64-75.
- Wilczak, A., E.W. Howe, E.M. Aieta, and R.G. Lee. (1992). How Preoxidation Affects Particle Removal During Clarification and Filtration. *Journal American Water Works Association*, V. 84, N. 12, 85-94.

CHAPTER 3

FUNDAMENTALS OF BUBBLE FORMATION DURING COAGULATION AND SEDIMENTATION PROCESSES

Paolo Scardina and Marc Edwards
Virginia Tech; 418 Durham Hall; Blacksburg, VA 24061

ABSTRACT:

Conventional coagulation and sedimentation processes can be significantly disrupted by gas bubbles forming, attaching, and then floating coagulant floc. This study sought to understand the fundamental factors that lead to bubble formation and corresponding floating floc during coagulation and sedimentation. Gas bubbles (causing the floating floc) can form whenever the total dissolved gas (TDG) pressure exceeds the local solution pressure, which can occur during rapid mixing since high fluid velocities impose minimum pressure within the coagulation system. Furthermore, very high rate rapid mixers, which often are preferred for instantaneous chemical dispersion, can cause bubble formation even in waters undersaturated with dissolved gas relative to the atmosphere. The formation and stability of floating floc are dependent on equilibrium and mass transfer kinetics of the system, both of which are a function of many system properties including the local solution pressure, amount and type of dissolved gas supersaturation, and temperature. Other design and operation properties also influences the formation and stability of floating floc including the length of rapid mixing, surface chemistry of the mixing paddle, and attachment forces.

INTRODUCTION:

Gas bubbles suspended in solution can attach to coagulated floc particles creating “floating” or “rising” floc in conventional drinking water treatment plants (Figure 3.1). Floating floc reduces settling efficiency during sedimentation. Subsequent floc carry-over can overload filters, such that in extreme events, the filter can become the only physical barrier for pathogen and particle removal. Even bubbles detectable only by close visual inspection (bubble diameters ≤ 0.5 mm) can potentially cause floating floc. For example, given that the density of floc particles (aluminum or iron hydroxide plus turbidity) is often only slightly greater than that of

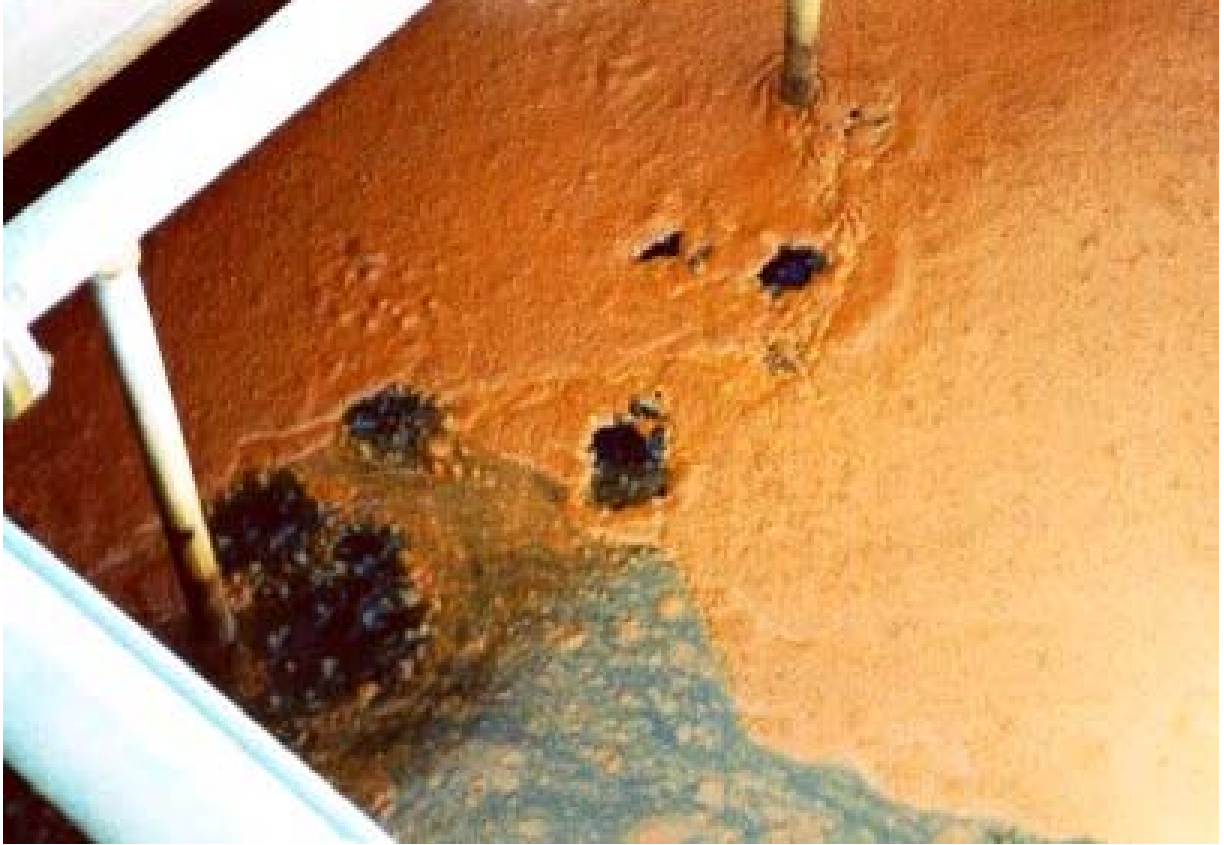


Figure 3.1 – Floating Floc Collected above a Filter at a Water Treatment Plant.

water (e.g., 1.1 g/mL floc), consideration of particle buoyancy indicates that settling of 1 g of floc would be prevented if 0.03 mL of bubbles were attached.

Gas bubbles can form in solution whenever the total dissolved gas (TDG) pressure exceeds the local solution pressure. Under such conditions, the water is considered supersaturated with dissolved gas. Since dissolved gas supersaturation can result from mechanical, chemical, or microbial processes (Scardina and Edwards, 2002), plants can experience daily, seasonal, or diurnal events that can lead to bubble formation and subsequent floating floc.

Utilities afflicted with these problems often make futile attempts to improve settling of the floating floc, and in other cases utility personnel do not even know how to recognize bubbles as the problem. A better fundamental understanding is necessary to educate treatment plant operators and managers as to the consequences of bubble formation with respect to plant operation. Root causes and possible solutions to these problems, therefore, need to be clearly identified.

This study investigated the initial formation and then stability of floating floc during conventional coagulation-sedimentation processes. Various design and operational parameters of a coagulation system and also intrinsic properties of the raw water solution were varied in benchscale laboratory experiments. The overall development of floating floc was observed, with the goal of determining simple procedures to mitigate this problem.

MATERIALS AND METHODS:

Benchscale laboratory coagulation experiments were conducted with a standard jar tester (maximum mixing speed = 160 rpm) using 1 L square jars (9 cm side length). The paddles had a dimension of 7.5 x 2.5 x 0.1 cm and were positioned in the middle of the jars. Portable devices (drills) were used in some experiments to rapid mix at higher rpm's as measured by a tachometer. When using the drills, the top of the jars had to be covered to prevent water loss.

For each experiment, 0.85 g of NaNO₃ and 1.0 mL of a 0.52 M as SO₄⁻² Na₂SO₄ stock solution were added to the jars prior to filling to 1 L with distilled-deionized source water. No additional turbidity particles were added to these solutions, which were then dosed with either a 0.13 M as Al liquid stock solution of alum (Al₂(SO₄)₃•18H₂O) or 0.27 M as Fe FeCl₃•6H₂O coagulant. Since coagulant flocs formed quickly at a dose of 14.5 mg/L as Al, this alum dosage was used throughout most of the study. At the start of rapid mixing (time, t = 0), the coagulant was added along with 1 M sodium hydroxide (NaOH). The two chemicals were dosed at opposing corners of each jar to produce a final coagulation pH of 6.0 ± 0.2. The ionic strength of most alum coagulated waters with dissolved nitrogen supersaturation was 0.016 M.

For all experiments, the waters were rapid mixed between 0 – 600 sec depending on the experiment, flocculated for 30 min, and allowed to settle for 30 min. The rapid mix and flocculation rates (revolutions per minute, rpm) were varied as specified for each experiment, and mixing intensities were converted into mean velocity gradients (G values) using equations outlined in Droste (1997).

The final settled turbidity, pH, total dissolved gas (TDG), and volume of floating floc were measured at the end of 30 min of sedimentation. Final settled turbidity samples were drawn from the middle of the jar and measured with a HACH 2100 N benchtop turbidimeter. It is understood that suspended gas bubbles measure as turbidity (HACH, 1997), and since samples were not degassed prior to measurement, gas bubbles may have contributed to the solution

turbidity. However, it is generally believed that their contribution was slight since 5 minutes was allowed for bubbles to rise from within mixed collected sample solutions.

In this study, the driving force for gas bubble formation was created by supersaturating the water with dissolved gas (Scardina and Edwards 2001). A total dissolved gas probe (TDGP) manufactured by Sweeney Aquametrics was used to measure the total dissolved gas (TDG) pressure of the solution. Most data are reported as gauge pressures (± 0.002 atm) referenced to the local barometric pressure which is also measured by the TDGP (± 0.002 atm). For example, a water at equilibrium with 1 atm barometric pressure (100% saturation) would have a TDG of 0 atm gauge pressure or 1 atm absolute pressure. Any dissolved gas supersaturation or undersaturation would have a positive or negative gauge pressure, respectively. The TDGP also corrects the TDG pressure based upon the solution temperature, which is also measured by the TDGP (± 0.1 °C).

The distilled and deionized source water was initially undersaturated with dissolved gas: TDG between -0.013 and -0.066 atm gauge pressure. The source water was then placed in an enclosed chamber where the headspace above the water was pressurized with nitrogen gas at 0.2 – 0.35 atm gauge pressure. The water in this pressurized chamber was stirred to increase transfer of gas into solution. Initial TDG measurements indicated that 0.07 atm gauge pressure was lost during transfer from the pressurized chamber to the coagulation jars, so the water was pressurized inside the chamber to 0.27 atm gauge pressure to give an initial supersaturation of 0.20 atm gauge pressure within the coagulant jars at the start of all experiments, unless otherwise indicated.

In some experiments, the solutions were supersaturated (0.20 atm total gauge pressure) with dissolved carbon dioxide. The source water was initially aerated to saturation (0.00 atm gauge pressure). Sodium bicarbonate was added to the aerated solution, and after acidifying to pH 6.0, the bicarbonate alkalinity was converted to dissolved carbon dioxide. Initial measurements determined that 1.50 g/L as NaHCO_3 produced 0.20 atm absolute pressure carbon dioxide after acidification, creating solutions that were supersaturated with dissolved gas at 0.20 atm total gauge pressure. The final ionic strength of these solutions was 0.029 M.

RESULTS AND DISCUSSION:

The fundamental factors that influence bubble formation and floating floc are first introduced, followed by a qualitative description of jar test observations. A series of jar tests are then shown that confirm key hypotheses. Finally, some additional considerations with respect to coagulation systems and floating floc are presented.

Fundamental Background on Bubble Formation during Coagulation and Mixing

Bubbles at Equilibrium with Dissolved Gas

A gas bubble can form in solution whenever the total dissolved gas (TDG) pressure exceeds the local solution pressure, i.e. dissolved gas supersaturation. Since most conventional treatment plants function essentially as closed systems with respect to the atmosphere in terms of gas transfer across the liquid atmosphere interface (Letterman and Shankar, 1996), bubble formation can be the major mechanism of alleviating dissolved gas supersaturation. Given the initial dissolved gas supersaturation in most of these experiments (0.2 atm gauge pressure), the bubbles originated via heterogeneous nucleation from pre-existing gas pockets located on solid surfaces, such as the mixing paddle or side of the jar (Figure 3.2) (Scardina and Edwards, 2001; Harvey, 1975). The number and type of nucleation sites are related to the roughness and hydrophobicity of the surfaces (Ryan and Hemmingsen, 1998), and surfactants can either promote or reduce bubble formation (Hilton et al., 1993).

Conceptually, a modified closed system analysis is useful for predicting gas transfer and bubble formation in treatment plants. Considering water initially supersaturated with dissolved gas at a concentration $[C(t = 0)]_x$ for each individual gas species x , bubbles can continue forming or growing until the system reaches equilibrium with the newly formed gas phase and not the atmosphere (Figure 3.3). For conditions typically present in water treatment (dilute solutions with respect to atmospheric gases), Henry's gas law is applicable, rather than Raoult's law (Betterton, 1992), for dissolved gas equilibrium of gas species x :

$$[C_E]_x = pG_x \cdot K_{h(x)}, \quad (\text{Equation 3.1})$$

where $[C_E]_x$ is the equilibrium dissolved gas concentration, pG_x is the partial pressure in the gas phase, and $K_{h(x)}$ is Henry's gas law constant which is temperature dependent. Equilibrium

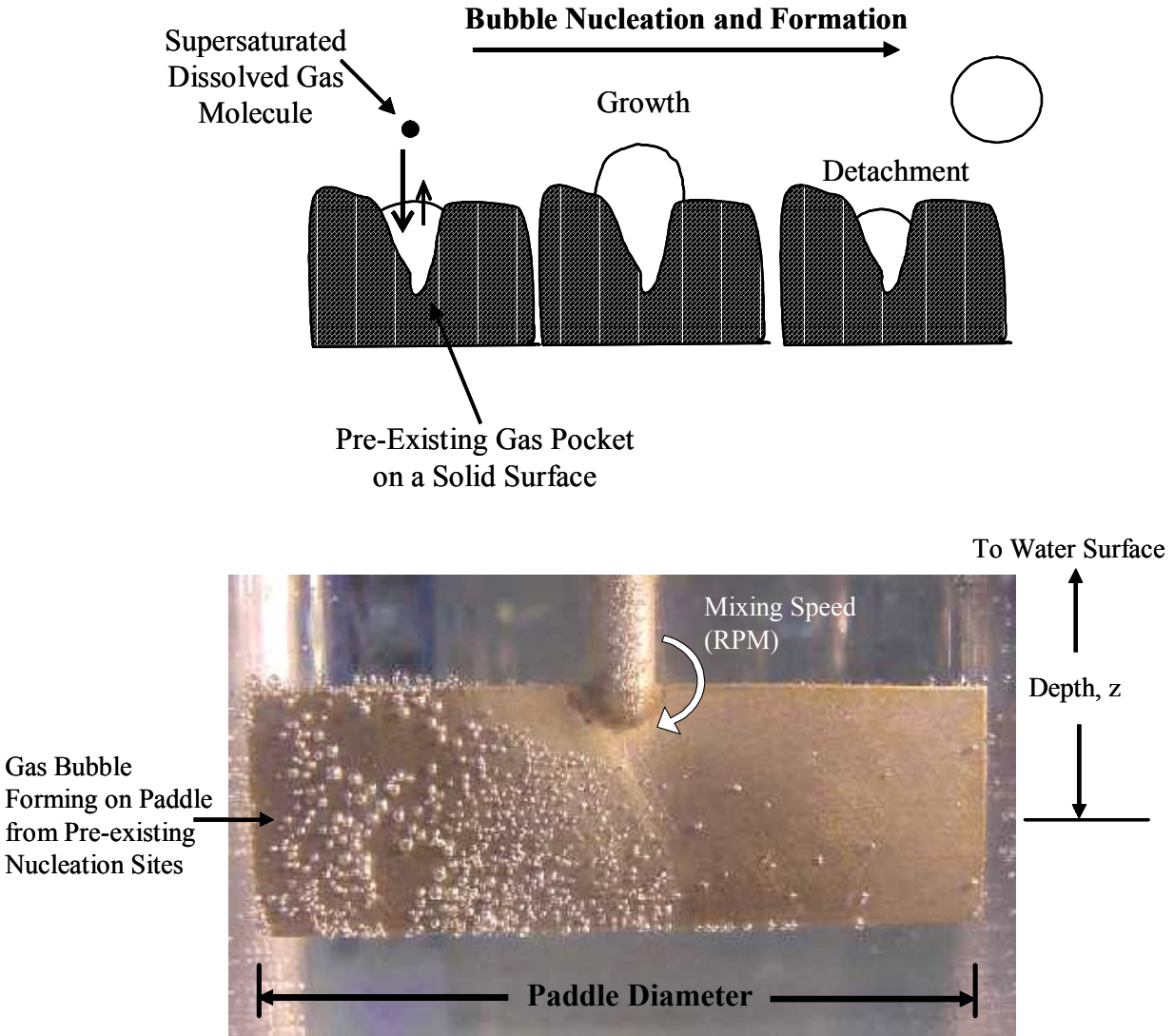


Figure 3.2 – Gas Bubble Formation by Heterogeneous Nucleation: Schematic (Top) and on the Mixing Paddle (Bottom).

Paddle Rotation Was Clockwise. Some Bubbles Are also Present on the Wall of the Jar.

conditions would, therefore, be a function of the amount of initial dissolved gas supersaturation, local pressure, dissolved gas type, and solution temperature.

A gas bubble equilibrium model based upon this modified closed system assumption (Scardina and Edwards, 2001) can be used to estimate the volume of bubbles formed (mL/L) and the equilibrium dissolved gas concentration $[C_E]_x$ for solutions initially supersaturated with dissolved gas. The volume of the gas bubble includes any dissolved gases that transferred to the gas phase plus water vapor, assuming that the pressure within the bubble equals the barometric

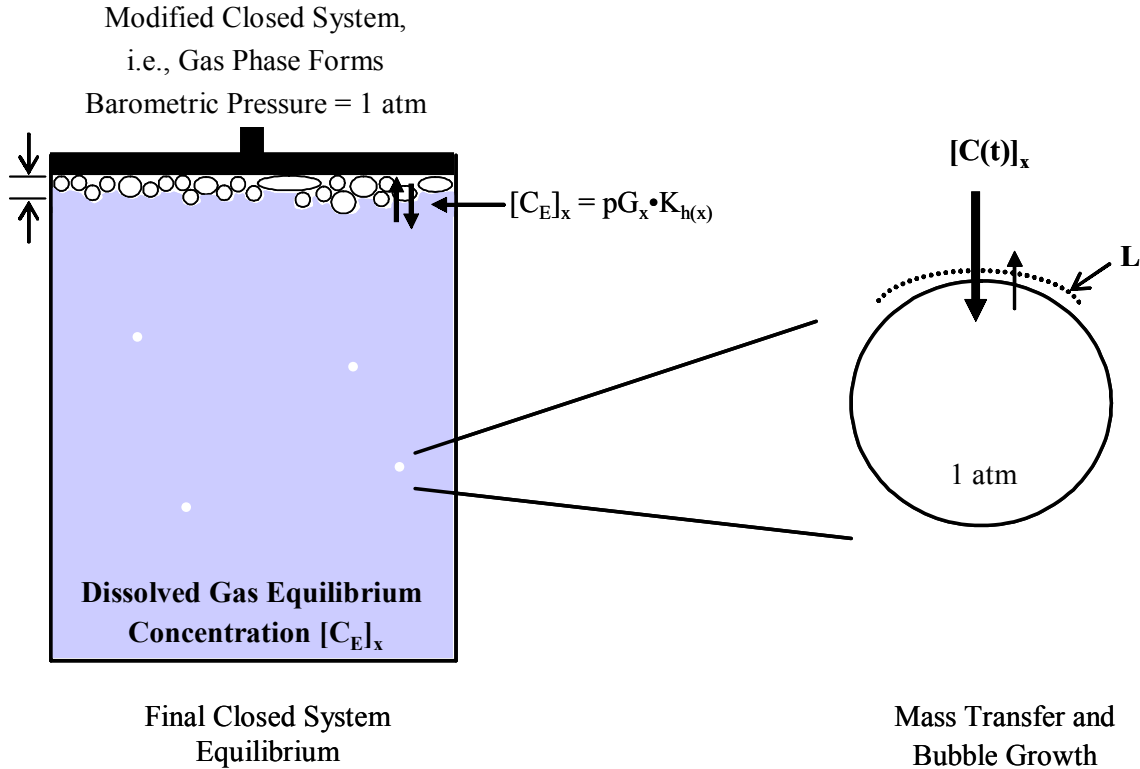


Figure 3.3 – Gas Bubbles Form until Equilibrium Is Reached Between Water and Local Atmosphere for Each Dissolved Gas(x) (Left), and Conceptualization of Gas Transfer Kinetics as System Approaches Equilibrium via Bubble Formation (Right).

pressure (Figure 3.3). For example, consider two types of waters at 20 °C both starting with 0.2 atm gauge pressure dissolved gas supersaturation (Table 3.1). One water is supersaturated with 1.2 atm absolute pressure dissolved nitrogen. The second water is initially aerated with 79% nitrogen and 21% oxygen at 1.0 atm absolute pressure, and an additional 0.2 atm absolute pressure dissolved carbon dioxide is formed by addition of NaHCO_3 and acid. Henry's law can be used to convert partial pressures to concentration units (Equation 3.1).

The difference between the initial known $[C(t)]_x$ and predicted equilibrium concentration $[C_E]_x$ (by the modified closed system model) of each individual dissolved gas (x) would be the amount of gas transferred to the gas bubbles per 1 L solution. In the system supersaturated at 0.2 atm gauge pressure nitrogen, the modified closed system model predicts that 1.6×10^{-4} moles of nitrogen would transfer to the gas bubbles, and including the additional contribution of water vapor, the total bubble volume formed would be 3.9 mL (Table 3.1). In the other water with 0.2 atm gauge pressure carbon dioxide supersaturation, only 0.5×10^{-4} moles of carbon dioxide are predicted to transfer to gas bubbles (Table 3.1). Although a smaller amount of carbon dioxide

Table 3.1 – Illustrative Calculation of Gas Type and Temperature Relative to Bubble Formation.

Type of Dissolved Gas Supersaturation	Initial TDG (atm, absolute)	Temperature (°C)	Initial Dissolved Gas Concentration [C(t)] _x (M)	Equilibrium Dissolved Gas Concentration ¹ [C _E] _x (M)	Initial Driving Force [C _I - C _E] _x (M)	Diffusion Constant ² (D _L) (cm ² /s)	Equilibrium Bubble Formation ¹ (mL/L)	Initial Mass Transfer Rate ³ (nanomoles/hr)	Measured Floating Floc ⁴ (mL/L)
Nitrogen	1.20	20	8.34x10 ⁻⁴	6.79x10 ⁻⁴	1.55x10 ⁻⁴	1.806x10 ⁻⁵	3.91	10	14.5
Carbon Dioxide ⁵	CO ₂	0.20	78.68x10 ⁻⁴	78.23x10 ⁻⁴	0.45x10 ⁻⁴	1.311x10 ⁻⁵	5.53	13.3	0
	N ₂	0.79	5.49x10 ⁻⁴	4.15x10 ⁻⁴	1.34x10 ⁻⁴	1.806x10 ⁻⁵			
	O ₂	0.21	2.91x10 ⁻⁴	2.50x10 ⁻⁴	0.41x10 ⁻⁴	1.643x10 ⁻⁵			
Carbon Dioxide ⁵	CO ₂	0.10	39.41x10 ⁻⁴	39.30x10 ⁻⁴	0.11x10 ⁻⁴	1.311x10 ⁻⁵	2.70	6.6	1.1
	N ₂	0.79	5.49x10 ⁻⁴	4.74x10 ⁻⁴	0.75x10 ⁻⁴	1.806x10 ⁻⁵			
	O ₂	0.21	2.91x10 ⁻⁴	2.70x10 ⁻⁴	0.21x10 ⁻⁴	1.643x10 ⁻⁵			
Nitrogen and Carbon Dioxide ⁵	N ₂	1.10	7.65x10 ⁻⁴	6.10x10 ⁻⁴	1.55x10 ⁻⁴	1.806x10 ⁻⁵	4.35	10.9	0
	CO ₂	0.10	39.41x10 ⁻⁴	39.23x10 ⁻⁴	0.18x10 ⁻⁴	1.311x10 ⁻⁵			
Nitrogen	1.20	10	10.02x10 ⁻⁴	8.25x10 ⁻⁴	1.77x10 ⁻⁴	0.690x10 ⁻⁵	4.22	4.4	5.2

¹Calculated with the Scardina and Edwards Modified Closed System Model (2001).

²Diffusion Constants Calculated from Hayduk and Laudie (1974) and Converted to Appropriate Temperature Using Selleck and et al. (1988).

³Diffusion Layer Thickness (L = 0.1 mm) and Surface Area (SA = 1 mm²) Assumed to Be Constant for Initial Conditions.

⁴Waters Rapid Mixed at 80 rpm (G = 120 sec⁻¹) for 60 sec and Flocculated at 5 rpm (G = 2 sec⁻¹).

⁵ Solution Initially Supersaturated by Acidifying Carbonate System to pH of 6.0.

transferred to the gas bubble phase, this carbon dioxide would cause the equilibrium to be altered for other dissolved gases in this system, nitrogen and oxygen. Nitrogen and oxygen would then transfer to the gas bubbles until their respective equilibrium is reached (Scardina and Edwards, 2001). Thus, including all the dissolved gases in this newly formed gas bubble, a larger total bubble volume 5.5 mL should result in this water which was initially only supersaturated with carbon dioxide (Table 3.1).

These examples illustrate the importance of the initial system conditions in relation to total bubble formation. A similar comparison of dissolved nitrogen supersaturation (0.2 atm gauge pressure) at 10 °C and 20 °C suggests that colder solutions also form more gas volume when equilibrium is reached (Table 3.1).

Mass Transfer of Dissolved Gas to Gas Bubbles

In the benchscale experiments to be discussed later, waters initially supersaturated with dissolved gas did not reach equilibrium, as indicated by TDG measurements on settled waters. Thus, the rate of mass transfer from the dissolved phase to the gaseous phase is also a controlling factor in bubble formation. The rate of mass transfer $(dM/dt)_x$ in units of nanomoles/hr would be a function of the system conditions (Figure 3.3):

$$\text{Mass Transfer} = (dM/dt)_x = K_L \cdot SA \cdot [C(t) - C_E]_x. \quad (\text{Equation 3.2})$$

The mass transfer parameter K_L (cm/sec) is the liquid diffusion constant D_L (cm²/sec) divided by the diffusion layer thickness L (mm) (Figure 3.3). Dissolved gases transfer across a bubble or pre-existing gas pocket surface area SA (mm²). The driving force of bubble formation is the difference between the actual (supersaturated) dissolved gas concentration and the concentration at equilibrium $[C(t) - C_E]_x$ (M) for each particular gas. For calculations of relative mass transfer rates, the diffusion layer thickness L and surface area SA were assumed to be 0.1 mm and 1 mm², respectively, for all systems.

The diffusion constant (D_L) varies for each dissolved gas (Hayduk and Laudie, 1974) and is a function of the solution temperature (Selleck and et al., 1988). The diffusion constant can have significant effects on the rate of bubble formation. For example, as shown previously the driving force is greater for a water at 10 °C and 1.2 atm absolute pressure dissolved nitrogen, than for a water with the same TDG at 20 °C. However, lower diffusion in the colder solution

causes a 56% reduction in the overall rate of mass transfer (Table 3.1). Yet, if this water was given sufficient time to reach equilibrium, then the total bubble formation would be about 8% greater in the colder solution (Table 3.1).

The concentration driving force $[C(t) - C_E]_x$ also affects mass transfer (Equation 3.2). Consider the previous example with a water supersaturated with nitrogen compared to a water supersaturated with carbon dioxide. Due to its larger total initial driving force, a greater mass transfer rate would be expected in the water supersaturated with carbon dioxide (Table 3.1). Again, carbon dioxide would only be a portion of the total bubble formation and gas transfer. The mass transfer of nitrogen, oxygen, and carbon dioxide causes a 31% faster rate of gas bubbles formation (13.3 nanomoles/hr), than if the water contained only dissolved nitrogen (10.0 nanomoles/hr) (Table 3.1).

Mass transfer, like equilibrium, is a fundamental property controlling bubble formation and the development of floating floc. As shown, the rate of mass transfer is also dependent on many initial system properties.

Location of Gas Bubble Nucleation

The mechanism by which bubbles form in water treatment plants is heterogeneous nucleation (Scardina and Edwards, 2001; Harvey, 1975). Bubbles could form primarily on the mixing paddle, since this is often a location of minimum pressure in the system (Figure 3.2). As the paddle rotates through the fluid at a high rate, the higher velocity would reduce the local solution pressure, which has been described by the energy equation for similar conditions of flow within pipes:

$$\frac{P}{\lambda} + \frac{V^2}{2g} + z = \text{Constant.} \quad (\text{Equation 3.3})$$

Due to the non-ideal turbulent mixing environment, the energy equation (Equation 3.3) is not a perfect description of the local solution pressure (P) in a jar test, but it can illustrate key concepts (Robertson and Crowe, 1993). The velocity (V) was assumed to be the product of the mixing speed (rpm) and the circumference made by the rotating paddle at a particular depth (z) (Figure 3.2, bottom). Even if bubbles cannot form on a paddle at rest because the local solution pressure

is greater than the TDG pressure, mixing can reduce the local solution pressure to conditions favorable for bubble formation ($TDG > \text{local pressure}$) (Figure 3.4).

Although the actual local solution pressure at the paddle surface is nearly impossible to calculate or measure directly, a manometer tube positioned on each side of the mixing paddle can provide another estimate of the local pressure (Figure 3.5). A lower local pressure during mixing would decrease the height of water in the manometer tube, as monitored with gradations marked on the shaft (Figure 3.5). Using this device, it was shown that the local solution pressure during rapid mixing was lower than the non-mixing hydrostatic pressure (Figure 3.6), and the local solution pressure rapidly decreased at higher mixing speeds (Figure 3.6, Bottom). At mixing speeds greater than 305 rpm, all of the water in the manometer tube was completely evacuated, suggesting negative local gauge pressures at the paddle surface (Figure 3.6, Bottom).

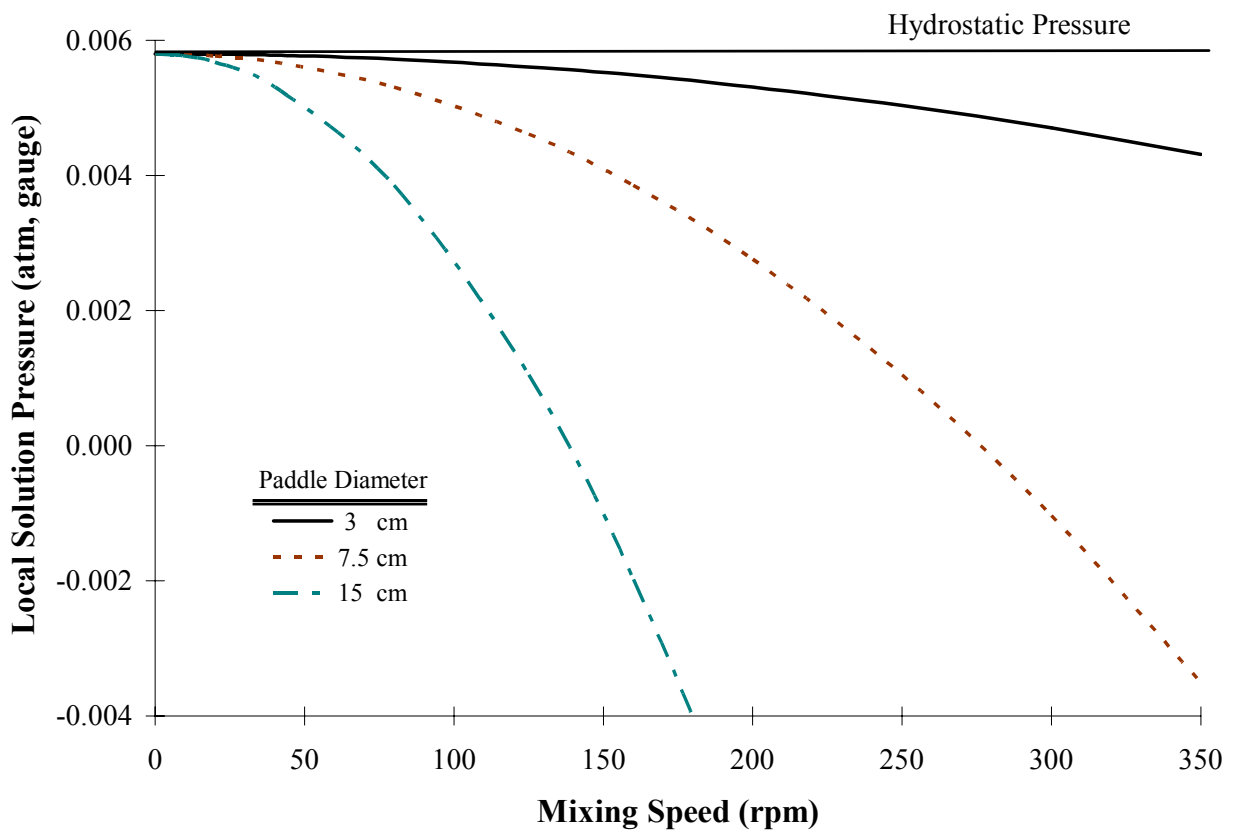


Figure 3.4 – Calculated Local Solution Pressure at the Outer Most Tip of the Paddle Estimated for the Jar Tester at a Depth of 6.0 cm Using the Energy Equation (Equation 3.3).



Figure 3.5 – Crude Manometer Tube Affixed to Mixing Paddle.

For a given mixing speed, the pressure was consistently lower on the back side of the paddle (Figure 3.6, Top). When a paddle moves through a solution, the fluid streamlines separate and break around the paddle, creating a very turbulent area on the backside of the paddle known as a wake (Birkhoff, 1957; Van't Riet and Smith, 1975). At very high mixing rates, the wakes can also become gaseous cavities (Birkhoff, 1957). This was in agreement with the fact that bubble formation was more prominent on the back of the paddle (left side of the paddle in Figure 3.2, Bottom).

The manometer data was actually fairly well approximated by the energy equation (Equation 3.3) (Figure 3.6). Given the formation of wakes, though, the measured local solution pressure on the backside of the paddle was on average 25% less than that predicted by the energy equation in these experiments.

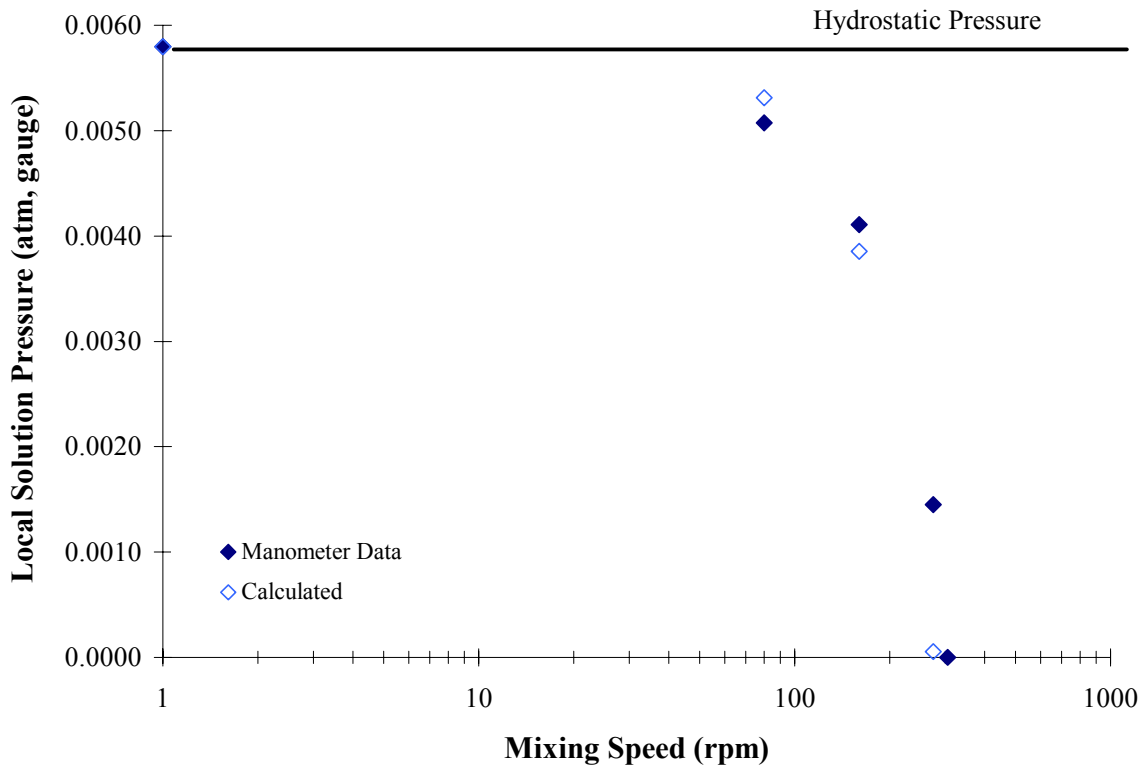
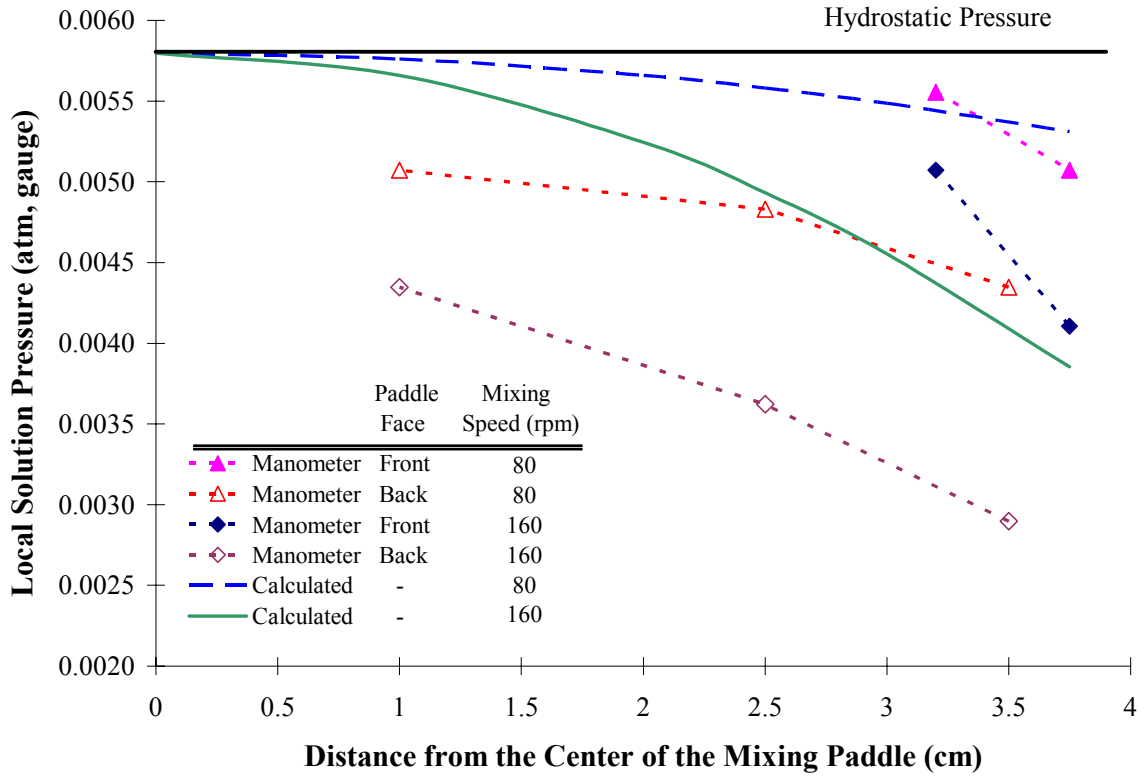


Figure 3.6 – Change in Local Solution Pressure while Mixing for the Front and Back of the Paddle Face (Top) and for the Front Face as a Function of Different Mixing Speeds (Bottom). The Energy Equation (Equation 3.3) Was Used to Calculate the Local Solution Pressure.

Generalized Observations Related to Bubble Phenomenon in Jar Tests

The formation of floating floc during jar tests was reproducible in benchscale laboratory experiments. Floating floc in most experiments was associated with reduced particle removal and settling efficiency, and the final turbidity of water after settling was sometimes higher in the solutions with floating floc than waters with no floating floc (Figure 3.7). However, it was evident that final settled turbidity was not a good indicator of treatment disruptions caused by gas bubbles, since so much of the floc was floating (Figure 3.7). To quantify the floating floc, a new parameter was developed where the diameter and thickness of the floc floating at the water surface was measured to estimate the total volume of floating floc (mL/L) (Figure 3.8). This estimation was reproducible between ± 1 mL or $\pm 10\%$, whichever is greater.

After filling the coagulant jars with water supersaturated with dissolved gas, many minute bubbles could be seen in solution upon close inspection originating from nucleation sites on the bottom and sides of the jars. Without mixing, these bubbles would float to the water surface in about one minute. Some of these “pre-existing” bubbles probably contributed to

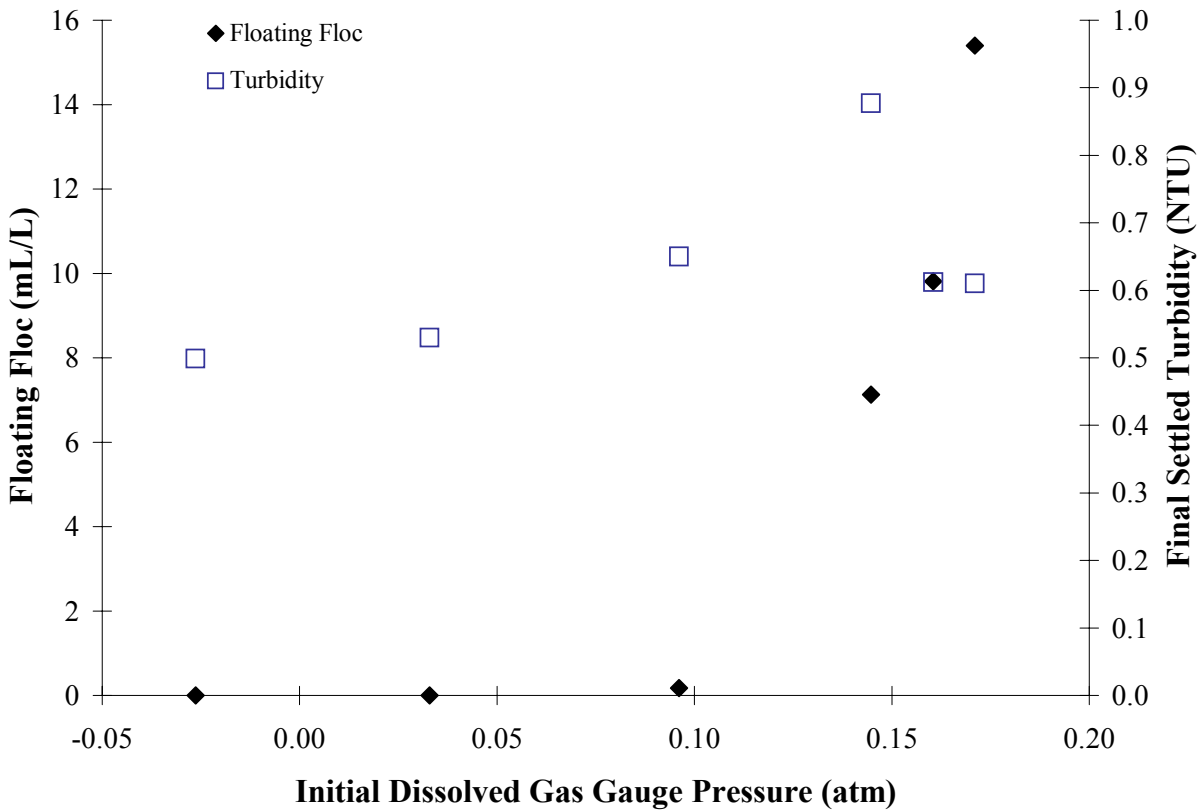


Figure 3.7 – Preliminary Alum Experiment.
Solutions Were Rapid Mixed at 80 rpm ($G = 120 \text{ sec}^{-1}$) for 60 sec and Flocculated at 5 rpm ($G = 2 \text{ sec}^{-1}$).

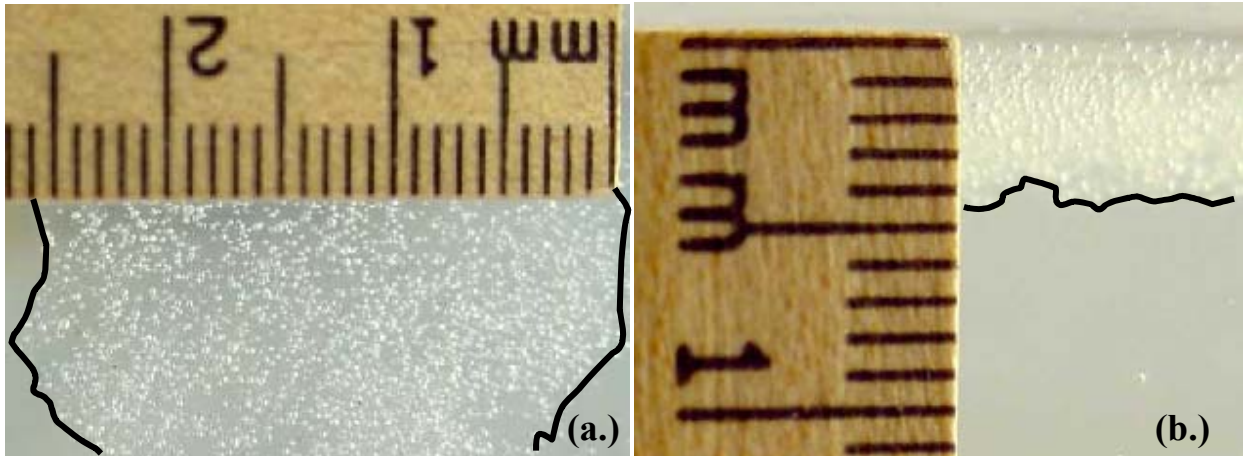


Figure 3.8 – Quantification of Alum Floating Floc by Estimating the Surface Diameter (a.) and the Depth/Thickness (b.) of the Floating Floc.

Black Lines Added to the Figure to Accent Outline of Floating Floc.

floating floc, since rapid mixing usually began within a minute of filling the first jar. In an experiment where these bubbles were allowed to leave solution prior to rapid mixing, there was 35% less floating floc than in similar waters that were rapid mixed [$G = 120 \text{ sec}^{-1}$ for 60 sec] immediately after filling the jars. It was clear, then, that most bubbles were forming during rapid mixing (Equation 3.3).

Bubble formation could be classified dependent on whether the bubbles attached to floc. That is, many of the larger gas bubbles (diameter = 1 – 2 mm) did not attach to coagulant floc and floated quickly to the water surface at the start of slow mixing without major disruptions to flocculation or sedimentation. Smaller gas bubbles (diameter ≤ 0.2 mm) were seemingly held in suspension during the slow mix flocculation and could readily attach to newly formed coagulant floc, and these bubbles often were not visible until after a few minutes of slow mixing.

The bubbles that initially attached to the coagulant floc were observed to have several possible fates:

1. bubble(s) floated the coagulant floc to the water surface,
2. some floc settled properly even with bubbles attached,
3. bubbles on settled floc sometimes continued to grow, causing previously settled floc to re-suspend with time,
4. bubbles detached from the floating floc, allowing the floc to settle,

5. bubbles floating to the water surface could disrupt other floating floc, separating previously attached bubbles from the floc.

Bubbles were sometimes broken free of the floc by mixing, and more rigorous mixing caused more detachment.

Changes in floating floc volume are therefore a function of factors causing its formation and factors that destroy it:

$$\frac{\partial \text{Floating Floc}}{\partial \text{Time}} = \text{Formation} - \text{Losses}. \quad (\text{Equation 3.4})$$

Conceptually, formation of floating floc is probably described by an equation with the following terms:

$$\text{Formation} \approx (\text{Bubble Concentration})(\text{Attachment Factors})(\text{Floc Concentration})(\text{Extent of Local Dissolved Gas Supersaturation}). \quad (\text{Equation 3.5})$$

That is, without floc or bubbles, floating floc formation is zero. Likewise, if the bubbles and floc are both present but do not attach, then floc cannot be floated. More detailed explanations of these phenomena can be found in the dissolved air floatation literature (Edzwald, 1995).

In addition, the surface properties of the coagulant could influence the degree of bubble attachment and nucleation, since a hydrophobic surface typically creates more nucleation sites for bubble formation and is more likely to attach to a preformed bubble than a hydrophilic surface (Harvey, 1975). Solid iron hydroxide $[\text{Fe}(\text{OH})_{3(s)}]$ is often considered more hydrophobic than solid aluminum hydroxide $[\text{Al}(\text{OH})_{3(s)}]$, which is more hydrated (Edzwald, 1995). Since the surface charge of gas bubbles and solid particles can vary significantly depending of properties of the solution, electrostatic forces can also influence bubble attachment to floc.

Losses in floating floc volume are probably described by an equation with the following terms:

$$\text{Losses} \approx (G)(\text{Volume of Floating Floc})(\text{Attachment Factors}). \quad (\text{Equation 3.6})$$

In other words, loss requires the presence of pre-existing floating floc volume. Faster mixing (G) will cause detachment, and the strength by which bubbles are held by floc will also play a role.

Consistent with these concepts, typical results at a given mixing speed (160 rpm, $G = 335 \text{ sec}^{-1}$) led to a maximum volume of floating floc at a specified time (Figure 3.9). Bubble concentrations were high early in the mixing sequence, so floating floc increased rapidly for a time (zone 1). At longer mixing times, the volume of floating floc declines (zone 2), which can be explained by two possibilities: bubble growth continued during rapid mixing with larger bubbles leaving the solution quickly (i.e., low bubble concentration in Equation 3.5) or bubbles attached to floc are detached by mixing (Equation 3.6). Eventually, if mixing times are long enough, no floating floc remains (zone 3). A sharp peak in floating floc volume was observed at a mixing time of 15 sec for this system (0.2 atm gauge pressure, 160 rpm, $G = 335 \text{ sec}^{-1}$). Experiments also demonstrated that bubble attachment to floc may be important and change with time. Specifically, if the water in Figure 3.9 was rapid mixed 600 sec without coagulant and then coagulant was suddenly dosed with 15 sec of additional rapid mixing, 2.9 mL/L floating floc formed. No floating floc was present after this total rapid mix time when coagulant was added at the start, even though the dissolved gas content was the same.

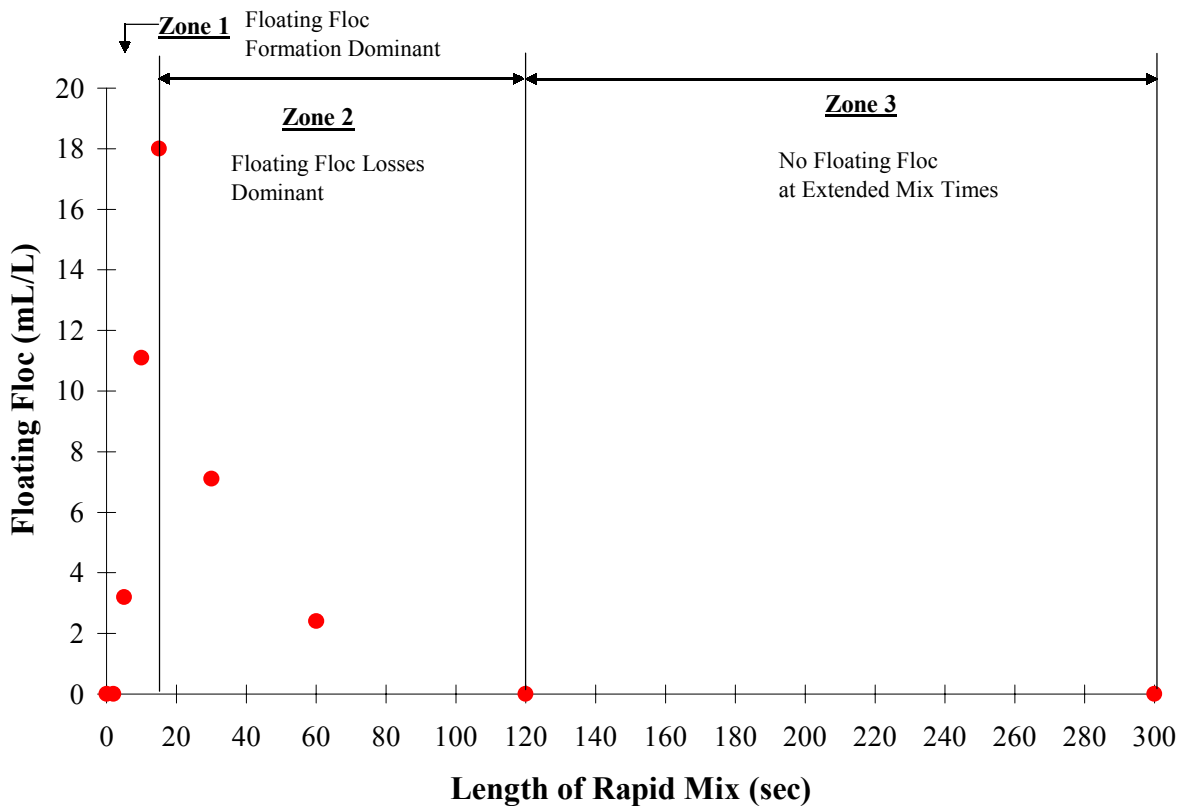


Figure 3.9 – Variations in Floating Floc as a Function of the Rapid Mix Length. Solutions Were Initially at 0.20 atm Gauge Pressure, Rapid Mixed at 160 rpm ($G = 335 \text{ sec}^{-1}$), and Flocculated at 5 rpm ($G = 2 \text{ sec}^{-1}$).

Quantitative Results in Relation to Background, Theory, and General Observations

Importance of Surface Nucleation Sites

Experiments tested the effects of altering either the mixing paddle surface or the water quality (by addition of surfactants), while the water was initially supersaturated at 0.2 atm dissolved nitrogen gauge pressure. The amount of bubble formation was observed on the paddle and photographed after 30 min while mixing at 40 rpm ($G = 42 \text{ sec}^{-1}$) (Figure 3.10). Each scenario was compared to a control solution with an unaltered paddle and without any surfactants (Figure 3.10, a.). Since regular dishwashing soap appeared to reduce the amount of gas bubble nucleation on the paddle (Figure 3.10, b.), further testing examined other surfactants at concentrations close to those applied during water treatment: hexametaphosphate and natural organic matter (NOM). Although NOM (2 mg/L as C) did not seem to significantly change the bubble formation compared to the control (Figure 3.10, c.), bubble formation was markedly reduced when hexametaphosphate (3.5 mg/L as P) was present in solution (Figure 3.10, d.).

Bubble nucleation was not significantly enhanced by roughing the paddle with coarse sand paper (Figure 3.10, e.), yet polishing the paddle with a smooth grinder did change the nature of nucleation, creating many gas bubbles with much smaller diameters than the control (Figure 3.10, f.). In this test, interestingly, no bubbles were noted on a colored mark that was used to designate the polished side (Figure 3.10, f.). When a regular paddle was completely marked with the same permanent marker, the amount of bubble formation was greatly reduced (Figure 3.10, g.). Similar results occurred with a completely painted paddle (Figure 3.10, h.). The marker and paint most likely made the surface more hydrophobic, but it is also speculated that the marker/paint smoothed surface imperfections, thereby reducing the number of nucleation sites. A smooth hydrophobic surface produces little bubble formation (Ryan and Hemmingsen, 1993). This result highlighted the importance of nucleation sites and the condition of the paddle.

If a modified, painted paddle surface caused a reduction in gas bubble nucleation, would this then lead to less floating floc in a jar test? To test this hypothesis, jar tests were conducted with waters that were supersaturated initially at 0.2 atm gauge pressure, rapid mixed at 80 rpm ($G = 120 \text{ sec}^{-1}$) for 60 sec, and flocculated at 5 rpm ($G = 2 \text{ sec}^{-1}$). When the paddles were completely painted with the permanent marker, the amount of floating floc was less (4.8 mL/L) than in control experiments with unmodified paddles (14.5 mL/L)—a result significant at greater than 95% confidence (Figure 3.11). The net conclusion is that for systems where bubble

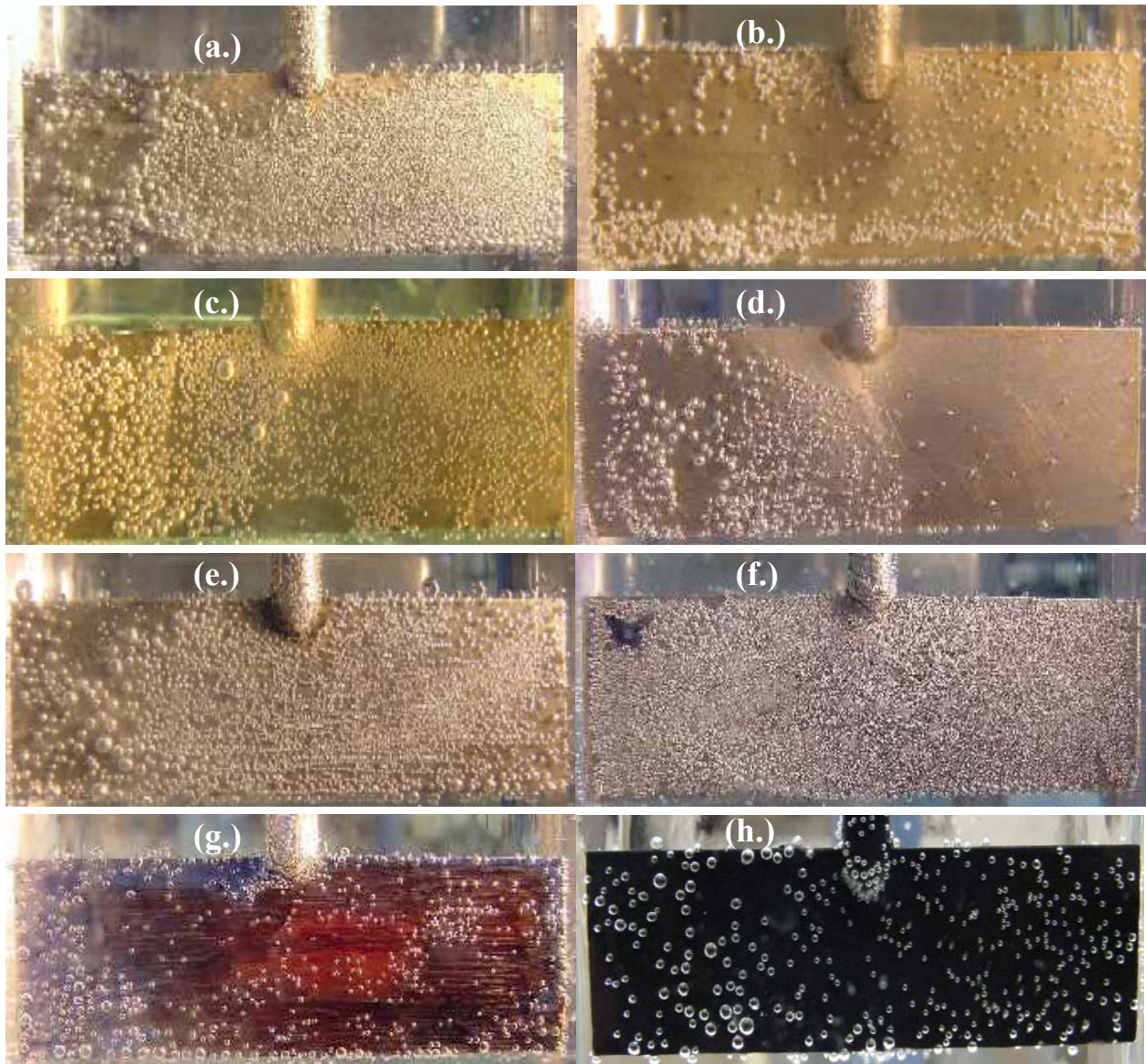


Figure 3.10 – Visual Observations of Bubble Nucleation on Paddle during Nucleation
 Experiments: (a.) Control, (b.) Dish Soap, (c.) NOM, (d.) Hexametaphosphate, (e.) Sandpaper,
 (f.) Fine Polish, (g.) Permanent Marker, (h.) Paint.
 Solutions Were Mixed at 40 rpm ($G = 42 \text{ sec}^{-1}$). Painting the Surface Could Smooth Surface Imperfections that
 Cause Gas Bubble Nucleation or Could Make the Surface More Hydrophobic.

formation occurs on the mixing paddle, painting or replacement with a different paddle material could greatly decrease the amount of bubble formation and floating floc.

Since the number and type of nucleation sites appeared to influence the amount of floating floc, it was anticipated that other sources of nucleation sites such as bentonite clay might also increase bubble formation. In another jar test with unmodified paddles, the waters initially

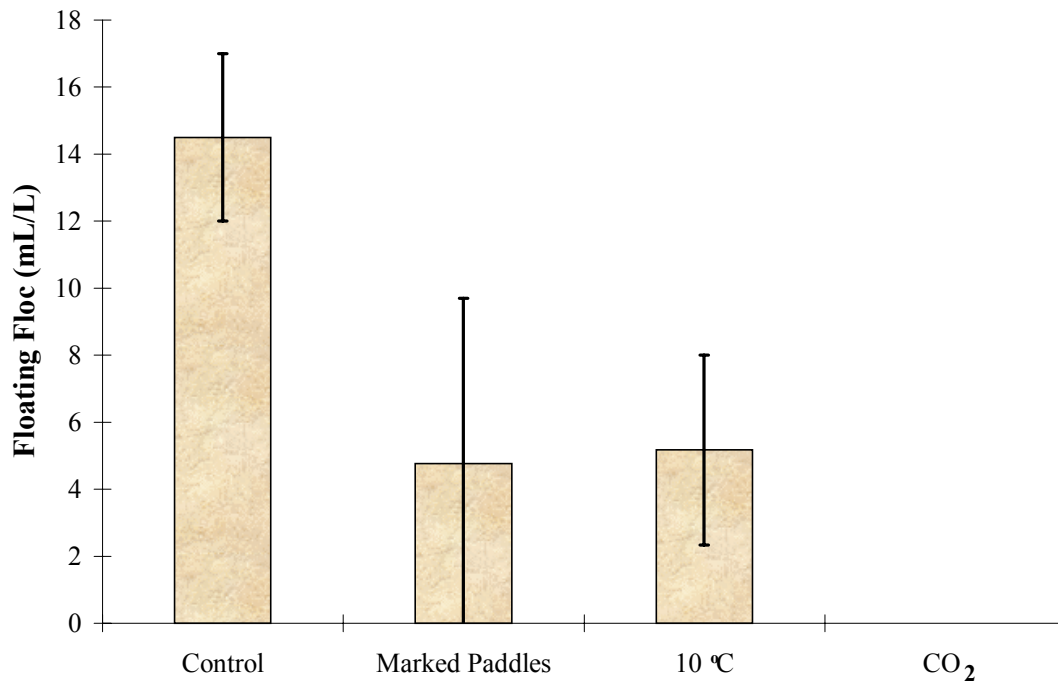


Figure 3.11 – Factors Affecting Gas Bubble Nucleation and Floating Floc.

Solutions Were Initially at 0.20 atm Gauge Pressure, Rapid Mixed at 80 rpm ($G = 120 \text{ sec}^{-1}$) for 60 sec, and Flocculated at 5 rpm ($G = 2 \text{ sec}^{-1}$). The Control Solution Was Dissolved Nitrogen Supersaturation at 20 °C with an Unaltered Paddle. The Experiments with Marked Paddles and at 10°C Had Dissolved Nitrogen Supersaturation. Error Bars Represent 95% Confidence.

had 0.2 atm gauge pressure and 10 NTU of bentonite clay turbidity. There was no statistical increase of floating floc in the turbid waters compared to control solutions with no initial turbidity (data not shown). Thus, the paddle type and surface exerted a primary controlling influence in these experiments.

Type of Dissolved Gas Supersaturation

Waters supersaturated with dissolved carbon dioxide (0.2 atm gauge pressure) were coagulated next to solutions supersaturated with dissolved nitrogen (0.2 atm gauge pressure). However, no floating floc resulted in solutions supersaturated with dissolved carbon dioxide (Figure 3.11), which was surprising given the previous predictions regarding kinetics and equilibrium (Table 3.1). The acid-base chemical reactions of carbon dioxide and carbonate species (H_2CO_3 , HCO_3^- , CO_3^{2-}) can affect mass transfer kinetics (Howe and Lawler, 1989), which is primarily a result of corresponding pH changes. In these experiments, a significant

buffering alkalinity still existed at the experimental coagulation pH 6, such that observed pH changes during course of the jar test were negligible with respect to the abundance of measured dissolved gas supersaturation. Furthermore, the presence carbonic acid (H_2CO_3) was also insignificant, since at pH 6 the relative equilibrium amount of carbon dioxide was 99.8% (0.2% H_2CO_3). Consequently, any effects from acid-base reactions were deemed negligible in these jar test experiments.

Extensive follow up experiments sought to explain the lack of floating floc during carbon dioxide supersaturation. The possibility that higher ionic strength in the carbon dioxide solution affected floating floc development was tested. Floating floc actually increased in solutions supersaturated with nitrogen at the equivalent higher ionic strength (0.029 M). In addition, zeta potential measurements of many different solutions showed that electrostatic forces did not control this phenomenon.

The higher mass transfer rate caused by the carbon dioxide supersaturation appeared to affect the formation and stability of floating floc in the solutions (Table 3.1). During and immediately after rapid mixing, gas bubbles in the carbon dioxide waters appeared to be larger (≈ 0.33 mm diameter) than bubbles in the nitrogen solutions (≈ 0.20 mm diameter) (Appendix F1). The corresponding rise velocity of these bubbles calculated using Stoke's law for spheres ($\rho_b = 1.20 \text{ kg/m}^3$ at 20°C) would be 6.0 and 2.2 cm/s, respectively, so perhaps it is not surprising that many of the bubbles in the carbon dioxide solutions floated quickly to the water surface without attaching to any coagulant floc. In terms of Equation 3.5, the larger carbon dioxide bubbles represented an overall lower concentration in the number of bubbles and had a lower tendency to attach to floc.

Some bubbles that remained in the carbon dioxide solutions (diameter ≤ 0.20 mm) did cause floating floc initially. Yet, the newly formed floating floc was disrupted by bubbles growth that steadily continued on the paddle or walls of the jar (elevated mass transfer). When these bubbles (1 – 2 mm diameter) floated quickly to the water surface, some of the new formed floating floc was agitated, separating previously attached bubbles from the coagulant floc (Equation 3.6). For example, the amount of floating floc in a carbon dioxide jar test that could be measured at the end of flocculation was 0.7 mL/L, but only 0.02 mL/L of floating floc remained following the 30 minutes of settling (Figure 3.11). This agitation caused by other gas bubbles was not normally observed in solutions supersaturated with only dissolved nitrogen but

did occur in waters with dissolved nitrogen and carbon dioxide both at 0.10 atm gauge pressure (Table 3.1).

Similar mass transfer observations have been documented previously in experiments that monitored size changes of a pre-formed bubble exposed to oscillatory pressure variations. With “air” present as the dissolved gas (i.e., nitrogen), any changes in the size of the bubble were not attributed to mass transfer of the dissolved “air” even during times of dissolved gas supersaturation (Ran and Katz, 1991). Yet, during similar experiments with carbon dioxide dissolved in solution, significant bubble size changes were observed, mainly caused by mass transfer of carbon dioxide (Ran and Katz, 1991). The net result is that in the Ran and Katz experiments (1991), mass transfer of dissolved carbon dioxide had a greater effect on bubble growth than did dissolved nitrogen.

In summary, bubble formation and subsequent floating floc varied depending on the type of dissolved gas supersaturation. Dissolved carbon dioxide supersaturation seemed to produce more overall bubble formation but also created scenarios unfavorable for floating floc. Again, these results were not anticipated and should be investigated further.

Dissolved Gas Supersaturation and Floating Floc

In a preliminary experiment, the amount of floating floc seemed to increase with the initial dissolved gas supersaturation, consistent with the initial idea that higher mass transfer and bubble formation would then lead to more floating floc (Figure 3.7). Consequently, most experiments were designed with water initially supersaturated at 0.2 atm gauge pressure. Yet, given the surprising results for the carbon dioxide jar tests, additional experiments considered more initial levels of dissolved nitrogen supersaturation (0.0 – 0.3 atm gauge pressure) for a range of rapid mix lengths (0 – 120 sec at 160 rpm ($G = 335 \text{ sec}^{-1}$)).

Except for one experiment at 2 sec of rapid mixing, waters with the highest initial dissolved gas supersaturation tested (0.3 atm gauge pressure) had less floating floc than all other solutions (Figure 3.12). Extensive bubble formation was definitely observed in these solutions, which continued throughout slow mix flocculation, yet bubbles floating to the water surface disrupted the newly formed floating floc as observed in the previous experiment with carbon dioxide supersaturation. This phenomenon, though, did not seem to be as apparent in the other solutions tested at lower initial dissolved nitrogen supersaturation. The implication from both of

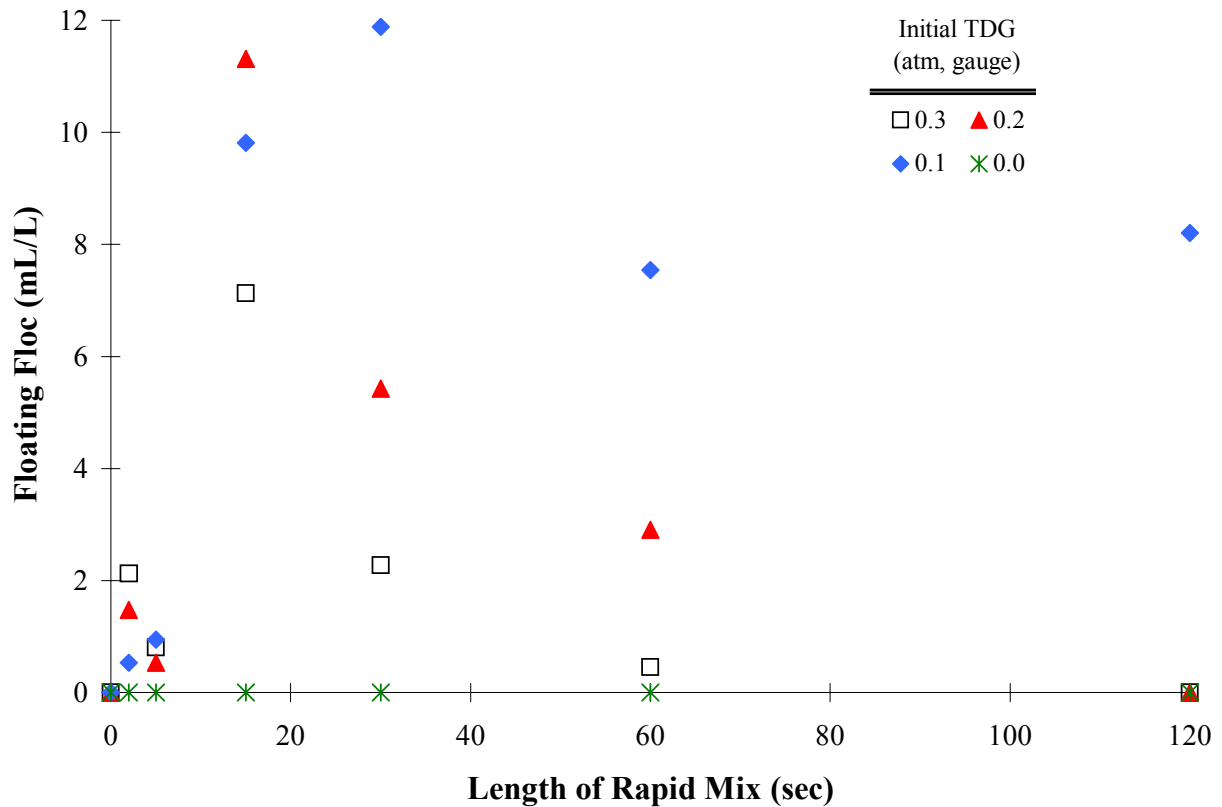


Figure 3.12 – Floating Floc as a Function of Initial TDG and Length of Rapid Mixing. Solutions Were Rapid Mixed at 160 rpm ($G = 335 \text{ sec}^{-1}$) for 60 sec, and Flocculated at 5 rpm ($G = 2 \text{ sec}^{-1}$).

these results suggests that there is an upper threshold where any additional dissolved gas supersaturation (which is dependent on the particular gas) actually decreases the occurrence of floating floc.

Intuitively conflicting results also occurred in the other solutions. Waters supersaturated at 0.2 atm gauge pressure produced the most floating floc when rapid mixed between 2 – 15 sec, but more floating floc developed in the lower 0.1 atm gauge pressure solutions when rapid mixing was 30 – 120 sec (Figure 3.12). The potential reduction of floating floc in the 0.2 atm gauge pressure waters rapid mixed longer than 15 sec have been considered previously (Figure 3.9). Clearly, the 0.1 atm gauge pressure solutions were not nearly as susceptible to these effects during this range of mixing times, and rapid mixing longer than 3.5 min was required for there to be no resulting floating floc in these particular solutions.

An additional aspect of these results has implication for other experiments. For example, the results and interpretation of an experimental series would have been much different if the

waters were rapid mixed at 160 rpm for 2 sec (the most floating floc at 0.3 atm gauge pressure) than if rapid mixed for 60 sec (the most floating floc at 0.1 atm gauge pressure). The major significance of the length of rapid mixing on floating floc development was not initially conceived for all experiments. In hindsight, it can be speculated that a more thorough analysis would probably find some conditions where floating floc would be maximize in solutions supersaturated with dissolved carbon dioxide.

Effects of Solution Temperature

Solutions supersaturated with 0.2 atm gauge pressure nitrogen at 10 °C were compared to similar solutions but at 20 °C. The measured floating floc in the 10 °C waters was significantly less than what formed in the 20 °C system (Figure 3.11). As predicted previously, the lower diffusion rate at 10 °C (Table 3.1) probably reduced overall mass transfer, causing less total bubble formation and corresponding floating floc. Even though colder solutions were less susceptible to floating floc in these experiments, any warming of a colder water within a treatment plant would increase the dissolved gas pressure, as indicated by Henry's gas law (Equation 3.1), and could increase the potential for bubble formation and floating floc.

Effects of Coagulant Type

The same alum dose (14.5 mg/L as Al) was used throughout this study, and for a comprehensive comparison, three iron concentrations were tested, equivalent to the molar (30 mg/L as Fe) and mass (14.5 mg/L as Fe) concentrations of the aluminum. Since iron and aluminum hydroxides can precipitate quite differently even at similar molar concentrations, a third iron dosage (6.25 mg/L as Fe) was visually selected from an iterative experiment in water undersaturated with dissolved gas to replicate the approximate floc size/volume observed for aluminum. All solutions were rapid mixed at 80 rpm ($G = 120 \text{ sec}^{-1}$) for 60 sec and flocculation at 5 rpm ($G = 2 \text{ sec}^{-1}$).

At the equivalent molar concentration (30 mg/L as Fe), the iron flocs also appeared to form instantaneously but became much larger and more abundant. As a consequence, these larger flocs seemed to have more gas bubbles attached, resulting in a very high average volume of floating floc (Figure 3.13). In contrast, in the same experiment with solutions undersaturated with dissolved gas, most of these iron flocs settled naturally during the flocculation stage (Figure

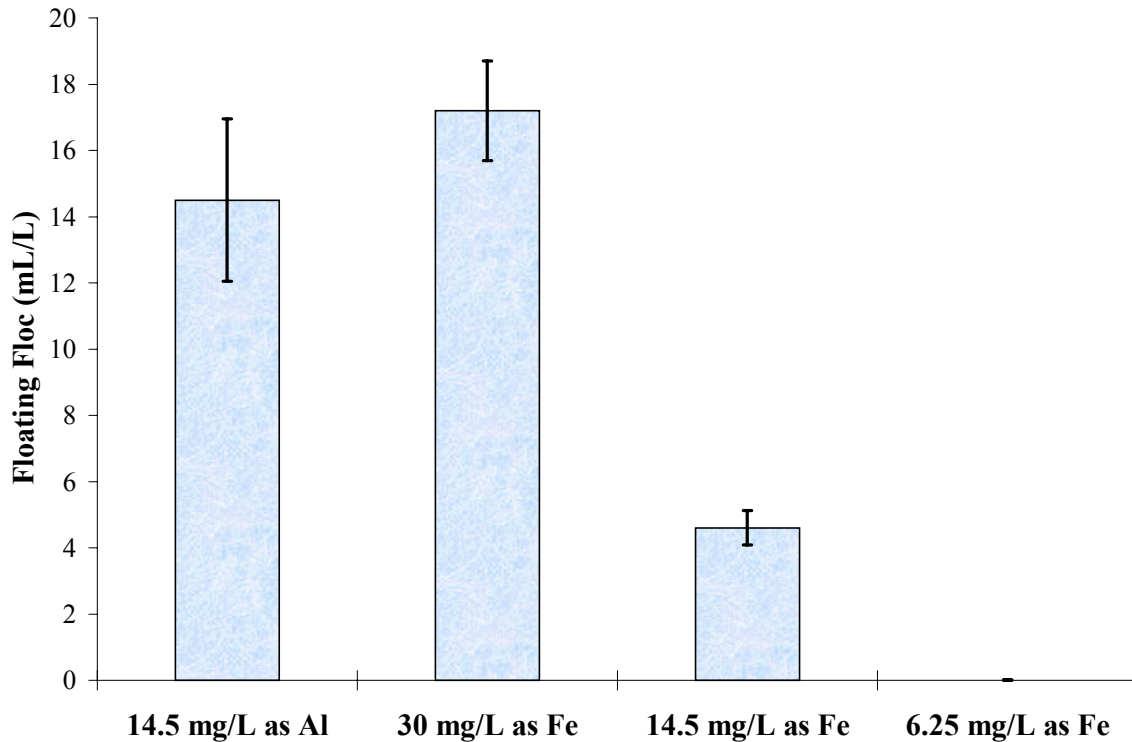


Figure 3.13 – Comparison of Alum and Iron (III) Chloride Coagulants. Solutions Were Rapid Mixed at 80 rpm ($G = 120 \text{ sec}^{-1}$) for 60 sec and Flocculated at 5 rpm ($G = 2 \text{ sec}^{-1}$). Error Bars Represent 95% Confidence.

3.14). The total amount of floating floc decreased at the lower iron dosages (Figure 3.13); therefore, in these particular experiments, larger floc particles did not improve settling efficiency but actually worsened floating floc.

Two additional observations are deemed noteworthy. First, at the lowest iron dose (6.25 mg/L as Fe), the coagulant flocs did not become visible until after 15 minutes of slow flocculation. At this point the vast majority of bubbles that formed during rapid mixing had naturally escaped to the water surface, such that there was almost no floating floc in this experiment due to a low number of available bubbles (Equation 3.5). Similar results occurred when experiments were done to replicate the classic study by Amirtharajah and Mills (1982). Although certain waters in that study were susceptible to dissolved gas supersaturation, the coagulant floc under those specific conditions also did not become visible until the middle of slow mix flocculation, so there was also no observed floating floc (Appendix). These results

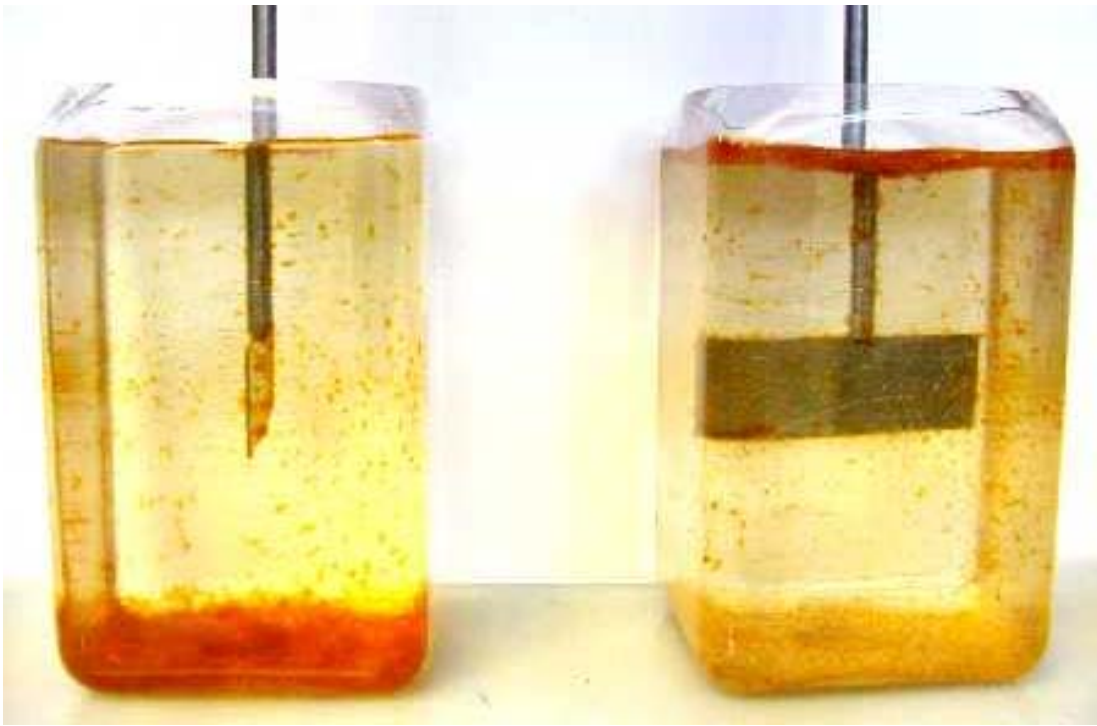


Figure 3.14 – Picture of Ferric (III) Chloride Jar Tests (30 mg/L as Fe). Most of the Coagulant Floc in the Water Undersaturated with Dissolved Gas Settled during Slow Mix Flocculation (Left), while the Floc Predominantly Floated to the Water Surface in Solutions Initially Supersaturated to 0.20 atm Gauge Pressure (Right).

have implications for reducing floating floc by selecting a coagulation system that does not instantaneously become visible during rapid mixing.

The second anomaly of interest occurred in the solutions undersaturated with dissolved gas and coagulated at 30 mg/L as Fe. Although no gas bubbles formed in these waters, some of the coagulant naturally floated at the water surface. No other floating floc appeared in any other experiments when the water was undersaturated with dissolved gas. The cause of this floating floc was not determined, but it might be an indication of the inherent hydrophobicity of precipitated iron hydroxide. This floating floc was of little consequence, since the vast majority of floc settled properly, but it does warrant further investigation.

Even if iron hydroxide precipitates are more hydrophobic, in waters prone to bubble formation, floating floc could result with either aluminum or iron coagulants (Figure 3.13). The type of coagulant did not seem to control the problem.

Effects of High Rate Mixers

Very high rate mixers are sometimes appealing to utilities for instantaneous chemical dispersal and have been found in some cases to be beneficial (Amirtharajah and Mills, 1982). Some experiments were conducted with rapid mix speeds of 1300 and 2200 rpm (7775 and 17,120 sec^{-1} , respectively), and as noted previously, mixing at these speeds induced negative local gauge pressures at the paddle (Figure 3.6, Bottom). Bubbles were scattered throughout solution following both high rate mixes, even in waters initially undersaturated with dissolved gas relative to the atmosphere. However, even though bubbles were readily produced by the high rate mixers, floating floc did not develop in solutions with no (0.0 atm gauge pressure) or very little dissolved gas supersaturation (0.03 atm gauge pressure). Many bubbles were indeed attached to the coagulant floc, but without a sufficient driving force of dissolved gas supersaturation, bubbles did not grow enough to buoy the floc.

High rate mixing waters supersaturated at 0.2 atm gauge pressure nitrogen was again dependent on the time length of rapid mixing. For example, essentially all of the coagulant floc was floated to the water surface in solutions with short rapid mix times (1 – 5 sec) (3.15, Top), while most all of the floc settled in waters with longer mixing times (10 – 15 sec) (3.15, Bottom). Unlike the previous experiments where settling improved at longer rapid mix times (Figure 3.9 and Figure 3.12), bubbles were enmeshed in these settled floc (3.15, Bottom), which was consistent at both high rate mixing speeds. Upon closer visual inspection, there appeared to be a difference between the coagulant flocs, such that flocs from shorter rapid mixes seemed to be much “fluffier” and less dense. Slight differences in pH were not the cause of these phenomena, since similar results occurred in solutions carefully maintained at pH 6. As observed in the Amirtharajah and Mills study (1982), how the water is rapid mixed can effect the corresponding precipitated coagulant floc. The inherent creation of denser floc would be less susceptible to floating in the presence of bubbles.

Additional Considerations

As apparent in the high rate mixer experiments, the presence of gas bubbles could have affected the mass density of newly precipitated coagulant floc. Obviously, if the presence of gas bubbles influenced formation of a less dense coagulant floc, then the overall effects of bubble formation would be compounded. As a first approximation in this work, the coagulant floc

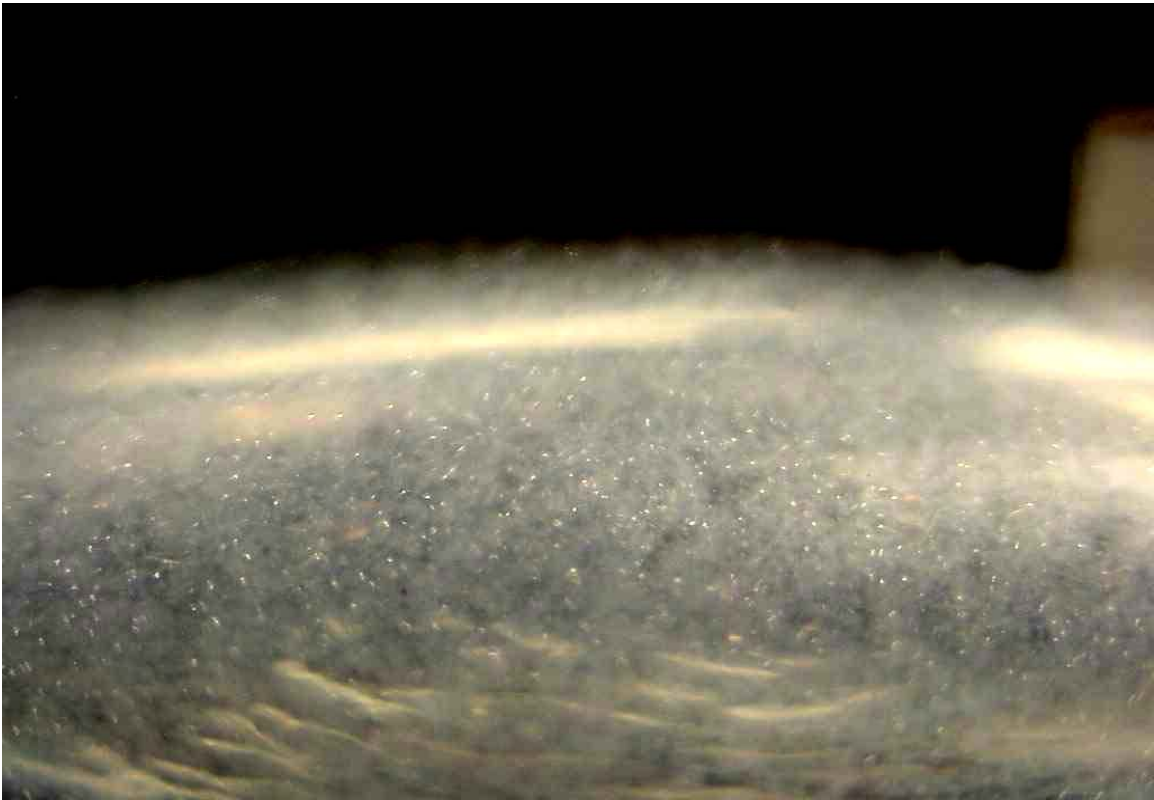


Figure 3.15 – High Rate Mixing Experiments at 1300 rpm. Floating Floc in Waters Rapid Mixed for 2 sec (Top), and Bubbles Enmeshed in Settled Floc Rapid Mixed at 10 sec (Bottom).

density was assumed to be constant for all experiments, such that any density variations were considered negligible in floating floc calculated volumes. Future studies should consider changes in the density of coagulant floc when gas bubble formation is also present. Furthermore, coagulant floc tensile strength measurements would confirm whether gas bubbles indirectly compromise floc integrity.

Other system properties might also influence bubble formation and floating floc. For example, any entity absorbed onto a coagulant could change the overall surface properties of the floc, such as natural organic matter (NOM). Even though NOM did not markedly affect bubble formation (Figure 3.10), NOM could change the surface charge (electrostatic forces) and make the surface more hydrophobic (hydrophobic forces). Ionic strength, acid-base properties of the surface, and the bubble surface charge could also affect bubble-floc attachment forces. Further analysis should systematically investigate surface chemistry interactions of the bubble and floc for conditions common in drinking water treatment.

SUMMARY AND CONCLUSIONS:

- Bubbles attached to coagulant floc can cause floating floc, which reduces settling and particle removal efficiency. Both aluminum and iron coagulants are susceptible to this problem.
- For waters supersaturated with dissolved gas, a rapid mix paddle can be a location of minimum pressure in the system and a source of bubble formation. If the local solution pressure during rapid mixing estimated by the energy equation is less than the measured total dissolved gas (TDG), then bubbles can form. Painting the paddle surface, though, could reduce the amount of bubble formation by smoothing surface imperfections that serve as nucleation sites for bubble formation.
- Very high rate rapid mixers can cause bubble formation, even in a water undersaturated with dissolved gas relative to the atmosphere.
- Many system properties control the formation and stability of floating floc including the local solution pressure, amount and type of dissolved gas supersaturation, and temperature. The time length of rapid mixing also influences floating floc, such that longer mixing times corresponded to no development of floating floc.

ACKNOWLEDGMENTS:

This work was supported by the American Water Works Association Research Foundation (AWWARF) under grant 2821. The opinions, findings, conclusions, or recommendations are those of the writers and do not necessarily reflect the views of AWWARF.

Many of these experiments were performed by Kenneth Craft, Jr as undergraduate research. His efforts are greatly appreciated.

APPENDIX:

Since high rate rapid mixing caused extensive bubble formation and some disruption of sedimentation processes in these experiments, it was speculated that the classic study by Amirtharajah and Mills (1982) could have also been influenced by bubbles. Given the sodium bicarbonate alkalinity (80 mg/L) and the final pH during some experiments, bubbles could have formed, especially with the high intensity mixer (Table 3.A1).

The previous experiment at pH 5.85 was replicated with close inspection to any adverse effects caused by bubble formation. As described in the Amirtharajah and Mills (1982) paper, the coagulant floc precipitation was not within the optimal range for sweep floc and was not visible until the middle of slow mix flocculation. Consequently, all bubbles that formed during rapid mixing had left solution and did not appear to disrupt the system, although observations were clouded by the turbidity (Table 3.A1). Thus, this classic study does not appear to have been influenced by gas bubbles.

Table 3.A1 – Comparison of the Amirtharajah and Mills (1982) and This Study.

Alum Dose (mg/L as Al ₂ (SO ₄) ₃ ·16H ₂ O)	pH	Equilibrium Bubble Formation ¹ (mL/L)	Initial Turbidity (NTU)	Settled Turbidity ² (30 min)	
				G = 300 sec ⁻¹	G = 16,000 sec ⁻¹
Amirtharajah and Mills (1982)					
5	5.85	1.07	-	24	18
1	6.45	0.79	-	17	18
30	6.45	0.79	-	16	3
This Study					
5	5.95	1.03	22.4	24	-
5	5.90	1.05	18.3	-	22

¹Calculated with the Scardina and Edwards Modified Closed System Model (2001).

²No Floating Floc Was Observed in These Experiments.

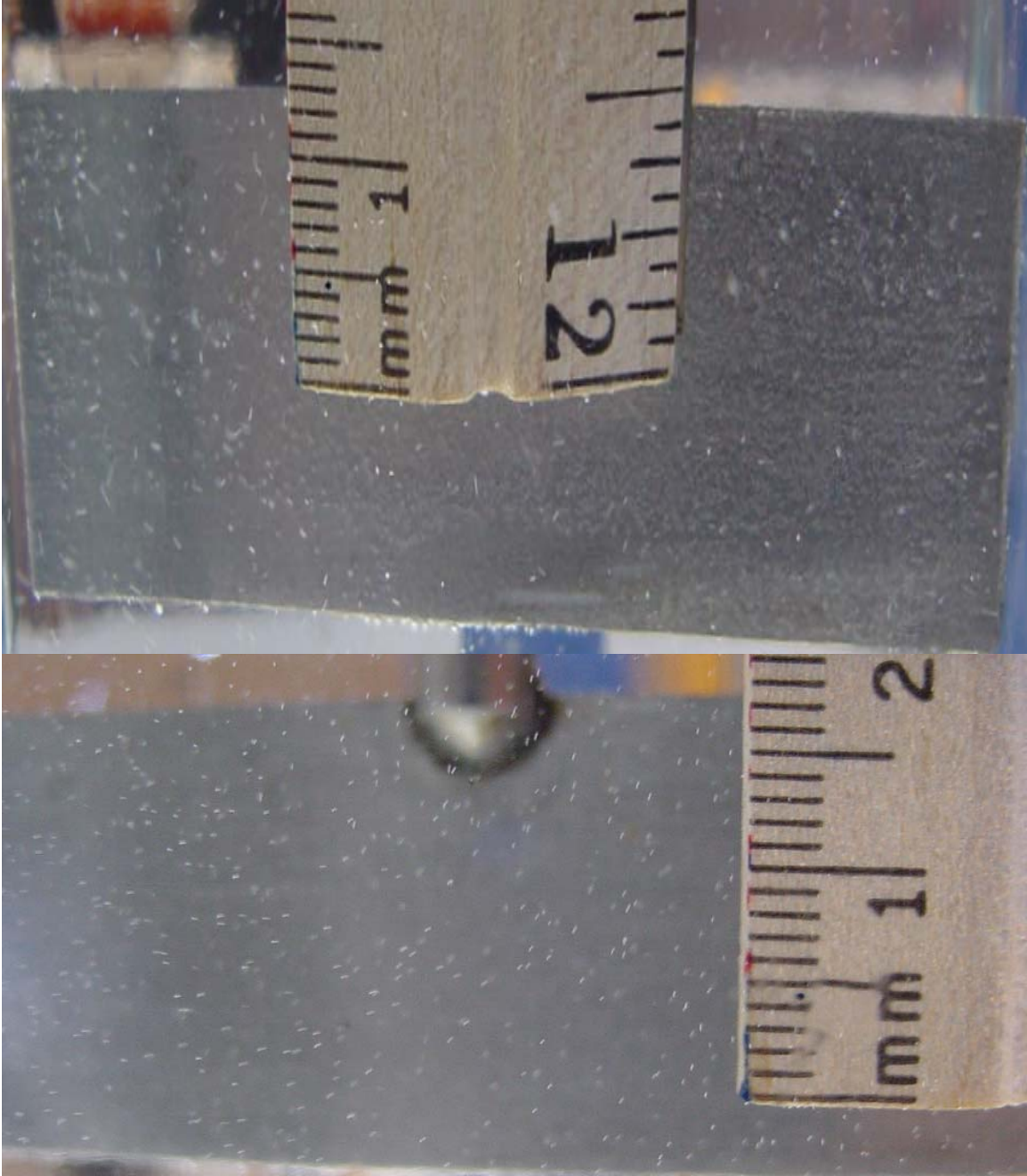


Figure 3.A1 – Bubble Formation after Rapid Mixing in Solutions Supersaturated with Dissolved Carbon Dioxide (Top) and Nitrogen (Bottom).

REFERENCES:

- Amirtharajah, A. and Mills, K. M. (1982). "Rapid Mix Design for Mechanisms of Alum Coagulation." *Journal American Water Works Association*, Vol. 74, 4, pg 210.
- Amirtharajah, A. and Tambo, N. (1991). *Mixing in Coagulation and Flocculation*. Eds., Amirtharajah, A., Clark, M.M., and Trussell, R.R. American Water Works Association Research Foundation, Denver, CO.
- Appleton, Davison, T. S., and Pearce, J. (2001). "Rapid Gravity Filter Modeling." *Advances in Rapid Granular Filtration in Water Treatment*. Conference Proceedings, The Chartered Institution of Water and Environmental Management, London, UK, pg 23-32.
- Betterton, E.A. (1992). "Henry's Law Constants of Soluble and Moderately Soluble Organic Gases: Effects on Aqueous Phase Chemistry." *Gaseous Pollutants: Characterization and Cycling*, Edt. J.O. Nriagu, John Wiley and Sons, Inc, New York.
- Birkhoff, G. (1957). *Jets, Wakes, and Cavities*. Academic Press, Inc., New York.
- Droste, R.L. (1997). *Theory and Practice of Water and Wastewater Treatment*. John Wiley and Sons, Inc, pg 389 – 394.
- Edzwald, J.K. (1995). Principles and Applications of Dissolved Air Flotation. *Water Science and Technology*, 31:3:1.
- HACH Model 2100N Laboratory Turbidimeter Instruction Manual*. (1997). HACH Company.
- Harvey, H. H. (1975). "Gas Disease in Fishes—A Review." *Proc., Chemistry and Physics of Aqueous Gas Solutions., Electrothermics and Metallurgy and Industrial Electrolytic Divisions, Electrochemical Society*, Princeton, N.J., 450-485.

- Hayduk, W. and H. Laudie. (1974). "Vinyl Chloride Gas Compressibility and Solubility in Water and Aqueous Potassium Laurate Solutions." *Journal of Chemical and Engineering Data*, Vol. 19, 3, pg 253.
- Head, R. and Shepherd, D. (2001). "Practical Experience of Using Rapid Gravity Filter Models to Improve Operational Performance at Water Treatment Works." *Advances in Rapid Granular Filtration in Water Treatment*. Conference Proceedings, The Chartered Institution of Water and Environmental Management, London, UK, pg 381-390.
- Hilton, A. M., Hey, M. J., Bee, R. D. (1993). "Nucleation and Growth of Carbon Dioxide Gas Bubbles." *Food Colloids and Polymers: Stability and Mechanical Properties, Special Publication 113*, Royal Society of Chemistry, Cambridge, U.K., 365-375.
- Howe, K.J. and Lawler, D.F. (1989). "Acid-Base Reactions in Gas Transfer: A Mathematical Approach." *Journal of American Water Works Association*, Vol. 81, 1, pg 61-66.
- Letterman, R. & Shankar, S. (1996). Modeling pH in Water Treatment Plants: The Effect of Carbon Dioxide Transport on pH Profiles. Poster at the 1996 AWWA National Conference in Toronto, Canada.
- Letterman, R.D., Johnson, C.E., Viswanathan, S., and Dawarakanathan, J. (2002). "A Study of Low-Level Turbidity Measurements," final project report published by the American Water Works Association Research Foundation, Denver, CO.
- O'Melia, C. R. and Ali, W. (1978). "The Role of Retained Particles in Deep Bed Filtration." *Progress in Water Technology*, Vol. 10, pg 167-187.
- Naylor, F., and Millward, A. (1984). "A Method of Predicting the Effect of the Dissolved Gas Content of Water on Cavitation Inception." *Proc Instn Mech Engineers*, V. 198C, No 12.

- Ran, B. and Katz, J. (1991). "The Response of Microscopic Bubbles to Sudden Changes in the Ambient Pressure." *J. Fluid Mech.*, Vol 224, pg 91-115.
- Robertson, J.A. and Crowe, C.T. (1993). *Engineering Fluid Mechanics*, 5th ed. Houghton Mifflin Company, Boston.
- Ryan, W. L., Hemmingsen, E. A. (1993). "Bubble Formation in Water at Smooth Hydrophobic Surfaces." *J. of Colloid and Interface Science*, 157, 312-317.
- Ryan, W. L. and Hemmingsen, E. A. (1998). "Bubble Formation at Porous Hydrophobic Surfaces." *J. of Colloid and Interface Science*, 197, 101-107.
- Sander, R. (1999). "Compilation of Henry's Law Constants for Inorganic and Organic Species of Potential Importance in Environmental Chemistry – Version 3," <http://wee.Mpchem-main2mpg.de/~sander/res/henry.html>.
- Scardina, P. and Edwards, M. (2001). "Prediction and Measurement of Bubble Formation in Water Treatment." *Journal of Environmental Engineering*, Vol. 127, 11, pg 968.
- Scardina, P. and Edwards, M. (2002). "Practical Implications of Bubble Formation in Conventional Treatment." *Journal American Water Works Association*, Vol. 94, 8, pg 85.
- Selleck, R.E., Mariñas, B.J., and Diyamandoglu, V. (1988). "Treatment of Water Contaminants with Aeration in Counterflow Packed Towers: Theory, Practice, and Economics." UCB/SEEHRL Report 88-3/1, University of California, Berkeley, CA.
- Stevenson, D. G. (2001). "Exploration of Variables in Granular Media Filtration Using the Filterflex Model." *Advances in Rapid Granular Filtration in Water Treatment*. Conference Proceedings, The Chartered Institution of Water and Environmental Management, London, UK, pg 1-10.

Van 't Riet, K. and Smith, J. M. (1975). "The Trailing Vortex System Produced by Rushton Turbine Agitators." *Chemical Engineering Science*, Vol. 30, pg 1093-1105.

Water Quality and Treatment: A Handbook of Community Water Supplies. (1999). Ed., Letterman, R. D. McGraw Hill, Inc. (5th ed.).

CHAPTER 4

ADDRESSING PROBLEMS WITH GAS SUPERSATURATION AT POTABLE WATER TREATMENT PLANTS

Paolo Scardina and Marc Edwards
Virginia Tech; 418 NEB; Blacksburg, VA 24061

ABSTRACT:

Complete failure or reduced efficiency of treatment processes can result when gas bubbles form within conventional water treatment plants. The most common problems caused by bubble formation are floating floc during coagulation and sedimentation, air binding in media filters and upflow clarifiers, and erroneous particle counts or turbidity. Gas bubbles form in areas that are supersaturated with dissolved gas with respect to the local solution pressure. A survey of dissolved gas measurements and estimates of the localized pressure through the treatment plant can identify locations of bubble formation. Measurements of total dissolved gas in source waters should become routine prior to design of any new treatment plant. Oftentimes, simple strategies can be employed to reduce the adverse effects of bubble formation in the plant such as extending the time length of rapid mixing. In other cases, multiple steps may be required to alleviate dissolved gas supersaturation. This paper will address some parameters that should be considered when either designing a new or modifying an existing treatment plant with respect to dissolved gas. In addition, some illustrative case studies are presented.

INTRODUCTION:

Gas bubbles forming in a water treatment plant can disrupt treatment processes and reduce plant operating efficiency (Scardina and Edwards, 2001, 2002, 2004a, 2004b; Scardina et al., 2004). Floating floc, air binding, erratic particle counting and turbidity measurements are frequently encountered manifestations of bubble formation. In using a total dissolved gas probe (TDGP) to diagnose and track such problems in recent years, the initial impression was that treatment problems arising from dissolved gas were a relative rare curiosity. However, as our experiences became more numerous, it became obvious that these phenomena were fairly commonplace, but that the drinking water industry had little training in recognizing and preventing such problems when they occur. Specifically, in some cases the bubbles disrupting

treatment are not easily visible, and even when they are, many personnel refuse to believe they can have major adverse impacts. More importantly, engineers sometimes do not directly consider water supersaturation when designing treatment plants. Consequences of our existing ignorance have ranged from simple nuisance to complete failure of new full-scale water treatment facilities. In still other instances, such as those where operators have felt compelled to implement “burping” of filters to extend filter run length beyond several hours, it is possible that treatment effectiveness is compromised.

In some cases, a detailed diagnosis indicates that an unfortunate treatment plant simply has a highly supersaturated source water, in which case additional treatment steps must be designed to explicitly deal with this highly supersaturated water or the plant might be modified to use dissolved air floatation. In other instances, poor design can directly cause a serious problem where it would not have otherwise existed. This paper will address some parameters that should be considered when either designing a new or modifying an existing treatment plant. In addition, to help the industry recognize such problems when they occur, some illustrative case studies are presented.

MATERIALS AND METHODS:

To illustrate a practical basis for the phenomena of gas bubble formation during rapid mixing, a conventional jar tester was used in benchtop laboratory experiments to mimic coagulation mixing processes. The mixing paddles had dimensions of 7.5 x 2.5 x 0.1 cm and were positioned in the middle of the jars. All solutions were initially saturated with air and then supersaturated with dissolved nitrogen to 0.2 atm gauge pressure using a pressure tank as in Scardina and Edwards (2004b). The jar test water contained 1×10^{-2} M NaNO_3 and 0.52×10^{-3} M as SO_4^{-2} after pressurization. At the start of rapid mixing (time, $t = 0$), the coagulant alum ($\text{Al}_2(\text{SO}_4)_3 \cdot 18\text{H}_2\text{O}$) was dosed to the water at a concentration of 14.5 mg/L as Al along with 1 M sodium hydroxide (NaOH). The two chemicals were dosed at opposing corners of each jar to produce a final coagulation pH of 6.0 ± 0.2 . The speed of rapid mixing and slow mix flocculation varied per experiment, as well as the length of rapid mixing. All solutions were flocculated for 30 min and allowed to settle for 30 min.

The amount of floating floc in these jar tests was estimated by measuring the diameter and thickness of floc floating at the water surface (Scardina and Edwards, 2004b). A volume

was then calculated (mL/L), and this estimation was reproducible between ± 1 mL or $\pm 10\%$, whichever is greater.

During site visits, the pH, alkalinity, dissolved oxygen (DO), total dissolved gas (TDG), and temperature were measured directly in the treatment plant process train. Whenever this was not possible, samples were collected from taps in a manner designed to minimize gas transfer to the extent possible. A total dissolved gas probe (TDGP) manufactured by either Common Sensing, Inc. or Sweeney Aquametries was used to measure the TDG (± 0.003 atm), barometric pressure (± 0.003 atm), and temperature (± 0.1 °C). Dissolved oxygen (DO) was measured by different meters, and the Common Sensing TDGP measured DO (± 0.003 atm). The TDG and DO were recorded as either a gauge or absolute pressure referenced to the local barometric pressure.

RESULTS AND DISCUSSION:

Discussion begins with an investigation of mixing in relation to formation of floating floc. Sampling and analytical protocols are then presented that can be used in detecting and diagnosing problems in treatment plants. This paper concludes with case studies, and decision trees are also shown as a guide to resolving bubble induced problems during coagulation and filtration.

Design of Coagulation Mixers and Bubble Formation

The formation of floating floc is a function of many different factors including the extent of dissolved gas supersaturation, type of dissolved gas supersaturation, temperature, rate of floc formation, and the speed of various mixing stages (Scardina and Edwards, 2004b). Somewhat surprising, in the jar test apparatus and in treatment plants, many floating floc problems originate at the mixing paddle(s). Consequently, it was deemed necessary to develop an engineering understanding of this issue in relation to mixer design.

In a mixing basin, the hydrostatic pressure at a depth will be reduced in the localized area of the mixing paddle due to high fluid velocities. Previous work demonstrated that the extent of pressure reduction could be reasonably approximated by the energy equation (Scardina and Edwards, 2004b):

$$\frac{P}{\lambda} + \frac{V^2}{2g} + z = \text{Constant.} \quad (\text{Equation 4.1})$$

On a given paddle, the maximum velocity relative to the water is a function of the mixing rate (rpm) and paddle diameter. If the local pressure at the surface of the paddle becomes less than the total dissolved gas (TDG) pressure, bubbles can potentially form on the paddle and then be released to the water. Hence, a mixing paddle can be a bubble generator. The water itself and the surface condition of the paddle play a major role in controlling the extent of the problem (Scardina and Edwards, 2004b), but it is also clear that bubble formation can often be completely eliminated if the mixing rate is maintained below certain critical values.

Conceptually, for every possible mixing paddle depth, there is a critical velocity at which the minimum pressure of the paddle is equal to the pressure of dissolved gases in the water. The energy equation (Equation 4.1) can be used to construct a line that demarcates combinations of mixing speed and depth where bubbles may and may not form (Figure 4.1). For example, if a

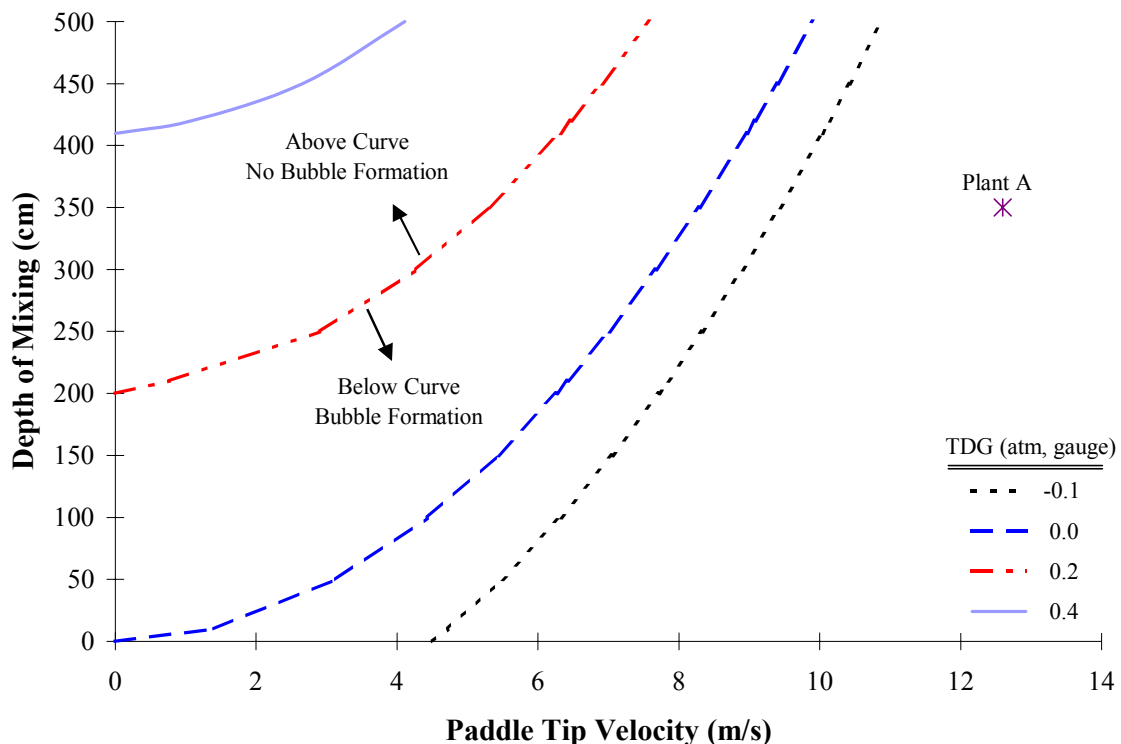


Figure 4.1 – Paddle Mixing Velocity Where the Local Solution Pressure Equals the Total Dissolved Gas (TDG) Pressure at a Given Depth, as Calculated by the Energy Equation (Equation 4.1).

water is at equilibrium with the atmosphere (TDG = 0 atm gauge pressure), the TDG pressure would equal the local solution pressure (0 atm gauge pressure) when the highest speed on the mixing paddle is 4.5 m/s at a depth of 1 m. Velocities greater than 4.5 m/s at a depth of 1 m would decrease the local solution pressure below the TDG pressure, creating a potential for bubble formation. Increasing the mixing depth or reducing the paddle tip velocity will reduce the potential of forming bubbles.

Since the energy equation is an imperfect prediction of the actual pressure at the surfaces of paddles, a correction factor is necessary. For instance, in previous work with a jar test apparatus (Scardina and Edwards, 2004b), it was determined that the local solution pressure on the backside of paddle was about 25% less than that predicted. Since the local solution pressure is proportional to the velocity squared, this implies an approximate correction factor of 0.85 to the paddle tip velocities to insure that the critical pressure is not exceeded. Additional research would be necessary to determine if this correction factor is appropriate for other paddle geometries.

Figure 4.1 has many potential applications in practice including:

- 1) if the dissolved gas content of the water is measured at the plant and the mixing paddle depth is fixed, operators can quickly determine the mixing speed below which bubbles will not form at the paddle surface;
- 2) if the range of dissolved gas content of the water is known and a certain paddle type and velocity are desirable, the diagram would provide information on the minimum depth of mixing to avoid bubble formation;
- 3) if the mixing depth, paddle type, and mixing speed are fixed, and aeration or other mitigation measures are employed to reduce dissolved gas supersaturation, the diagram provides a target TDG treatment level;
- 4) if bubbles were not forming in the treatment plant but were forming in the jar tester, the diagram allows determination of a range of jar test rapid mix velocities that may better simulate plant performance.

Other uses are quite possible as will be discussed in later sections.

The diagram is also useful in considering tradeoffs between G value, rapid mix speed, and paddle diameter for a fixed mixing speed. That is, to maintain the same velocity gradient, a smaller diameter paddle would have to be mixed at higher revolutions, which could potentially worsen bubble formation. For example, a conventional jar test paddle (7.5 cm diameter) mixing at 160 rpm creates a predicted velocity gradient and local solution pressure at 6.0 cm depth of 335 sec^{-1} and 3.9×10^{-3} atm gauge pressure, respectively. In order to maintain a G of 335 sec^{-1} , a

3.4 cm diameter paddle would need to be mixed at 565 rpm, thereby lowering the estimated local solution pressure to 0.8×10^{-3} atm gauge pressure for the same depth. For these two paddles at the same G, the smaller diameter paddle is more likely to create bubbles due to its lower localized pressure.

Previous work also showed that the length of rapid mixing influenced formation and stability of floating floc (Scardina and Edwards, 2004b). Based on variations in the length of rapid mix only, floating floc production increases to a worst case value at a given mixing rate (rpm), with virtually no floating floc at rapid mix times that are much shorter or much longer than this mixing time (Figure 4.2). An operational mixing curve should be developed for different mixing scenarios at existing plants in order to avoid floating floc (Figure 4.2). For example, in the jar test data of Figure 4.2, specific rapid mix options would minimize floating floc. Mixing at 80 rpm for up to 10 sec reduced bubble formation and floating floc. Alternatively, mixing at 160 rpm for greater than 120 sec or at 1300 rpm for longer than 15 sec would also minimize floating floc. Secondly, for a fixed mixing rate, shortening the rapid mix time could reduce the amount of bubble formation, or longer rapid mixing could separate bubbles and floc. Even for the worst case conditions in Figure 4.2, there is no floating floc in waters undersaturated with dissolved gas (Table 4.1).

Even if a utility was unable to change its rapid mix protocol, the floating floc could still be reduced by altering the rate of slow mix flocculation (Figure 4.3). To illustrate, waters were rapid mixed at 80 rpm ($G = 120 \text{ sec}^{-1}$) for 60 sec, which led to reproducible formation of greater than 10 mL/L floating floc, and were then slow mix flocculated between 5 and 40 rpm. There was a major reduction in the turbidity and floating floc at a slow mix flocculation speed of 20 rpm or greater ($G = 15 \text{ sec}^{-1}$). Higher flocculation speeds physically detaches gas bubbles from the flocs, as observed in the rapid mix study. In summary, the mixing protocol is important to reducing the amount of floating floc.

Analysis of Bubble Formation at Treatment Plants

A few treatment plants were visited that historically have had problems caused by bubble formation. The measurement and troubleshooting protocol is described first, followed by results of each site visit (Table 4.2).

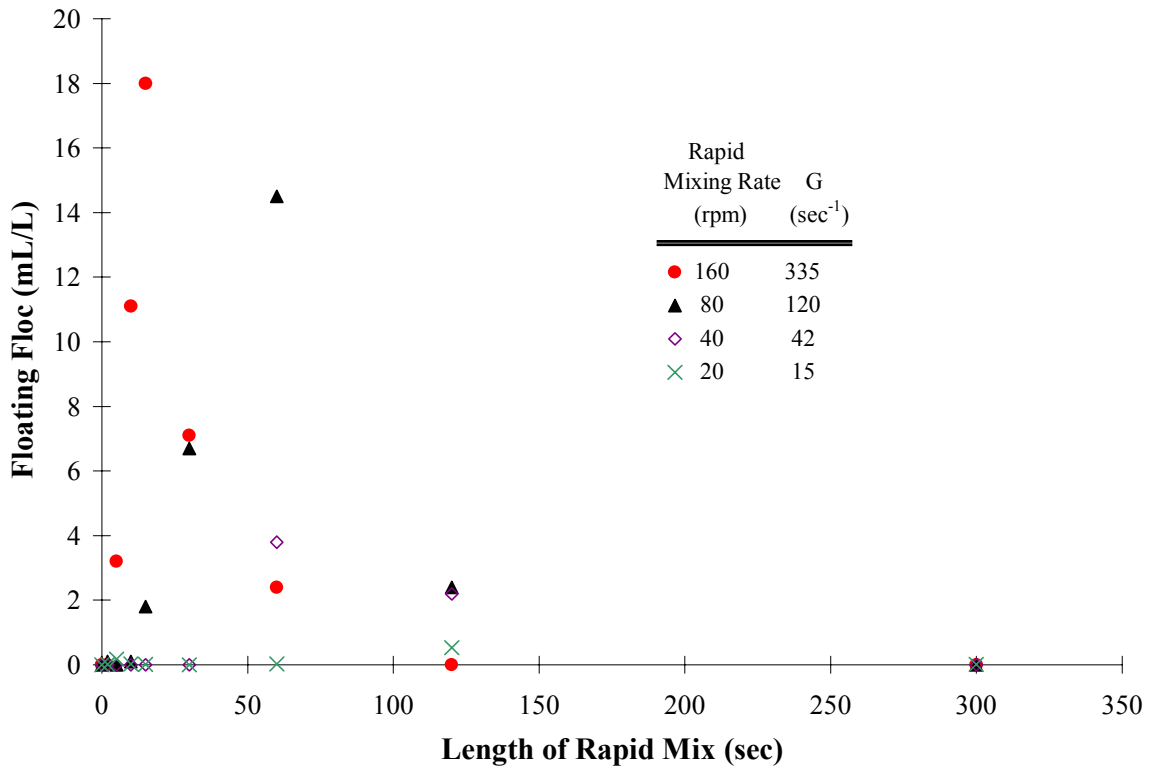
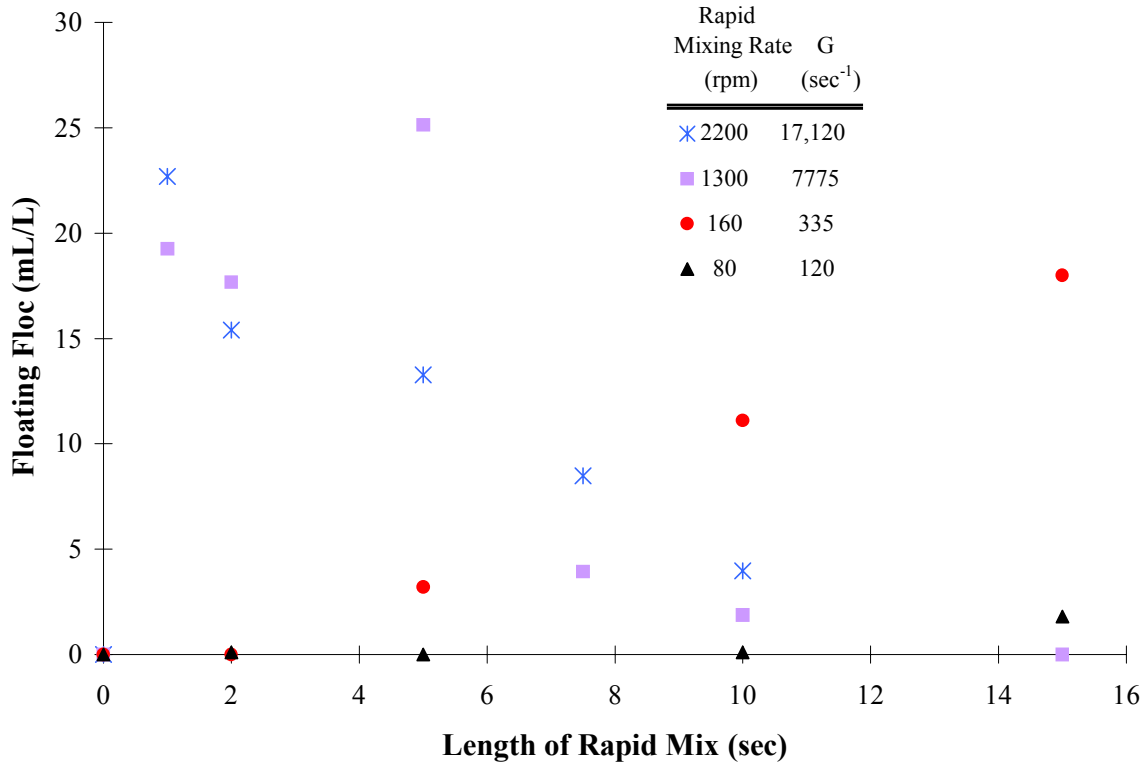


Figure 4.2 – Operational Curves for Different Mixing Scenarios. Solutions Were Initially at 0.2 atm Gauge Pressure and Were Flocculated at 5 rpm ($G = 2 \text{ sec}^{-1}$).

Table 4.1 – Single Comparison of Waters Supersaturated and Undersaturated with Dissolved Gas.

Solutions Were Flocculated at 5 rpm ($G = 2 \text{ sec}^{-1}$).

Rapid Mix Rate (rpm)	G (sec^{-1})	Rapid Mix Length (sec)	Initial Solution Gauge Pressure			
			TDG = 0.2 atm		TDG < 0 atm	
			Floating Floc (mL/L)	Turbidity (NTU)	Floating Floc (mL/L)	Turbidity (NTU)
160	335	10	11.1	0.75	0	0.51
80	120	60	14.5	0.49	0	0.41
40	42	60	3.8	0.65	0	0.74
20	15	120	0.5	0.58	0	0.88

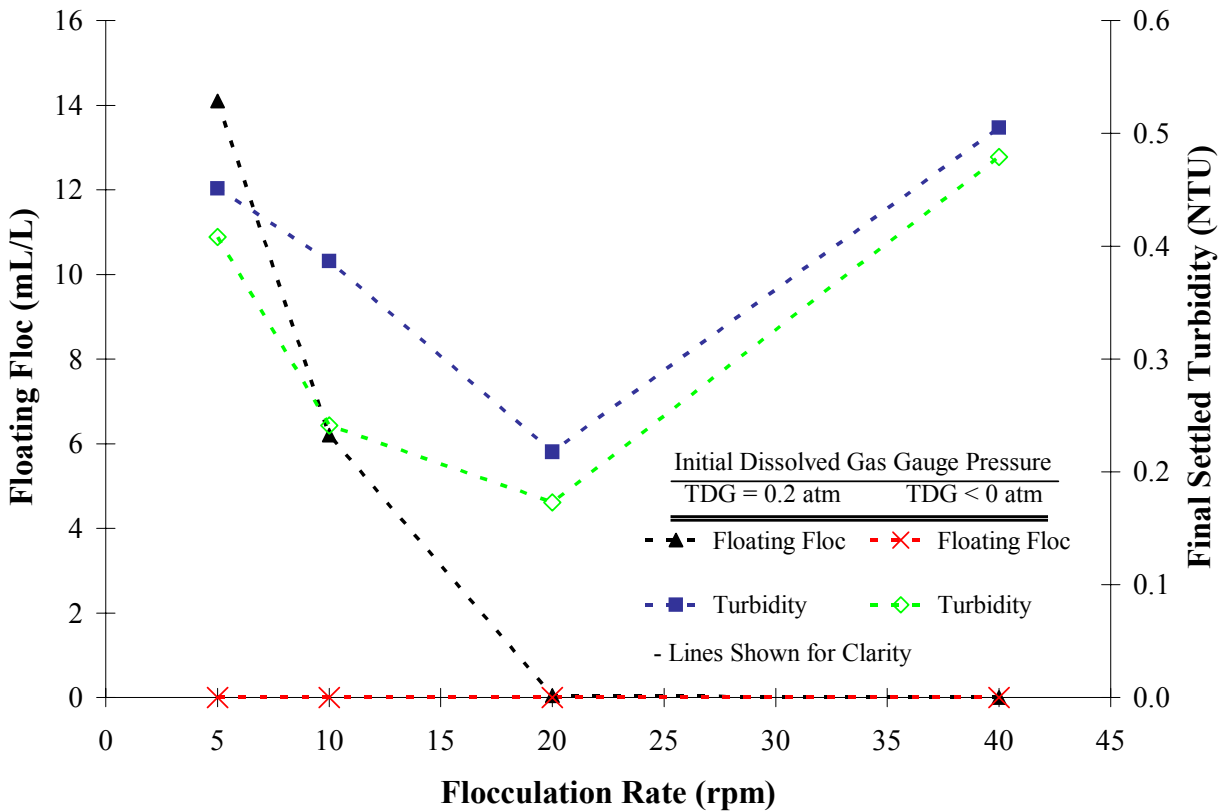


Figure 4.3 – Effects of the Rate of Flocculation on the Amount of Floating Floc. Solutions Were Rapid Mixed at 80 rpm ($G = 120 \text{ sec}^{-1}$) for 60 sec.

Table 4.2 – On-site Analysis of Dissolved Gas Supersaturation and Bubble Formation at Various Water Treatment Plants.

Treatment Plant	Major Problems	Suspected Cause	Measured Total Dissolved Gas (TDG) (atm, gauge)						
			Raw	Ozone Effluent	Rapid Mix	Flocculation Basin	Sedimentation Basin or Upflow Clarifier	Filter Influent	Filter Effluent
A	Floating Floc	High Rate Mixer	-0.033	–	-0.029	-0.029	–	–	–
B	Filter Air Binding	Pipeline Air Entrainment	0.032	–	0.038	0.037	0.037	0.037	0.038
C	Floating Floc, Filter Air Binding	Pipeline Air Entrainment	0.174	–	0.184	0.189	0.193	0.140	0.138
D	Filter Air Binding	Algae Photosynthesis, Pipeline Air Entrainment	–	–	–	–	-0.034	0.087	–
E	Filter Air Binding	Ozonation	-0.014	0.084	0.145	0.147	0.150	0.141	0.059
F	Clarifier Air Binding	Algae Photosynthesis	0.141	–	–	–	0.132	0.116	0.100

Sampling and Data Analysis Protocol

Simple visual observations are useful in detecting treatment disruptions caused by bubble formation. Often, the bubbles are very small (diameter ≤ 0.5 mm) and are only visible upon close inspection, such as in a carefully collected beaker grab sample held toward light. Bubbles causing filter air binding can be observed during filter backwashing but should not be confused with an air scour on the filter surface.

A total dissolved gas probe (TDGP) is a powerful tool for diagnosing sources of dissolved gas supersaturation and bubble formation. Since a treatment plant essentially operates as a closed system with respect to gas transfer across the atmosphere-water interface (Letterman and Shankar, 1996), any decrease in total dissolved gas (TDG) can be assumed to be from bubble formation. Dissolved oxygen (DO) measurements alone have limitations, since oxygen may not be the particular dissolved gas that is supersaturated. A profile of TDG through the plant provides further knowledge of dissolved gas supersaturation and bubble formation, and profiles with depth from a raw water source could indicate a better location of an intake to avoid gas supersaturation. That is, sometimes only the epilimnion of a reservoir is supersaturated with dissolved gas. Therefore, TDG measurements of a source water is recommended before designing a new water treatment plant, since improper design for the supersaturated water can cause failure of the plant to perform. Problems with dissolved gas are sometimes a seasonal problem; for instance, they can be caused by algae activity in the summer and increasing solution temperatures in the spring (Scardina and Edwards, 2002).

A thorough analysis would attempt to isolate the amount of each dissolved gas of interest at each sample location. It can be assumed that the measured TDG is the sum of the partial pressure of the three primary dissolved gases nitrogen, oxygen, and carbon dioxide:

$$\text{TDG} = p\text{N}_2 + p\text{O}_2 + p\text{CO}_2. \quad (\text{Equation 4.2})$$

The $p\text{N}_2$ is actually the sum of nitrogen, argon, and other gases, as it is determined by difference between the TDG measurement and the measured values of $p\text{O}_2$ and $p\text{CO}_2$. All values in Equation 4.2 should be absolute pressures (mmHg or atm), and whenever needed, Henry's gas law can be used to convert a dissolved gas molar concentration [Gas] (M) to a partial pressure $p\text{Gas}$ (mmHg or atm absolute pressure):

$$[\text{Gas}] = K_H \cdot p\text{Gas}. \quad (\text{Equation 4.3})$$

Henry's gas law constant K_H (M/atm) varies for each gas and is also dependent on temperature.

The amount of dissolved oxygen can be measured with a DO probe. The concentration of dissolved carbon dioxide can be calculated from pH and alkalinity measurements, assuming that all of the alkalinity is in the form of bicarbonate $[\text{HCO}_3^-]$:

$$K_{a1} = \frac{[\text{H}^+][\text{HCO}_3^-]}{[\text{CO}_2]}. \quad (\text{Equation 4.4})$$

The first carbonate equilibrium constant K_{a1} also varies with temperature. After converting the partial pressure of oxygen and carbon dioxide to the appropriate pressure units, the partial pressure of nitrogen can then be estimated by Equation 4.2. It is possible that in rare circumstances, methane, sulfides, and other gases could also be significant, but these are believed to be rare.

Comparing two points in the treatment plant, formation of gas bubbles can alleviate dissolved gas supersaturation, leading to lower concentrations of dissolved gas in the water. The ideal gas law can then be used to estimate the total volume of bubble (V) formed between the two points per 1 L volume of water:

$$PV = nRT \quad (\text{Equation 4.5})$$

The decrease in the concentration [Gas] of each dissolved gas species is the number of moles transferred to the gas bubble phase (n). The pressure within the bubble (P) can be assumed to equal the barometric pressure, and R is a constant. A thorough analysis of dissolved gases can therefore be completed with a few simple measurements.

On-site Analysis at Treatment Plant A

Treatment plant A has had a long history of floating floc (Figure 4.4). This utility attempted different coagulant chemical combinations over a 10 yr period, but were unable to improve settling of their floc. The floating floc did not appear to be seasonal or diurnal, and filter air binding had not been observed. Measurements of the raw water through the plant did not indicate any dissolved gas supersaturation (Table 4.2), even though bubbles could be easily seen attached to floating floc in beaker grab samples.

Further analysis identified the coagulant rapid mixer as the potential source of bubble formation. This mixer had a paddle diameter of 19 cm (7.5 in) and rotated at approximately



Figure 4.4 – Floating Floc at Utility A.

1268 rpm for a maximum paddle velocity of 12.6 m/s. The static hydrostatic pressure at the point of mixing was estimated to be 0.35 atm gauge pressure at an approximate depth of 350 cm. Thus, these mixing conditions are well in the range of gas bubble formation in Figure 4.1 even at TDG \approx -0.1 atm gauge pressure. The solution pressure within the localized area of the paddle mixer was estimated to be -0.43 atm gauge pressure. On the basis of this information, the utility is currently in the process of re-designing the rapid mixer.

Attempts to diagnose the problem initially led away from the rapid mixer, since floating floc was also noted to occur in the conventional benchscale jar tests. However, analysis indicated that significant changes in the solution temperature were occurring in the jar test but not in the treatment plant. As shown by Henry's gas law constants (Equation 4.3), the TDG pressure increases with temperature for a given amount of dissolved gas. For instance, at the start of one jar test, the raw water had a measured TDG and temperature of 0 atm gauge pressure and 12.5 °C. By the end of settling, the jar test solutions had warmed to 21.5 °C, which increased the measured TDG to 0.072 atm gauge pressure. Since this water became

supersaturated with TDG, bubbles formed during this jar test and even floated some floc that was previously settled. This divergence between the plant and jar test performance could be resolved by submerging the jars in re-circulating raw water.

On-site Analysis at Treatment Plants B and C

Utility B and C have unique source waters. Both plants experience filter air binding, and utility C also has had substantial problems with floating floc. Filter air binding has been so severe at utility C that 3 – 5 hr filter runs can be common, and bubbles could be easily seen floating media out of the system during backwashes. It is believed that pipeline air entrainment is the source of the dissolved gas supersaturation for both utilities. Air trapped within a pipeline can be forced into solution by high hydrostatic pressure, so elevated concentrations of nitrogen and oxygen would be expected (Scardina and Edwards, 2002).

Utility B had recently installed a type of deaerator at their source water intake. This equipment may have helped reduce some dissolved gas supersaturation, since the source water was only slightly supersaturated (Table 4.2). Measurements across the filter were at first perplexing, since the measured TDG increased from 0.037 atm gauge pressure in the filter influent to 0.038 atm gauge pressure in the filter effluent (Table 4.2). However, the water had warmed through the filter from 13.5 to 14.3 °C, which was shown previously to affect TDG pressures. Additional measurements and Equations 4.2 – 4.5 were needed to fully characterize the dissolved gases through the filter.

After converting all of the dissolved gases to concentration units, it was evident that nitrogen was the main dissolved gas in excess, and the concentration of nitrogen did actually decrease through the filter, corresponding to a 0.21 mL of bubbles forming per L water treated (Table 4.3). The actual volume of solid particles collected within the filter was also determined by measuring the volume of particles that settled in the neck of an inverted 1 L volumetric flask (± 0.5 mL/L). For the conditions measured at utility B, bubble formation was equal to about 20% of the particle volume (1 mL/L) loaded to filters (Table 4.3). Even though the water was only slightly supersaturated with dissolved gas, the resulting bubble formation still occupied a significantly volume of pore spaces within the filter media, increasing total filter headloss.

A similar analysis was performed on the data collected at utility C. The level of dissolved gas supersaturation was much higher at this utility (Table 4.2), which in turn led to

Table 4.3 – Analyses at Utilities B and C.

	Dissolved Gas Concentrations (M)						Captured within Filter (mL/L)	
	Filter Influent			Filter Effluent			Measured Particles	Calculated Bubble Formation
	[N ₂]	[O ₂]	[CO ₂]	[N ₂]	[O ₂]	[CO ₂]		
Utility B	5.35x10 ⁻⁴	2.59x10 ⁻⁴	2.10x10 ⁻⁴	5.26x10 ⁻⁴	2.59x10 ⁻⁴	2.10x10 ⁻⁴	1.0	0.21
Utility C	5.55x10 ⁻⁴	2.96x10 ⁻⁴	0.23x10 ⁻⁴	5.48x10 ⁻⁴	2.89x10 ⁻⁴	0.23x10 ⁻⁴	0.5	0.35

more filter air binding (Table 4.3). The volume of bubbles formed in the filter (0.35 mL/L) was about 70% of the particle volume loading to the filter (0.5 mL/L). As has been noted elsewhere (Scardina and Edwards, 2004a), air bubbles tend to deposit almost exclusively within certain zones of the filter bed, so their impact on headloss can be much higher than would be indicated by comparing volumes.

On-site Analysis at Treatment Plant D

Utility D had speculated that air binding occurs within its filters. This utility can have severe algal blooms in the source water and also within the treatment plant. Algae photosynthesis can cause dissolved gas supersaturation, since the partial pressure of newly created oxygen exceeds the reduction in the partial pressure of consumed dissolved carbon dioxide (Scardina and Edwards, 2002). Algal activity can also increase taste and odors and increase substances that cause disinfection byproducts when chlorinated. To control algae growth within the treatment plant, this utility covered the sedimentation basins with a pool cover that blocks sunlight. A study sought to quantify the benefits of covering the basins by comparing a covered and un-covered sedimentation basin. This utility was even reluctant at first to remove one of the covers, since consumer taste and odor complaints were reported to increase whenever the covers were not used.

Effluent from the sedimentation basin was undersaturated with dissolved gas, which may have been another benefit of reduced algal activity in the covered basin (Table 4.2). Yet, surprisingly, on route to the filter, there was a significant change in TDG, and the water became supersaturated with dissolved gas (Table 4.2). An investigation revealed that water is channeled from the sedimentation basin and falls down a conical funnel to a final water depth of approximately 3 – 4.5 m (10 – 15 ft), where it is then redistributed upward to the top of the filters (Figure 4.5). During this funneling process, the turbulent water entrains and traps air in solution, which is easily visible. As the water falls downward, the hydrostatic pressure at depth (3 – 4.5 m) could force the entrained air to dissolve into solution, supersaturating the water with dissolved gases similar to pipeline air entrainment. Measurements were not possible for the filter effluent, but based upon the observations at other utilities (Utility B in particular), bubbles could

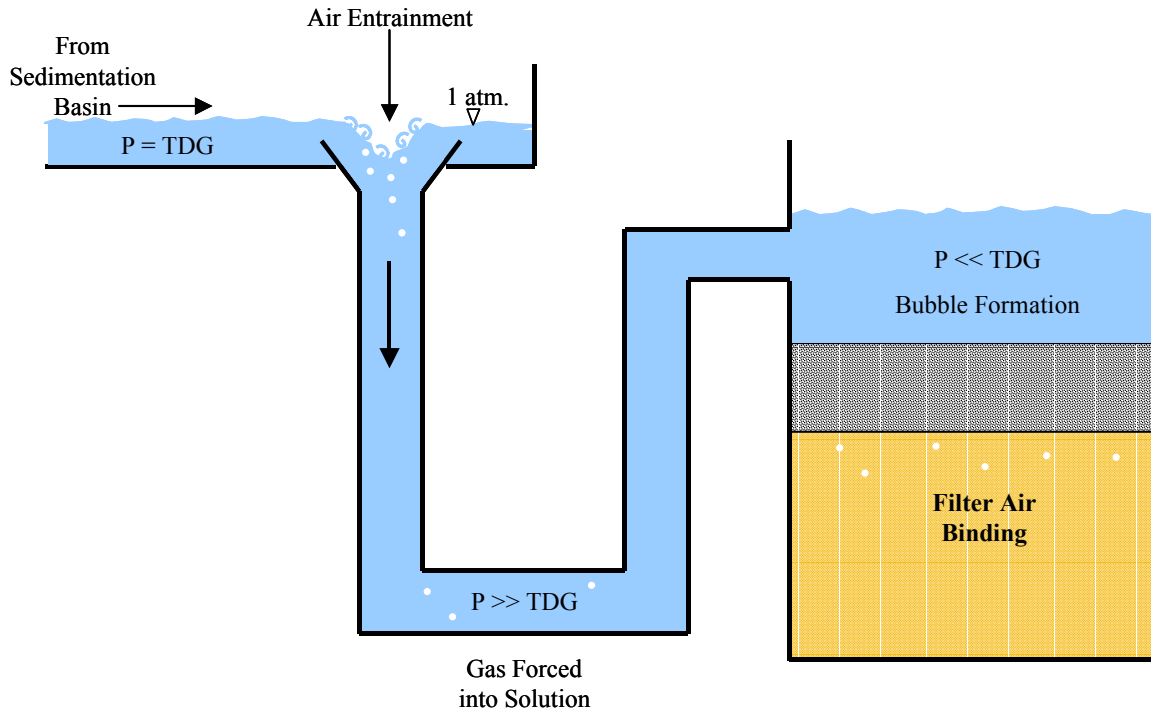


Figure 4.5 – Water Flow Schematic from the Sedimentation Basin to the Filters at Utility D. Air Entrainment at the Entrance Causes Trapped Air to Diffuse into Solution at Depth, which then Leads to Dissolved Gas Supersaturation and Filter Air Binding.

potentially form within these filters. All potential filter air binding could be eliminated by modifying the design of the intake to these filters to prevent air entrainment.

On-site Analysis at Treatment Plant E

Utility E has routinely experienced filter air binding. Measurements through the plant suggested that the ozonation process caused the dissolved gas supersaturation (Table 4.2). Diffusing ozone and its carrier gas at depths can drive gases into solution (Scardina and Edwards, 2002). The filter effluent measurements were taken from a laboratory tap that naturally allowed some loss of TDG, so the actual TDG in the filter effluent is probably higher than the value listed (Table 4.2). Dissolved gas supersaturation can be decreased by reducing the depth of ozone diffusion. Another utility plagued by the same problems (Scardina and Edwards, 2002) reduced the flow rate injection of ozone and carrier gas without changing the depth of diffusion. Since the rate of gas injection decreased, this seemed to reduce some of the dissolved gas supersaturation and corresponding filter air binding at this utility.

On-site Analysis at Treatment Plant F

Utility F has had problems with bubbles forming within its upflow clarifier. Following rapid mixing at utility F, the water enters the bottom of an upflow clarifier where coagulant floc is removed within a mixed media (Figure 4.6). This treated water then proceeds directly to a conventional media filter. The source water typically has prolific algal blooms during the summer, and the resulting dissolved gas supersaturation in the source water induces severe bubble formation within the upflow clarifier. In addition to increasing the rate of backwashing in this clarifier, the gas bubbles periodically release from the media in a “burping” phenomenon (Figure 4.7). In some cases, the upflow clarifier exhibited burping 30 – 45 minutes after backwashing. This phenomenon proved to be very problematic, since the burping from the clarifier reduced the effectiveness of treatment for pathogens and particles removal at utility F.

Measurements confirmed that TDG was lost within the upflow clarifier (Table 4.2). During one afternoon, water entered the upflow clarifier with 0.132 atm gauge pressure and left the clarifier at 0.116 atm gauge pressure TDG. A boat was used to travel across the source water. Thick mats of algae were visible located around the source water intake, and TDG measurements confirmed dissolved gas supersaturation in the source water reservoir.

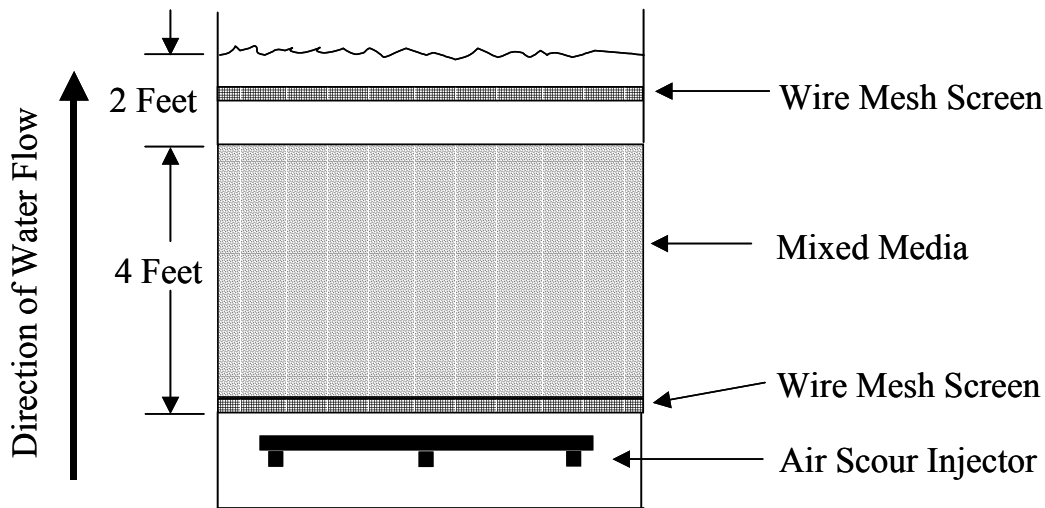


Figure 4.6 – Schematic of Upflow Clarifier at Utility F.

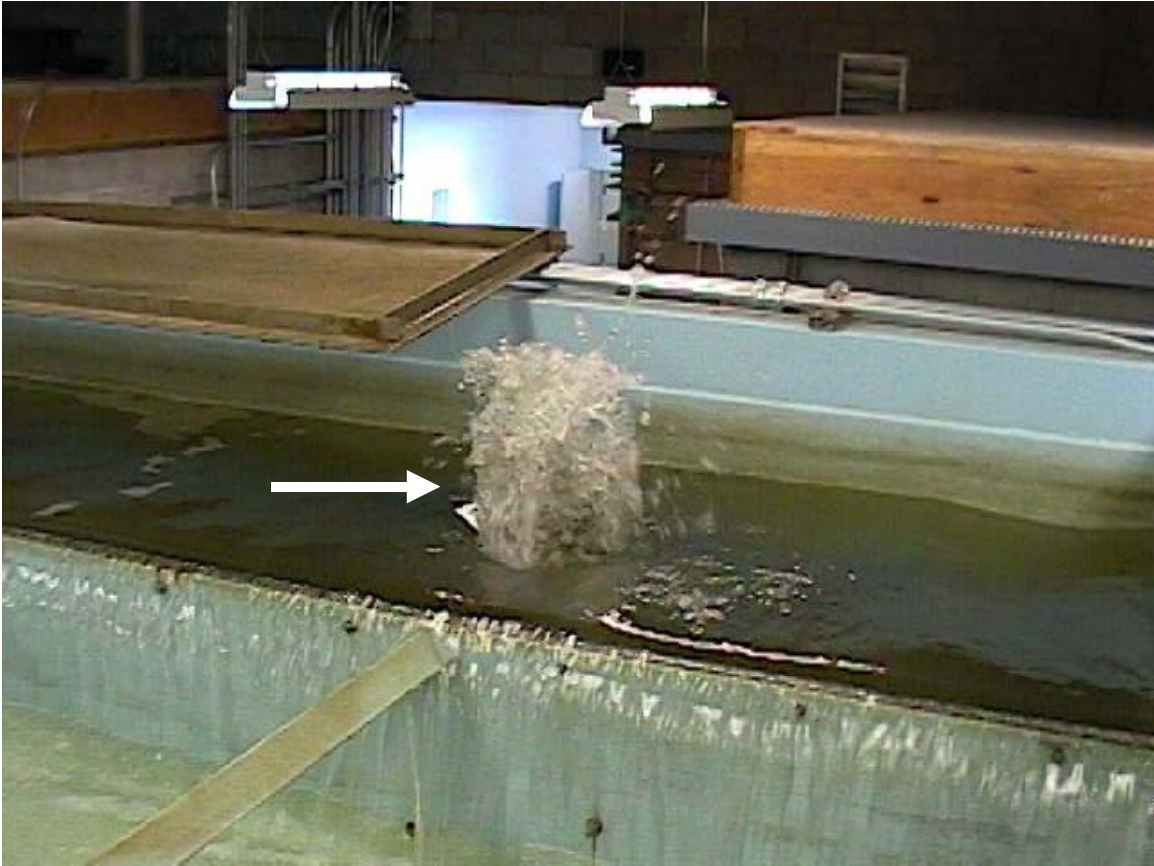


Figure 4.7 – Bubble Release (Burping) from the Upflow Clarifier at Utility F.

A neighboring utility uses the same source water, but less algae was observed around the source water intake for this utility. The neighboring treatment plant has a similar design and operation as utility F but uses a different type of media in their upflow clarifier. Although the source water seemed to have less dissolved gas supersaturation entering the neighboring plant, bubbles are seldom released (burping) from their upflow clarifier. Without any quantitative data, it has been assumed that the type of media in this clarifier was less likely to allow release of gas bubbles (burping) to the effluent.

Utility F chose to change the media in their upflow clarifier to a type similar to that used at the neighboring treatment plant, with hope of controlling bubble release from their clarifier. During a second visit, the water was only slightly supersaturated at 0.024 atm gauge pressure, and there did not appear to be any gas bubble release (burping) from the clarifier with the new media. A future follow up study is needed to determine if this was effective.

On-site Analysis at Treatment Plant G

Large algal blooms are quite common during the summer months in both the source water and in treatment plant G. High levels of dissolved oxygen are typically measured during algal activity, and the staff at utility G speculated that this caused air binding in their filters. A diurnal study was designed to understand how filter performance can change throughout the day and during the summer months, from both algae photosynthesis and temperature changes. To monitor the peak water quality variations during the day when algal activity would be the greatest, measurements began at 6:30 am and concluded on 11:00 pm. Filter influent and effluent were collected with a bucket from 4 filters.

As mentioned previously, algae photosynthesis can cause a net increase in the TDG, since dissolved oxygen production exceeds dissolved carbon dioxide consumption. During the evening when algae would undergo respiration, the opposite should occur for a net decrease in TDG. The measured dissolved gases in the filter influent of all four filters followed the expected trends with a diurnal variation throughout the day (Figure 4.8, Top). The water early in the morning was undersaturated with TDG, and the TDG increased with the algal activity throughout the day, with the water eventually becoming supersaturated with dissolved gas. During this sampling event, the amount of algal activity was considered much lower than an average year, due to an abnormally rainy summer; consequently, the peak of dissolved gas supersaturation was not deemed very high. Dissolved oxygen and carbon dioxide also varied according to algae activity.

For all data measurements throughout the day, the TDG decreased after the water passed through the filter (negative change in TDG through the filter) (Figure 4.8, Bottom), and more TDG was removed when the influent had the greatest amount of TDG supersaturation (at 6 pm) (Figure 4.8, Top) and dissolved oxygen. Three different scenarios could explain this reduction of TDG through the filters:

1. Gas bubbles could be forming within the filter media (filter air binding). This bubble formation would cause a reduction of all dissolved gases in solution.
2. Algae could be growing in the filters. Peak algal activity would be expected during sunlight intensity. As a result of photosynthesis, dissolved carbon dioxide would decrease, dissolved oxygen would increase, and pH would also increase.

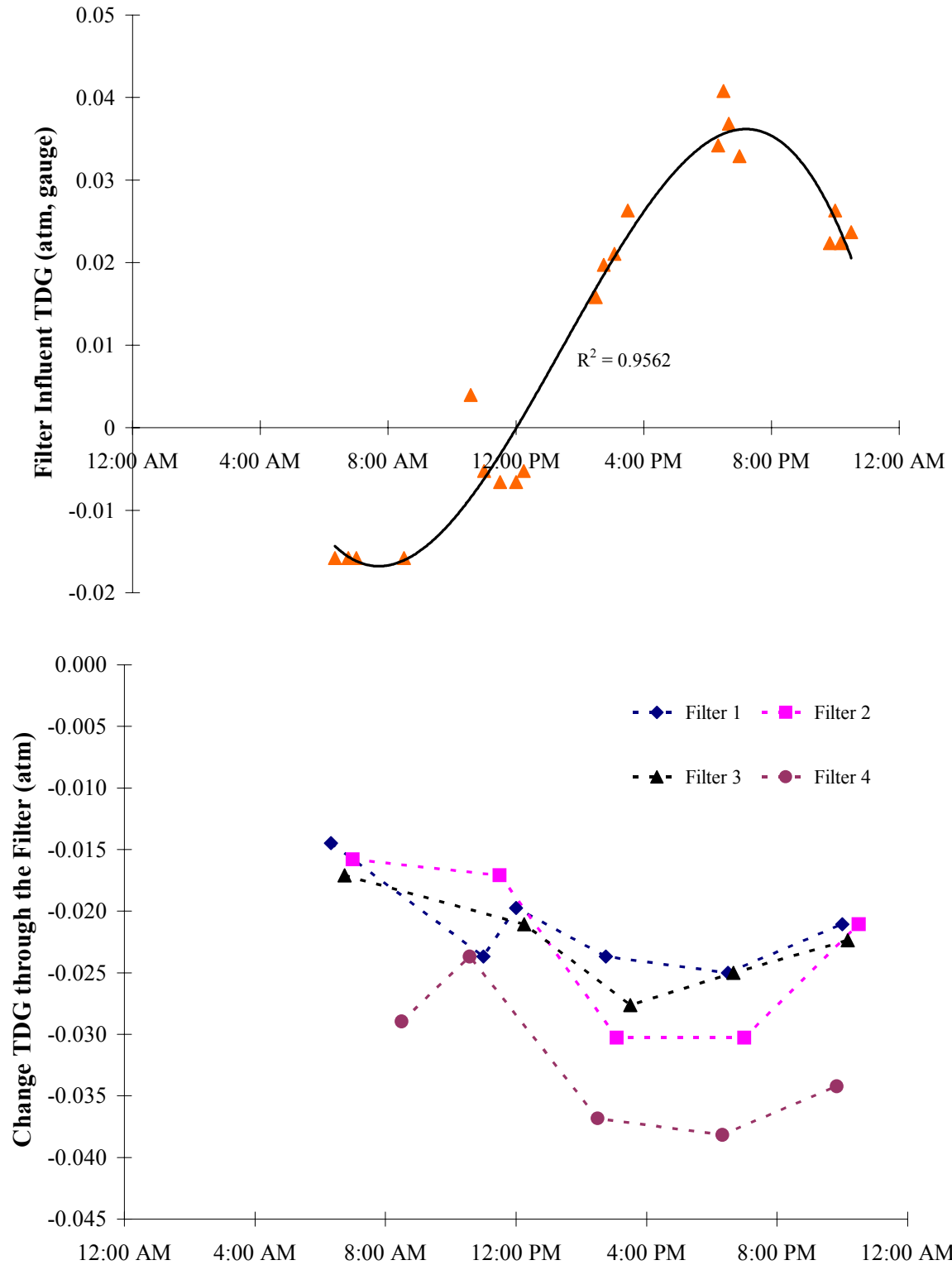


Figure 4.8 – Diurnal Variation of TDG in the Filter Influent for All Four Filters at Utility G (Top), and Change in the Total Dissolved Gas (TDG) through Each Filter at Utility G (Bottom). A Negative Change in TDG Indicates a Loss Within the Filter.

3. Heterotrophic bacteria could be growing as a fixed film attached to the filter media. Bacteria respiration would tend to increase dissolved carbon dioxide, decrease the pH, and remove dissolved oxygen.

In all of the filters, there was a decrease in dissolved oxygen (negative change through the filter) and an increase in dissolved carbon dioxide (positive change through the filter) (Figure 4.9), consistent with active heterotrophic bacteria changing the dissolved gas content. The pH was also lower in the filter effluent. Although green algae could be seen attached to some of the structures on top of the filters, the net effects of this algae had to be overwhelmed by action of the bacteria.

The activity of heterotrophic bacteria was unexpected but does explain why gas bubbles were not observed during filter backwashes when air binding was suspected. The extent of algal activity, again, was considered less than a typical year, so filter air binding might still be a problem during higher levels of dissolved gas supersaturation. Yet, higher dissolved gas supersaturation could lead to more bacteria activity (Figure 4.8, Top). This diurnal filter study broadened the understanding of what can happen to dissolved gas within a media filter.

Future Analysis

The total extent of bubble formation problems within water treatment plants is unknown. Although many utilities such as those presented previously have historically had obvious bubble induced disruptions, these problems could be very widespread across the water industry but less severe. Indeed, simple observations may have been overlooked or regarded as negligible. As was shown with utility B, even a small degree of bubble formation can significantly reduce plant efficiency (Table 4.3). A thorough survey measuring total dissolved gases is needed to determine the distribution of dissolved gas supersaturation and subsequent bubble related problems. In addition, a survey may provide insight into other sources of dissolved gas supersaturation or simple mitigation techniques.

Mitigating the Effects of Bubble Formation

Utilities face many obstacles in reducing problems associated with gas bubble formation. Experiences were synthesized to provide a starting point for their analysis of problems with floating floc (Figure 4.10) and filter air binding (Figure 4.11). Occurrences of floating floc or filter air binding should be confirmed first, and then the source causing the dissolved gas

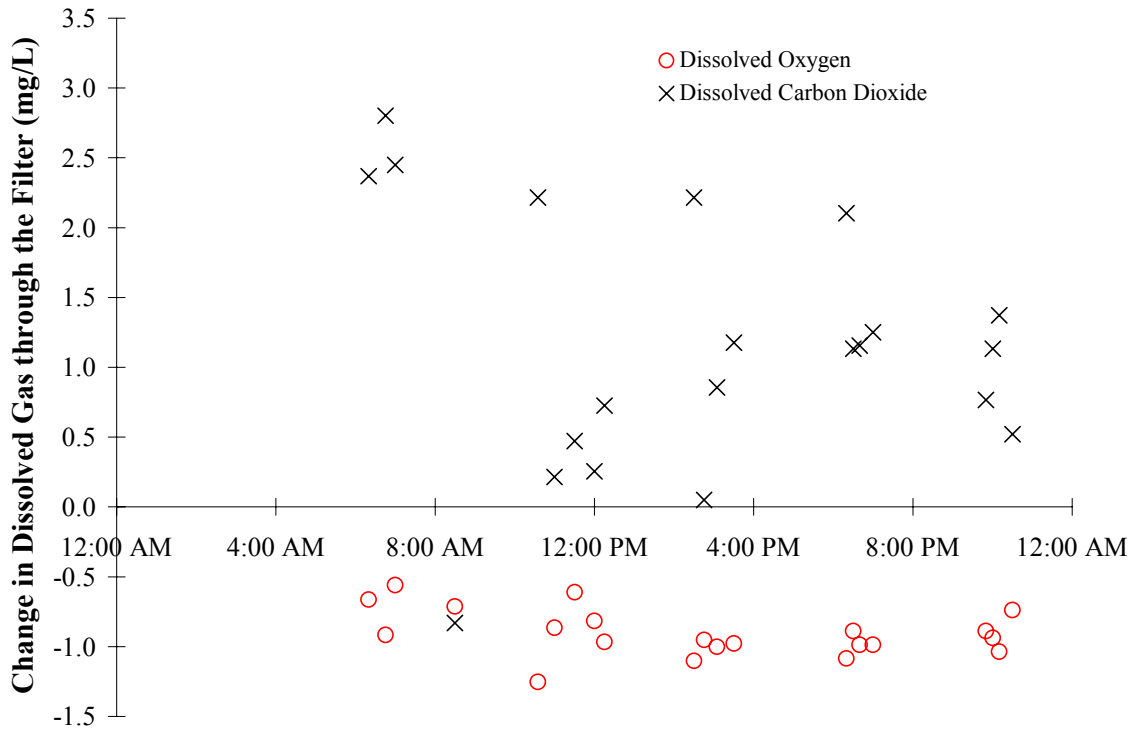


Figure 4.9 – Change in the Dissolved Oxygen and Carbon Dioxide for All Filters at Utility G. A Negative Change in TDG Indicates a Loss within the Filter, and a Positive Change Indicates an Increase through the Filter.

supersaturation or bubble formation should be identified and eliminated whenever possible. In some cases there could be multiple causes of dissolved gas supersaturation.

Unfortunately, reducing dissolved gas supersaturation in a source water (algae photosynthesis or pipeline air entrainment for example) can be very complex, expensive, or unfeasible. Furthermore, altering treatment processes that cause dissolved gas supersaturation, such as ozonation, may not be an option, so other options need to be considered. For example, many of the principles outlined in Figures 4.1, 4.2, and 4.3 can be used to reduce the occurrence of floating floc (Figure 4.10). In fact, if the water is actually undersaturated with respect to the atmosphere, re-designing the rapid mixer could stop all bubble and floating floc formation (Scardina and Edwards, 2004b).

A few operational changes can also reduce filter air binding (Figure 4.11). Increasing the water head above the media (submergence) increases the local pressure profile through the media, thereby reducing the potential for bubble formation (Scardina and Edwards, 2004a). Likewise, decreasing the flow rate or using a higher porosity media can increase the local

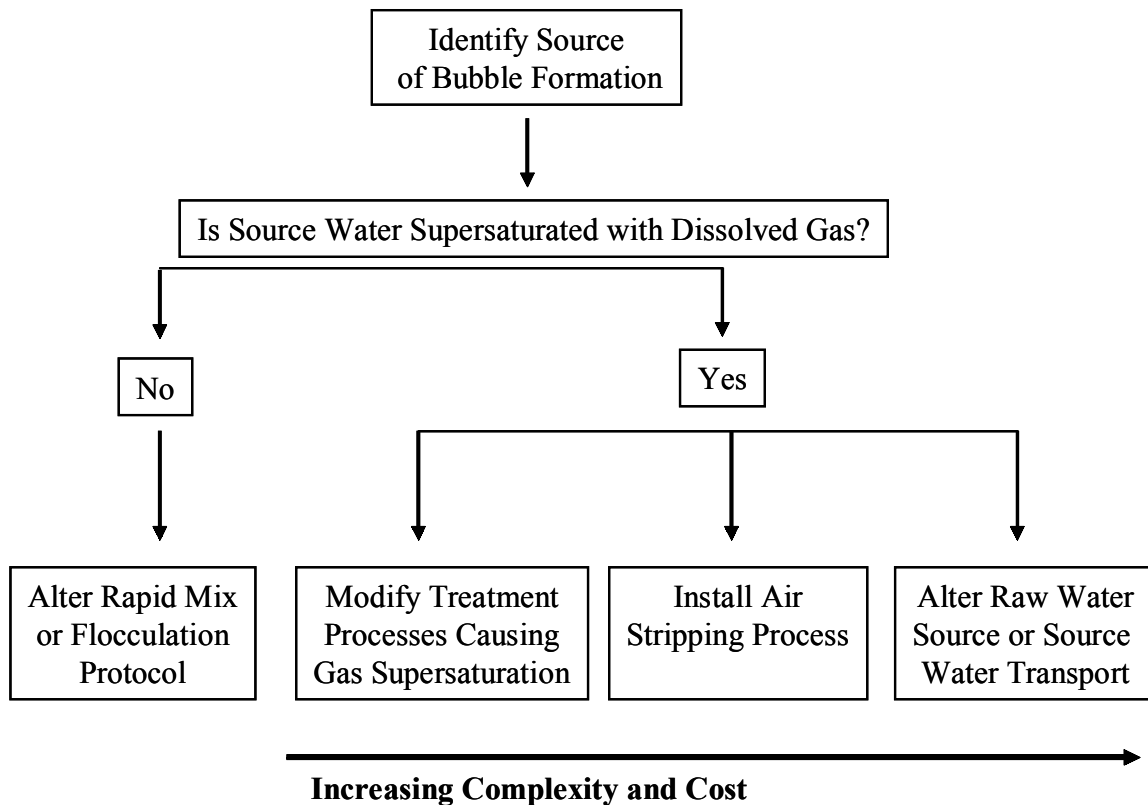


Figure 4.10 – Decision Tree for Reducing Bubble Formation, Floating Floc, and Hindered Settling.

pressure in the filter (Scardina and Edwards, 2004a). The use of an anthracite top layer can also be beneficial in reducing the effects of air binding. Due to its hydrophobicity and higher porosity, bubbles form readily in anthracite, such that less bubble formation would be expected deeper within the media bed; in addition, gas bubbles are also more likely to be released from an anthracite layer in a burping action, which would alleviate some of the bubble induced headloss (Scardina and Edwards, 2004a). These operational changes may improve filter performance but might not completely eliminate the air binding.

If the source of the dissolved gas supersaturation cannot be eliminated and operational changes do improve plant performance, then an additional treatment step should be installed that enhances gas transfer. Freefall aeration towers, freefall weirs, and air diffusion at a shallow depth can strip dissolved gas supersaturation. Given the slow kinetics of gas transfer across an air-water interface, multiple treatment steps might be needed to remove the dissolved gas supersaturation. For source waters supersaturated with dissolved gas, the first treatment step should remove this dissolved gas supersaturation, since all subsequent treatment processes could

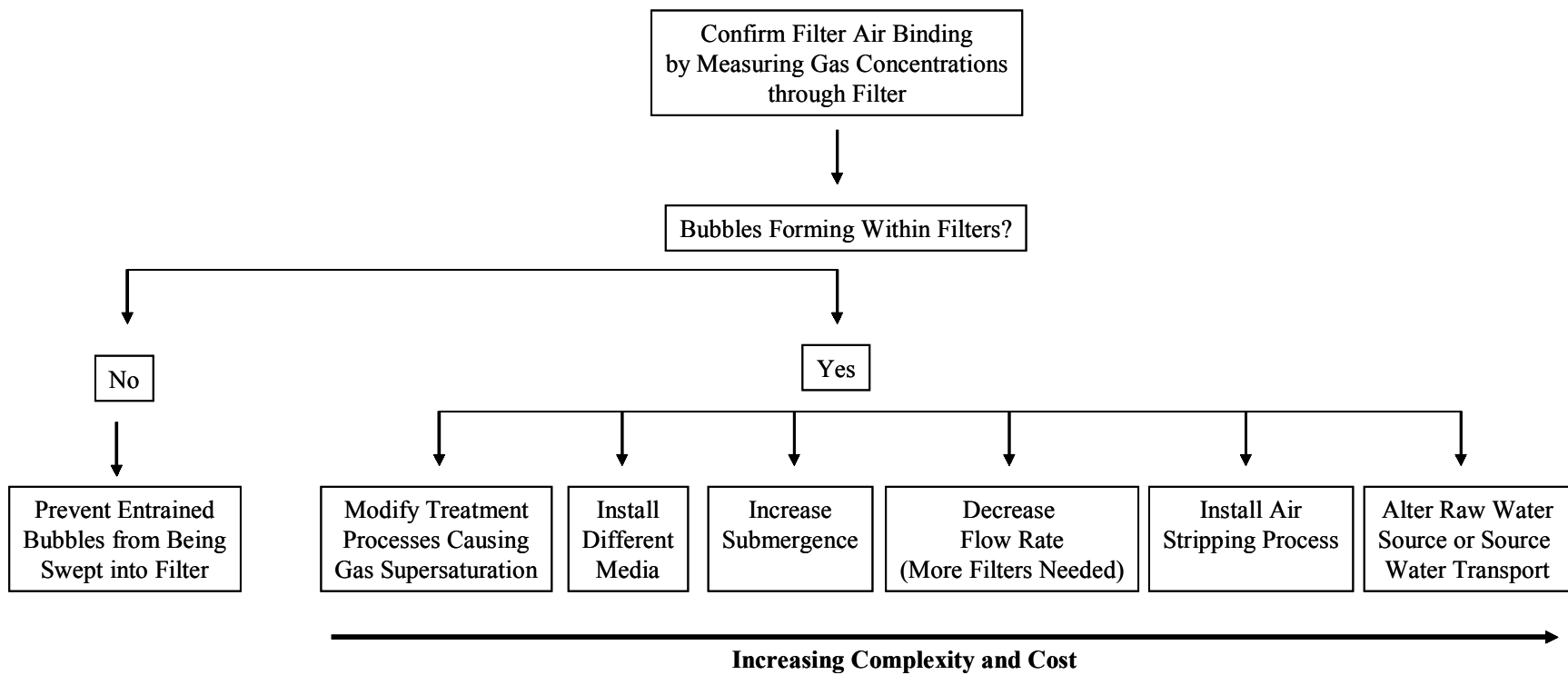


Figure 4.11 – Decision Tree for Reducing Filter Air Binding and Burping.

be compromised. Implementing additional treatment might appear to be cumbersome or expensive, but failure to do so can be more detrimental in terms of lost plant efficiency and operational costs, as well as potentially compromising water quality.

SUMMARY AND CONCLUSIONS:

- Bubble formation within treatment plants can reduce plant efficiency or cause complete failure of treatment processes. The most common problems caused by bubble formation observed in treatment plants are floating floc during coagulation and sedimentation, air binding in media filters and upflow clarifiers, and erroneous particle counts or turbidity.
- Sampling with a total dissolved gas probe (TDGP) can indicate sources of dissolved gas supersaturation and locations of bubble formation. A detailed analysis would track changes of all dissolved gas.
- Measuring dissolved gas in a source water can provide information on dissolved gas supersaturation, selection of better intake locations, and should be performed prior to design of a new treatment plant. In some cases dissolved air floatation should be considered if a water is supersaturated.
- The effects of bubble formation upon treatment processes can sometimes be mitigated by modifying plant operation. In some cases, multiple treatment steps might need to be installed to reduce dissolved gas supersaturation prior to further treatment.
- Modification of mixing during coagulation and flocculation can effect the formation and stability of floating floc. The localized solution pressure in the vicinity of an operating rapid mix paddle can be increased by increasing the depth of mixing or decreasing the velocity at the edge of the paddle. Rapid mixing for longer time lengths or increasing the flocculation rate can help separate bubbles from floc and improve floc settling.

ACKNOWLEDGMENTS:

This work was supported by the American Water Works Association Research Foundation (AWWARF) under grant 2821. The opinions, findings, conclusions, or recommendations are those of the writers and do not necessarily reflect the views of AWWARF.

REFERENCES:

- Letterman, R. & Shankar, S. (1996). Modeling pH in Water Treatment Plants: The Effect of Carbon Dioxide Transport on pH Profiles. Poster at the 1996 AWWA National Conference in Toronto, Canada.
- Scardina, P. and M. Edwards. (2001). "Prediction and Measurement of Bubble Formation in Water Treatment." *Journal of Environmental Engineering*, Vol. 127, 11, pg 968.
- Scardina, P. and M. Edwards. (2002). "Practical Implications of Bubble Formation in Conventional Treatment." *Journal American Water Works Association*, Vol. 94, 8, pg 85.
- Scardina, P. and M. Edwards. (2004a). Air Binding of Granular Media Filters. Pending Publication in *Journal of Environmental Engineering*.
- Scardina, P. and M. Edwards. (2004b). Fundamentals of Bubble Formation during Coagulation and Sedimentation Processes. Submitted to *Journal of Environmental Engineering*.
- Scardina, P., R.D. Letterman, and M. Edwards. (2004). Interference to Particle Count and Turbidity Measurements from Dissolved Gas and Bubble Formation. Submitted to *Journal of Environmental Engineering*.

APPENDIX I

PREDICTION AND MEASUREMENT OF BUBBLE FORMATION IN WATER TREATMENT

Paolo Scardina and Marc Edwards¹

Keywords: bubble, air binding, filters, nucleation, equilibrium, water treatment, headloss, filtration, gas transfer

Journal of Environmental Engineering 2001, 127, 11, pg 968.

ABSTRACT:

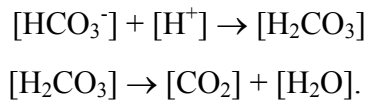
Water utilities can experience problems from bubble formation during conventional treatment, including impaired particle settling, filter air binding, and measurement as false turbidity in filter effluent. Coagulation processes can cause supersaturation and bubble formation by converting bicarbonate alkalinity to carbon dioxide by acidification. A model was developed to predict potential bubble formation during coagulation, and its accuracy was confirmed using an apparatus designed to physically measure the actual volume of bubbles formed. Alum acted similar to hydrochloric acid for initializing bubble formation, and higher initial alkalinity, lower final solution pH, and increased mixing rate tended to increase bubble formation at a given pH.

INTRODUCTION:

Gas bubble formation is of established importance to divers and fish (i.e., the bends), carbonated beverages, solid liquid separation in mining, cavitation in pumps, gas transfer, stripping, and dissolved air flotation processes. Moreover, it is common knowledge that formation of gas bubbles in conventional sedimentation and filtration facilities is a significant nuisance at many utilities, because bubbles are believed to hinder sedimentation, cause headloss in filters through a phenomenon referred to as “air binding” (*AWWA* 1999), and measure as turbidity in effluents without posing a microbial hazard (Sadar 2000). There is currently no rigorous basis for predicting when such problems will occur or correcting them if they do.

¹ Paolo Scardina is a graduate student at Virginia Tech, Marc Edwards is an associate professor of environmental engineering at Virginia Tech, 418 NEB, Blacksburg, VA 24061.

In the past, many utilities having problems with bubble formation from waters supersaturated with dissolved gas have traced the source of the problem to air entrainment at water intakes. However, with the increasing popularity of “enhanced coagulation” at lower pHs, utilities may increasingly see problems arising from carbon dioxide driven bubble formation upon acidification of waters under some circumstances. Even if a source water is initially at equilibrium with the atmosphere and has no potential to form bubbles, the water can become supersaturated with carbon dioxide upon coagulant addition by conversion of bicarbonate to carbon dioxide:



This newly formed carbon dioxide supersaturation can then lead to bubble formation through various mechanisms.

Since the surface area is small compared to the volume of water in municipalities, treatment plants have been found to function as a relatively closed system with respect to the atmosphere (Letterman and Shankar 1996). In support of this hypothesis, although a conventional jar test would be expected to allow more transfer than a treatment plant, predictions of coagulation pH are most closely approximated by closed system assumptions (Tseng 1997, Tseng and Edwards 1999). To the extent that a treatment plant was approximated by a closed system assumption, bubble formation would be the only means of releasing dissolved gas supersaturation.

The goal of this paper is to describe the fundamental chemistry of bubble formation with a particular emphasis on carbonate supersaturation in water treatment plants. Equations are developed to predict the maximum volume of bubbles that might form during treatment processes, and a new device to physically measure this parameter in a water sample. The merits and drawbacks of other approaches to predict bubble formation are also discussed.

FUNDAMENTALS OF BUBBLE FORMATION:

Bubble Nucleation

Following supersaturation of a dissolved gas, a nucleation step is necessary before bubbles can form in solution. Homogenous or *de novo* nucleation describes spontaneous bubble

formation within the bulk water, which typically occurs only if the difference between the ambient and dissolved gas pressure is greater than 100 atm. (Harvey 1975). Consequently, homogenous nucleation is not expected to be observed in water treatment.

Bubbles can also form within pre-existing gas pockets located in surface cracks and imperfections of solids in a process known as heterogeneous nucleation (Figure 1). Supersaturated gas diffuses into the gas pockets, causing bubble growth and eventual detachment from the solid support. Unlike homogeneous nucleation, heterogeneous bubble nucleation can occur whenever a water is supersaturated (Hey et al. 1994) and is expected to prevail in most environmental systems.

The size and number of bubbles nucleated depends on the history of the water body and type of suspended particles (Keller 1972). The number of nucleation sites generally increases in the presence of surface active agents (Jackson 1994). Rough hydrophobic surfaces nucleate bubbles easily even at low supersaturations, while hydrophilic or even smooth hydrophobic surfaces nucleate bubbles only at exceptionally large supersaturations (Ryan and Hemmingsen 1998; Ryan and Hemmingsen 1993). The gaseous nucleation site can persist indefinitely on surfaces (Liebermann 1957; Tikuisis 1984). Surfactants such as soap reduce bubble nucleation at low micelle concentrations; whereas, above the critical micelle concentration they can increase nucleation (Hilton et al. 1993).

The crevice surface geometry dictates the curvature and internal pressure of the pre-existing gas pockets, which can be estimated using various approaches for use in modeling and predicting bubble formation. Unfortunately, no reliable analytical techniques can currently validate the predictions experimentally for the ideal geometries (Hey et al. 1994), although successful data can be obtained with arbitrary, irregular surfaces (Ryan and Hemmingsen 1998).

Other system factors affect bubble formation. Increasing gas supersaturation activates previously dormant nucleation sites and generates more bubbles from these sites (Hilton et al. 1993; Hikita and Konishi 1984), as will increased mixing intensity (Jackson 1994; Hikita and Konishi 1984). Finally, the tendency for bubble formation increases with temperature due to reduced Henry's equilibrium constants and more rapid diffusion kinetics (Hikita and Konishi 1984).

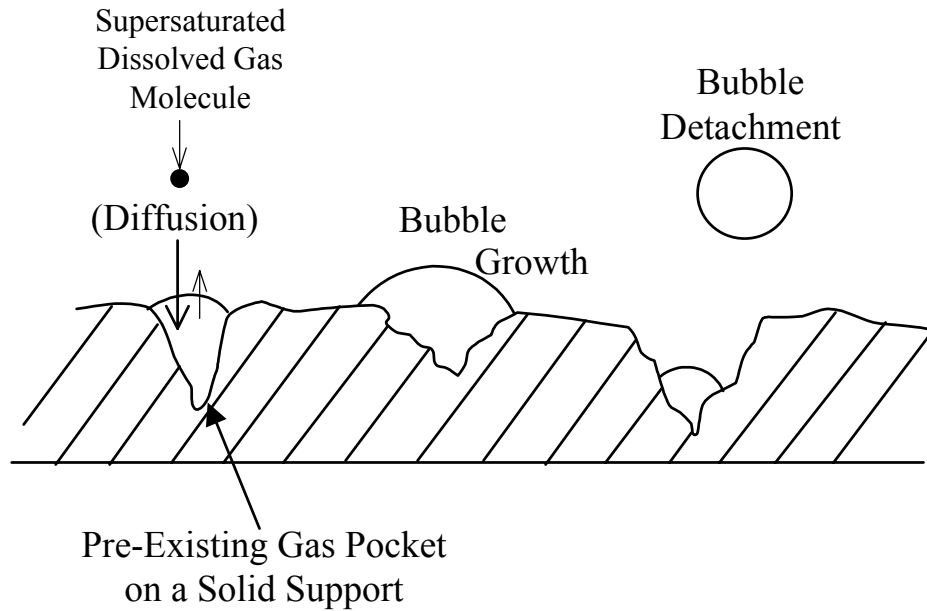


Figure 1 – Heterogeneous Nucleation.

Model Conceptualization

The preceding section described how supersaturated waters could form bubbles. Although models exist for gas stripping processes, no model has been proposed that allows prediction of possible bubble formation in water treatment (Boulder, 1994; Hess et al. 1996). A simple conceptualization was developed to predict the volume of bubbles that could form from this phenomenon (Figure 2). Consider a natural water initially at equilibrium with the atmosphere with no bubble forming potential. Upon acid addition, the bicarbonate is converted to carbon dioxide and the system will become supersaturated. If nucleation occurs, a new equilibrium can be approached by forming a volume of gas (ΔV_{gas}). This conceptualization is a hybrid of the classic open and closed system assumptions: it is a closed in that no exchange with the atmosphere occurs, but a gas phase is allowed to form. Although supersaturated carbon dioxide can drive the bubble formation, the gas formed includes nitrogen, oxygen, and carbon dioxide.

Using conventional equations for all equilibria, partial pressures, and mass balance equations for nitrogen, oxygen, and carbon dioxide, equilibrium for the system can be computed using the following equations (Stumm and Morgan 1970).

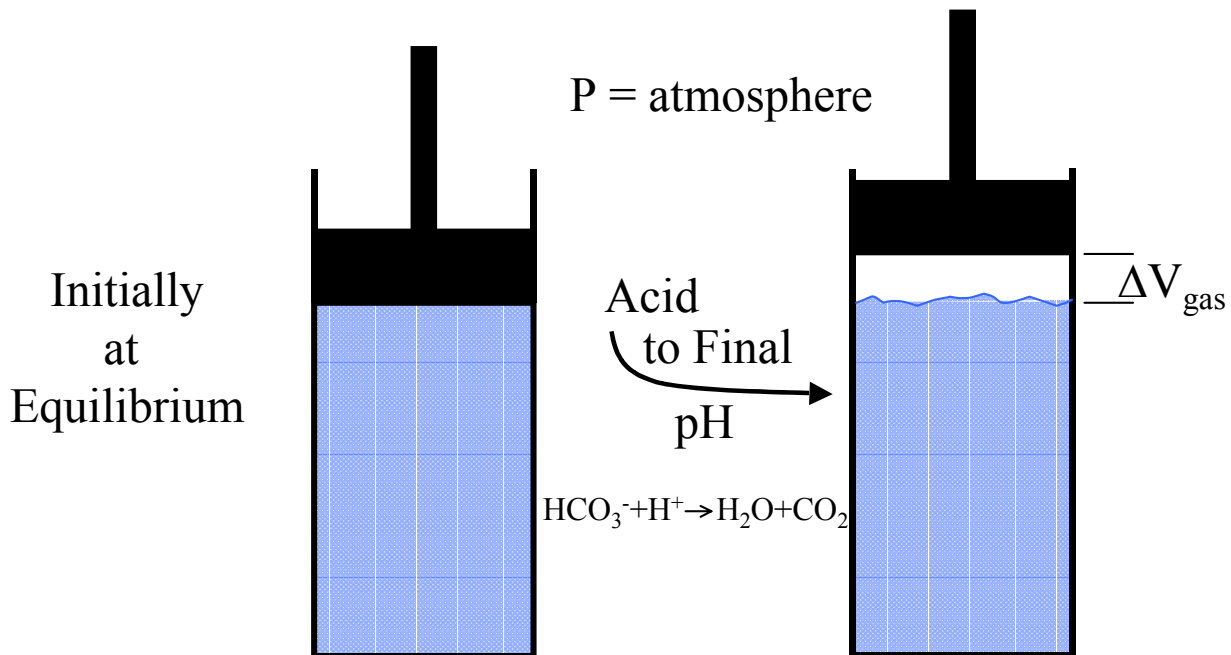


Figure 2 – Modified Closed System Conceptualization.

Bubble Atmosphere and Solution Equilibrium

$$[\text{O}_2]_{\text{aq}} = k_{\text{O}_2} p\text{O}_2 \quad \text{Equation 1}$$

$$[\text{N}_2]_{\text{aq}} = k_{\text{N}_2} p\text{N}_2 \quad \text{Equation 2}$$

$$[\text{CO}_2]_{\text{aq}} = k_{\text{CO}_2} p\text{CO}_2 \quad \text{Equation 3}$$

Sum of Bubble Partial Pressures

$$p\text{O}_2 = (P_b - P_{\text{wv}}) \times \frac{\text{O}_{2(\text{g})}}{\text{O}_{2(\text{g})} + \text{N}_{2(\text{g})} + \text{CO}_{2(\text{g})}} \quad \text{Equation 4}$$

$$p\text{N}_2 = (P_b - P_{\text{wv}}) \times \frac{\text{N}_{2(\text{g})}}{\text{O}_{2(\text{g})} + \text{N}_{2(\text{g})} + \text{CO}_{2(\text{g})}} \quad \text{Equation 5}$$

$$p\text{CO}_2 = (P_b - P_{\text{wv}}) \times \frac{\text{CO}_{2(\text{g})}}{\text{O}_{2(\text{g})} + \text{N}_{2(\text{g})} + \text{CO}_{2(\text{g})}} \quad \text{Equation 6}$$

Gaseous Mass Balances

$$P_{\text{atm}} (\%O_2) k_{O_2} V = [O_2]_{\text{aq}} V + O_{2(g)} \quad \text{Equation 7}$$

$$P_{\text{atm}} (\%N_2) k_{N_2} V = [N_2]_{\text{aq}} V + N_{2(g)} \quad \text{Equation 8}$$

$$P_{\text{atm}} (\%CO_2) k_{CO_2} + \text{Alk.} - \frac{K_{\text{HCO}_3^-} \times [CO_2]_{\text{aq}}}{[H^+]} = [CO_2]_{\text{aq}} + \frac{CO_{2(g)}}{V} \quad \text{Equation 9}$$

where:

$[O_2]_{\text{aq}}, [N_2]_{\text{aq}}, [CO_2]_{\text{aq}}$ = Concentrations of Respective Dissolved Gases (M)

pO_2, pN_2, pCO_2 = Partial Pressures in Gaseous State (atm)

k = Henry's Law Constants (M/atm)

$O_{2(g)}, N_{2(g)}, CO_{2(g)}$ = Amount of Respective Gas in Gaseous State (moles)

P_b = Pressure of Gases within Bubble (Assumed Atmospheric Pressure) (atm)

P_{wv} = Water Vapor Pressure (atm)

P_{atm} = Atmospheric Pressure (atm)

$\%O_2, \%N_2, \%CO_2$ = Normal Percentage Occurring in Atmospheric Air

V = Solution Volume (Assume 1 L) (L)

Alk. = Bicarbonate Alkalinity (M)

$K_{\text{HCO}_3^-}$ = First Acid Dissociation Constant for Bicarbonate

$[H^+]$ = Hydrogen Ion Concentration (M)

The model considers the presence of water vapor, and for simplicity the percentage of remaining trace gases, like argon, are included with nitrogen through the convention known as “atmospheric nitrogen” (Harvey 1975). Henry's gas law (Equations 1 – 3) is more applicable for dilute solutions with respect to atmospheric gases, rather than Raoult's law (Betterton, 1992). The carbon dioxide mass balance includes terms that consider the conversion of bicarbonate to carbon dioxide depending on the final pH and does not account for additional sources such as biological activity. If the actual initial dissolved gas concentrations for the dissolved gases (nitrogen and oxygen) are known, then the starting concentrations in their mass balances can be adjusted accordingly to account for more realistic conditions. All equilibria were adjusted for the appropriate temperature and taken from *Lange's Handbook of Chemistry* (1987).

After solving the system of equations listed above, the ideal gas law can then be used to calculate the total volume of bubbles formed at equilibrium. The ideal gas law was used since our calculations indicated that use of the real gas law only alters predictions by less than 0.4% under conditions typical of water treatment.

$$PV_g = nR'T \quad \text{Equation 10}$$

$$P = P_b - P_{wv} \quad \text{Equation 11}$$

$$n = O_{2(g)} + N_{2(g)} + CO_{2(g)} \quad \text{Equation 12}$$

$$\frac{P_{wv}}{P_b} = \frac{V_{wv}}{V_b} \quad \text{Equation 13}$$

$$V_b = V_{wv} + V_g \quad \text{Equation 14}$$

where:

V_g = Bubble Volume from Aqueous Dissolved Gases (O_2 , N_2 , CO_2)

R' = Ideal Gas Law Constant

V_{wv} = Bubble Volume from Water Vapor

V_b = Total Bubble Volume

Illustrative Calculation

With the known initial alkalinity and pH, final pH (or moles of acid addition), and the ambient temperature and pressure as starting inputs to the model, a computer program was used to solve the system of equations for various circumstances. For example, consider a closed system containing 1 L water with 300 mg/L as $CaCO_3$ alkalinity initially at pH of 8.7 and at equilibrium with the atmosphere (Table 1). Following acidification to pH 6.3, the system will shift to a new equilibrium with 1.62 mL of gas predicted to form. Although nitrogen and oxygen were not supersaturated with respect to the atmosphere before acidification, they constitute approximately 90% of the nucleated bubble volume with the remainder attributed to carbon dioxide (7.7%) and water vapor (2.3%). At equilibrium in this modified “closed” system, the final carbon dioxide concentration in solution remains supersaturated 100 times relative to the external atmosphere.

Table 1 – Illustrative Calculation Example.

Solution Parameter	Initial Conditions	Equilibrium Following Acidification
pH	8.7	6.3
Alkalinity, [HCO ₃ ⁻] (mg/L as CaCO ₃)	300	150
[N ₂] _{aq} (M)	5.37E-04	4.90E-04
[O ₂] _{aq} (M)	2.84E-04	2.71E-04
[CO ₂] _{aq} (M)	1.34E-05	3.01E-03
[N ₂] _g (moles)	-	4.70E-05
[O ₂] _g (moles)	-	1.30E-05
[CO ₂] _g (moles)	-	5.00E-06
pN ₂	-	70.51%
pO ₂	-	19.54%
pCO ₂	-	7.65%
Water Vapor	-	2.30%
Bubble Volume (mL/L)	-	1.62

Intuitively, higher initial alkalinity or lower final pH after acidification would be expected to lead to more bubble formation. The model confirms this expectation with a direct relationship between the initial alkalinity and bubble volume for a given final pH (Figure 3 and Figure 4). For a water at a given initial alkalinity, predicted bubble volume increases as pH decreases.

The model also predicts increased gas volume production at higher temperatures (Figure 4). For example, a water with 250 mg/l as CaCO₃ alkalinity initially at equilibrium with the atmosphere would form about 50% more bubbles at 25 °C than for the corresponding conditions at 5 °C. The enhanced bubble formation at higher temperatures is due to the changing Henry's constant with temperature. The carbon dioxide from acidification of the water at 25 °C exerts a partial pressure of 0.15 atm when pH is depressed to below 5 (1.15 atm. initial total pressure) as compared to 0.08 atm. (1.08 atm. total pressure) at 5 °C. This effect overwhelms the decreased volume of initial dissolved gas in solution at the higher temperature. Of course, all equilibrium constants should be corrected to the actual system temperature or significant errors will result.

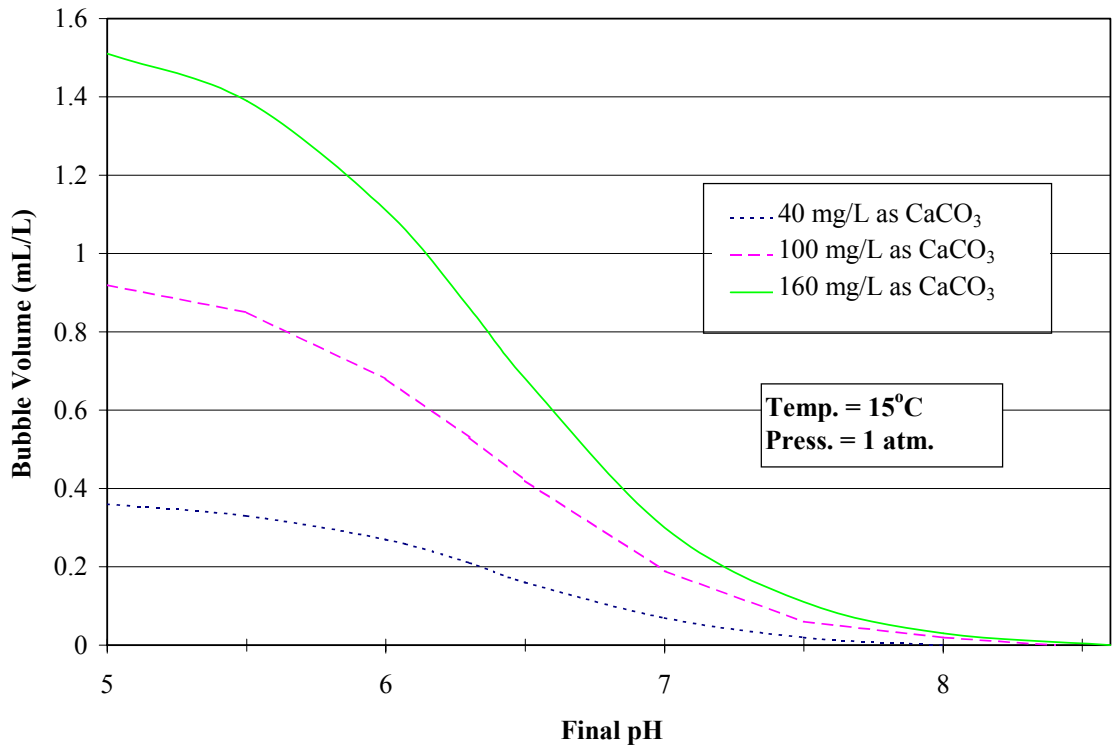


Figure 3 – Bubble Formation Potential Calculated Using Equations 1 – 14 as a Function of Initial Alkalinity and pH.

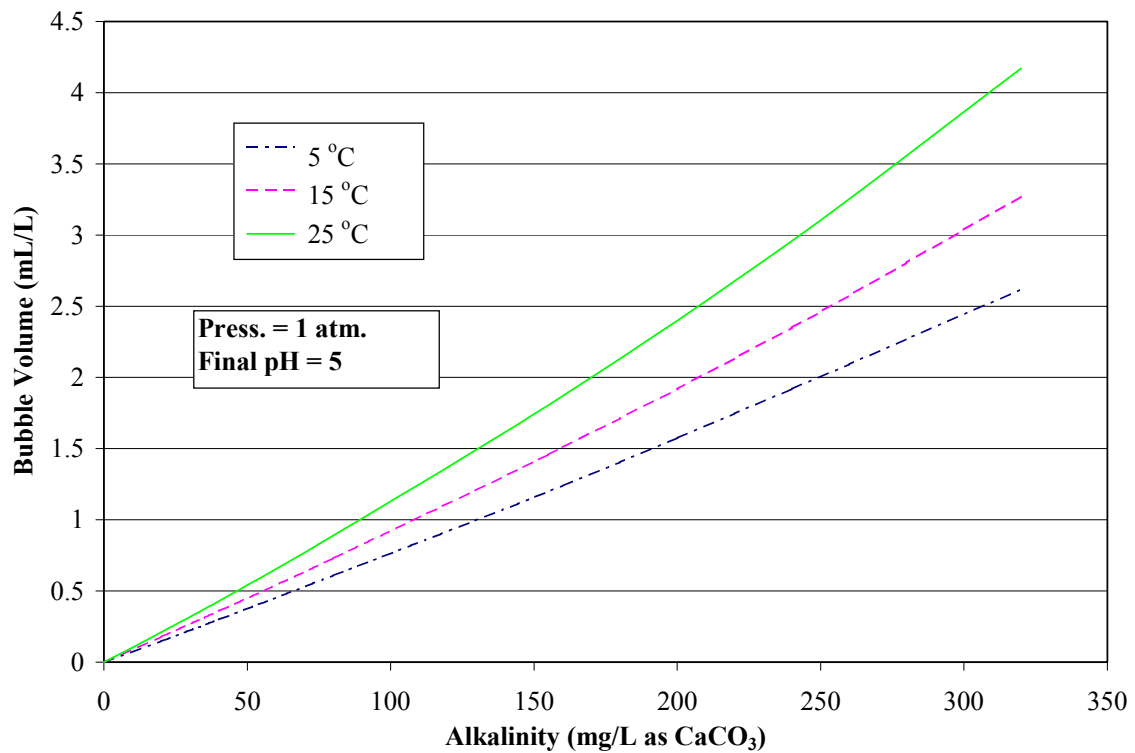


Figure 4 – Bubble Formation Potential Calculated Using Equations 1 – 14 as a Function of Temperature.

Like temperature, the ambient pressure or the depth of the solution can impact bubble formation. The model assumes atmospheric pressure for the pre-existing gas pockets and the final internal pressure of nucleated bubbles. Hydrostatic forces increase pressures, and the net result is that at a depth of 1.5 meters the bubble formation potential is greatly reduced (Figure 5).

MODEL CONFIRMATION:

Development of Bubble Apparatus

In order to validate the model predictions and provide a tool for use in practical situations, an apparatus was developed to physically measure the total volume of gas released from solution. The apparatus (Figure 6) follows the idealized conceptualization (Figure 2), with gas release occupying some volume within the closed system as indicated by a water level drop within the measuring pipette. Volume measurements are taken after the pressure within the pipette is normalized with respect to the atmosphere by moving the pipette upwards until the water levels (and pressure) in the pipette and holding container are equal.

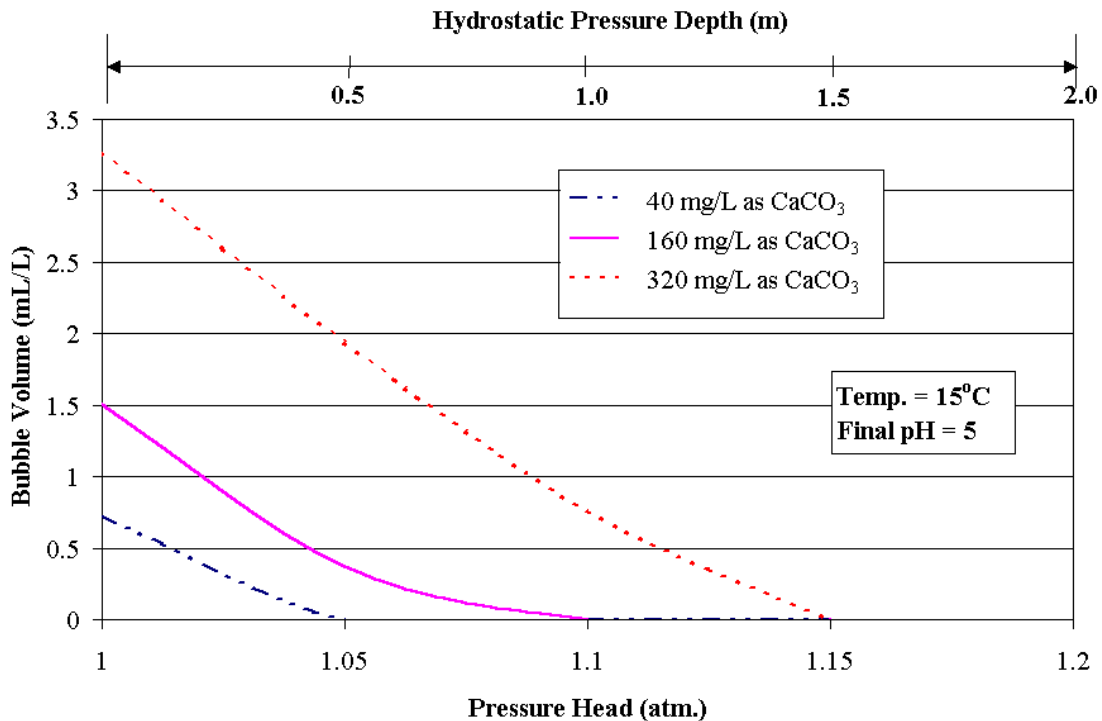


Figure 5 – Bubble Formation Potential Calculated Using Equations 1 – 14 as a Function of Pressure.

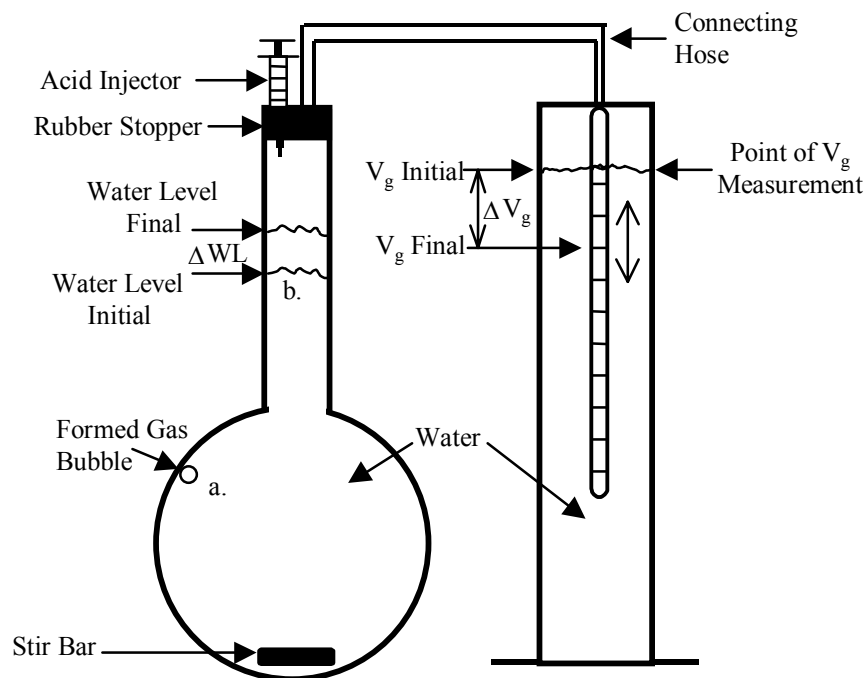


Figure 6 – Schematic of Bubble Volume Measuring Apparatus. Either bubbles forming in solution (a) or gases transferred at the interface (b) can be measured (ΔV_g).

Gases evolved in the apparatus can remain as bubbles in the original liquid volume, producing a rise in the flask's water level ΔWL , or transferred to the headspace of the container. In either case, the total volume of gas formed appears as ΔV_g (Figure 6), and ΔWL directly measures bubbles remaining in solution.

Materials and Methods

Construction materials included either a 1 or 2 L volumetric flask with a rubber stopper and teflon stirbar. Rubber stoppers were fitted with a 10 mL syringe for acid addition and nonexpandable teflon tubing—both secured with silicon glue. A 10 mL with 0.1 mL graduations pipette, submerged in a 1 L graduated cylinder containing water equilibrated with temperature and dissolved gases, measured the bubble volume produced. In a modified experiment to measure the bubble volume contained in solution, the necks of the 1 and 2 L flasks were reduced from their original 2 and 2.5 cm diameter, respectively, to a consistent 0.6 cm diameter, creating greater sensitivity for measuring the change in water level (ΔWL). With a 10 mL pipette, standard deviations in measurement were typically ± 0.03 mL. The practical quantitation limit ($\pm 20\%$ RSD) for the instrument is approximately 0.28 mL.

Sample waters were prepared with 0.01 M sodium nitrate (electrolyte) and aerated overnight in constant temperature rooms (either 20 or 5 °C ± 0.1.), and alkalinity was added as sodium bicarbonate immediately before experiments began. After checking the system for leaks, the sample was acidified by either 8.8 M hydrochloric acid or 0.2 M Al₂(SO₄)₃•18H₂O (alum), rapid mixed for 10 seconds at 300 rpm, and then stirred slowly at the desired rate for the remainder of the test. Preliminary tests at 160 mg/L as CaCO₃ found that the solutions approached equilibrium in the apparatus in approximately 4 hours; consequently, all subsequent experiments were stopped after four hours. When gas supersaturation was rather low (80 mg/L as CaCO₃ lowered to pH 6.3), gas evolution ended as quickly as two hours. Lastly, in extended preliminary experiments, there was no indication that gases transferred as bubbles to the headspace were transferred (redissolved) in the solution contacting the measuring pipette.

At least two apparatuses were simultaneously operated during initial experimental runs: one with analyte water for the actual gas measurement and the other with plain distilled water (containing no alkalinity or supersaturated dissolved gases) as a control. Any movement in the control pipette, due to barometric pressure changes or temperature warming, was subtracted from the measurements of the actual sample trial. As discussed later, alternative methods of dealing with these errors were developed.

Mixing Effects

More available energy or increased mixing intensity promotes and enhances bubble nucleation and growth (Jackson 1994). Consistent with expectations, a water, initially at 160 mg/L as CaCO₃ alkalinity lowered to pH 5, stirred at 500 rpm approached equilibrium quicker than the same water mixed at 120 rpm (Figure 7). An arbitrary mixing rate of 200 rpm was chosen for all remaining tests, but it is noted that a higher mixing rate would evolve gas faster. Modeling the treatment process with mixing rates that correlate to the rapid mix and flocculation cycles would be expected to provide valuable information on kinetics in an actual treatment plant.

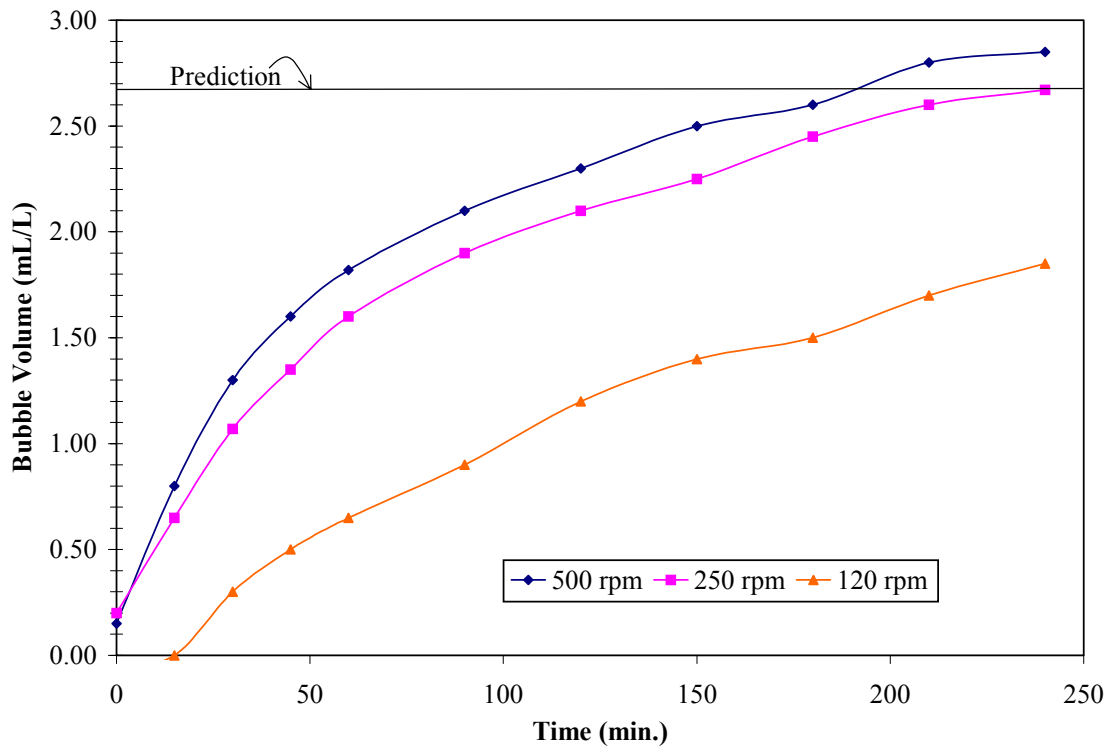


Figure 7 – Mixing Intensity Effects on Bubble Kinetics.

Realistic Water Condition Testing

The model predictions were compared to experimental data at a variety of conditions. A simple ratio (R) was developed to compare the experimental data to the mathematical prediction, with a ratio of 1 indicating a perfect prediction for the experiment.

$$R = \frac{\text{Actual Bubble Volume Produced Experimentally}}{\text{Bubble Volume Predicted by the Model}} \quad \text{Equation 15}$$

Initial alkalinities ranging between 40 and 320 mg/L as CaCO₃ and pH's lowered to 5 provided practical and extreme testing conditions (Figure 8). Although a few data points deviated in excess of 20% from the model, the majority lie well within the expected error. There was no distinguishable difference between the effects of hydrochloric acid (HCl) and alum (Al₂(SO₄)₃•18(H₂O)), and the mathematical model functioned equally well at temperatures of 20 and 5°C. The model was also accurate when more realistic coagulation pHs were examined (Figure 9).

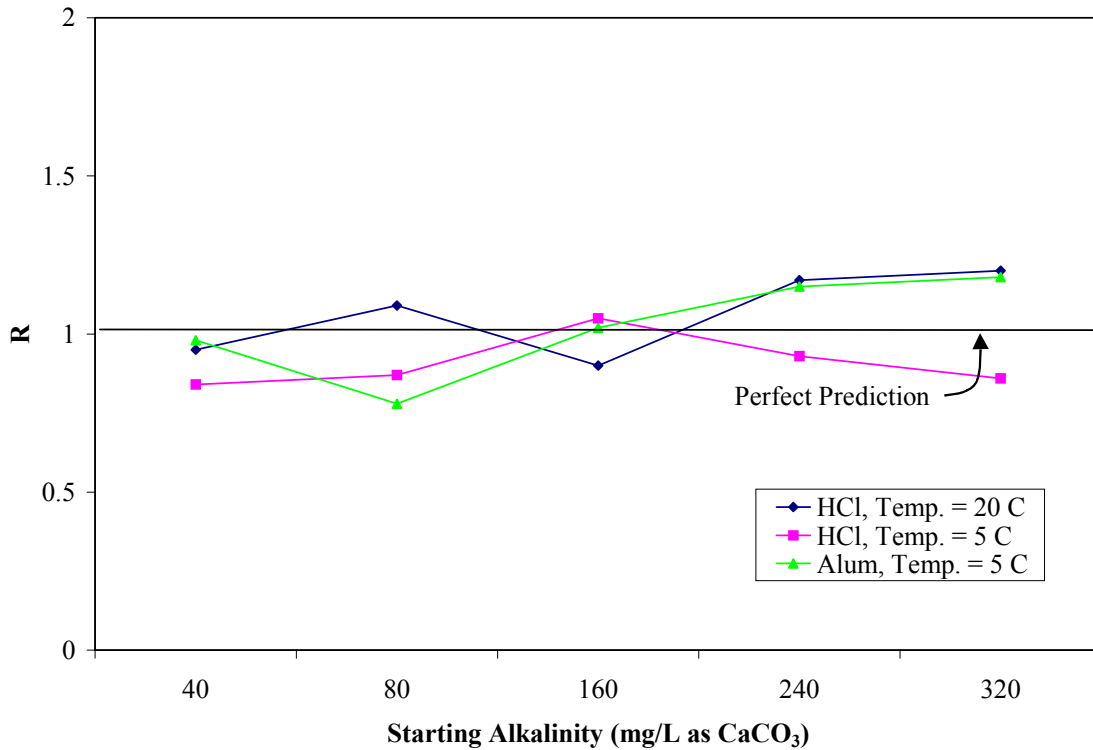


Figure 8 – Model Verification with Extreme Conditions. R is the Ratio of the Measured to the Predicted Bubble Volume (Equation 15). R Equals 1 when the Prediction Equals Experimental Measurements.

With higher gas supersaturations (320 mg/l as CaCO₃ lowered to pH 5), bubbles became visible on the glass surface and teflon stirbar minutes after acidification, characteristic of heterogeneous nucleation. Bubbles grew progressively and detached from the stirbar, eventually becoming visible on the glass flask.

Modified Analysis

The modified flasks with the reduced neck diameter were used to quantify bubble formation in the solution. Almost instantly, noticeable differences in the water level occurred in solutions of 320 mg/L as CaCO₃ initial alkalinity at 5 and 20 °C. The quantity of *in situ* bubbles seemed to level to a relatively constant value of 0.15 mL/L average for both temperatures; whereas, the ultimate gas production steadily increased implying that a certain number of nucleation sites growing, emitting, and re-forming bubbles.

The overall gas production was significantly lower than that produced during the normal tests, even with an extended test time length of 12 hours. For example, at 20 °C with the normal

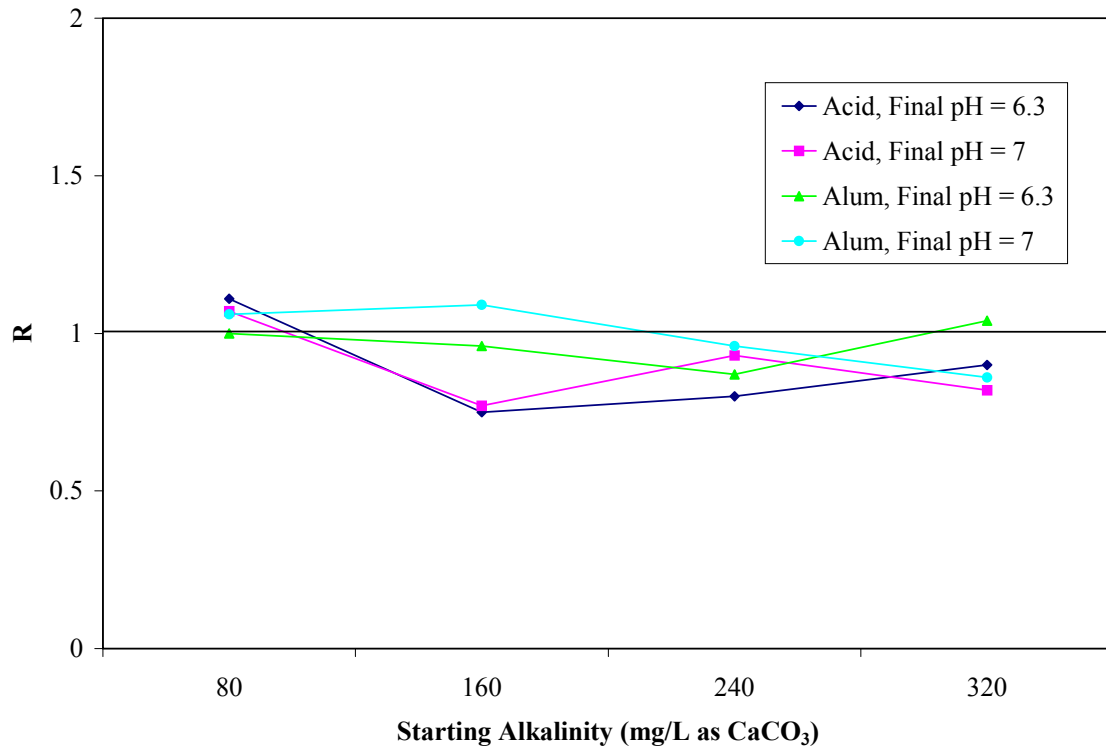


Figure 9 – Model Verification for 2 Different Acids and pH's. R is the Ratio of the Measured to the Predicted Bubble Volume (Equation 15). R Equals 1 when the Prediction Equals Experimental Measurements.

volumetric flask 6.7 mL/L of gas evolved compared to 3 mL/L for the same water within the modified flask. Surface interfacial gas transfer probably constituted a considerable amount to the measured bubble volume for the experiments in Figures 8 and 9, and modified flasks might be more appropriate to simulate actual treatment. Additional research is needed to resolve this issue.

Modeling and Experimental Errors

The system pressure where the supersaturated dissolved gas transfers (pre-existing gas pockets, pre-existing bubbles, or surface interfacial transfer) was assumed equal to atmospheric pressure. The assumption holds for interfacial surface gas transfer, but a bubble at depth would have a higher internal pressure limiting gas transfer (decreased concentration gradient), which may indicate the overall reduced measured volume in the modified experiment. Since the Laplace equation can predict internal pressures for the pre-existing nuclei either greater or less than solution pressure, atmospheric pressure was the safest assumption.

For most of the experiments, aeration was accomplished using compressed air jets located on the lab benches. Coupled with the air entering the solution at depth and probably being at a pressure greater than barometric, part or all of the solution water could have been supersaturated with dissolved gases prior to usage.

Ultimately, ambient pressure proved to be the largest factor. On a typical day, the barometric pressure varied up to 2% during experiments thereby changing the amount of bubbles produced. For instance, a water with 160 mg/L as CaCO₃ initial alkalinity at 5 °C acidified to pH 5 produces 1.23 mL/L of bubbles when the pressure was 1 atm. at the beginning and end of the test. If pressure drops 2% during the test, the model predicts 1.78 mL/L of bubble produced (45% increase), and a 2% increase in pressure during the test would decrease bubbles products by 41%. Use of a digital barometer during tests allowed for compensation of these effects.

Prior to applying the model to real waters, alkalinity buffering from non-carbonate species should be determined and subtracted from the total alkalinity.

PRACTICAL EXTENSIONS:

Other Analytical Techniques

Most analytical procedures only measure the aqueous gas supersaturation rather than a physical bubble volume produced. Although volumetric extraction and gas chromatography can measure dissolved gas concentration, these tests are labor intensive and expensive. The current edition of Standard Methods outlines a test for measuring gas supersaturation in a liquid by use of a sampling probe. Gases diffuse through the membrane until the pressure within the hose is at equilibrium and total pressure in solution is measured.

These devices report the data in terms of partial pressures, which indicates a potential for bubble formation, but does give equations to predict the potential volume of bubbles formed. Equations 10, 11, 13, 14, and 16 defined in this work and the measured supersaturation can be used to predict bubble formation potential, assuming that only nitrogen and oxygen contribute and the internal bubble pressure is atmospheric pressure.

$$n = (P_s - P_{atm})[k_{O_2} (\%O_2) + k_{N_2} (\%N_2)] \quad \text{Equation 16}$$

where:

P_s = Supersaturated Dissolved Gas Pressure in Solution (measured)

Standard Methods and other sources state that the main constituents of gas supersaturation are oxygen and nitrogen with carbon dioxide and argon considered negligible. The error introduced into Equation 16 by ignoring carbon dioxide is dependent on the initial alkalinity, system temperature, and final pH. For example, ignoring carbon dioxide in a water at 25 °C with 320 mg/L as CaCO₃ initial alkalinity and acidified to pH 3, 3.69 mL/L of bubbles are predicted, which would produce an error of 16% compared to the model calculation of 4.4 mL/L. The error increases substantially when very large alkalinities become acidified and results from incorrect assumptions stated in Standard Methods (Figure 10). As shown with the hypothesis and model, carbon dioxide cannot be ignored in all circumstances, which is especially true in anaerobic digesters, where the alkalinity is typically greater than 2,000 mg/L as CaCO₃ (Droste 1997).

Other problems can arise with these sampling probes. Under certain circumstances, accurate pressure measurements require up to two hours. Operators skilled in instrument usage are required for measurement precision because considerable errors result when bubbles form on the sampling hose. Although a 1.5 – 2% precision is documented for skilled operators, some researchers noticed up to 20% error from bubble growth on the sampling hose (Bouck 1982). Even though modifications of the original device helped eliminate this problem, usage of these dissolved gas probes mandates conscious operators and considerable care.

Future Work

The enhanced coagulation rule with possible reductions in coagulation pH will increase the likelihood of air binding problems. Thus, future work will apply these principles to a practical study of settling problems and filter binding which result from bubble formation.

ACKNOWLEDGMENTS:

This work was supported by the National Science Foundation (NSF) under grant BES-9729008. The opinions, findings, conclusions, or recommendations are those of the authors and do not necessarily reflect the views of NSF.

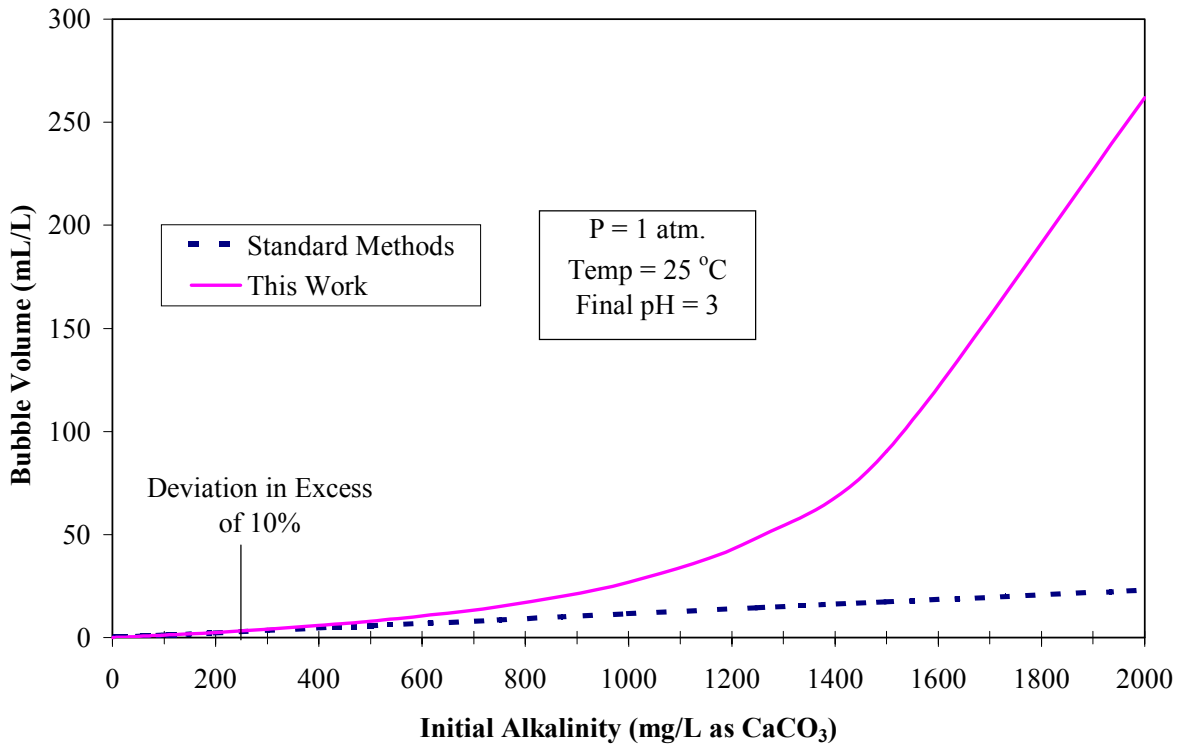


Figure 10 – Predictions of this Work Considering CO₂ Compared to Standard Methods Assumptions.

CONCLUSIONS:

- A model was developed to apply the science of bubble formation to the water treatment field. Bubble forming potential (mL gas/L solution) can be readily predicted or measured in waters, and this is likely to be an important operational parameter under some circumstances.
- Acidifying normal alkalinity waters, even if the water is not initially supersaturated with gas, can drive bubble formation.
- The model accurately predicted the volume of bubbles using a new apparatus.
- It is possible to measure bubble formation potential using a variety of approaches.

REFERENCES:

- Betterton, E.A. (1992). "Henry's Law Constants of Soluble and Moderately Soluble Organic Gases: Effects on Aqueous Phase Chemistry." *Gaseous Pollutants: Characterization and Cycling*, Edt. J.O. Nriagu, John Wiley and Sons, Inc, New York.
- Bouck, G. R. (1982). "Gasometer: An Inexpensive Device for Continuous Monitoring of Dissolved Gases and Supersaturation." *Trans. American Fisheries Society*, 111, 505-516.
- Boulder, CO. (1994). Conceptual Design Memorandum. Report prepared by Richard P. Arber Associates for Boulder, CO.
- "Dissolved Gas Supersaturation." (1998). *Standard Methods for the Examination of Water and Wastewater*. L. S. Clesceri, A. E. Greenberg, and A. D. Eaton, eds., United Book Press, Inc., Baltimore, 2-90-2-94.
- Droste, R. L. (1997). *Theory and Practice of Water and Wastewater Treatment*. John Wiley and Sons, Inc., New York, 626.
- Harvey, E. N., Barnes, D. K., McElroy, W. D., Whiteley, A. H., Pease, D.C., and Cooper, K. W. (1944). "Bubble Formation in Animals." *J. of Cellular and Comparative Physiology*, 24 (1), 1-22.
- Harvey, H. H. (1975). "Gas Disease in Fishes—A Review." *Proc., Chemistry and Physics of Aqueous Gas Solutions., Electrothermics and Metallurgy and Industrial Electrolytic Divisions, Electrochemical Society*, Princeton, N.J., 450-485.
- Hess, T.F., Chwirka, J.D., and Noble, A.M. (1996). "Use of Response Surface Modeling in Pilot Testing for Design." *Environmental Technology*, 17, 1205-1214.
- Hey, M. J., Hilton, A. M., Bee, R. D. (1994). "The Formation and Growth of Carbon Dioxide Gas Bubbles from Supersaturated Aqueous Solutions." *Food Chemistry*, 51, 349-357.

- Hikita, H. Konishi, Y. (1984). "Desorption of Carbon Dioxide from Supersaturated Water in an Agitated Vessel." *AIChE J.*, 30 (6), 945-950.
- Hilton, A. M., Hey, M. J., Bee, R. D. (1993). "Nucleation and Growth of Carbon Dioxide Gas Bubbles." *Food Colloids and Polymers: Stability and Mechanical Properties, Special Publication 113*, Royal Society of Chemistry, Cambridge, U.K., 365-375.
- Jackson, M. L. (1994). "Energy Effects in Bubble Nucleation." *Ind. Eng. Chem. Res.*, 33, 929-933.
- Keller, A. (1972). "The Influence of the Cavitation Nucleus Spectrum on Cavitation Inception, Investigated with a Scattered Light Counting Method." *J. Basic Eng., Trans. ASME*, 94 (4), 917-925.
- Lange's Handbook of Chemistry*. (1987). Crawford H. B. and Weine, R. L. Eds., McGraw-Hill, NY, 5-14, 10-3, 10-5.
- Letterman, R., Shankar, S. (1996). "Modeling pH in Water Treatment Plants: The Effect of Carbon Dioxide Transport on pH Profiles." Poster at the 1996 AWWA National Conference in Toronto, Canada.
- Liebermann, L. (1957). "Air Bubbles in Water." *J. of Applied Physics*, 28 (2), 205-211.
- Ryan, W. L., Hemmingsen, E. A. (1993). "Bubble Formation in Water at Smooth Hydrophobic Surfaces." *J. of Colloid and Interface Science*, 157, 312-317.
- Ryan, W. L., Hemmingsen, E. A. (1998). "Bubble Formation at Porous Hydrophobic Surfaces." *J. of Colloid and Interface Science*, 197, 101-107.

Sadar, M. (2000) "Calibration Methods for Low-Level Turbidimeter Measurements." *Virginia Section Newsletter, American Water Works Association*, July, 8.

Stumm, W., Morgan, J.J. (1970). *Aquatic Chemistry: An Introduction Emphasizing Chemical Equilibria in Natural Waters*. Wiley-Interscience, NY.

Tikuisis, P., Johnson, R. (1984). "Conditions for Heterogeneous Nucleation in the Physiological Environment." *Underwater Physiology VIII, Proceedings of the Eighth Symposium on Underwater Physiology*. A. J. Bachrach and M. M. Matzen, eds., Undersea Medical Society, Bethesda, MD, 107-118.

Tseng, T. "Considerations in Optimizing Coagulation." Master thesis, University of Colorado, Boulder, (1997).

Tseng, T. and Edwards, M. (1999). "Predicting Full-Scale TOC Removal." *Journal American Water Works Association*, 91 (4) 159-170.

Water Quality and Treatment: A Handbook of Community Water Supplies. Ed., Letterman, R. D. McGraw Hill, Inc. (5th ed., 1999).

APPENDIX II

PRACTICAL IMPLICATIONS OF BUBBLE FORMATION IN CONVENTIONAL TREATMENT

Paolo Scardina and Marc Edwards
418 Durham Hall, Blacksburg, VA 24061

JAWWA 94, 8, 2002, 85-94.

ABSTRACT:

Air entrainment and ozonation are the key causes of dissolved gas supersaturation and eventual bubble formation in water treatment plants. Total dissolved gas probes (TDGP) are now available to directly measure supersaturation and have many advantages compared to conventional techniques. Bubble formation during coagulation-flocculation hindered particle sedimentation, producing settled turbidities double that of solutions without dissolved gases. In a filtration study, run time to one half of initial flow was decreased by 54% when the source water was increased from 0.1 to 0.2 atm supersaturation. Indeed, even at 0.05 atm supersaturation, run length was only 21 hours in solutions without added particulate matter. A case study confirmed that bubble formation can interfere with coagulation and filtration processes at conventional treatment plants.

INTRODUCTION:

Dissolved gas supersaturation can lead to air bubble formation in water treatment plants and cause some unusual problems. Treatment plant operators have long suspected that bubble formation hinders particle agglomeration and can even float flocs particles during conventional coagulation-flocculation-sedimentation, resulting in solids carry over and overloading of the filters. Bubble formation within filter media also hinder performance by creating unwanted headloss—a phenomenon commonly termed “air binding” (*Water Quality and Treatment*, 1999). Finally, air bubbles in water have been reported to measure as turbidity (*Model 2100N Laboratory Turbidimeter Instruction Manual*, 1997), and filter media loss is believed to occur from bubble release during backwashing.

Although these problems routinely affect water utilities such as Metropolitan Water District, California, City of Myrtle Beach, South Carolina, and Boulder, Colorado, very little

fundamental research has been aimed at confirming, understanding, or eliminating this common problem. The goal of this paper is to discuss practical situations that lead to bubble formation at water treatment plants, to illustrate how bubble formation can affect treatment processes such as coagulation and filtration, and to confirm some key predictions in a case study.

BUBBLE FORMATION AND DISSOLVED GAS SUPERSATURATION:

Bubbles can form whenever the activity of dissolved gas(es) in solution—as measured by partial pressure—exceeds the ambient hydrostatic pressure.

$$\Sigma \text{Dissolved Gas(es) Partial Pressure} > \text{Ambient Hydrostatic Pressure} \rightarrow \text{Bubble Formation}$$

Since it is believed that water treatment plants (WTP) typically operate as closed systems (Letterman and Shanka, 1996), bubble formation might be the preferred means of alleviating dissolved gas supersaturation, rather than interfacial transfer. The mechanism by which bubbles are expected to form at WTP is heterogeneous nucleation, that is, dissolved gases diffuse into air cavities (nucleation sites) located on imperfections of solid surfaces (Scardina and Edwards, 2000). As supersaturated dissolved gas diffuses into the nucleation site, the air cavity grows and eventually creates a bubble which can detach.

Waters can become supersaturated through a number of processes (Table 1), although the most common are either air entrainment or ozonation. Air can be entrained in pipelines during cascading or turbulent conditions at the source water intake or through drawing of air into pipes at air/vacuum release valves by excessive pipe flow velocities (Figure 1). Increased hydrostatic pressure in the pipeline drives subsequent gas dissolution, as observed when there are large elevation differences between the source and the WTP (1800 feet elevation drop at Boulder, CO). This entrained air is then released in the form of bubbles when it enters the treatment plant. Greater hydrostatic pressures and quantities of entrained air can increase the degree of gas supersaturation.

Ozonation can either increase or decrease gas supersaturation, depending on the specific circumstances. In general, gas diffusion at depth in a contact chamber will directly cause supersaturation of ozone even assuming it does not react or degrade (Figure 2). With air as the carrier gas, the partial pressures of all atmospheric gases will increase, while oxygen saturation increases and other gases are stripped in situations if a pure oxygen carrier gas is used.

Table 1 – Sources of Dissolved Gas Supersaturation

Source	Key Reaction
Air Entrainment	$[G] = k_h * \rho G$: Increased partial pressure at depth
Ozonation ¹	$O_3 \rightarrow O_2$, $[G] = k_h * \rho G$: 1 mole of O_3 can degrade to 1 mole O_2 , and increase of carrier gas partial pressure at depth
Coagulant Addition	$[HCO_3^-] + [H^+] \rightarrow [H_2CO_3]$: Acidic coagulants convert alkalinity to carbon dioxide
Lake/Reservoir Aeration, CO_2 Addition, Dissolved Air Flotation	$[G] = k_h * \rho G$: Increased partial pressure at depth
Photosynthesis and Anaerobic Growth	$106CO_2 + 16NO_3^- + HPO_4^{2-} + 122H_2O + 18H^+ \rightarrow C_{106}H_{263}O_{110}N_{16}P + 138O_2$ (Algae Photosynthesis ²) Microbial and algae growth can potentially supersaturate waters
Hypochlorite ³	$H^+OCl + H^+OCl \rightarrow O_2 + 2HCl$, Hypochlorite disinfectant can degrade to form O_2
Thermal Warming	$[G] = k_h * \rho G$: Waters hold less gas at increased temperatures
Barometric Pressure Change	$[G] = k_h * \rho G$: Waters hold less gas at lower barometric pressures

¹(AWWA, 1991)

²(Masters, 1991)

³(Baur)

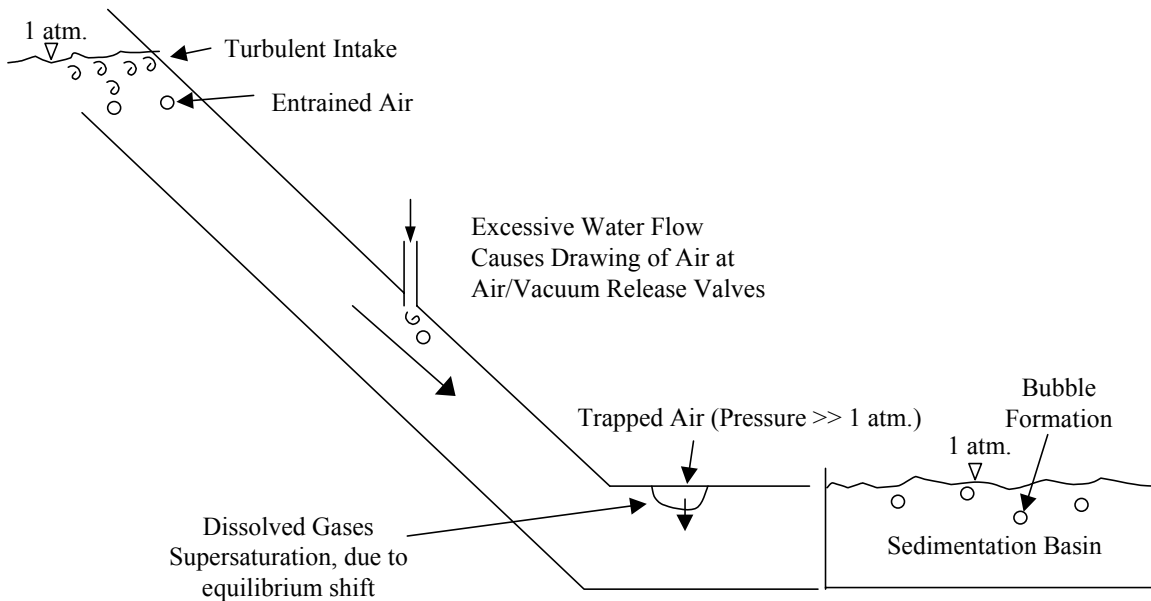


Figure 1 – Dissolve Gas Supersaturation from Source Water Air Entrainment.

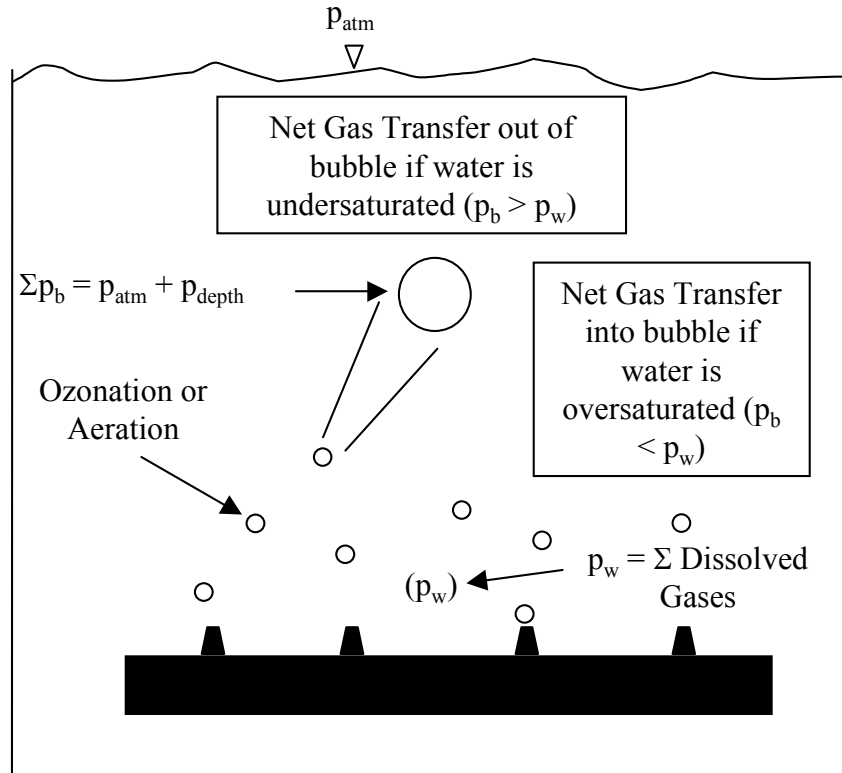


Figure 2 – The Effects of Ozonation on the Dissolved Gas Saturation.

Supersaturation will tend to increase with depth of bubble injection and increased airflow due to the additional hydrostatic pressure and the added air-water contact time.

Ozone can also directly cause supersaturation by chemical degradation to oxygen at a molar ratio of one oxygen to one ozone (AWWA, 1991). For example, consider a water at equilibrium with a 2% ozone and 98% oxygen gas phase at 1 atm. After the ozone completely degrades to oxygen at 25 °C (77 °F), the solution would then be supersaturated 0.18 atm with pure oxygen. Finally, ozonation can actually decrease dissolved gas supersaturation if the water is already highly saturated, since the injected bubbles provide for more rapid release of supersaturated gas transfer than is possible through heterogeneous nucleation. A pilot study for the City of San Diego found 67% reductions in headloss buildup, due to reduced air binding from ozonation prior to filtration (San Diego, 1990).

Lake or reservoir aeration, carbon dioxide gas injection, and dissolved air flotation can supersaturate waters through mechanisms similar to ozonation by diffused injection at depth. Although carbon dioxide is not commonly considered a factor in bubble formation, coagulant

addition can cause bubble formation by converting bicarbonate alkalinity to supersaturated carbon dioxide. Typical stoichiometries of microbe growth predict that aerobic bacterial respiration is expected to decrease the total gas partial pressure in solution, while anaerobic bacterial growth or photosynthesis can supersaturate oxygen. For example, if a water is initially at equilibrium with the atmosphere at 25 °C (77 °F), the total partial pressure will increase above 1 atm from algae photosynthesis: oxygen production outweighs carbon dioxide consumption. Net supersaturation becomes even greater if bicarbonate alkalinity is used as an algal carbon source. Warming of water and decreased local barometric pressure can supersaturate waters, assuming the solutions were initially at atmospheric equilibrium. Dissolved oxygen can also be formed from hypochlorite degradation.

MEASURING DISSOLVED GAS SUPERSATURATION:

Measurements of dissolved oxygen via a membrane probe or Winkler method is a common surrogate measure for total dissolved gas supersaturation. These methods are useful and reliable if all dissolved gases are proportionally supersaturated (i.e., air entrainment, ozonation with air as the carrier gas, dissolved air flotation, thermal warming and barometric pressure changes if all gases are initially at equilibrium) or if the water is supersaturated with oxygen (i.e., ozonation with oxygen carrier gas, hypochlorite, photosynthetic algae growth). However, these methods are clearly ineffective when oxygen concentrations are not supersaturated but the water is, as in the case of lake aeration or carbon dioxide supersaturation arising from acidification of solutions with inorganic carbon.

A direct measure of dissolved gases in solution is possible using a total dissolved gas probe (TDGP). The TDGP contains a hollow cylindrical silicon membrane (silastic) that rejects water but allows the transfer of dissolved gases from solution until the pressure within the membrane's cavity is in equilibrium with the pressure of gases in solution. The total partial pressure of gases in solution is displayed digitally, and the instrument can therefore detect gas supersaturation whenever it occurs. If desired, oxygen could be measured with a separate probe and subtracted from the total partial pressure, with various assumptions used to quantify the remaining gases.

There are few drawbacks to the method. Bubbles can form on the silastic membrane and interfere with the TDGP by causing a constant drop in the reported partial pressure, although this

can be prevented by pressurizing the sample container. In addition, although gases diffuse at approximately similar rates through air and water (Masterton and Hurley, 1993), (Baird and Davidson, 1962), (Thomas and Adams, 1965), gases transfer at different rates through the silastic on the TDGP. As a result, while it can take about 20 minutes for an accurate measurement of 1.1 atm total pressure from pure nitrogen which permeates through the silastic at a rate of $227 \times 10^{-10} \text{ s}^{-1}(\text{cm Hg})^{-1}$, the same measurement can be made for carbon dioxide in 5 minutes since it diffuses at $3240 \times 10^{-10} \text{ s}^{-1}(\text{cm Hg})^{-1}$ (*Lange's Handbook of Chemistry*, 1992). Certain TDGP's report an erroneously high total gas partial pressure, when the probe is immersed at considerable depth. Once identified, these hydrostatic effects can be corrected. Also, like dissolved oxygen measurements, the TDGP cannot discern micro bubbles in solution.

An alternative form of determining bubble formation potential is the bubble apparatus described by Scardina and Edwards (2000). This method is advantageous since it is less expensive to build and also has the potential to give a better indication of bubble formation in the treatment plant. However, field testing showed that the apparatus must be submerged in a water bath to prevent errors introduced by changing temperature.

PREVIOUS WORK:

The majority of published research to date on the subject is from consulting firms, contracted by specific utilities to determine feasible degassing strategies and in a few cases to identify the source of dissolve gas supersaturation (Table 2). Care should be taken when reviewing the consulting reports, since errors have been found concerning the fundamental science of bubble formation in treatment plants, as might be expected given the lack of previous research on the subject.

MATERIALS AND METHODS:

Coagulation Study

Three different levels of dissolved gas supersaturation were created in solution during coagulation tests in a jar apparatus: a water which contained very low dissolved gases, a water saturated with dissolved nitrogen gas, and a water supersaturated with a specified level of dissolved nitrogen gas. All waters were initially boiled, and solutions termed "low dissolved gases" in this work were sealed and allowed to cool. To saturate and supersaturate solutions,

Table 2 – Previous Work on Bubble Formation in Treatment Plants. All Plants Except Shreveport and South Bay Aqueduct Identified Air Entrainment as Source of Gas Supersaturation.

Utility	Project Summary
Boulder, CO	Described degasification alternatives, and pilot tested freefall weir treatment. ⁴ Investigated vacuum packed towers, heating dearators, and multi cone aerator by Infilco Degremont for degasification. ^{5*-8}
Denver, CO	Described degasification alternatives and conducted a dissolved oxygen profile through the plant including a pilot filter study on air binding. ⁹
MWD	Surveyed air binding at other utilities including site visits, described degasification alternatives, measured profiles of total dissolved gases and dissolved oxygen through plant, measured effects from ozonation, pilot tested freefall weir, paddle wheel, and degasification tower for degasification. ¹⁰
San Diego	Pilot tested effects of various filter submergences, ozonation, and aeration on filter air binding. ^{11**}
Shreveport	Measured degasification from freefall weir. ^{12**}
South Bay Aqueduct	Pilot tested the effects of ozonation on coagulation and filtration and tested aeration degasification. ^{13**}

⁴(Boulder, 1980)

⁵(Hess, 1980)

⁶(Boulder, 1993)

⁷(Boulder, 1994)

⁸(Hess, et. al, 1996)

⁹(Denver, 1997)

¹⁰(Metropolitan Water District, 1995)

¹¹(San Diego, 1990)

¹²(Ferguson and Beuhler, 1990)

¹³(Camp Dresser & McKee Inc., 1990)

*As discussed in Boulder (1993), **As discussed in Metropolitan Water District (1995)

subsamples of this solution were subject to nitrogen gas at pressure, mixed, and measured with a TDGP. Error was always less than 0.005 atm of the target value.

For the coagulation test, one liter 0.01 M sodium nitrate solutions were saturated with gases as desired. These solutions were then dosed with 2.5 or 5 mg/L as Fe from a 0.15 M stock ferric (III) chloride solution, and to maintain pH, 70 and 140 µL of 2 M sodium hydroxide was added just prior to the coagulant, respectively. Due to a smaller atmospheric surface area to volume ratio, one liter Erlenmeyer flasks were deemed a better approximation to treatment plants than traditional square jars. Solutions were rapid mixed at 300 rpm for 10 seconds and flocculated at 60 or 100 rpm for 30 minutes using a 1.5 inches (3.8 cm) Teflon coated magnetic stirbar. Samples were collected at a depth of 3.5 inches (8.9 cm) from the surface for measurements of settled turbidity.

Filtration Study

All filtration studies were carried out using a mono-media column filter with a circular diameter of 1.75 inches (4.45 cm) and sand media between the size range 0.417 and 0.589 millimeters (0.016 and 0.023 inch) as collected by wet sieving (Figure 3). The intermediate material was a mix of 0.125 and 0.25 inches (.32 and .64 cm) media, and the ballast material was approximately 1 inch (2.5 cm) in size. The media was thoroughly backwashed prior to each experiment to remove any bubbles and was settled such that initial flow through the filter was always within $\pm 5\%$ of 3 gpm/ft² (8.3 L/hr). A constant head of 6 inches was maintained above the filter at all times, and water entered the filter at 2 inches (5.1 cm) above the media surface, to prevent splashing of the water.

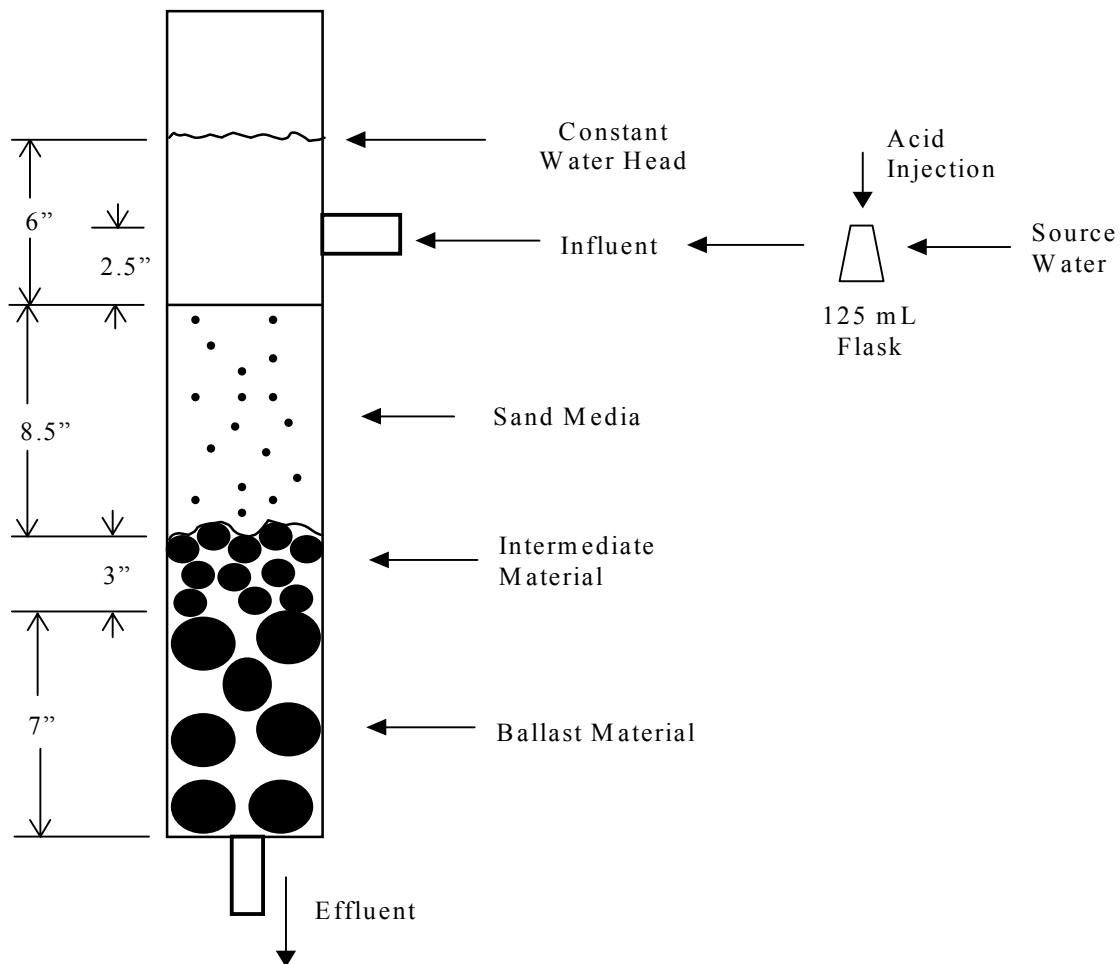


Figure 3 – Pilot Filter Schematic.

The influent was distilled deionized water equilibrated with atmospheric gases. For every 0.1 atm of desired gas supersaturation, 170 mg/L as CaCO₃ alkalinity (added as sodium bicarbonate) was added to the source water, with supersaturation created by acidification to a pH below 4.5 using 1 molar nitric acid. To minimize the amount of gas desorption, the source water was pumped into a 125 mL flask where nitric acid was added, after which the supersaturated water was immediately introduced to the filter.

RESULTS AND DISCUSSION:

Implications of Bubble Formation in Coagulation

Despite normal precautions taken to minimize degassing, during the jar test experiment the measured total dissolved gas (TDG) pressure decreased markedly during the rapid mix and flocculation cycles before leveling off (Figure 4). Between the experimental time of 0-5 minutes, the cumulative degassing was due to transferring solution from the pressurized flask to the testing flask, turbulent rapid mixing, and in situ bubble nucleation. Following rapid mixing in the 1.2 atm supersaturated solution, significantly more micro bubbles were seen in solution than in the comparable water saturated with 1.1 atm gas, which undoubtedly resulted from a greater rate of gas transfer from solution.

In all scenarios, the solutions containing supersaturated dissolved nitrogen gas exhibited slightly higher measured turbidity during flocculation than the solutions at equilibrium with nitrogen (Figure 5). The increased measured turbidity in supersaturated solutions could have been caused by air bubbles, altered floc particle sizes, or bubbles contributing to measurements of the turbidimeter. The specific cause was not identified in this work. Within minutes of starting flocculation, bubbles began forming on the wall of the flask and on the stirbar in the supersaturated gas solutions. Toward the middle to end of flocculation, bubbles were also attached to the flocs or floating freely in solution (See Photograph). Many of the iron hydroxide flocs had a natural tendency to float at the water surface, and the supersaturated waters typically appeared to have a greater mass of particles at the interface.

During all three tests with a 2.5 mg/L as Fe dose, different agglomerates formed dependent on supersaturation (See Photograph). Solutions that were low in dissolved gases and equilibrated with 1 atm nitrogen had “normal” iron hydroxide particles with a slight yellow-orange color after flocculation. In contrast flocs never formed properly in the solutions saturated

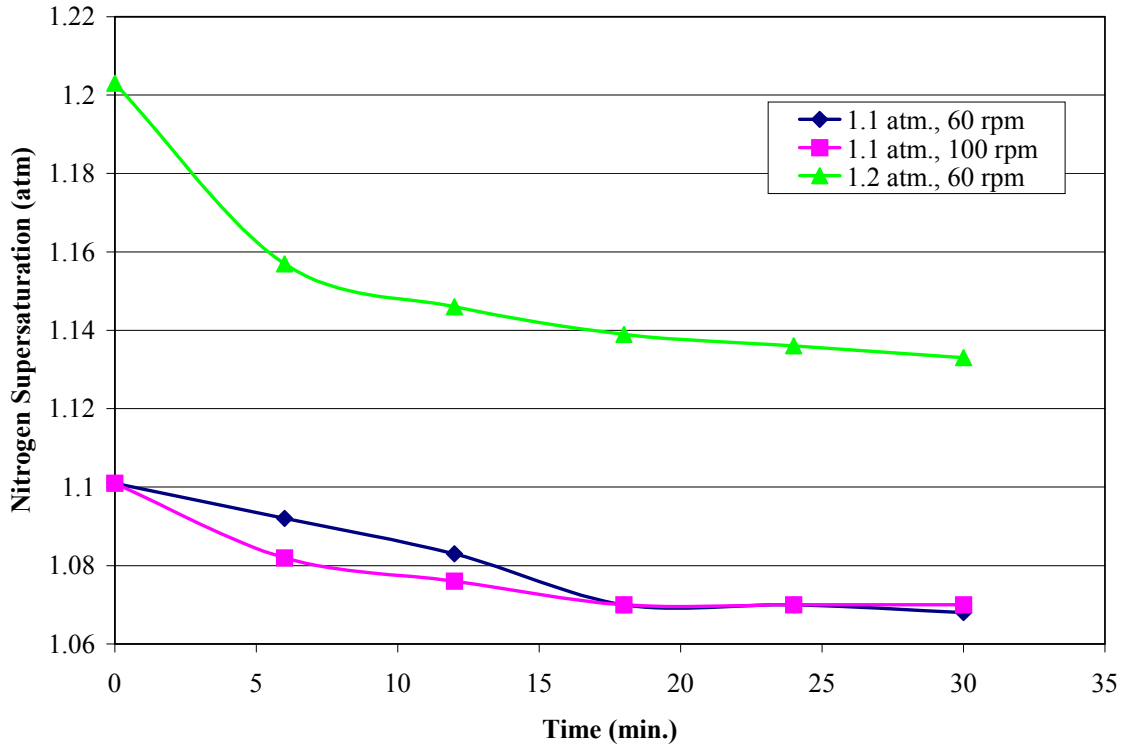


Figure 4 – Extent of Dissolved Nitrogen Supersaturation during Coagulation Experiment.

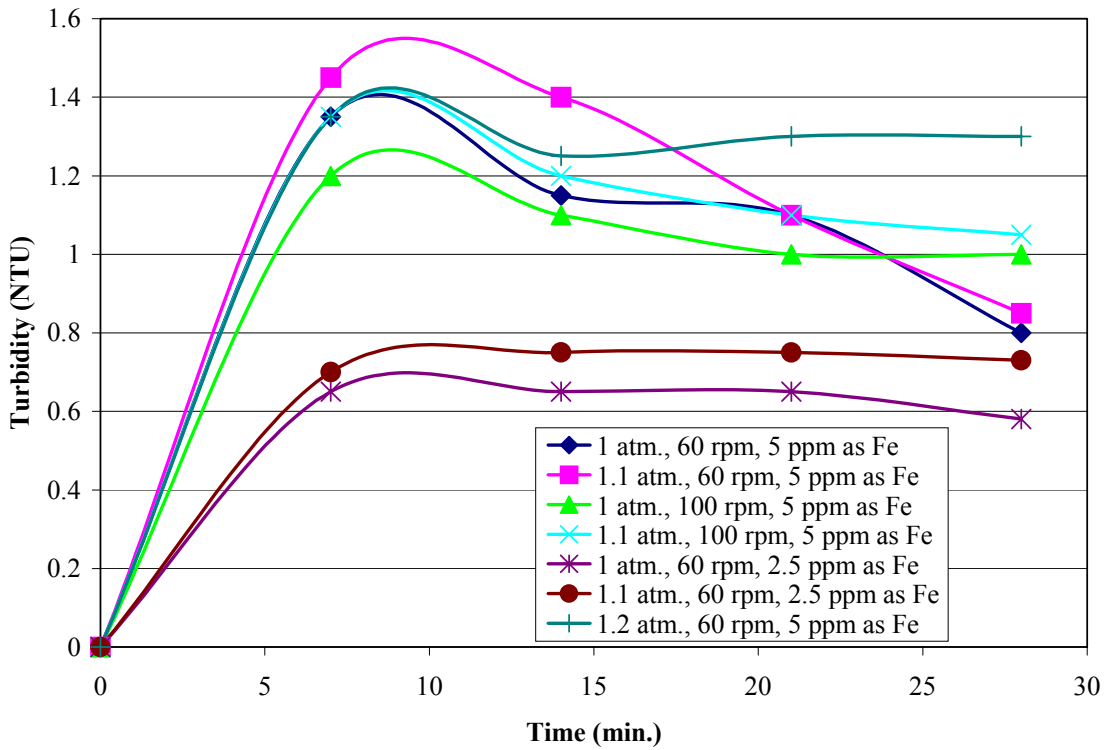


Figure 5 – Turbidity Measurements during Flocculation.



Photo 1 – Bubbles Attached to Floc Particles. Bubbles attached to iron hydroxide particles in solution (a), and enlargement (b).

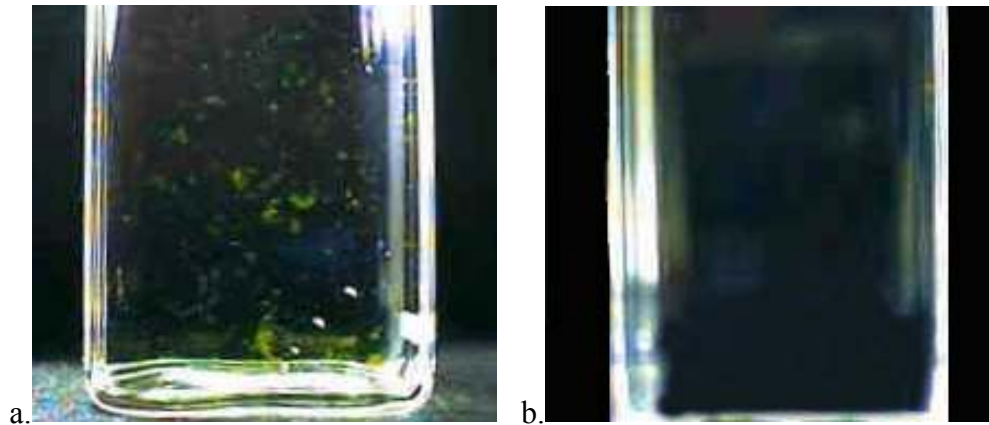


Photo 2 – Comparison of Floc Formation at 2.5 mg/L Fe. Visible Agglomerates in the Solution at Equilibrium with the Atmosphere (a), and No Visible Flocs in the Supersaturated Solution (b).

with 1.1 atm nitrogen, with only white agglomerates or no flocs visible. We do not know exactly why these changes occurred, and these changes deserve future investigation. The final settled turbidity in the supersaturated solutions was approximately double that of the other solutions at this coagulant dose (Figure 6).

For the solutions coagulated with 5 mg/L Fe, there was a 20% increase in settled turbidity in the 1.1 atm supersaturated solutions when flocculated at 60 rpm compared to the unsaturated waters (Figure 6). This increase was significant at 95% confidence. However, in the same experiment but at 100 rpm flocculation the bubbles were separated from the flocs at the higher mixing rate, and there was no significant difference between the saturated and unsaturated solutions. Tests with a solution at 1.2 atm did not lead to a significant worsening of settled

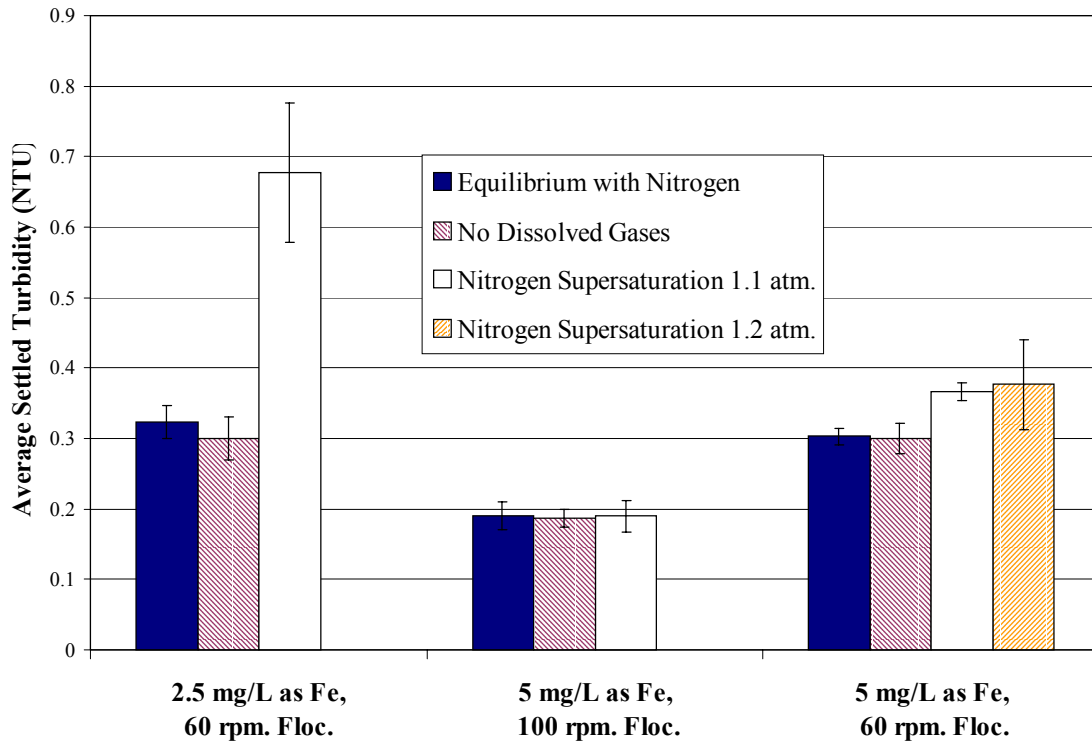


Figure 6 – Final Settled Turbidity for Coagulation Experiments. Error Bars Indicate 95% Confidence. The 2.5 and 5 mg/L Fe solutions settled for 45 and 30 minutes, respectively.

turbidity compared to 1.1 atm solutions, even though the TDG and turbidity were much greater at the end of flocculation in the 1.2 atm waters.

A treatment plant would be expected to respond in a similar manner as the jar tests with only a small percentage of TDG removed between rapid mixing and flocculation since the ratio of surface area to volume is approximately $0 \text{ cm}^2/\text{L}$ for both the surface with respect to the atmosphere and the solid surface of the reactor. Yet, due to dramatically different areas for gas transfer, a conventional or modified jar test is not very representative of treatment plants. For example, a conventional jar test would have surface area to volume ratios of 80 and $475 \text{ cm}^2/\text{L}$ for the atmosphere and solid surface, respectively, and the Erlenmeyer flasks used in the modified jar test had ratios of 20 and $405 \text{ cm}^2/\text{L}$, respectively. It is not possible to know whether this lessened or worsened effects of bubble formation in these experiments relative to treatment plants.

Given that dissolved gas supersaturation was proven to have profound effects on coagulation in this study, the question arises whether this phenomenon was influential in previous research results. In the classic study by Amirtharajah (1982) on rapid mixing design,

solutions were coagulated at different final pHs with alum concentrations at 1-30 mg/L and with initial alkalinity of 80 mg/L as CaCO₃. The waters were then rapid mixed at either 300, 1000, or 16,000 s⁻¹ and turbidity measurements were taken following settling. Plotting the settled turbidity in that study after 90 minutes of settling versus the potential bubble formation (calculated for a water initially at equilibrium with the atmosphere) using the model outlined by Scardina and Edwards (2000) illustrates that trends in the Amirtharajah work are consistent with the observations of this study (Figure 7). That is, settled turbidity increased when the potential for bubble formation was higher. Rapid mixing at a higher G value markedly improved settling analogous to results in Figure 6, but mixing had nearly no effect on settled turbidity when bubble formation potential was nearly zero.

Similarly, in Chowdury's (1991) coagulation experiments at a constant pH 6.5 and coagulant dose, reduced settling occurred when the solution's initial carbonate alkalinity was increased from 0.002 to 0.01 molar. The Scardina model predicts 2.15 and 0.4 mL/L bubble formation potential at 0.01 and 0.002 molar alkalinities, respectively; thus, reduced settling

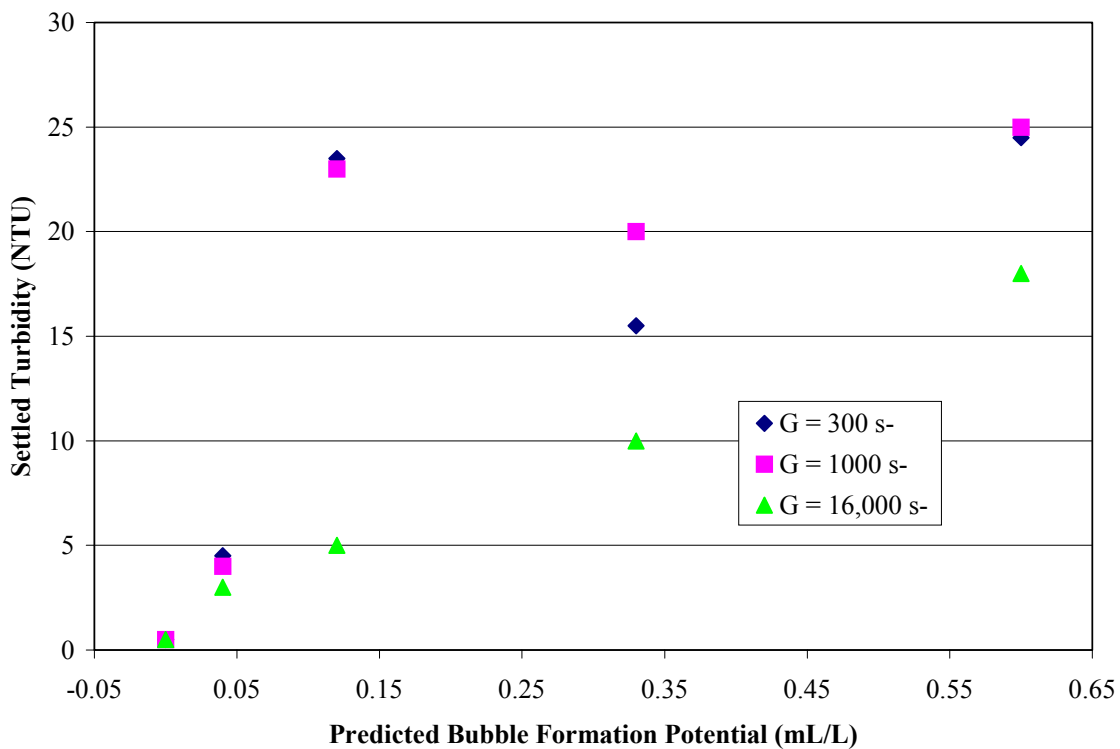


Figure 7 – Relationship between Bubble Formation Potential and Settled Turbidity in the Amirtharajah Study (Amirtharajah and Mills, 1982).

occurred at higher supersaturation as was the case in this work. Even more than 75 years ago, Miller (1925) examined effects of alkalinity on coagulation at several doses of alum, and noted that some solutions tested were completely opaque, consistent with micro bubble formation.

In summary, while it is uncertain as to the extent to which actual bubbles formed and influenced results in the cited research, it is clear that many phenomena in the literature are consistent with findings from this study and that bubble formation was not considered as a possible cause. Future work should examine the fundamental role of bubble formation in the context of coagulation and flocculation, repeating classic experiments if possible and re-interpreting results if necessary.

Implications of Bubble Formation in Filtration

Supersaturated dissolved gases in treatment plants are expected to interfere with filter performance through a phenomenon known as air binding. In addition to the criteria described earlier that can favor bubble formation, the velocity of water passing through the filter media will create a headloss, dropping the hydrostatic pressure and creating a greater driving force for bubble formation, according to Bernoulli's equation:

$$\frac{p}{\lambda} + \frac{V^2}{2g} + z = C$$

In the filtration experiments, it was not determined whether the decreased pressure predicted by the Bernoulli equation increased bubble formation in the filter media.

Bubbles began forming on top of the filter media within a few minutes if the influent was supersaturated at 0.2 atm or greater, and they occasionally detached and floated filter media to the water surface. Most bubbles were observed in the top 0.75 inches of the media, and bubble growth actually pushed the media upward as they grew (See Photograph). In addition, bubbles also formed in the underdrain rocks, with large gas pockets forming and almost completely covering the underdrain at the higher levels of supersaturation tested. This occurrence of bubble formation where space was available is an adaptation to the current theory of air binding, which mainly considered minute bubbles forming between the filter media similar to particles.

The headloss steadily increased in the pilot filter as bubbles grew and restricted flow (Figure 8). The time required to obtain 50% reduction of the initial flow appeared to decrease exponentially with the degree of supersaturation (Figure 9). No significant decrease in flow

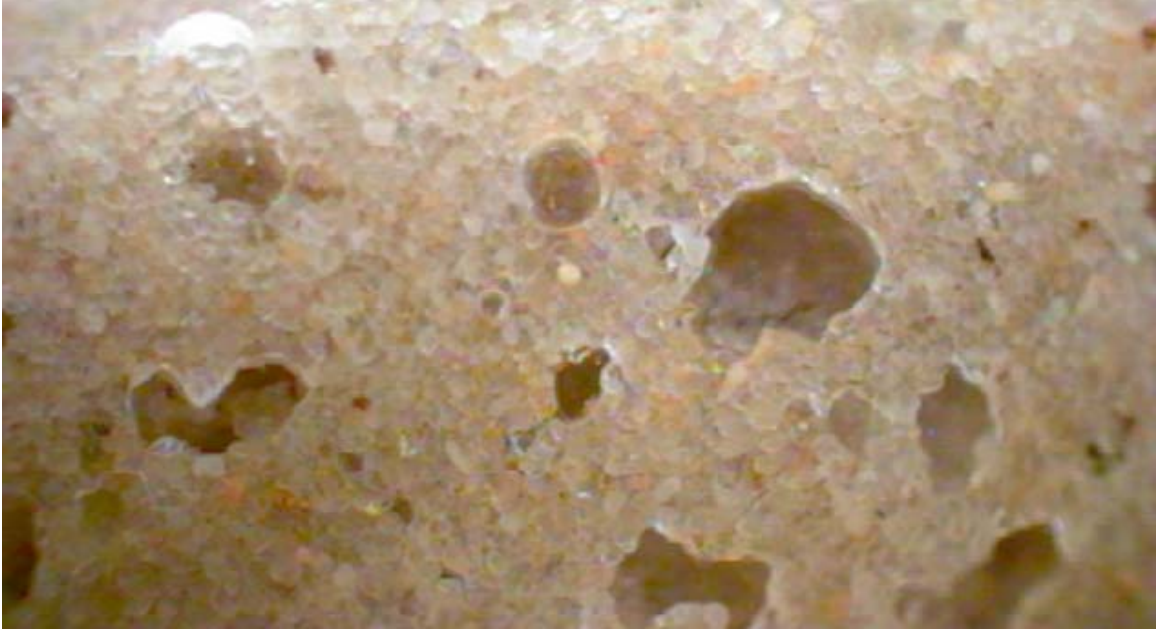


Photo 3 – Air Bubble Formation in Media during Filtration of Supersaturated Waters.

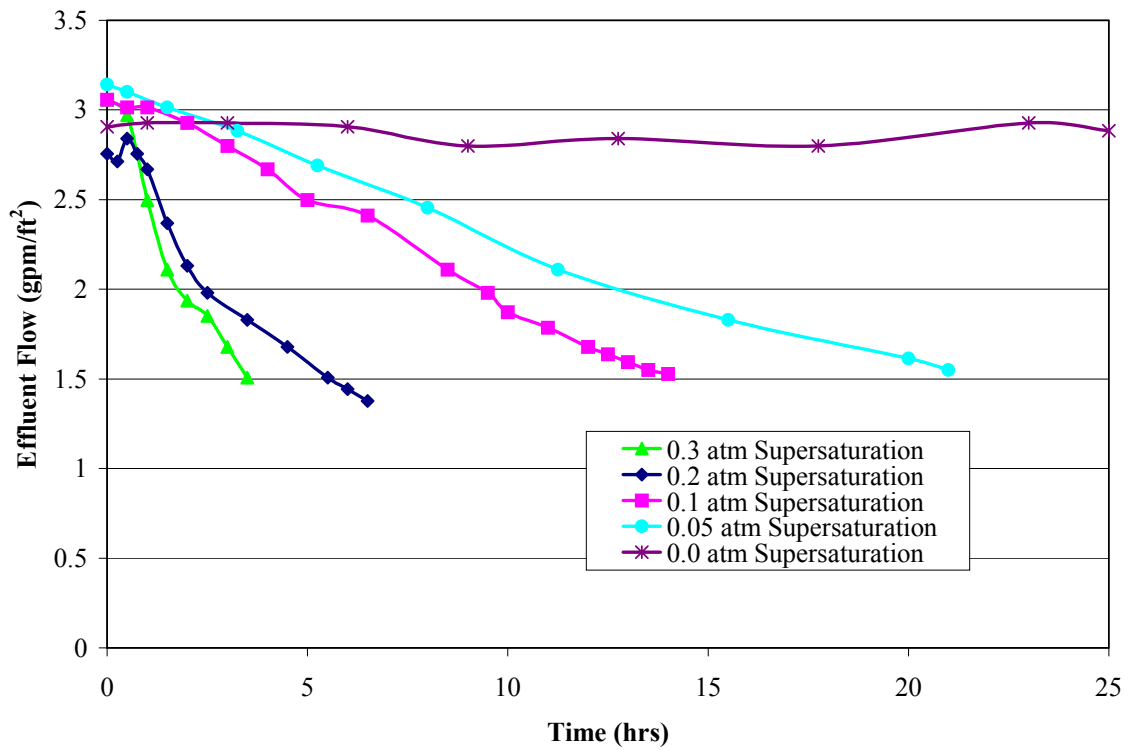


Figure 8 – Effluent Filter Flow at Constant Head.

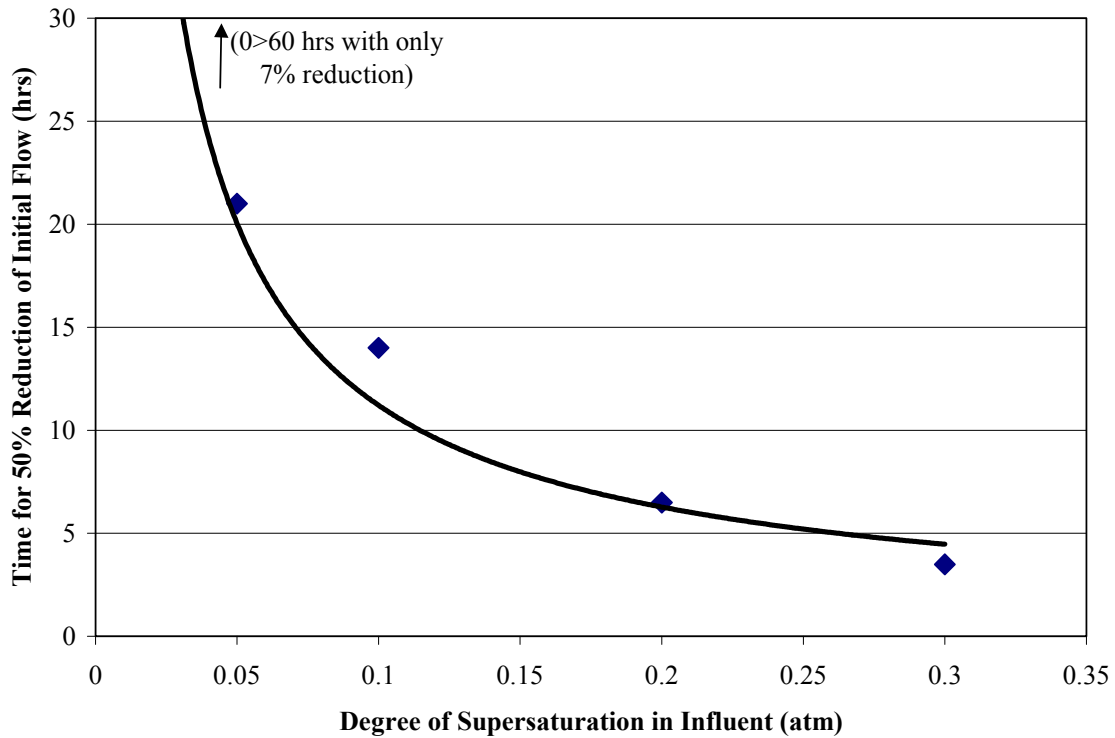


Figure 9 – Time for 50% Reduction of Effluent Flow per Supersaturation.

through the filter occurred in a water at saturation. However, even at 0.05 atm supersaturation, flow was decreased by 50% in 24 hours. Since plants commonly have filter runs between 24-100 hours (Montgomery, 1985), the above results suggest that even slight degree of supersaturation can have substantial effects upon headloss.

A rough comparison of the volume of floc and bubbles per liter suggest that such impacts are not surprising. Consider coagulation of a water with 160 mg/L as CaCO_3 alkalinity and raw turbidity of 10 NTU (~ 70 mg/L bentonite (Tseng, 1997) with a specific gravity of approximately 2.65 (Ojha, 1993)) with 5.8 mg/L as FeCl_3 coagulant to a final pH 7. Assuming all the iron forms flocs with a specific gravity of 1.01, the total volume of particles per liter including associated water is 0.4 mL/L, and it would be expected that most of these particles would be removed in the sedimentation basin. In contrast, if the water was initially at equilibrium with the atmosphere, acidification from the coagulant would lead to a bubble formation potential of 0.3 mL/L. Thus, bubble formation could dominate particle deposition as a source of filter headloss under some circumstances.

WATER TREATMENT PLANT CASE STUDY:

A case study at utility A provided confirmation of key principles developed in the laboratory. The study was conducted at the end of July 1999 when air binding in the filters is most noticeable due to higher plant flows and increased water temperature. This conventional treatment plant has the potential for pre-ozonation but currently only ozonates following sedimentation using air as the carrier gas—full details of the WTP can be found in Scardina (2000). The raw water has a typical pH of 6.9, 30 mg/L as CaCO₃ alkalinity, 300 color units, and total organic carbon between 20 and 60 mg/L. The water temperature was about 30 °C during sampling. A typical coagulant dose is 150 mg/L of alum, with lime addition to maintain pH at 5.8.

The raw water at the plant during normal operation was slightly undersaturated, but after rapid mixing was at equilibrium with dissolved gases (Figure 10). Total dissolved gases increased to 0.22 atm gauge pressure after post-ozonation, and since the plant usually experiences a zero measured ozone residual due to its reaction with contaminants, diffusion of the carrier gas at depth was assumed the source of supersaturation. Operators believed that filter headloss increased at the plant from bubble formation in sand media, and this was verified by the reduction in total dissolved gases after filtration (Figure 10). These TDG measurements and equations outlined by Scardina and Edwards (2000) for predicting bubble formation, indicate that 1.2 mL of bubbles formed per liter of water passed through the filtration process. As the head lowers above the filter for backwashing, bubbles physically boil the media, and the operators let the air release for five minutes prior to initiating backwash flow to help reduce filter media loss (See Photograph). Clearly, bubble formation was causing a serious operational problem at this plant, and the profile in Figure 10 illustrates the power of the TDGP to detect and interpret these phenomena.

After the sampling event, the operators began diffused aeration in the pre-ozonation cell to rapid mix the coagulant. The aeration at depth increased the partial pressure of dissolved gases from -0.039 to 0.092 atm gauge pressure (Figure 10), causing obvious bubble formation in the flocculation basin. Normally with the high coagulant dose, large, fluffy flocs form and settle quickly, and the bottom of the sedimentation basin (15 feet deep) (4.5 m) is often visible. With the onset of bubble formation, however, particle agglomeration was hindered, and many agglomerates passed into the filter since settling was impaired. This is consistent with the solids

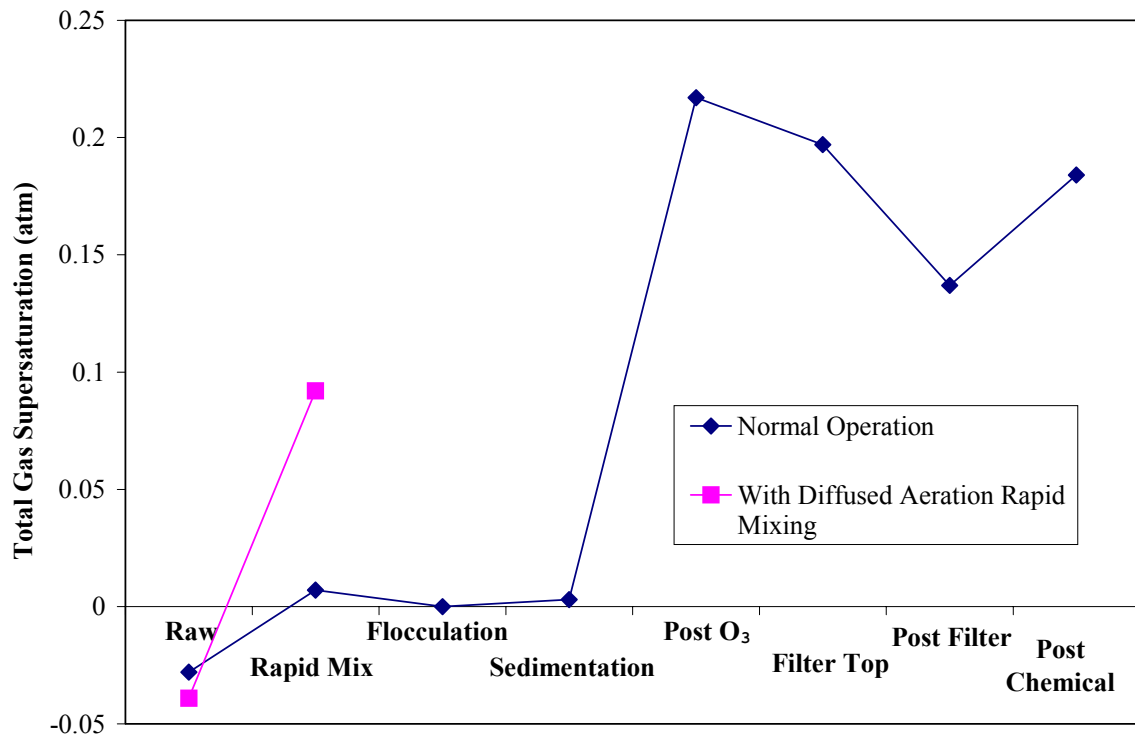


Figure 10 – Total Dissolved Gas Profile through Utility A.



Photo 4 – Air Bubble Release during Filter Backwashing at Utility A.

flotation observed from pre-ozonation in the South Bay Aqueduct pilot study (Camp Dresser & McKee Inc., 1990) and in Figure 5 and 6 of this work. Bubbles were visible on the flocs when samples were taken from the flocculation cell, and when the diffused aeration mixing was terminated, coagulation immediately improved.

ACKNOWLEDGEMENTS:

The authors would like to thank the generous anonymous operators at utility A who helped in the case study presented in this work. This work was supported by the National Science Foundation (NSF) under grant BES-9729008. The opinions, findings, conclusions, or recommendations are those of the authors and do not necessarily reflect the views of NSF. Parts of this work were presented at the *Advances in Rapid Granular Filtration in Water Treatment* conference at London, England, April 2001.

NOTATION:

[G] = Dissolved gas concentration for a particular gas

k_h = Henry Law's constant for a particular gas

pG = partial pressure of a particular gas

CONCLUSIONS:

- Sources of dissolved gas supersaturation in water treatment have been documented, and new techniques are described to measure the degree of supersaturation.
- Bubble formation during coagulation and flocculation can potentially inhibit particle sedimentation. In some cases, settled water turbidity was at least double that of a water without supersaturated gases.
- Increasing the degree of supersaturation decreases filter run time, even at 0.05 atm supersaturation. Bubble formation in filters can be an important, even dominant, contributor to filter headloss.
- A case study at a water treatment plant confirmed that bubble formation can dramatically decrease operational efficiency in coagulation-flocculation and filtration.

REFERENCES:

- Amirtharajah, A. & Mills, K.M. Rapid-mix Design for Mechanisms of Alum Coagulation. *Journal of American Water Works Association*, 74:4:210, (1982).
- AWWA. *Ozone in Water Treatment: Application and Engineering*. Eds., Langlais, B., Reckhow, D.A., & Brink, D.R. Lewis Publishers, Michigan (1991).
- Baird, M.H.I & Davidson, J.F. Annular Jets II: Gas Absorption. *Chemical Engineering Science*, 17:473 (1962).
- Baur, R. "Hypochlorite Problems and Some Solutions." Unified Sewerage Agency Memo.
- Boulder, CO. Conceptual Design Memorandum. Report prepared by Richard P. Arber Associates for Boulder, CO, (1993).
- Boulder, CO. Pilot Vacuum Deaeration Study. Report prepared by Richard P. Arber Associates for Boulder, CO, (1994).
- Boulder, CO. Reduction of Entrained/Dissolved Air in the Silver Lake Water Supply. Report prepared by CH2M-Hill for Boulder, CO, (1980).
- Camp Dresser & McKee Inc. South Bay Aqueduct Pilot Plant Studies. Technical Memorandum No. 10, (1990).
- Chowdhury, Z.K., Amy, G.L., & Bales, R.C. Coagulation of Submicron Colloids in Water Treatment by Incorporation into Aluminum Hydroxide Floc. *Environmental Science and Technology*, 25:10:1766, (1991).
- Denver, CO. Report prepared by HDR Engineering Inc. for Denver, CO, (1997).

- Ferguson, D. & Beuhler, M. Metropolitan Water District of Southern California, Internal Memorandum on Air Binding Data, (1990).
- Hess, T.F. Removal of Entrained Air from a Source Water. Master thesis, University of Colorado, Boulder, (1980).
- Hess, T.F., Chwirka, J.D., & Noble, A.M. Use of Response Surface Modeling in Pilot Testing for Design. *Environmental Technology*, 17:1205, (1996).
- Lange's Handbook of Chemistry*. Ed. Dean, J.A. McGraw-Hill, Inc., New York (14th ed., 1992).
- Letterman, R. & Shankar, S. Modeling pH in Water Treatment Plants: The Effect of Carbon Dioxide Transport on pH Profiles. Poster at the 1996 AWWA National Conference in Toronto, Canada (1996).
- Masters, G.M. *Introduction to Environmental Engineering and Science*. Prentice Hall, New Jersey (1991).
- Masterton, W.L. & Hurley, C.N. *Chemistry: Principles and Reactions*. Saunders College Publishing, New York (2nd ed., 1993).
- Metropolitan Water District. Degasification and Filter Air Binding Studies. Report prepared by Camp Dresser & McKee Inc. for Metropolitan Water District of Southern California, (1995).
- Miller, L.B. A Study of the Effects of anions Upon the Properties of 'Alum Floc.' (1925).
- Model 2100N Laboratory Turbidimeter Instruction Manual*. HACH Company, (1997).
- Montgomery, J.M. *Water Treatment Principles and Design*. (1985).

Ojha, C.S.P. & Graham, N.J.D. Theoretical Estimates of Bulk Specific Deposit in Deep Bed Filters. *Water Research*, 27:3:377, (1993).

San Diego. Water Quality Report. Report by Powell/Pirnie Assoc. for City of San Diego, CA, (1990).

Scardina, P. Water Treatment: Fundamentals and Practical Implications of Bubble Formation. Masters Thesis. (2000).

Scardina, P. & Edwards, M. Submitted to *Journal of Environmental Engineering*. (2000).

Thomas, W.J. & Adams, M.J. Measurement of the Diffusion Coefficients of Carbon Dioxide and Nitrous Oxide in Water and Aqueous Solutions of Glycerol. *Transactions of the Faraday Society*, 61:668 (1965).

Tseng, T. Considerations in Optimizing Coagulation. Master thesis, University of Colorado, Boulder, (1997).

Water Quality and Treatment: A Handbook of Community Water Supplies. Ed., Letterman, R. D. McGraw Hill, Inc. (5th ed., 1999).

AUTHOR'S VITA

Robert Paolo Scardina

Paolo Scardina has Bachelors of Science Degree in Mining and Minerals Engineering from Virginia Tech and a Master's Degree in Environmental Engineering also from Virginia Tech.